Simulation Studies of Correlations, Dynamics and Phase Transitions in Diblock Copolymer Melts

A THESIS
SUBMITTED TO THE FACULTY OF THE GRADUATE SCHOOL
OF THE UNIVERSITY OF MINNESOTA
BY

Taher Ghasimakbari

IN PARTIAL FULFILLMENT OF THE REQUIREMENTS
FOR THE DEGREE OF
DOCTOR OF PHILOSOPHY

Advisor: David Morse

May 30, 2018

Acknowledgments

I owe everything I have achieved in life to my beautiful, loving, and caring parents. Every step of the way in my growing up, they emphasized the importance of setting high goals and the possibility of achieving it by hard works. They have showered my brother and me with unconditional love and support. No collection of words would contain my sincere appreciation and gratitude for the wonderful parents they have been to us. I would also like to thank my little brother(Farzam Ghasimakbari) who have been my best friend since his birth. He has been an abundant source of joy and love in my life.

Far from home, I found a beautiful and loving girlfriend(Elspeth Hardy) with whom I have grown over last four years. She has been the source of many moments of happiness and love in my life away from Family. Without her presence in my life, this achievement would not have meant as much.

Over the years of my Ph.D. in Minnesota, I have made many friends. I have learned from them spent time with them and shared my concerns and seek their advice. They have always been very generous in their support for me. I want to thank them all for many years of friendship and support. My colleagues in the Prof. Morse group have in particular been wonderful friends with whom I have had many scientific and non-scientific discussion.

I want to thank my advisor Prof. David Morse. It has been a pleasure working with him and seeing up close what makes a great scientist. He has been more than generous with his time answering my countless questions over the years with enthusiasm and patience.

Dedicated to My Parents,
Shafigheh Afsharzadeh and Mohammad Ghasimakbari

Abstract

The limitations of approximate theories of diblock copolymers have motivated the computational study of these materials. Recent breakthroughs in the analysis of coarse-grained simulation models have led to an improved level of accuracy and consistency in the modeling of symmetric diblock copolymers. Simple bead-spring simulation models with a few parameters, f (relative volume fraction), χN (interaction strength), and $\overline{N}$ (a measure of polymer-polymer overlap) can predict the behaviors of diblock copolymers. The work presented in thesis focuses attention on the study of asymmetric diblock copolymers and the study of dynamics of symmetric copolymers.

Composition fluctuations in the disordered phase of asymmetric diblock copolymers have been investigated over a range of values of volume fraction, f, and fluctuation parameter, $\overline{N}$. Results for the structure factor are shown to obey a principle of corresponding states, which states that equivalent results should be obtained for systems with equal values of f, χN and $\overline{N}$. An empirical relationship is presented for the dependence of the peak in the structure factor of symmetric and moderately asymmetric diblock copolymers upon these state parameters.

Coarse-grained simulation models have been used to study dynamical properties and linear viscoelastic properties of symmetric diblock copolymers. Among dynamical properties measured are diffusion, end-to-end autocorrelation, Van Hove relaxation time, and stress relaxation modulus. The evolution of these properties has been studied from $\chi N = 0$ all the way up to the value $(\chi N)_{ODT}$ at the order-disorder transition (ODT). A simple description is provided for the behavior of the intermediate structure factor $S(q,t)$, and existing theoretical predictions for $G(t)$ are compared to simulation results.

Locations of order-disorder transitions have been identified for asymmetric diblock copolymers over a range of values of f and $\overline{N}$. Simulation results for $(\chi N)_{ODT}$ for several models are shown to obey the principle of corresponding states and exceed self-consistent field (SCFT) predictions by an amount that increases systematically with decreasing $\overline{N}$. SCFT predictions for the free energy in a hexagonal ordered phase are shown to be quite accurate, in contrast to the inaccuracy of predictions for the free energy in the disordered phase near the ODT. New methods are introduced to identify gyroid-disorder transitions, which are found to pose a particular technical challenge.

Contents

List of Tables

List of Figures

Chapter 1

Theoretical Background

Diblock copolymers are linear polymer chains with a structure that contain two linear blocks constructed from distinct chemical repeat units, denoted here by A and B, giving a molecule with the structure A_nB_m. Diblock copolymer melts exhibit a rich variety of properties, and have been heavily studied by physicists, chemists, and chemical engineers for several decades [1, 2, 3, 4, 5, 3, 6, 7, 8, 9, 10, 11, 12, 13]. A melt of diblock copolymers can undergo a phase transition to an ordered structure below a critical temperature[14, 15, 16, 17, 18, 19, 20, 21]. The nature of the resulting ordered structure depends on the relative length of the two blocks, and could be a lamellar (LAM), gyroid (GYR), hexagonal (HEX), or body centered cubic (BCC) phase.

This chapter briefly reviews some of the theoretical background to the content of this thesis and provides a summary of the remainder of the thesis. Section 1.1 discusses theories developed to understand equilibrium properties of disordered melt of diblock copolymers. Section 1.2 discusses the Rouse model of dynamical behavior in unentangled polymer liquids. Section 1.3 is an overview of the thesis.

1.1 Equilibrium Properties

Throughout this thesis, we consider the behavior of a melt of AB diblock copolymers. The standard theoretical descriptions of diblock copolymers describes this type of

system in terms of a few key parameters[14, 22, 23, 24, 25]. We consider a liquid of identical polymers in which each polymer has a total of N monomers, with a block of N_A A monomers, and $N_B = N - N_A$ B monomers. Let $f = f_A = N_A/N$ denote the fraction of A monomers and $f_B = 1 - f_A = N_B/N$. In a model of polymers as random walks, the A and B blocks are characterized by statistical segment lengths b_A and b_B. All of the work presented in this thesis, we consider simulation models in which A and B blocks are structurally similar, so that $b_A = b_B$.

When discussing simulation results, we use N to denote the number of beads in a simple bead-spring model of a polymer chain. The number of beads in such a simple coarse-grained model need not be the same as the number of chemical repeat units in a corresponding experimental system. The beads in a coarse-grained simulation model or theoretical description generally represent collections of chemical monomers that interact with sort of smooth pseudo-potential chosen to mimic the more complex interactions of real polymers.

In a melt containing M chains in a total volume V, let $c = MN/V$ denote the average monomer concentration. Let $c_i(\mathbf{r})$ denote the local monomer concentration of monomers of type i at a position $\mathbf{r}$, where i is a monomer type index with allowed values i =A or B. Coarse-grained theories often assume that the melt is effectively incompressible, and thus that $c_A(\mathbf{r}) + c_B(\mathbf{r})$ is constrained to a constant value c at every point $\mathbf{r}$. In an incompressible system, we use $\phi_i(\mathbf{r}) = \langle c_i(\mathbf{r})\rangle/c$ to denote the average volume fraction of monomers of type i at each point, with $\phi_A(\mathbf{r})+\phi_B(\mathbf{r}) = 1$ by construction.

Self-Consistent Field Theories

The self-consistent field theory (SCFT) of diblock copolymers is the most widely used method to predict order-disorder and order-order transitions in diblock copolymers[25, 26], and is the starting point of more advanced theories.

SCFT is itself rooted in the Flory-Huggins theory of homogeneous polymer blends and reduces to Flory-Huggins theory when applied to a homogeneous mixture. We thus begin with a brief discussion of Flory-Huggins theory. In its most

general form, the Flory-Huggins theory for a homogeneous mixture of A and B homopolymers yields a free energy of mixing per unit volume of the form

$$f_{\mathrm{mix}} = ck_{\mathrm{B}}T \sum_{i=A}^{B} \frac{\phi_i \ln \phi_i}{N_i} + f_{\mathrm{ex}}(\phi_A, T) \tag{1.1}$$

in which ϕ_A and ϕ_B are macroscopic average volume fractions of A and B monomers, N_i is the number of beads per homopolymer of type i, k_{B} is the Boltzmann constant and T is absolute temperature.

The original Flory-Huggins lattice theories [27] predicted a purely enthalpic excess free energy density, for which

$$f_{\mathrm{ex}}(\phi_A, T) = ck_{\mathrm{B}}T\chi(T)\phi_A\phi_B \quad , \tag{1.2}$$

with an interaction parameter $\chi(T) = A/T$ that was predicted to be independent of composition and inversely proportional to absolute temperature T. The simplicity of this prediction was, however, a result of the random-mixing approximation underlying those lattice theories. The more general expression given in Eq. (1.1) instead allows f_{ex} to be an arbitrary function of temperature and composition in a real mixture, or of simulation parameters in a simple simulation model. This level of generality is necessary to describe the thermodynamics of some real chemical systems and is believed to be sufficient to capture the dominant dependence of the free energy on chain length in the limit of long chains.

Self-consistent field theory [28, 23] for dense polymer liquids is a type of density functional theory of effectively incompressible liquids of idealized Gaussian polymers [29, 30]. SCFT yields an approximation for the free energy F of an inhomogeneous structure (e.g., an interface or an ordered phase) as a functional of the average volume fraction $\phi_A(\mathbf{r}) = \langle c_A(\mathbf{r})\rangle/c$ of A monomers at each point within the structure. SCFT approximates this functional as a sum of

$$F[\phi_A] = F_{\mathrm{id}}[\phi_A] + F_{\mathrm{ex}}[\phi_A] \tag{1.3}$$

of the free energy functional $F_{\rm id}[\phi_A]$ of an ideal gas of non-interacting Gaussian polymers with a specified composition profile plus an excess free energy $F_{\rm ex}$ that arises from interactions between polymers. The equilibrium state is obtained by minimizing this subject to a incompressibility constraint requiring a homogeneous total concentration $\langle c_A(\mathbf{r})+c_B(\mathbf{r})\rangle = c$. The excess free energy $F_{\rm ex}[\phi_A]$ in this theory is usually approximated as a local functional, i.e., as an integral of the form

$$F_{\rm ex}[\phi_A] \simeq \int d\mathbf{r}\; f_{\rm ex}(\phi_A(\mathbf{r})) \tag{1.4}$$

in which $f_{\rm ex}(\phi_A(\mathbf{r}))$ is a free energy density per volume at position $\mathbf{r}$ that depends only on the average composition at the same position $\mathbf{r}$.

The first numerical solution for SCFT of diblock copolymers was introduced by Helfand. However, Matsen and Schick were the first to determine the phase diagram of the diblock copolymers for the known phases of LAM, GYD, HEX, and BCC[23, 24, 29]. The original paper by Matsen and Schick is frequently used by experimental groups in their comparisons of results with theoretical predictions. While the experimental[18] and SCFT phase diagrams are in qualitative agreement, there are apparent quantitative differences due to the fluctuation effects.

The SCFT approach to diblock copolymers assumes a set of ideal Gaussian chains interacting via a mean field. This approach by design fails to incorporate the non-Gaussian chain effects and the composition fluctuations. Therefore the results of the SCFT are expected to be valid only in the absence of fluctuation effects.

Structure Factor

Correlations in the DBC melts, or any two component melt, in general, can be characterized by a 2×2 structure factor matrix given by

$$S_{ij}(\mathbf{q}) \equiv \int d\mathbf{r}\; e^{i\mathbf{q}\cdot\mathbf{r}} \langle \delta c_i(\mathbf{r}) \delta c_j(\mathbf{0})\rangle \tag{1.5}$$

where i and j are monomer type indices that can take on values denoting A and B monomer. Here $\delta c_i(\mathbf{r})$ is the deviation of the local concentration of monomers of

type i from its spatial average. This structure factor matrix is the Fourier transformation of the cross-composition correlation matrix. In a dense liquid, the structure factor matrix has two eigen-vectors with widely disparate eigenvalues. One eigenvector, denoted by $\epsilon^{+} = (+1, +1)$, is associated with changes in total monomer concentration, characterized by an amplitude

$$\delta c(\mathbf{r}) \equiv \delta c_A(\mathbf{r}) + \delta c_B(\mathbf{r}) \quad . \tag{1.6}$$

In the limit of an incompressible melt of diblock copolymers, the total concentration of the melt does not fluctuate,

$$\delta c(\mathbf{r}) = \delta c_A(\mathbf{r}) + \delta c_B(\mathbf{r}) = 0 \quad , \tag{1.7}$$

and so the eigenvalue associated with this mode becomes vanishingly small, creating a nearly singular matrix. The second eigenvector, denoted by $\epsilon^{-} = (+1, -1)$, is associated with composition fluctuations at fixed total composition and is characterized by a mode amplitude

$$\psi(\mathbf{r}) \equiv [\delta c_A(\mathbf{r}) - \delta c_B(\mathbf{r})]/2 \quad . \tag{1.8}$$

The eigenvalue associated with this composition mode is related to the scalar structure factor $S(\mathbf{q})$, given by

$$S(\mathbf{q}) \equiv \int d\mathbf{r}\; e^{i\mathbf{q}\cdot\mathbf{r}} \langle \psi(\mathbf{r})\psi(\mathbf{0})\rangle \quad . \tag{1.9}$$

The scalar correlation function $S(\mathbf{q})$, which is the spatial Fourier transform of the correlation function of the composition field $\psi(\mathbf{r})$, is often referred to as the structure factor in the literature. Since the disordered phase of DBCs lack any long-range order and is isotropic, the structure factor in an large system only depends on the magnitude of the wave-vector $|\mathbf{q}| = q$. The scalar structure factor of diblock copolymers may be experimentally measured using small-angle neutron scattering(SANS) or X-ray scattering(SAXS).

Random Phase Approximation

The mean-field approach to investigate the disordered and the weakly ordered melt of diblock copolymers was first developed by Leibler[14]. In Leibler's approach, the free energy functional of the diblock copolymer system is represented by a Landau expansion in terms of the composition field. In this approach, the particle-particle interactions were approximated by an effective external field proportional to the χ parameter and the local average concentration of A and B monomers. This mean-field theory provides predictions for the scalar structure factor, $S(q)$, in the disordered phase as well as predictions for the phase diagram of diblock copolymers.

The Leibler theory for $S(q)$ is usually referred to as the random-phase approximation (RPA). The RPA theory for $S(q)$ can be derived by using a self-consistent field approximation to compute the free energy cost of infinitesimal composition fluctuations [14], to harmonic order in the amplitude of the fluctuation. The RPA for $S(q)$ in a diblock copolymer melt with equal A and B statistical segment lengths, denoted here by $S_0(q)$, is given by an equation of the form

$$cNS_0^{-1}(q) = F(qR_{g0}, f) - 2\chi_e N \quad , \tag{1.10}$$

where $F(qR_{g0}, f)$ is a known analytic function, $R_{g0} = \sqrt{Nb^2/6}$ is the ideal random walk radius of gyration for a chain with a statistical segment length b, and χ_e is an effective RPA interaction function given by

$$\chi_e \equiv -\frac{1}{2ck_BT}\frac{\partial^2 f_{\rm ex}(\phi_A)}{\partial \phi_A^2} \quad , \tag{1.11}$$

in which the derivative is evaluated at average composition $\phi_A = f$ of the disordered diblock copolymer melt. Eq. (1.11) for χ_e yields a function χ_e that is independent of average composition f if and only if $f_{\rm ex}$ has the simple quadratic composition dependence, $f_{\rm ex} \propto \phi_A\phi_B$, predicted by the original Flory-Huggins mean-field lattice theories. Leibler's prediction for the structure factor is widely used by experimental groups in their analysis of scattering results.

The function $F(q)$ has a minimum around $1/R_g$ which produces a maximum

in the structure factor. The maximum in the structure factor is the manifestation of the correlation-hole peak in the disordered phase[31]. The Leibler prediction of the structure factor adequately describes the observations of most SANS and SAXS measurements, especially those performed at low χN, deep in the disordered phase of diblock copolymers[32, 33].

The Leibler theory, although successful in many aspects, has several limitations. Despite the Leibler's prediction for linear dependence of inverse structure factor on χ, experimental observations of the inverse structure factor over a wide range of χN do not show such a linear dependence[32, 15, 12, 19]. Also, Leibler's theory predicts that the position of the peak structure factor, q^*, does not vary with χN. This is in contrast with experimental observations where q^* decreases as the melt temperature approaches the ODT temperature[34, 33, 5, 15]. Deviations from the RPA predictions are attributed to the failure of the mean-field approximation and the emergence of strong composition fluctuations in the melt of DBCs.

Fredrickson-Helfand and Renormalized-One Loop Fluctuation Theories

Early theoretical approaches to the study of diblock copolymers were based on the self-consistent field approximation. This approach captures the essence of the diblock copolymer behavior, and yields accurate predictions for some properties, but fails to take into account the effects of composition fluctuations that become strong in the vicinity of the order-disorder transition.

The first attempt to theoretically predict deviations from SCFT was given in the theory of Fredrickson and Helfand[22]. This theory attempted to describe the behavior in the vicinity of the order-disorder transition of symmetric diblock. The Fredrickson-Helfand (FH) theory was based directly on a more general phenomenological theory of weakly-first order crystallization by Brazovskii [35]. The FH theory correctly predicted that one effect of strong composition fluctuations would be to change ODT of the symmetric diblock copolymer from a second order transition, as predicted by the RPA theory, to a first order transition, as observed in experiments.

FH adapted Brazovskii's weak-crystallization theory to construct quantitative predictions for the structure factor and the location of the order-disorder transition of the symmetric diblock copolymers[22].

In all of the predictions of the FH theory, the magnitude of corrections to SCFT and RPA predictions are controlled by a dimensionless parameter

$$\overline{N} = N(cb^3)^2 \quad , \tag{1.12}$$

which is sometimes referred to as the invariant degree of polymerization. All predictions of the theory can be expressed in terms of universal functions of the dimensionless parameter χN and f that appear in analogous predictions of SCFT and, in addition, the parameter $\overline{N}$. All predictions of the theory also reduce to the corresponding self-consistent field predictions in the limit $\overline{N} \to \infty$, with fluctuation effects becoming more important with decreasing $\overline{N}$.

The FH theory successfully explained the non-linear dependence of the inverse structure factor on χN near the ODT [32, 15, 12, 19]. It also predicted a value for the value of χN at the ODT, denoted by $(\chi N)_{ODT}$, which depends on $\overline{N}$, and decreases with increasing $\overline{N}$ and gave results for the location of the transition in reasonable quantitative agreement with the experiment on long chains.[15]. The original FH theory did not predict the observed shift of q^* with decreasing temperature near the ODT. To address this issue, Barrat and Fredrickson refined the original Fredrickson-Helfand theory to incorporate the wave-vector dependence of the quartic term in the Landau expansion of the symmetric diblock copolymers free energy functional, and showed that this was sufficient to yield a variation of q^* consistent with that observed in experiments[36].

The Fredrickson-Helfand-Barrat(FHB) theory was successful in addressing some aspects of the observed fluctuation effects for symmetric diblock copolymers but suffered from lack of rigorous theoretical basis and a limited range of validity. Both Fredrickson-Helfand and Fredrickson-Helfand-Barrat theories use the mean-field free energy functional as an effective Hamiltonian without justification. The theory also relied on a set of mathematical approximations that were justifiable only for values

of χN that lie in a relatively narrow range near the ODT, and for very large values of $\overline{N}$. Finally, the Fredrickson-Helfand theory suffers from an ultraviolet divergence that was swept under the rug somewhat in the presentation of the original theory.

The renormalized one-loop (ROL) theory is a more recent theory of correlations in disordered diblock copolymer melts that avoids many of the limitations of the FH theory.[37, 38, 39, 40] The ROL theory avoids the problem of UV divergence by showing how the UV divergences in the related theory can be absorbed into a redefinition of the values of phenomenological parameters such as the effective interaction parameter and the statistical segment length. Like the Fredrickson-Helfand theory, the ROL theory yields predictions for $S(q)$ that depend explicitly on $\overline{N}$, as well as f, χN and wavenumber q. When applied to symmetric diblock copolymers, the theory has been shown to have a much wider range of validity than the Fredrickson-Helfand theory, and to provide accurate predictions for values of χN over the entire range from $\chi N = 0$ to the value at the ODT. [41, 42] When applied to sufficiently asymmetric diblock copolymers, however, the theory exhibits unphysical behavior near the ODT. When applied to asymmetric diblock copolymers, the theory is thus expected to be accurate only at low values of χN, far from the ODT.[39, 40]

Universality and Corresponding States

The SCFT and RPA theories for diblock copolymer melts yields predictions in which free energy per chain depends on only a few dimensionless state parameters. Let g denote the free energy per chain divided by the thermal energy $k_{\mathrm{B}}T$. SCFT yields a prediction for g in a melt of diblock copolymers with equal A and B statistical segment lengths that depends only on the parameters f and χN, so that

$$g = g(f, \chi N) \quad . \tag{1.13}$$

As a result of this, SCFT yields a phase map for this class of systems that can be plotted on a graph of χN vs. f, in which phase boundaries represent lines along which values of g for neighboring phases become equal. Similarly, the RPA

theory for $S(q)$ in such systems yields a prediction for non-dimensionalized inverse structure factor $cNS^{-1}(q)$ that depends only on the state parameters f and χN and on the nondimensionlized wavenumber qR_{g0}, in which $R_{g0} = \sqrt{Nb^2/6}$ is the unperturbed radius of gyration of a diblock copolymer in a homogeneous liquid. The self-consistent field approximation thus leads to a theory in which f and χN are the only relevant thermodynamic state parameters, and in which the polymer coil size is the only relevant length scale.

The Fredrickson-Helfand and ROL theories instead yield predictions for the free energy per chain and the nondimensionalized structure factor that depend on $\overline{N}$ as well as on the parameters that appear in the corresponding SCFT and RPA predictions. The analysis underlying the ROL theory provided a hint that this feature might be more general. The authors of ROL theory showed that the one-loop correction to SCFT that they compute is actually the first correction to SCFT in a Taylor series expansion in powers of $\overline{N}^{-1/2}$, in which the coefficients in the expansion appear to be functions of the SCFT state parameters. This suggested that the ROL theory is part of an asymptotic expansion of the free energy and structure factor in which the state of the system can be specified as a function of the state parameters f, χN, and $\overline{N}$ alone.

Morse and coworkers have proposed a generalization of this observation that they refer to as a corresponding states hypothesis. When applied to diblock copolymer melts for chains with $b_A = b_B$, this hypothesis states that equivalent results should be obtained in different simulations or different chemical systems in states with matched values of the state parameters f, χN, and $\overline{N}$. When applied to measurements of the free energy, it implies that the non-dimensional free energy per chain g should be a function of f, χN and $\overline{N}$. When applied to the behavior of the structure factor in the disordered phase, it implies that $cNS^{-1}(q)$ should depend only on the state parameters f, χN and $\overline{N}$ and the non-dimensionalized wavenumber qR_{g0}.

Implications of the corresponding states hypothesis for symmetric diblock copolymers have been thoroughly tested and verified in a series of simulation studies of the behavior of the structure factor [43, 42] and of the order-disorder transition and free energy [44, 45]. One immediate implication of this hypothesis is that the value of

χN at the order-disorder, where the values of g in the ordered and disordered phase become equal, must be a universal function of f and $\overline{N}$, or a universal function of $\overline{N}$ alone in the special case of symmetric copolymers. The validity of this statement was demonstrated for symmetric copolymers by comparing results for the location of the ODT for a series of models with different values of $\overline{N}$ [44, 45].

1.2 Dynamical Properties

In addition to their structure forming tendencies, DBCs have interesting dynamical properties.[4]. Chapter 4 of this thesis is a study of the relationship among various measures of dynamic and viscoelastic properties in a melt of unentangled diblock copolymers. The starting point for the description of dynamical properties in such a system is the Rouse model [46], which we briefly review here for reference.

In the Rouse dynamical picture, the beads of the homopolymer chains experience a friction force due to the relative motion of the chains, the drag force. In addition, the beads experience a random thermal force. In other words, the Rouse model is the study of the Brownian motion of beads connected with springs. The Rouse model provides a complete picture of the dynamics of homopolymer melts, and diblock copolymer melts at low χN. Consider a chain of N beads with positions $\mathbf{R}_1(t), \ldots, \mathbf{R}_N(t)$. The motion of the beads is described in the Rouse model by the following sets of equations

$$\frac{d\mathbf{R}_1}{dt} = -\frac{3k_BT}{\zeta b^2}(\mathbf{R}_1 - \mathbf{R}_2) + \mathbf{f}_1 \tag{1.14}$$

$$\frac{d\mathbf{R}_n}{dt} = -\frac{3k_BT}{\zeta b^2}(2\mathbf{R}_n - \mathbf{R}_{n-1} - \mathbf{R}_{n+1}) + \mathbf{f}_n \tag{1.15}$$

$$\frac{d\mathbf{R}_N}{dt} = -\frac{3k_BT}{\zeta b^2}(\mathbf{R}_N - \mathbf{R}_{N-1}) + \mathbf{f}_N \tag{1.16}$$

in which ζ is a bead friction coefficient, b is the root-mean-square equilibrium bond length (i.e., the statistical segment length), and $\mathbf{f}_n$ is a random force on bead n, for

which

$$\langle \mathbf{f}_n \rangle = 0 \tag{1.17}$$

$$\langle \mathbf{f}_n(t)\mathbf{f}_m(t') \rangle = 2\zeta \mathbf{I}\delta_{nm}\delta(t-t'). \tag{1.18}$$

This coupled set of linear stochastic differential equations can be decoupled using a canonical transformation of the form

$$\mathbf{R}_n = \mathbf{X}_0 + 2\sum_{p=1}^{p=N} \mathbf{X}_p \cos\left(\frac{p\pi}{N}(n-1/2)\right) \tag{1.19}$$

Different terms of this sum relax with different time constants. Placing the above equation in the Rouse equations of motion we get

$$\frac{d\mathbf{X}_p}{dt} = \frac{-1}{\tau_p}\mathbf{X}_p + \mathbf{F}_p \tag{1.20}$$

in which $\mathbf{F}_p$ is a random white noise for the canonically transformed coordinates , and

$$\tau_p = \frac{\zeta b^2}{3k_{\mathrm{B}}T}\left[4\sin^2\left(\frac{p\pi}{2N}\right)\right]^{-1} \tag{1.21}$$

is the relaxation time of pth mode. The shorter the wavelength of the wave, the faster the wave relaxes.

The Rouse model predicts the chain diffusion constant D to be related to the bead fricion coefficient as

$$D = \frac{k_{\mathrm{B}}T}{\zeta N} \quad . \tag{1.22}$$

Chain diffusion is thus N-times slower than diffusion of single unchained bead in the same melt.

Another dynamical response function that the Rouse model provides the prediction for is the chain end-to-end auto-correlation function. Let $\mathbf{R}_e(t)$ denote the vector connecting the first and last beads of a polymer chain, given by

$$\mathbf{R}_e = \mathbf{R}_N - \mathbf{R}_1 \tag{1.23}$$

The end-to-end autocorrelation function, denoted here by $E(t)$, is given by the average

$$E(t) = \langle \mathbf{R}_e(t+\tau) \cdot \mathbf{R}_e(\tau) \rangle \tag{1.24}$$

for a randomly chosen chain, and an arbitrary reference time τ. The Rouse model prediction for $E(t)$ is given in the limit $N \gg 1$ by a sum

$$E(t) = \frac{8b^2N}{\pi^2} \sum_{p=1,3,5}^{\infty} \frac{1}{p^2} \exp\left(-\frac{t}{\tau_p}\right) \tag{1.25}$$

where the sum is taken only over odd values of $p = 1, 3, 5, \ldots, \infty$, $\tau_p \simeq \tau_1/p^2$ and

$$\tau_1 \simeq \frac{1}{6\pi^2} \frac{\zeta N b^2}{k_{\mathrm{B}}T} \tag{1.26}$$

is the longest relaxation time for $N \gg 1$.

The Rouse model also provides predictions for the shear stress relaxation modulus of a homopolymer melt. The Rouse model prediction for the stress relaxation modulus $G(t)$ may be approximated in the continuum limit $N \gg 1$ by a sum

$$G(t) = \frac{ck_BT}{N} \sum_{p=1,2,3,\ldots}^{\infty} \exp\left(-\frac{2t}{\tau_p}\right) \tag{1.27}$$

where c is the monomer concentration and the τ_p's are the Rouse chain relaxation times. The viscosity of such a melt can be calculated as well by integrating the shear relaxation modulus

$$\eta = \int_{t=0}^{t=\infty} G(t)dt \simeq \frac{c\zeta N b^2}{36} \tag{1.28}$$

The Rouse model however successful in describing the dynamics of a concentrated unentangled diblock copolymer melt deep in the disordered phase, it fails as the melt approaches the order-disorder transition, as a result of the appearance of long-lived A and B rich regions near the transition.[22].

1.3 Contents of Thesis

We now summarize the contents of each of the remaining chapters of the thesis.

Chapter 2 provides some details about the coarse-grained simulation models that are used in the simulations presented in chapters 3-6.

Chapter 3 is a study of the behavior of the structure factor $S(q)$ in the disordered phase of asymmetric diblock copolymers. We explore the corresponding states hypothesis and the applicability of the χ calibrated for the symmetric diblock copolymers to asymmetric diblock copolymers. The limitations of the RPA and ROL theories are discussed alongside the simulation results. A new fit is introduced to extend the range of applicability of the RPA and ROL theories to the relevant range of $\overline{N}$ for experimentalists.

Chapter 4 is a study of dynamical and linear viscoelastic properties of disorderd symmetric diblock copolymers. A variety of dynamical properties have been investigated in this chapter. The evolution of these properties with changes in χN is characterized to show how dynamics and viscoelasticity are affected by the emergence of strong composition fluctuations near the order-disorder transition.

Chapter 5 focuses on the phase diagram of diblock copolymers. We have used well-tempered metadynamics to precisely locate values of χN along the lamellar-disorder and hexagonal-disorder phase boundaries as functions of f for systems of varying $\overline{N}$, and study the behavior of the underlying free energy per chain at a single value of $f = 1/4$.

Chapter 6 is dedicated to a more detailed study of the gyroid-disorder transition.

Chapter 2

Simulation Models

All of the simulation presented in Chapters 3-6 use a set of simple bead-spring simulations models that were developed in earlier studies of equilibrium properties of symmetric diblock copolymer melts [47, 45, 42, 44, 48]. This sequence of models all use similar functional forms for the pair and bond potentials, and differ only in choices of the values of a few parameters. The specific parameter values in these models were chosen to given values for the dimensionless quantity $\overline{N}/N = (cb^3)^2$ that differ by powers of 2 between different models. This convention was chosen in order to simpify construct of pairs of systems for which the number N of beads per chain differ by a factor of 2 (e.g., 16 vs. 32 beads) but for which two systems have equal values of the invariant degree of polymerization $\overline{N} = N(cb^3)^2$. A signficant effort was also spent to develop accurate estimates of the dependence of the effective χ parameters upon simulation input parameters for these models. In the remainder of this chapter, we describe these bead-spring models and discuss some of the procedures used to choose specific sets of parameters and estimate physical properties.

2.1 Simulation Models

All of the simulations presented in this thesis use a model in which the nonbonded pair interaction between beads of types i and j are givn by a potential $V_{ij}(r)$ that

is zero when the distance r between particles exceeds a cutoff length σ, and is given by a function

$$V_{ij} = \frac{1}{2}\epsilon_{ij}(1 - r/\sigma)^2 \tag{2.1}$$

for all $r < \sigma$. Here, ϵ_{ij} is an energy parameter that controls the strength of interaction between i and j beads, for which $\epsilon_{ij} = \epsilon_{ji}$. In all of the models studied here we take $\epsilon_{AA} = \epsilon_{BB}$, thus preserving the symmetry between A and B monomers. Consecutive beads in the same chain also interact via a harmonic bond potential, of the form

$$V_{bond} = \kappa r^2/2 \quad , \tag{2.2}$$

in which κ is a spring constant.

In a model of this form, the degree of thermodynamic repulsion between A and B monomers in a melt of AB diblock copolymers is varied by varying the value of a control parameter

$$\alpha \equiv \epsilon_{AB} - \epsilon_{AA} \quad . \tag{2.3}$$

The control parameter α plays a role in simulations analogous to the role of temperature in an experiment, as a parameter that one can vary to modify the effective interaction parameter.

The definition of what we call a "model" is specified by specifying constant values for all of the parameters of the simulation *except* the value of α, which can be varied for each model in order to control the degree of segregation. In a constant pressure, constant temperature simulation, the definition of a model is thus given by specifying values for the temperature, pressure, the spring constant κ, and the value of $\epsilon_{AA} = \epsilon_{BB}$. In all of the models studied here, we take

$$\epsilon_{AA} = \epsilon_{BB} = 25 k_{\mathrm{B}} T \tag{2.4}$$

where T is absolute temperature and k_{B} is Boltzmann's constant.

Previous work on symmetric diblock copolymers used three models of the type

described above, which were referred to in that work models S1, S2, and S3. The parameters of these models were chosen so that the values of $\overline{N}/N = (cb^3)^2$ had values with ratios of $1:4:8$ for S1, S2 and S3, respectively[47, 45, 42, 44, 48]. In this prior work, the choice of the letter S was used to indicate that these are "soft" models, in contrast to a model with a "hard" truncated Lennard-Jones potential that was also used in that work. Throughout this thesis, these three pre-existing models are instead referred to as models D1, D3, and D4. The letter "D" in these names is used to indicate that the form of the potential and the specific choice of some of the parameters is chosen to be the same as that used in previous dissipative particle dynamics simulations. The work presented here also includes some results obtained with another model of the same type that we refer to as model D2, for which $\overline{N}/N$ is twice as high as for model D1. The complete sequence of models D1, D2, D3, and D4 thus has values of $\overline{N}/N = (cb^3)^2$ with ratios 1:2:4:8 that form a series of numbers that differ by factors of 2.

This series of models was designed so as to make it simple to design pairs of systems with matched values of $\overline{N}$ but values of N that differ by factors of 2 in order to test the corresponding state hypothesis. For example a simulation of model D3-16, which consists of D3 polymer chains of chain length 16, would have $\overline{N} = 960$, which is the same as the value of $\overline{N}$ for a simulation of model D1-64. All of the tests of the principle of corresponding states presented in this thesis involve a comparison of simulations of model D2-32 and D1-64, both of which have $\overline{N} = 480$.

The following table presents the parameters used in NPT simulations of this sequence of 4 models. The procedures used to arrive at these choices of parameters are described in the remainder of this chapter.

Model	ϵ_{AA}	κ	P	c	b
D1	25.0	3.406	20.249	3.0	1.088
D2	25.0	2.428	20.412	3.0	1.222
D3	25.0	1.135	4.111	1.5	1.727
D4	25.0	0.867	4.132	1.5	1.938

Table 2.1: Simulation parameters for the bead-spring models in units in which $k_BT = 1$ and $\sigma = 1$. Here, c and b denotes the extrapolated bead concentration and statistical segment length, respectively, for infinitely long homopolymers at the specified pressure. Models D1, D3, and D4 have been studied in earlier work, while model D2 was developed and calibrated for use in this thesis work.

Different models have been used in various chapters for different studies. In chapter 3, we have used simulation models D1-32, D1-64, D2-32, D3-32, D4-32 to study the disordered phase of diblock copolymers as well as the corresponding state hypothesis for asymmetric diblock copolymers. In chapter 4, we have used models D1-16 and D1-32 to investigate the dynamical properties of diblock copolymers. In chapter 5, the phase diagram of simulation models D1-32 and D3-32 is determined. In chapter 6, model D1-32 has been used to study the formation and stability of the gyroid structure.

2.2 Calibrating Model Parameters

In this section, we discuss some details of the procedure used to choose values for the parameters of models D1 - D4. The parameters of each model in this sequence are chosen to give a predetermined value for the monomer concentration c and for the value of the ratio $\overline{N}/N = (cb^3)^2$ in the limit $N \to \infty$ and $\alpha = 0$ of infinite hompolymers. The value of $\overline{N}/N$ for model D1 was chosen to be 4 times that of a model with repulsive Lennard-Jones pair interaction to which it was compared in earlier work [42]. Values of the ratio $\overline{N}/N$ for models D2, D3, and D4 were then chosen to form a geometric series with neighboring values differ by factors of 2. The target value monomer concentration c was arbitrarily chosen to be $c = 3.0\sigma^{-3}$ for

models D1 and D2, and $c = 1.5\sigma^{-3}$ for models D3 and D4.

Statistical Segment Length vs. Spring Constant

The statistical segment length, b, for any fixed set of values of the other parameters can be obtained from measurements of the radius of gyration $R_g(N)$. The ROL theory predicts that the radius of gyration R_g of a polymeric model at $\chi N = 0$, the homopolymer state, varies with chain length, N, as

$$R_g^2(N) = \frac{Nb^2}{6}\left[1 - \frac{1.42}{\sqrt{\overline{N}}} + \frac{\gamma}{\overline{N}} + \cdots\right] \tag{2.5}$$

The first correction term is a universal correction arising from the interactions between chains in an incompressible melt. The prefactor factor 1.42 is a universal characteristic of mono-disperse melts that was calculated by Qin and Morse[49].

To find the statistical segment length, b, a series of simulations of hompolymers (with $\alpha = 0$) are performed for several chain lengths for systems with constant concentration, $c = 3.0$ for D1 and D2 and $c = 1.5$ for D3 and D4, in NVT ensemble. The simulation results are then fitted to the equation Eq. (2.5), with b and γ considered as fitting parameters, to determine the statistical segment length b.

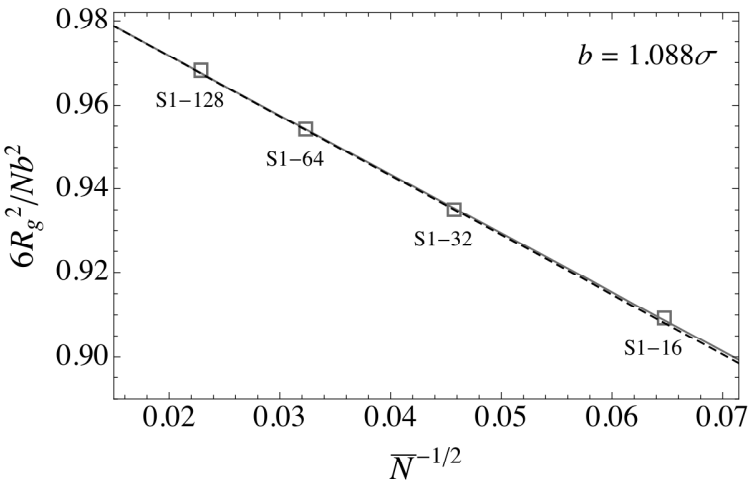

Figure 2.1: The fit of squared and normalized radius of gyration, $R_g^2(N)/N$ vs. $\overline{N}^{-1/2}$ at $\alpha = 0$ for model D1. The data is shown for $N = 16, 32, 64, 128$. The solid line represents the fit to equation 2.5. The dashed line is the obtained by setting $\gamma = 0$. This figure reproduced with permission from the Ph.D. thesis of Pavani Medapuram[50].

In order to find the value of the spring constant κ required to obtain a specified value of b, the procedure described above is repeated for several values of κ, thus giving a set of values of b at different values of κ. By fitting $b(\kappa)$ to a linear function, we can then chose the value of κ required to obtain a specified value for b, and thus a specified value for $\overline{N}/N = (cb^3)^2$.

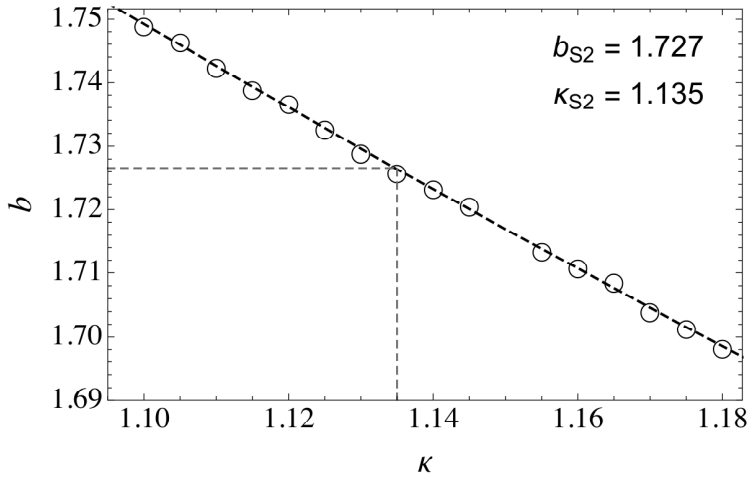

Figure 2.2: Dependence of the statistical segment length $b(\kappa)$ on spring constant κ for a sequence of models with $c = 1.5\sigma^{-3}$. The values obtained for κ for model D3 (or S2) by this procedure is shown above. This figure reproduced with permission from the Ph.D. thesis of Pavani Medapuram[50].

Pressure Calibration

The choice of a value for the pressure P in an NPT simulation is straightforward. The pressure is selected such that infinitely long homopolymers would have the targeted bead concentration c. NVT ensemble simulations are used to determine the functional dependence of pressure, P, on chain length, N, at the target concentration, $c = 1.5, 3.0$. The pressure in a homopolymer melt was found to vary with N

$$P(N) = P_\infty + \frac{\delta}{N} \quad . \tag{2.6}$$

The $1/N$ correction is presumably an end effect arising from the excess free volume associated with chain ends. The value P_∞ is the pressure used in NPT simulations with the specified target concentration.

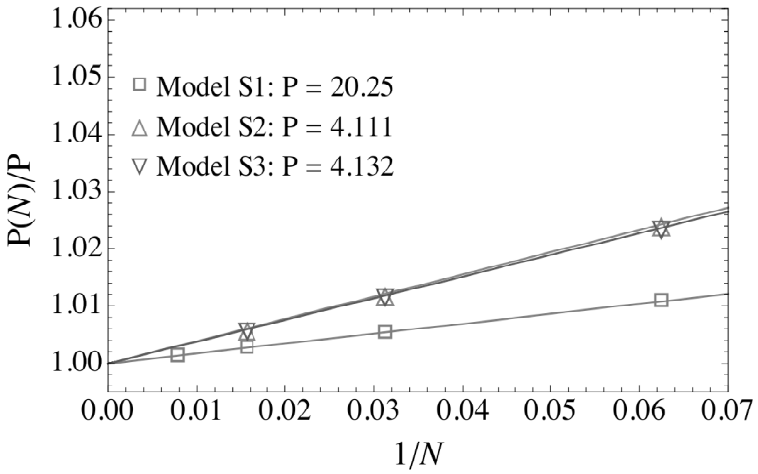

Figure 2.3: The normalized pressure, $P(N)/P_\infty$ vs. chain length, N, obtained from NVT simulations of homopolymers for three models that were referred to in earlier work as S1, S2 and S3. The solid line represents the fit to equation2.6. This figure reproduced with permission from the Ph.D. thesis of Pavani Medapuram[50].

2.3 Estimating $\chi(\alpha)$

In all of the simultions models used here, the parameter $\alpha = \epsilon_{AB} - \epsilon_{AA}$ is used as a control parameter that is varied in order to vary the effective interaction parameter χ. To interpret the simulation results in a manner that allows quantitative comparison of a variety of simulation models to theoretical predictions, experimental results, or results of different models, one needs to know how χ varies with changes in α.

Chung and Morse [51] showed that the relationship between χ and α can be defined to first order in a series in powers of α by a straightforward application of thermodynamic perturbation theory. They considered a binary blend of structurally similar A and B homopolymers and showed that the free energy mixing per monomer, denoted by f_{mix}, is given to first order in powers of α by a function of the form

$$f_{\text{mix}} \simeq \alpha z(N) \phi_A \phi_B \tag{2.7}$$

where $z(N)$ is an effective coordination number that can be easily extracted from simulations of melt of homopolymers of N beads. For the type of model considered here, $z(N)$ is given by the ratio

$$z(N) = u_{\text{inter}}/\epsilon \tag{2.8}$$

of the average intermolecular pair energy per monomer u_{inter} to the value of the energy parameter $\epsilon = \epsilon_{AA}$ used in the homopolymer limit $\alpha = 0$. This did not by itself, however, lead to an unambiguous approximation for the χ parameter at low values of α because the χ parameter should be independent of chain length, but the effective coordination number $z(N)$ depends slightly on chain length N: The shorter the chains, the more they are exposed to other chains and thus the larger $z(N)$. Morse and Chung developed an analytic theory for the dependence of $z(N)$ on N and showed that, for $N \gg 1$,

$$z(N) = z_\infty \left[1 + \frac{(6/\pi)^{3/2}}{\sqrt{\overline{N}}} + \frac{\delta}{\overline{N}}\right] \tag{2.9}$$

where z_∞ is the effective coordination number for infinitely long chains. Morse and Chung further argued that, in order to define χ in a manner that allows SCFT to be recovered in the limit of infinitely long chains, we must assume that χ is given to first order in α by a ratio

$$\chi \simeq z_\alpha \alpha / k_B T \quad , \tag{2.10}$$

in which the effective coordination number z_∞ is defined by using Eq. (2.9) to extrapolate results for $z(N)$ for finite chains to the limit of infinite N.

Attempts to compare results obtained using several simulation models for the structure factor $S(q)$ in the disordered phase using this linear approximation for χ were found to work well for very small values of α, but to fail for values of α obtained near the ODT of short chains. The nature of the errors suggested to Glaser and coworkers that these discrepancies might be the result of use of a linear approximation for $\chi(\alpha)$ outside its range of validity, and might therefore be corrected by allow for the possibility of a nonlinear functional form for $\chi(\alpha)$.

Glaser et al. [42] then proposed that the dependence of χ on α could be estimated outside of the range in which the relationship is linear by allowing for the possibility of a nonlinear functional dependence of $\chi(\alpha)$, and adjusting the parameters in this function so as to fit the behavior of the peak in $S(q)$ predictions of the renormalized one-loop theory. For this purpose, Glaser et al. assumed a functional dependence of the form

$$\chi(\alpha) = \frac{z_\infty \alpha + a\alpha^2}{1 + b\alpha} \tag{2.11}$$

for all of the models considered here, in which the parameter z_∞ is determined independently from analysis of simulations of homopolymer, while a and b are treated as fitting parameters. Their study showed that the ROL theory with a nonlinear dependence of $\chi(\alpha)$ could provide a consistent description of the behavior of the inverse peak intensity observed in simulations of systems of widely varying chain length, using a definition of the χ parameter with no explicit dependence on N. An example of this comparison of simulation results and ROL predictions is shown in Fig. 2.3.

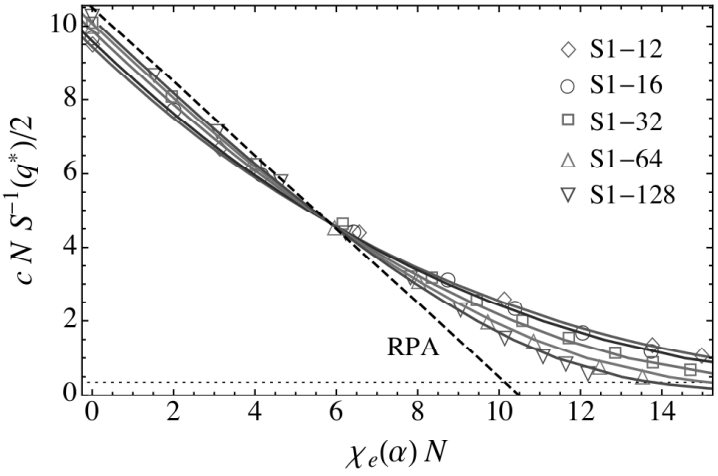

Figure 2.4: Comparison of simulations results for inverse peak scattering intensity $cNS^{-1}(q^*)$ for symmetric D1 model (open symbols) for chains of length $N = 16, 32, 64, 128$ to ROL predictions (solid lines). The dashed line represents the RPA prediction. The solid line on top corresponds to $N = 16$ and the one at the bottom is corresponding to $N = 128$. The non-linear $\chi(\alpha)$ form has been used to map α values to χ values when plotting simulation results. This figure reproduced with permission from the Ph.D. thesis of Pavani Medapuram[50].

Throughout the analysis of simulation results presented in Chapters 3-6, all reported values of χ_e are values that were estimated by using the methods and results of Glaser and coworkers to estimate the function $\chi(\alpha)$ for each model of interest.

Chapter 3

Correlations in Disordered Melts of Asymmetric Diblock Copolymers

This chapter is based on the publication
T. Ghasimakbari and D.C. Morse, "Correlations in Disordered Melts of Asymetric Diblock Copolymers", *Macromolecules* **51**, 2335-2348, 2018. [52]

Abstract: Simulations of several different coarse-grained models are used to characterize how the structure factor $S(q)$ in melts of compositionally asymmetric diblock copolymers varies with changes in the volume fraction f of the minority block, the parameter $\chi_e N$ (where χ_e is an effective interaction parameter and N is degree of polymerization), and the invariant degree of polymerization $\overline{N}$. We focus here on systems with $0.25 \leq f < 0.5$. Results obtained with several different models are consistent in the expected sense, demonstrating the validity of the corresponding states principle when applied to asymmetric copolymers. The analysis is simplified by a demonstration that the effective χ parameter for these simple models is almost independent of composition. Results are compared to renormalized one-loop theory predic-

tions, which become rapidly less accurate with increasing asymmetry. In the absence of an adequate predictive theory, a quantitative empirical relationship is developed to describe the dependence of peak intensity on $\chi_e N$, f and $\overline{N}$ over the range $0.25 < f < 0.5$. The dependence of the peak intensity on χN in asymmetric and symmetric copolymers are qualitatively similar, and exhibit a crossover from a weakly fluctuating regime in which the random-phase approximation (RPA) is nearly valid to a regime of strong composition fluctuations, with a crossover centered on the RPA spinodal value of χN. This crossover becomes noticeably sharper for more asymmetric systems, however, reflecting a more abrupt appearance of well segregated disordered domains with increasing χ in asymmetric copolymer melts.

3.1 Introduction

Disordered diblock copolymer melts exhibit composition fluctuations that become strong near an order-disorder transition. These fluctuations are quantified by the structure factor $S(q)$, which can be measured experimentally by small-angle X-ray and neutron scattering experiments [31, 32, 15]. The magnitude of the characteristic peak in $S(q)$ in the disordered phase depends upon the free energy cost of mixing in the melt, as characterized by a Flory-Huggins χ parameter. Measurements of $S(q)$ in the disordered phase are thus often analyzed in order to estimate how χ depends on the temperature in experimental systems, or on temperature or other control parameters in simulations. The development of more sophisticated methods of comparing between simulations, theory and experiment thus rely critically on the development of a reliable quantitative understanding of the behavior of $S(q)$ in the disordered phase.

Recent simulation studies of symmetric diblock copolymers [41, 43, 42, 44, 45, 53, 48, 54] have compared the results obtained with a variety of simple models to one other, to theoretical predictions, and to experimental results. One motivation for these comparisons is to assess the degree of universality of the behavior. Specif-

ically, these studies aimed to test the hypothesis that the thermodynamic behavior of a diblock copolymer melt exhibits a universal dependence on a small set of dimensionless state parameters, which consist of the dimensionless parameters that appear in self-consistent field theory and the invariant degree of polymerization $\overline{N}$ [43]. Because this hypothesis asserts that equivalent behavior should be obtained in corresponding thermodynamic states of different systems, we refer to this here as a corresponding states hypothesis. The results of these simulations of symmetric diblock copolymers strongly supported this hypothesis, and provided a comprehensive picture of how the properties of symmetric copolymer melts depend on $\overline{N}$ in the disordered phase and in the ordered phase near the order-disorder transition (ODT).

The present work uses simulations to study the disordered phase of asymmetric diblock copolymers, with A and B blocks of different length. For simplicity, we restrict ourselves in this study to simulation models in which the two blocks have structurally identical monomers of equal statistical segment length, which differ only in the number of monomers in each block. We present results here for the behavior of the structure factor in the disordered phase of several well-calibrated simulation models similar to those used in Refs. [42, 44]. The first goal of this study is testing whether the corresponding states hypothesis also applies to asymmetric copolymers. The results presented here, along with earlier similar results by Sethuraman, Nguyen and Ganesan [53], suggest that it does. The second and more important goal is to quantitatively characterize the behavior of $S(q)$ for asymmetric copolymers in a form that can be referred to by other workers, by quantifying how $S(q)$ depends on the volume fraction f of the minority block, on the product $\chi_e N$ of an effective interaction parameter and degree of polymerization N, and on the invariant degree of polymerization $\overline{N}$.

The rest of the chapter is organized as follows. Sec. 2 reviews some theoretical background and notation that is relevant to our analysis. Sec. 3 discusses details of our simulations and analysis. Sec. 4 presents tests of the universality of results from different models, in which we compare results from systems with matched values of $\overline{N}$. Sec. 5 presents a summary of results for how the structure factor $S(q)$ varies

with changes in parameters, and some comparison of results to predictions of the renormalized one-loop (ROL) theory. Sec. 6 presents a more detailed analysis of the parameter dependence of the peak intensity. Conclusions are summarized in Sec. 7.

3.2 Background

In the simulations presented here, we study several bead-spring models of a dense melt of AB diblock copolymers. Each chain contains N beads, with N_A beads of type A and a fraction $f = f_A = N_A/N$ of A beads. The average total monomer concentration for a sytem of M chains in volume V is denoted by $c = MN/V$. The function $c_i(\mathbf{r})$ instead denotes the instantaneous concentration of beads of type $i = A$, or B at a position $\mathbf{r}$, which has an average value $\langle c_i(\mathbf{r})\rangle = f_i c$, where $f_i = N_i/N$.

The main quantity of interest in this chapter is the structure factor

$$S(q) = \int d\mathbf{r}\langle\psi(r)\psi(0)\rangle e^{i\mathbf{q}\cdot\mathbf{r}} \quad , \tag{3.1}$$

in which $\psi(\mathbf{r}) = [\delta c_A(\mathbf{r}) - \delta c_B(\mathbf{r})]/2$, $\delta c_i(r) = c_i(\mathbf{r}) - f_i c$ is the local deviation of $c_i(\mathbf{r})$ from its average value, and $q = |\mathbf{q}|$. The structure function $S(q)$ for a diblock copolyer melt exhibits a maximum at a wavenumber that we denote by q^*.

Random-Phase Approximation:

The starting point for our analysis of $S(q)$ is the random-phase approximation (RPA). The RPA theory for $S(q)$ can be derived by using a self-consistent field approximation to compute the free energy cost of infinitesimal composition fluctuations [14]. The RPA for $S(q)$ in a diblock copolymer melt with equal A and B statistical segment lengths, denoted here by $S_0(q)$, is given by an equation of the form

$$cNS_0^{-1}(q) = F(qR_{g0}, f) - 2\chi_e N \quad , \tag{3.2}$$

where $F(qR_{g0}, f)$ is a known analytic function, $R_{g0} = \sqrt{Nb^2/6}$ is the ideal random walk radius of gyration for a chain with a statistical segment length b, and χ_e is an

effective RPA interaction function given by

$$\chi_e \equiv -\frac{1}{2ck_BT}\frac{\partial^2 f_{ex}(\phi_A)}{\partial \phi_A^2} \quad , \tag{3.3}$$

in which the derivative is evaluated at average composition $\phi_A = f$ of the disordered diblock copolymer melt. Here $f_{ex}(\phi_A)$ is the excess free energy per volume that is added to the combinatorical entropy of mixing in the generalized Flory-Huggins theory, or added to the free energy of an ideal gas reference system in the SCFT of inhomogeous systems, as discussed in chapter 1. Eq. (3.3) for χ_e yields a function χ_e that is independent of average composition f if and only if f_{ex} has the simple quadratic composition dependence, $f_{ex} \propto \phi_A\phi_B$, predicted by the original Flory-Huggins mean-field lattice theories. More generally, however, the interpretation of SCFT as a density functional theory allows for the possibility of an effective interaction parameter χ_e with an arbitrary dependence on composition and temperature.

Eq. (3.2) yields a prediction for $S(q)$ with a maximum at a wavenumber that we denote by q_0^*, for which the dimensionless product $q_0^* R_{g0}$ is given by a function

$$q_0^* R_{g0} = Q_0^*(f) \tag{3.4}$$

that is independent of $\chi_e N$ but that depends weakly on composition f. The RPA predicts that the peak in $S(q)$ should diverge at a spinodal value

$$(\chi N)_s \equiv F(q_0^* R_{g0}, f)/2 \quad , \tag{3.5}$$

where $(\chi N)_s$ denotes the spinodal value of $\chi_e N$.

Table 3.1 presents RPA predictions for $q_0^* R_{g0}$ and the spinodal value of $\chi_e N$ at compositions examined in our simulations.

f	$q_0^* R_{g0}$	$(\chi N)_s$
0.1875	2.134	27.037
0.2500	2.053	18.172
0.3125	2.001	14.012
0.3750	1.969	11.869
0.4350	1.951	10.815
0.5000	1.946	10.495

Table 3.1: RPA predictions for $q^* R_{g0}$ and $(\chi N)_s$.

Because SCFT and the RPA are based on a model of continuous Gaussian threads, with no chemical structure, they yield predictions that are invariant under an arbitrary redefinition of N, the number of "monomers" per chain. The quantity $S(q)/cN$ is the natural invariant form of the structure factor in any such theory. The RPA yields a prediction for this quantity that, for AB copolymers with equal statistical segment length, depends only on the nondimensionalized wavenumber qR_{g0} and the SCFT state variables f and $\chi_e N$.

Corresponding States:

The corresponding states hypothesis [43, 44, 45] posits that $S(q)/cN$ is well approximated for systems with A and B monomers of equal statistical segment lengths as a function

$$cNS^{-1}(q) = H(qR_{g0}, \chi_e N, f, \overline{N}) \tag{3.6}$$

of the non-dimensionalized wavenumber qR_{g0}, the SCFT state parameters f and $\chi_e N$ and the invariant degree of polymerization,

$$\overline{N} \equiv N(cb^3)^2 \quad . \tag{3.7}$$

In Eq. (3.6), $H(qR_{g0}, f, \chi_e N, \overline{N})$ is a universal function that is predicted to approach the RPA prediction in the limit $\overline{N} \to \infty$.

The analysis presented here focuses on the behavior of the peak scattering intensity $S(q^*)$ and peak wavenumber q^*. The corresponding states hypothesis predicts that the non-dimensionalized peak wavenumber $q^* R_{g0}$ and the invariant peak scat-

tering intensity should be universal (i.e., model-independent) functions of the state parameters $\chi_e N$, f, and $\overline{N}$, given by a pair of functions

$$q^* R_{g0} = Q^*(\chi_e N, f, \overline{N}) \tag{3.8}$$

$$cNS^{-1}(q^*) = H^*(\chi_e N, f, \overline{N}) \quad . \tag{3.9}$$

This implies that the ratio q^*/q_0^* of the true peak position to the RPA prediction q_0^* should also be a universal function of the state variables $\chi_e N$, f and $\overline{N}$, which is given by the ratio $q^*/q_0^* = Q^*(\chi_e N, f, \overline{N})/Q_0^*(f)$.

As an alternate way of characterizing the invariant peak intensity $cNS^{-1}(q^*)$, we also define an "apparent" interaction parameter $\chi_a^* N$. The quantity $\chi_a^* N$ is defined to be the value of $\chi_e N$ that would be obtained by fitting the observed peak intensity to the RPA prediction, using the equation

$$cNS^{-1}(q^*) = 2[(\chi N)_s - \chi_a^* N] \quad , \tag{3.10}$$

in which $(\chi N)_s$ is the spinodal value predicted by the RPA.

Renormalized One-Loop Theory:

The renormalized one-loop (ROL) [37, 55, 40] theory provides an explicit prediction for $S(q)$ that has been shown accurately describe the behavior found in simple bead-spring models of symmetric diblock copolymers[41, 42].

The ROL theory is believed to predict the dominant universal corrections to the RPA prediction within a power series in $\overline{N}^{-1/2}$. Because it is based on a power series expansion of deviations from the RPA, the ROL theory is expected to provide quantitatively accurate predictions in regions of parameters space in which corrections to the RPA remain sufficiently small, corresponding to long chains far from the ODT. The use of a rigorous expansion in powers of $\overline{N}^{-1/2}$ is not, however, sufficient to guarantee accuracy near the ODT, because the theory predicts large corrections to the RPA near the ODT for any finite value of $\overline{N}$, causing a breakdown in the underlying Taylor expansion. To allow predictions to be made near the ODT, the form of the ROL theory that was used to analyze simulations of symmetric di-

block copolymer combined the perturbative one-loop theory with a self-consistent treatment of strong fluctuations analogous that introduced by Brazovskii [35] and later adopted by Fredrickson and Helfand [22]. When applied to symmetric diblock copolymers, this self-consistent approximation is believed to capture the dominant corrections to the RPA near the ODT. The theoretical arguments are given to justify the validity of this approximation for very long symmetric copolymers near the ODT [22] do not, however, apply to asymmetric copolymers, because they ignore a set of strongly divergent terms in the expansion of $S^{-1}(q)$ that vanish in the special case of symmetric copolymers, but that become rapidly more important for $f \neq 0.5$. It has been shown that when applied to asymmetric copolymers the self-consistent ROL theory yields predictions for the peak intensity that becomes pathological near the ODT [55, 40], as discussed in greater detail in Sec. 4.

One important difference between the present study and previous work on symmetric diblock copolymers is thus the absence of an adequate analytic theory for the peak intensity in the case of asymmetric copolymers. The method used in Refs. [42, 44, 45] to estimate how χ_e depends on a simulation parameters relied in part on a fit of simulation results for the peak intensity to ROL predictions. Because the ROL theory is known to fail for asymmetric copolymers, we cannot simply repeat this analysis with asymmetric copolymers of varying composition to estimate χ_e as a function of composition. Instead, in the analysis presented here, we are forced to start from the hypothesis that χ_e for these simple simulation models is approximately independent of composition, and then test if this simplifying assumption is consistent with our simulation data.

3.3 Simulation Methodology

The simulations presented here are molecular dynamics (MD) simulations of simple bead-spring models similar to those introduced in dissipative particle dynamics simulations by Groot and Madden[56, 57]. All simulations use a pair potential $V_{ij}(r)$

between monomers of types i and j of the form

$$V_{ij}(r) = \epsilon_{ij}\left(1 - \frac{r}{\sigma}\right)^2 \tag{3.11}$$

with a cut off at $r_c = \sigma$, with $\epsilon_{AA} = \epsilon_{BB}$ and varying values of a parameter

$$\alpha \equiv \epsilon_{AB} - \epsilon_{AA} \tag{3.12}$$

that we vary to control the free energy cost of contact between A and B monomers. A harmonic bond potential of the form

$$V_{\rm bond}(r) = \frac{1}{2}\kappa r^2 \tag{3.13}$$

also acts between consecutive beads within each chain. The non-bonded pair interaction acts between all monomers, including bonded monomers. All simulations are isothermal, isobaric MD simulations.

We have studied four models of this type, denoted here D1, D2, D3, and D4. Models D1, D3, and D4 are identical to models studied in Refs. [42, 44, 45], where they were referred to as models S1, S2 and S3, respectively. Model D2 has not been studied previously. Parameters of all 4 models were chosen so as to give values of $\overline{N}/N = (cb^3)^2$ with ratios of $1 : 2 : 4 : 8$ for models D1, D2, D3, D4. Model D2 was added to those studied previously in order to complete this sequence of values, and was calibrated using methods identical to those applied previously to models D1, D3, and D4 in order to determine values of b and other parameters. As in Refs. [44, 45], which also used NPT simulations, each "model" is defined by a fixed set of choices for the values of the pressure P, and the parameters ϵ_{AA}, and κ in a system of units with $k_BT = \sigma = 1$. Table 3.2 summarizes input parameters and a few structural properties for these models.

Model	ϵ_{AA}	κ	P	c	b	$\overline{N}(32)$	z_∞	A	B
D1	25.0	3.406	20.249	3.0	1.088	480	0.237	0.138	0.438
D2	25.0	1.135	4.111	1.5	1.222	960	0.269	0.072	0.207
D3	25.0	0.867	4.132	1.5	1.727	1920	0.0916	-0.00087	0.00420
D4	25.0	2.428	20.412	3.0	1.938	3840	0.0977	-0.00144	0.00086

Table 3.2: Simulation parameters for the bead-spring models in units in which $k_BT = 1$ and $\sigma = 1$. Models D1, D3, and D4 have been studied in prevous work [42, 44, 45], in which they were referred to as models S1, S2 and S3, respectively. The parameters ϵ_{AA}, κ and P are simulation input parameters. The values of c and b denote extrapolated monomer concentration and statistical segment length, respectively, for infinite homopolymers at the specified pressure. The quantity $\overline{N}(32)$ is the value of $\overline{N}$ for chains of $N = 32$ beads. The quantities z_∞, A and B are parameters in Eq. (3.15) for $\chi_e(\alpha)$.

Each system simulated here is defined by a choice of model (D1, D2, D3, or D4), chain length N and fraction f of A monomers. Simulations for each system are performed over a range of values of a control parameter $\alpha = \epsilon_{AB} - \epsilon_{AA}$. In what follows in which we indicate a choice of model and chain length using a notation in which, for example, D1-32 denotes a simulation of model D1 with chains of $N = 64$ beads.

Figure 3.1 shows an example of how $S(q)$ varies with varying α for simulations of model D1-64 for $f = 0.25$. Estimated values of the peak intensity $S(q^*)$ and the peak wavenumber q^* are extracted for each system by fitting the wavenumber dependence of $S(q)$ to a smooth function similar to that used in earlier work on symmetric diblock copolymers. For this purpose, we fit simulation results for $S^{-1}(q)$ to a function of the form

$$S^{-1}(q) = S_0^{-1}(q, \chi = 0) + a + bq^2 + cq^4 \tag{3.14}$$

in which $S_0(q, \chi = 0)$ is the RPA prediction for a system with $\chi = 0$ and the appropriate values of c, N, f, and R_{g0}, and in which a, b and c are parameters that are adjusted to minimize the error of the fit. This functional form generally yields

a very good fit, which is used here only for the purpose of estimating $S(q^*)$ and q^*.

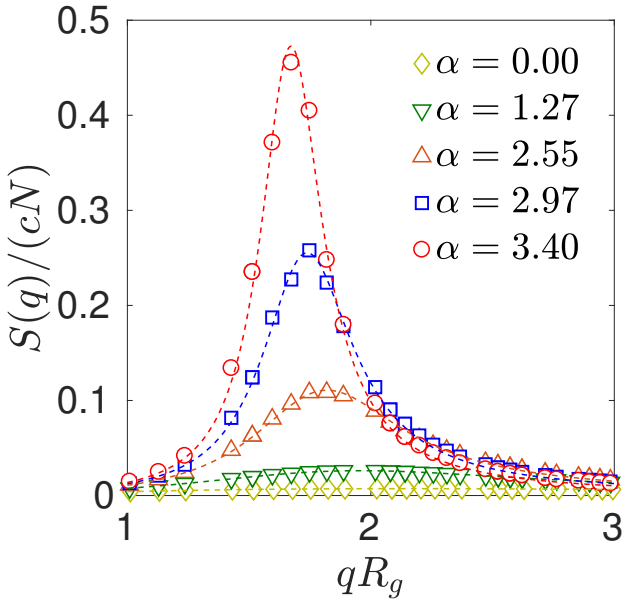

Figure 3.1: Structure factor $S(q)$ as a function of dimensionless wavenumber qR_{g0} from simulations of model D1 for $N = 32$ ($\overline{N} = 480$) and $f = 1/4$, for a range of values $\alpha = \epsilon_{AB} - \epsilon_{AA} = 0.0, ..., 3.4$(from bottom to top). The order-disorder transition for this system occurs at $\alpha = 3.52$. Dashed lines are fits to Eq. (3.14).

In each of the models studied here, the effective interaction parameter χ_e is a model-dependent function of our control parameter α. Estimates of the dependence of χ_e on α in symmetric diblock copolymers been developed previously for models D1, D3 and D4 by combining results from thermodynamic perturbation theory [41, 51] with a fit of results for the peak intensity in symmetric diblock copolymers to predictions of the ROL theory [42, 44, 45]. We have applied the same calibration procedure to symmetric copolymers of model D2. For each model studied here, $\chi_e(\alpha)$ has been fit to a function of the form

$$\chi_e(\alpha) = \frac{z_\infty \alpha + A\alpha^2}{1 + B\alpha} \quad , \tag{3.15}$$

in which z_∞ is an effective coordination number was obtained independently from simulations of a reference homopolymer ($\alpha = 0$) melt [51], and A and B are pa-

rameters that were obtained by fitting results for the dependence of $S(q^*)$ on α to ROL predictions. Values for the coefficients z_∞, A and B are given for each model in table Table 3.2.

The corresponding states hypothesis for $S(q)$ is based on a model of polymer chains as continuous random walks. It is thus expected to fail if applied to sufficiently short chains, for which the non-universal effects of discrete chain structure become important. The effect of discrete chain structure upon $S(q)$ has been analyzed previously by Medapuram et al. [42] for several models of symmetric diblock copolymers with potential energies similar to those used here. For simplicity, that analysis focused on systems with $\chi_e = 0$, for which the behavior of $S(q)$ is completely determined by the nature of intramolecular correlations. Plots of $S(q)$ vs. qR_{g0} obtained with simulations with matched values of $\overline{N}$ but different numbers of beads per chain, shown in Fig. 6 of that article, were found to differ somewhat at high values of q but to agree at $q \simeq q^*$ for symmetric copolymers with soft interactions similar to those used here, for chains with as few as $N = 16$ beads, or 8 beads per block. The analysis presented here focuses on the behavior of peak wavenumber q^* and peak intensity $S(q^*)$ for models in which the minority block always contains 8 or more beads, for which this prior experience suggested that a continuous chain model should be adequate. The adequacy of a continuous Gaussian chain model is verified in the next section by directly comparing results obtained using models of asymmetric copolymers with different numbers of beads per chain.

3.4 Testing Universality

To test the consistency of the results obtained from corresponding states of different simulations, we have compared results for $S(q)$ from simulations of pairs of systems with matched values of $\overline{N}$ and f but different values of N and monomer concentration c. For this purpose, we have compared simulations of model D2-32 and model D1-64, which have values of $N = 32$ and $N = 64$, respectively, but both have $\overline{N} \simeq 960$. This comparison was carried out for two such matched pairs systems,

with $f = 1/4$ and $f = 3/8$.

Peak Wavenumber

As a first test of the corresponding states hypothesis, we have compared plots of simulation results for q^*/q_0^* plotted vs. $\chi_a^* N$ from simulations of models with matched values of $\overline{N}$ and f, as done previously for symmetric copolymers [43]. As first emphasized in Ref. [43], this way plotting the data allows us to characterize the shift in q^* a manner that does not rely on any estimate of the parameter dependence of χ_e, because of the use of the measured quantity $\chi_a^* N$ as the absicca, rather than an estimated value of $\chi_e N$.

Figure 3.2 shows the resulting comparison of results for q^*/q_0^* for pairs of systems with matched values of $\overline{N} \sim 960$ and matched values of $f = 1/4$ and $f = 3/8$. Results for each system are shown over a range of values of α from $\alpha = 0$ up to near the value at the ODT. The results show near perfect collapse of results from simulations with matched values of $\overline{N}$ and f, as predicted by the corresponding states hypothesis.

Because Figure 3.2 compares results obtained using models different numbers of beads per chain ($N = 32$ vs. $N = 64$), this comparison is a very direct test of the adequacy of a continuous chain model. We expect the continuous random walk model to become exact in the limit of finely discretized chains, and for the effects of discrete chain structure (if any) to show up as differences between results obtained using models with different numbers of beads. The fact that these pairs of models agree indicates that behavior of q^* is already adequately described by a continuous chain model for the simulation models with 32 beads per chain.

The value of q_0^* that is used to compute the ratio q_0^*/q_0^* shown in Fig. 3.2 is calculated for each model using the statistical segment $b = b_A = b_B$ that we measured in the limit $\alpha = 0$ and $N \to \infty$ of infinite homopolymers. The statistical segment lengths b_A and b_B could, in general, depend somewhat upon both macroscopic parameters (e.g., upon α in our simulation or temperature in an experiment) and the local composition (i.e., the fraction of A and B monomers in the local environment

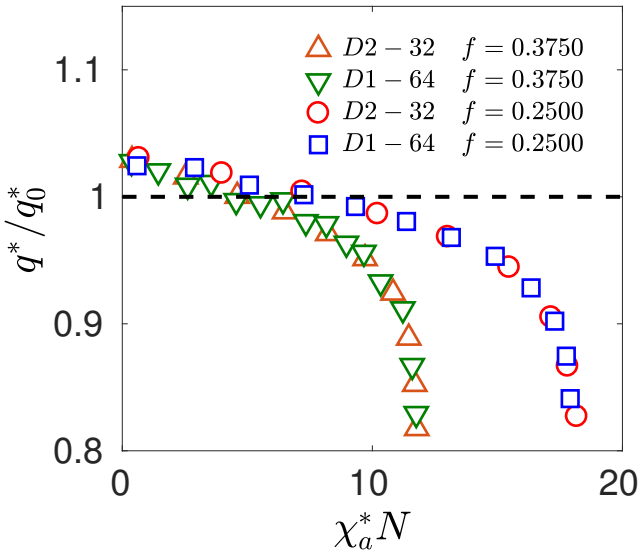

Figure 3.2: Normalized peak scattering wavenumber q^*/q_0^* vs. $\chi_a^* N$ for model D2, $N = 32(\overline{N} = 960)$, and model D1, $N = 64(\overline{N} = 960)$, of asymmetric diblock copolymers at compositions, $\frac{N_A}{N} = 0.3750, 0.2500$. q_0^* represents the RPA prediction for the peak scattering wavenumber. The RPA prediction is shown by a horizontal dashed line.

of a chain segment). Our use of a fixed value for statistical segment length to describe simulations carried out over a range of values of α and f instead implicitly assumes that b_A and b_B are approximately independent of both α and composition. Because of the structural symmetry of A and B monomers in the model studied here, b_A and b_B must be equal to one another and independent of composition in the limit $\alpha = 0$ (where A and B monomers become indistinguishable), but could in principle depend on both α and composition for $\alpha \neq 0$. Previous work on symmetric diblock copolymers [43, 42] has already shown, however, that consistent results for q^*/q_0^* could be obtained from a variety of models similar to those used here while approximating both statistical segments by a constant in the required analysis. The simulation results for both symmetric and asymmetric copolymers thus indicating that, for the simple models studied here, any dependence of the statistical segment lengths on α and composition is small enough to be neglected.

Peak Intensity

Figure 3.3 shows a comparison of results for invariant inverse peak intensity $cNS^{-1}(q^*)$ vs. $\chi_e N$ for the same two models and compositions. The value of the absicca $\chi_e N$ for each data point was calculated here by using the nonlinear relationship for $\chi_e(\alpha)$ that was obtained for each model by analyzing simulations of symmetric diblock copolymers. Because values of the absicca were calculated using an estimate of $\chi_e(\alpha)$ that was obtained by analyzing data from symmetric copolymers, but is applied here to data from asymmetric copolymers, we expect to obtain a collapse of results from systems with matched values of $\overline{N}$ if and only if the effective interaction parameter χ_e for these models is approximately independent of composition.

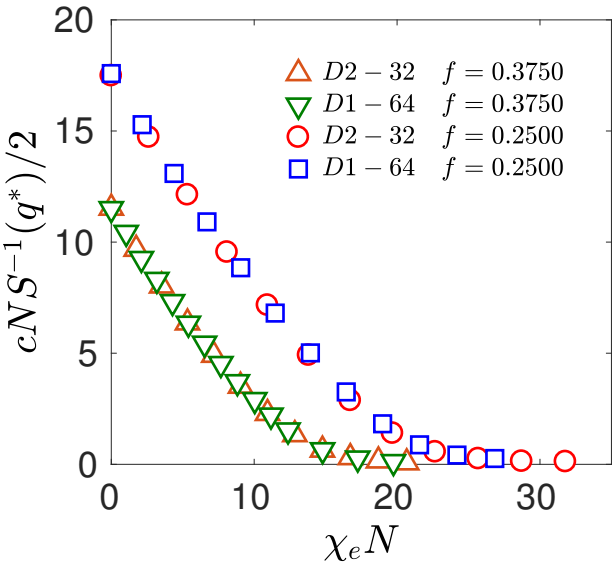

Figure 3.3: Collapse of the invariant inverse structure factor cNS^{-1} vs. $\chi_e N$ for model D2, $N = 32(\overline{N} = 960)$, and model D1, $N = 64(\overline{N} = 960)$, of asymmetric diblock copolymers at compositions, $f = N_A/N = 0.3750, 0.2500$.

The results shown in Figure 3.3 exhibit near perfect collapse of results for $cNS^{-1}(q^*)$ vs. $\chi_e N$ from simulations of corresponding states of different models (i.e., from simulations of systems with matched values of $\overline{N}$ and f). Similar results were obtained previously by Sethuraman, Nguyen and Ganesan [53] in a comparison of model S1-16 and model H-64 of Refs. [42, 44], in which these authors also

used an estimate of $\chi_e(\alpha)$ that had been obtained earlier by analyzing simulations of symmetric copolymers. As discussed above, the success of this collapse indicates both that these models of asymmetric copolymer melts obey the principle of corresponding states even for surprisingly rather short chains, and that χ_e for these models is almost independent of composition.

The statement of the corresponding states hypothesis given in Eq. (3.6) assumes that the effects of excess free energy upon $S(q)$ can be parameterized by a single interaction parameter, which we call χ_e. The meaning of χ_e is clearest in the random-phase approximation (RPA), which is valid sufficiently far from the ODT. In the RPA, χ_e is a function of the average composition f that is given explicitly by Eq. (3.3). The RPA definition of χ_e yields a value that is independent of f, however, if and only if the underlying excess free energy $f_{ex}(\phi_A)$ is a simple quadratic function of ϕ_A, of the form $f_{ex}(\phi_A, \alpha) = ck_BT\chi_e(\alpha)\phi_A\phi_B$. For structurally symmetric models of the type studied here, it has been shown that the RPA interaction parameter $\chi_{ex}(\phi_A, \alpha)$ must be independent of ϕ_A to first order in a Taylor expansion in powers of α, or that $f_{ex}(\phi_A, \alpha)$ is a quadratic function of ϕ_A to the same order in α. Because models with fewer beads have larger values of α at a given value of $\chi_e N$, we would expect any composition dependence of $\chi_e(\phi_A, \alpha)$ in structurally symmetric models to be different for models with different numbers of beads, and to be stronger for models with smaller values of N. If the RPA definition of χ_e depended significantly on f for any of the models studied here, we would thus expect to see discrepancies between matched pairs of models with different values of N even in the weakly-segregated regime $\chi_e N < (\chi N)_s$ in which the RPA is approximately valid. The apparent consistency between results of different models obtained here thus indicates that the RPA interaction parameter is approximately independent of f for the models considered here, and thus that $f_{ex}(\phi_A, \alpha)$ is a nearly quadratic function of ϕ_A.

3.5 Parameter Dependence of $S(q)$

This section presents results for how the peak wavenumber q^* and the peak intensity $S(q^*)$ depend on $\chi_e N$, $\overline{N}$ and f in the disordered phase of asymmetric diblock copolymer melts.

Peak Wavenumber

We first consider the behavior of the peak wavenumber q^*. The RPA predicts a value of the product $q^* R_{g0} = \hat{Q}_0(f)$ that is independent of $\chi_e N$ but that depends somewhat on f. Here $R_{g0} = \sqrt{N/6}b$, where b is the statisical segment length that we estimate by measuring R_g for homopolymers of varying N and estimating the limit $b = \lim_{N\to\infty} R_g\sqrt{6/N}$. The ROL theory and the principle of corresponding states predict that $q^* R_{g0}$ should exhibit a nontrivial dependence $\chi_e N$ and $\overline{N}$, but should approach the value predicted by the RPA in the limit $\overline{N} \to \infty$.

Figure 3.4 and Figure 3.5 show the behavior of the normalized peak intensity q^*/q_0^* vs. $\chi_a^* N$ for $f = 0.375$ and $f = 0.25$, respectively, for models with varying values of $\overline{N}$. Here, q_0^* denotes the RPA prediction for q^*. Results at both compositions show a peak wavenumber that decreases with increasing $\chi_a^* N$ (i.e., with increasing scattering intensity), with a particularly rapid decrease near the ODT. Results for both compositions also show a clear tendency for the value of q^*/q_0^* obtained at any fixed value of $\chi_a^* N$ to approach unity with increasing $\overline{N}$, as predicted by the one-loop theory.

Figure 3.6 shows a comparison of simulation results for q^*/q_0^* vs. $\chi_a^* N$ from model S1-32 to predictions of the ROL theory, for asymmetric polymers with $0.1875 \leq f \leq 0.5$. ROL predictions for this quantity are qualitatively correct and nearly quantitative for symmetric and nearly symmetric copolymers, and for conditions far from the ODT. The quantitative accuracy of predictions of behavior near the ODT deteriorates somewhat with increasing asymmetry, with a pronounced tendency for the ROL theory to predict too large a decrease in q_0^* near the ODT for highly asymmetric copolymers. These quantitative errors in predictions for the relationship

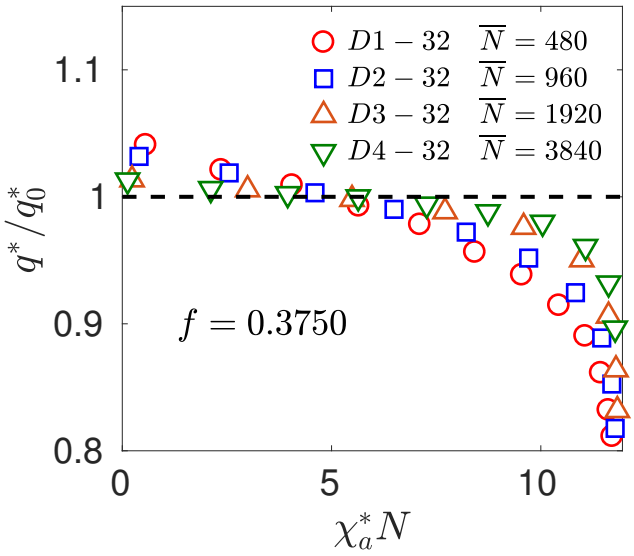

Figure 3.4: Normalized peak scattering location q^*/q_0^* vs. $\chi_a^* N$ for asymmetric diblock copolymers with compositions $f = 0.375$ for four models of chains with $N = 32$ beads but varying values of $\overline{N}$. The RPA prediction $q^*/q_0^* = 1$ is shown by a horizontal dashed line.

between peak position q^* and peak scattering intensity (as quantified by $\chi_a^* N$) are, however, much less problematic than the qualitative errors found in ROL predictions for the parameter dependence of peak intensity itself.

Inverse Peak Intensity

We now consider how the normalized inverse peak intensity $cNS^{-1}(q^*)$ depends on $\chi_e N$, f, and $\overline{N}$. Figure 3.7 and Figure 3.8 show results for the $cNS^{-1}(q^*)/2$ as a function of $\chi_e N$ for systems with $f = 0.375$ and $f = 0.25$, respectively. In each plot, results are shown for systems with a common value of f, for chains of $N = 32$ beads, but varying values of $\overline{N}$, corresponding to all four of the models studied here. Values of the absicca $\chi_e N$ for each simulation were computed using the calibration of $\chi_e(\alpha)$ that was obtained for each model by fitting similar results for symmetric copolymers to the ROL theory. The dot-dashed straight line in each of these figures

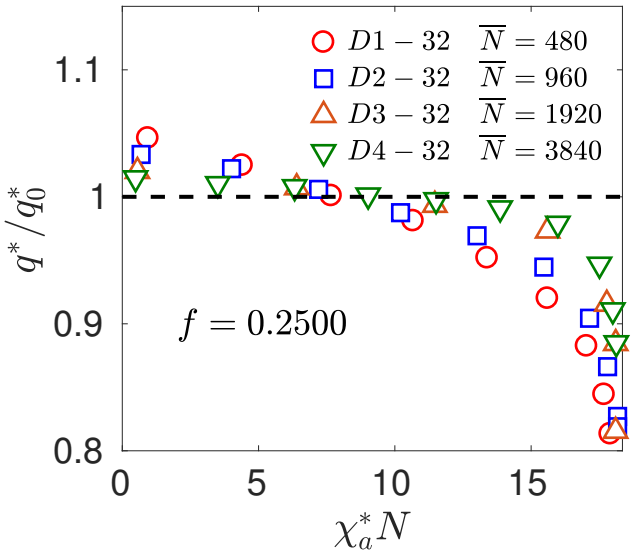

Figure 3.5: Normalized peak scattering location q^*/q_0^* vs. $\chi_a^* N$ for asymmetric diblock copolymers with coposition $f = 0.25$ for four models with varying values of $\overline{N}$.

it is the RPA prediction

$$cNS_0^{-1}(q_0^*)/2 = (\chi N)_s - \chi_e N \quad , \tag{3.16}$$

in which $(\chi N)_s$ is the RPA prediction for the spinodal value at the relevant value of f. The results for both compositions show a qualititative behavior very similar to that observed for symmetric diblock copolymers:Simulation results differ only slightly from RPA prediction for $\chi_e N < (\chi N)_s$ and exhibit a broad crossover centered at $\chi_e N \sim (\chi_e N)_s$ to a much more slowly decreasing function for $\chi_e N > (\chi N)_s$. Results at both compositions also show a clear tendency for the results obtained from different models at the same value of f to systematically approach the RPA prediction with increasing $\overline{N}$, in agreement with theoretical predictions.

We now turn to a comparison of simulation results for the peak intensity to ROL predictions. This comparison is shown in Figure 3.9, which shows a comparison of ROL predictions for the inverse peak intensity vs. $\chi_e N$ to simulation result from

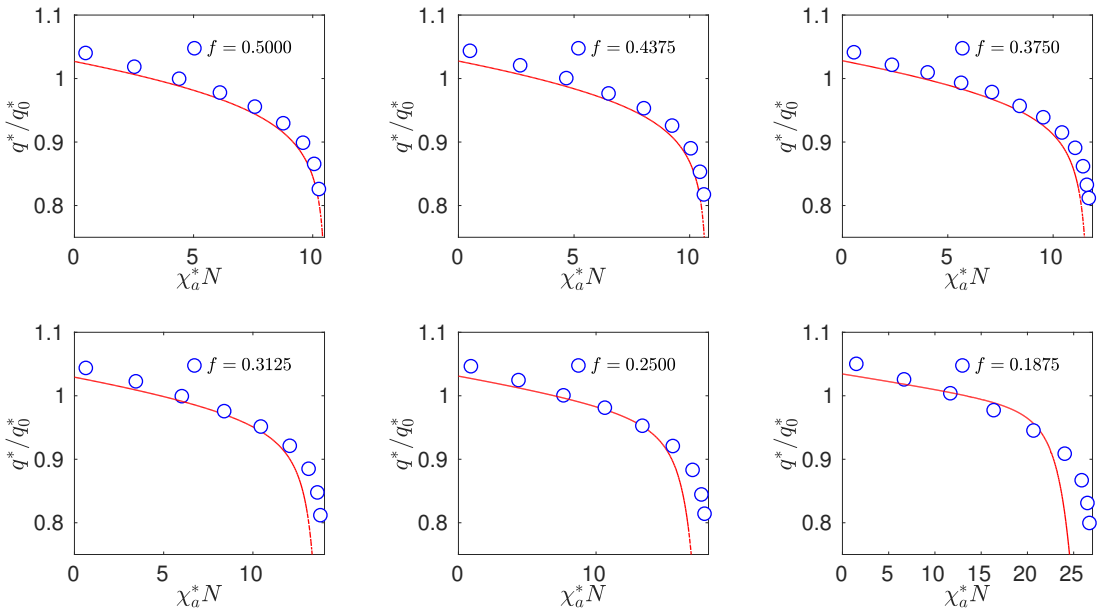

Figure 3.6: Comparison of simulation results (symbols) and ROL predictions (solid curves) for normalized peak scattering location q^*/q_0^* vs. $\chi_a N$ for diblock copolymers of length $N = 32(\overline{N} = 480)$ with varying values of f. Values of f are indicated in each plot. The upper-limit of the range of $\chi_a^* N$ shown in each plot (i.e., the right-hand edge of the plot) is chosen to be equal to the RPA spinodal value, $\chi_a^* N = (\chi N)_s$, and thus corresponds to a point at which the scattering intensity diverges.

model S1-32 ($\overline{N} = 480$) for asymmetric polymers with $f = 0.375$ (12/32), 0.4166 (14/32), and 0.5 (16/32). These ROL predictions are expected to fail because the self-consistent form of ROL theory used in this and previous work is known to yield pathological predictions for $S(q^*)$ in the case of asymmetric diblock copolymers. The nature of the problem is clearly visible in the the results shown in Figure 3.9(a) for $f = 0.375$: The ROL prediction for $cNS^{-1}(q^*)$ vs. $\chi_e N$ can be seen to "double over", forming a saddle-node bifurcation. We denote the value of $\chi_e N$ at this birfucation by $(\chi_e N)_b$. This yields a prediction for $cNS^{-1}(q^*)$ as a function of $\chi_e N$ that is double valued for $\chi_e N < (\chi_e N)_b$ and undefined for $\chi_e N > (\chi_e N)_b$. Only the upper branch of the ROL predictions qualitatively resembles the simulation results, while the lower branch is an artifact that should be ignored. This bifurcation in the ROL prediction is known to exist in diblock copolymer melts with $b_A = b_B$ for all

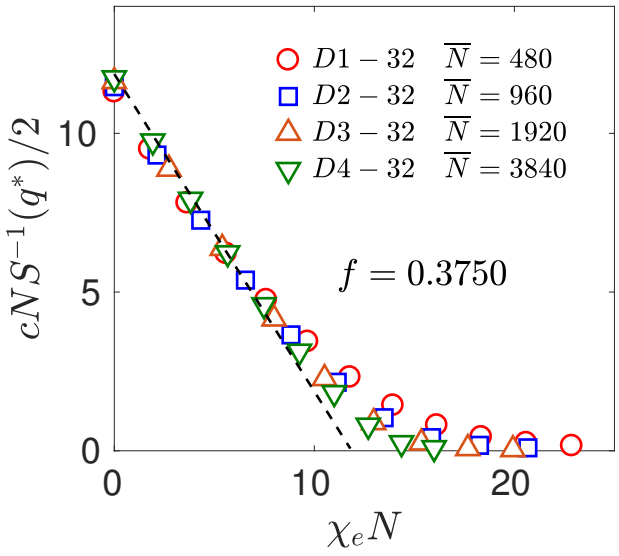

Figure 3.7: Normalized inverse peak structure factor $cNS^{-1}(q^*)/2$ vs. $\chi_e N$ for asymmetric diblock copolymers with $f = 0.375$ for models with different values of $\overline{N} = 480, ..., 3840$. The RPA prediction is shown by a straight dotted line in this and the following figure.

$f \neq 1/2$. The magnitude of the birfucation value $(\chi_e N)_b$ does, however, tend to increase as $f \to 1/2$ for any fixed value of $\overline{N}$. Its divergence at $f = 1/2$ removes the bifurcation and allows the theory to be used for symmetric copolymers. For nearly symmetric copolymers, with values of f sufficiently close to $1/2$, the value $(\chi_e N)_b$ may also exceed the value $(\chi_e N)_{ODT}$ at the first-order ODT, since $(\chi_e N)_{ODT}$ remains finite as $f \to 1/2$ while $(\chi_e N)_b$ diverges. This still the case for $f = 14/32$, for which we show only the upper branch of the ROL prediction. Unfortunately, the value of $(\chi_e N)_b$ drops rapidly with increasing deviation of f from $1/2$, becoming less than the RPA spinodal value $(\chi_e N)_{ODT}$ and then the SCFT prediction for the $(\chi_e N)_{ODT}$, both of which are always below the true ODT. The ROL theory thus yields meaningful predictions near the ODT only for nearly symmetric copolymers. Generally, however, the upper branch of the ROL predictions agree rather well with simulation results at sufficiently low values of $\chi_e N$, well below $(\chi_e N)_b$. Predictions of the ROL theory appear accurately describe the slight deviations from the RPA near

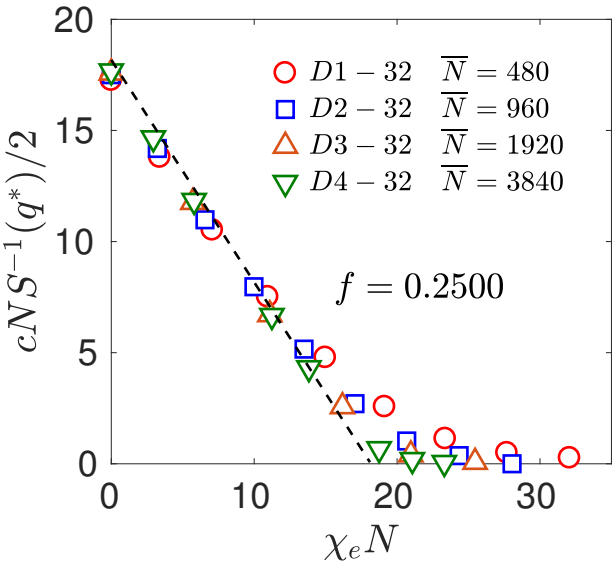

Figure 3.8: Normalized inverse peak structure factor $cNS^{-1}(q^*)/2$ vs. $\chi_e N$ for asymmetric diblock copolymers with $f = 0.25$ for several models with differing values of $\overline{N} = 480, ..., 3840$.

$\chi_e N = 0$ even for highly asymmetric copolymers, and generally remain reasonably accurate with increasing $\chi_e N$ until $\chi_e N$ approaches $(\chi_e N)_b$.

3.6 Analysis of Peak Intensity

The failure of the ROL theory to describe the peak intensity $S(q^*)$ for asymmetric copolymers leaves us without any adequate quantitative theory for the behavior of $S(q)$ in asymmetric polymers near the ODT. In the absence of an adequate theory, we focus in this section on analysis of the parameter dependence of the peak intensity at a more empirical level.

Scaling by Spinodal Values

The behavior seen when one plots $cNS^{-1}(q^*)$ vs. $\chi_e N$ for asymmetric polymers is qualitatively very similar to that obtained for symmetric polymers, despite the dif-

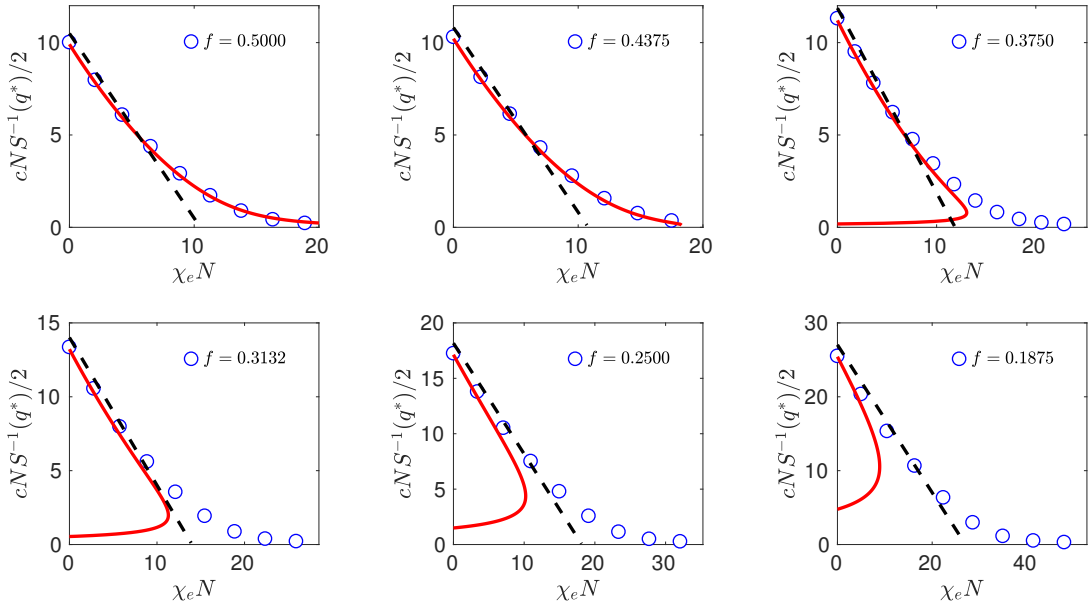

Figure 3.9: Comparison of simulation results (solid circles) and theoretical predictions for normalized inverse structure factor $cNS^{-1}(q^*)/2$ vs. $\chi_e N$ for model $D1$, $N = 32$ ($\overline{N}$=480). The solid red curves are ROL predictions, while straight dashed lines are RPA predictions.

ferences in the nature of ROL theoretical predictions. The most obvious differences between simulation results for symmetric and asymmetric copolymers arise from the composition dependence of the RPA spinodal value, which controls both the value of $\chi_e N$ at the "knee" in the plot of $cNS^{-1}(q^*)$ vs. $\chi_e N$ and the maximum value of $cNS^{-1}(q^*)$ at $\chi_e N = 0$. The RPA prediction for the inverse peak intensity, given by Eq. (3.16), predicts a value of $cNS^{-1}(q^*)/2$ that is equal to $(\chi N)_s$ at $\chi_e = 0$ and approaches zero as $\chi_e N$ approaches $(\chi N)_s$ from below, where $(\chi N)_s$ is a function of f. In order to take into account the relatively simple dependence on f predicted by the RPA, and thus focus our attention on the nature of deviations from the RPA, it is useful to plot a reduced inverse peak intensity

$$y \equiv cNS^{-1}(q^*)/[2(\chi N)_s] \quad , \tag{3.17}$$

in which $cNS^{-1}(q^*)$ is normalized by its RPA value at $\chi_e N = 0$, and to define a normalized interaction parameter

$$x \equiv \chi_e N/(\chi N)_s \quad . \tag{3.18}$$

The RPA prediction for the peak intensity, when expressed in these variables, is simply that $y = 1 - x$.

Plots of y vs. x are shown in Figure 3.10 for systems with $\overline{N} = 480$ (model S1-32, leftmost), $\overline{N} = 1920$ (model (D3-32, middle panel), and $\overline{N} = 3840$ (D4-32, right panel). In each of these plots, results are compared for simulations of the same model and overall chain length but different values of $f = N_A/N$. Plotting the data in this manner is found to almost collapse results from chains with different compositions, though some noticeable differences remain. Results for systems with the lowest value of $\overline{N} = 480$ almost collapse when plotted in this reduced form, over the range $f = 0.25 - 0.5$ shown here. Results for the two larger values of $\overline{N} = 1920$ and $\overline{N} = 3840$, however, show a tendency for the crossover or "knee" in this plot to become signficantly sharper for melts of more asymmetric polymers.

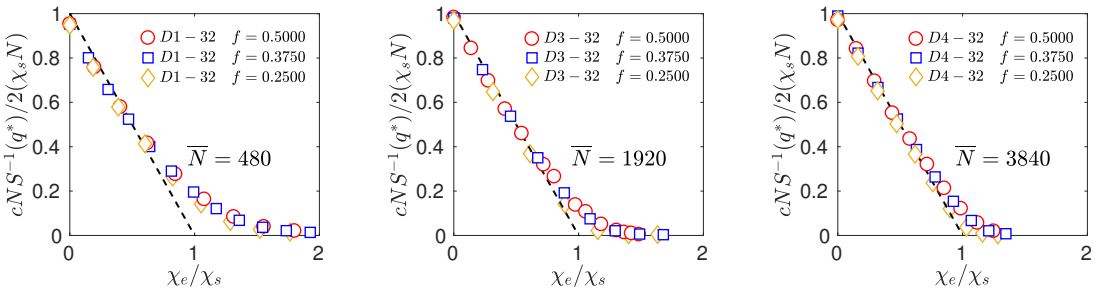

Figure 3.10: Comparison of normalized inverse peak structure factor $y = cNS^{-1}/2\chi_s N$ vs. the normalized interaction parameter $x = (\chi_e N)/(\chi_s N)$ for diblock copolymers. Each plots shows results for systems with a common value of $\overline{N}$ but differing values of f. Diagonal dashed lines show the RPA prediction $y = 1 - x$.

In order to emphasize the tendency for the crossover in behavior near χ_s to become sharper with increasing asymmetry for large $\overline{N}$, Figure 3.11 shows an expanded view of a comparison of results for systems with $f = 0.5$ and $f = 0.25$ and

a common value of $\overline{N} = 3840$ in a smaller region near the crossover at $\chi_e \simeq \chi_s$. The diagonal dashed line is again the RPA prediction. The two solid curves through the symbols are results of an empirical approximation that is developed in the next section, which is used here simply as a guide to the eye. When the region near the crossover is expanded, it becomes clear that the inverse peak intensity for the asymmetric system with $f = 0.25$ stays quite close to the RPA prediction until χ_e is almost equal to χ_s and then crosses over rather rapidly to a low plateau value, corresponding to saturation of $S(q^*)$ to a large value. By comparison, results for symmetric copolymers exhibit a much broader crossover. The appearance of a more abrupt crossover in the behavior of $S^{-1}(q^*)$ near the RPA spinodal suggests that strong local composition fluctuations appear more abruptly with increasing χ_e in more asymmetric copolymers than in symmetric copolymers.

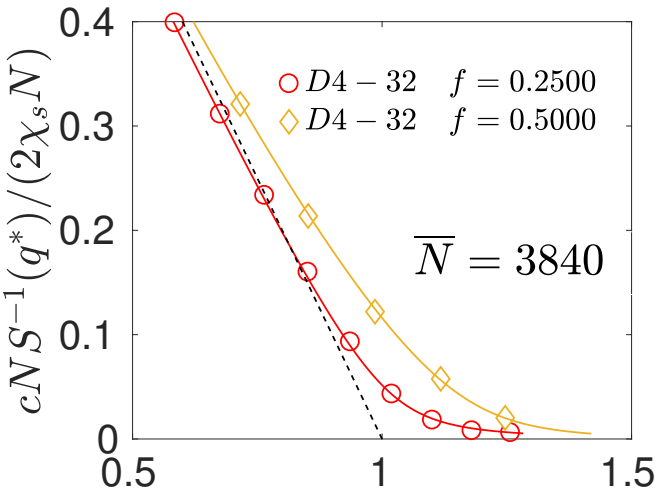

Figure 3.11: Expanded view of normalized inverse peak structure factor $y = cNS^{-1}/2\chi_s N$ vs. normalized interaction parameter $x = (\chi_e N)/(\chi_s N)$ for copolymers with a common value of $\overline{N} = 3840$ but differing values of $f = 0.50$ and $f = 0.25$. Solid lines through the data show the empirical relation that is defined in Eq. (3.25) and Eqs. 3.27-3.31, which is used here to guide the eye.

Dependence on $\overline{N}$

To characterize how the peak intensity depends on $\overline{N}$, it is useful to plot deviations from RPA predictions in a manner inspired by the Fredrickson-Helfand and ROL theories. Let $\delta S^{-1}(q^*)$ denote the difference

$$\delta S^{-1}(q^*) \equiv S^{-1}(q^*) - S_0^{-1}(q_0^*) \tag{3.19}$$

between the true inverse peak intensity $S^{-1}(q^*)$ and the value $S_0^{-1}(q_0^*)$ predicted by the RPA at the relevant values of χ_e, N and f. The ROL theory is based on an expansion of the normalized deviation $cN\delta S^{-1}(q)$ in powers of $\overline{N}^{-1/2}$ that is truncated at order $\overline{N}^{-1/2}$, corresponding to the "one-loop" approximation in the corresponding diagrammatic expansion. The self-consistent form of the ROL theory yields a prediction for the inverse peak intensity, for systems with $b_A = b_B$, of the form

$$cN\delta S^{-1}(q^*) = \overline{N}^{-1/2} K(\chi_a^* N, f) \quad , \tag{3.20}$$

in which $K(\chi_a^* N, f)$ is a universal function of the apparent segregation strength $\chi_a^* N$. The self-consistency in the theory arises from the fact that the function K is evaluated as a function of apparent interaction parameter $\chi_a^* N$, which is itself related to the resulting value for the peak intensity $S(q^*)$ by Eq. (3.10).

In light of the success and failures of the ROL theory, it is reasonable to ask whether the dependence of our results for $\delta S^{-1}(q^*)$ on $\overline{N}$ can be adequately described by any function of the form given in Eq. (3.20), if we treat $K(\chi_a N, f_A)$ as arbitrary function. This is equivalent to asking whether the deviation $cN\delta S^{-1}(q^*)$ at fixed value of f and $\chi_a^* N$ scales as $\overline{N}^{-1/2}$. It is convenient to express this hypothesis in a form in which we scale values of both the inverse peak intensity and $\chi_e N$ by the RPA spinodal value since we have shown that this removes most of the dependence of the results upon f. We thus define a scaled deviation variable

$$\delta y = y - (1 - x) = \frac{cN\delta S^{-1}(q^*)}{2(\chi_s N)} \quad , \tag{3.21}$$

and a scaled apparent interaction parameter

$$x_a = 1 - y = \frac{\chi_a^* N}{\chi_s N} \quad . \tag{3.22}$$

When expressed in terms of these rescaled variables, Eq. (3.20) requires that δy be a function of the form

$$\delta y = \overline{N}^{-1/2} \hat{K}(x_a, f) \quad . \tag{3.23}$$

in which $x_a = 1 - y$, and in which

$$\hat{K}(x_a, f) \equiv \frac{K(\chi_a^* N, f)}{2(\chi_s N)} \quad . \tag{3.24}$$

Figure 3.23 for δy implies that y itself obeys a non-linear equation

$$y = 1 - x + \overline{N}^{-1/2} \hat{K}(1 - y, f) \quad , \tag{3.25}$$

in which we have set $x_a = 1 - y$. This is a self-consistency relation for y identical in form to that used in the Fredrickson-Helfand and ROL theories, which produces the correct qualitative behavior as long as $K(x_a, f)$ is a function that diverges to $+\infty$ as $x_a \to 1$ from below.

To test how well this hypothesis fits our data, we have computed values of the rescaled variables x and y for each of our simulations, converted these to corresponding values of $\delta y = y - (1 - x)$ and $x_a = 1 - y$, and then plotted the product $\overline{N}^{1/2} \delta y$ vs. x_a for sets of simulations with varying $\overline{N}$ but the same value of f. If Eq. (3.20) or (equivalently) Eq. (3.23) were exact, this presentation of the data would result in a perfect collapse of data from simulations with different values of $\overline{N}$ but a common value of f onto a single function, and would result in a plot of the function $K(x_a, f)$ as a function of x_a at a fixed value f.

Results of this comparison are shown in Figure 3.12 for sets of systems with $f = 0.5000$, $f = 0.375$ and $f = 0.25$. For the systems with $f = 0.5$ (left panel) and $f = 0.375$ (middle panel) the extent of collapse of data from systems with different values of $\overline{N}$ but equal values of f is remarkable. This confirms that, for

symmetric and modestly asymmetric copolymers, deviations from the RPA scale as $\overline{N}^{-1/2}$ even for relatively low values of N and $\overline{N}$. For the most asymmetric polymers shown here, with $f = 0.25$, results for different values of $\overline{N}$ deviate more from one another. For $f = 0.25$, results from the two largest values of $\overline{N}$ do nearly collapse in this representation, but results for the shortest chains ($\overline{N} = 480$) differ significantly from the other two. This behavior suggests that the scaling predicted by the one-loop theory is obtained at sufficiently large values of $\overline{N}$. The results all appear to be consistent with the prediction that the dominant correction to the RPA should scale as $\overline{N}^{-1/2}$ for sufficiently large values of $\overline{N}$, but show that the range of values of $\overline{N}$ for which this simple asymptotic scaling is observed is widest for symmetric copolymers.

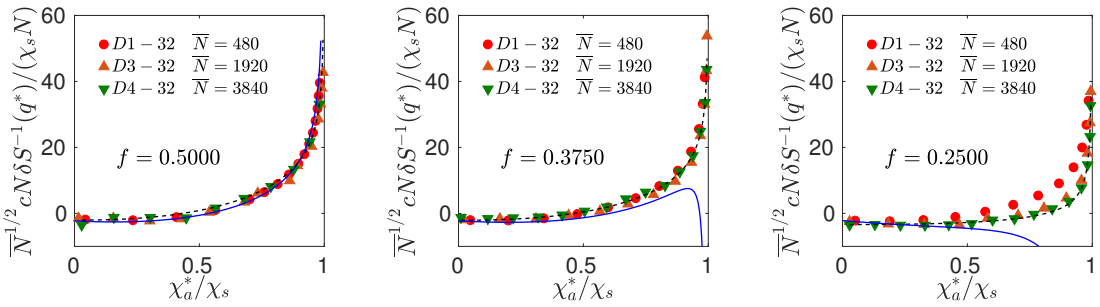

Figure 3.12: Normalized deviation $\overline{N}^{\frac{1}{2}} cN\delta S^{-1}(q^*/(2\chi_s N)$ of the inverse peak structure factor from RPA prediction vs. $x_a = \chi_a^*/\chi_s$. Each plot shows results for a single value of $f = 0.5000$, 0.3750, or 0.2500 over a range of values $\overline{N} = 480$ - 3840. Solid blue lines are ROL predictions. Dashed black lines are the proposed empirical fit.

Empirical Fit

The analysis presented above indicates that deviations in the behavior of the peak intensity $S(q^*)$ in melts of sufficiently long asymmetric copololymers can be described by a universal function $\hat{K}(x_a, f)$ that is independent of $\overline{N}$, and that is related to the peak intensity by Eq. (3.25). We now present an attempt to fit the function $\hat{K}(x_a, f)$ to an empirical function, as a way of summarizing the data presented here in an easily reproducible form.

An empirical fit to the ROL predictions for $\delta S^{-1}(q)$ for diblock copolmers with $b_A = b_B$ has been presented previously by Qin et al. [40]. In that work the ROL prediction for the function $K(\chi_a^* N, f) = \overline{N}^{1/2} c N \delta S^{-1}(q^*)$ was fit to a function of the form

$$K(\chi_a^* N, f) = \left[\frac{\beta(f)}{\sqrt{\chi_s N - \chi_a^* N}} + \frac{\gamma(f)}{\chi_s N - \chi_a^* N} \right] (\chi_a^* N)^{\delta(f)} + \epsilon(f) \quad (3.26)$$

in which $\beta(f)$, $\gamma(f)$, $\delta(f)$ and $\epsilon(f)$ were all taken to be quadratic functions of composition $(f - 1/2)$, and in which $\gamma(1/2) = 0$. The choice of this functional form was based in part on knowledge of the asymptotic behavior of $K(\chi_a^* N, f)$ predicted by the ROL theory in the limit $\chi_a^* N \to \chi_s N$. The ROL theory is known [55, 40] to yield two competing terms that diverge near the spinodal, corresponding to the divergent terms in this expansion. Analysis of the behavior of the ROL theory in the limit of strong scattering yields a positive coefficient $\beta(f) > 0$ for the first divergent term, and a coefficient $\gamma(f)$ that vanishes by symmetry at $f = 1/2$, with $\gamma(f) < 0$ for $f \neq 1/2$. The presence of the term proportional to $\gamma(f)/[\chi_s N - \chi_a^* N]$ with a negative prefactor, $\gamma(f) < 0$, is precisely what causes the ROL theory to make pathological predictions for asymmetric polymers near the ODT, where this term dominates. Because the resulting predictions do not resemble our simulation results, we have thus not included a term with this behavior when attempting to fit our data.

Here, we instead attempted to fit the function $\hat{K}(x_a, f)$ to a somewhat simpler function

$$\hat{K}(x_a, f) = \frac{\beta(f) x_a^{\epsilon(f)}}{(1 - x_a)^{\gamma(f)}} + \delta(f) \quad (3.27)$$

in which the coefficients $\beta(f)$, $\gamma(f)$, $\delta(f)$ and $\epsilon(f)$ are smooth functions of f. We have fit each of these four function of f by a three-parameter function of the form, for example,

$$\beta(f) = \beta_0 + \beta_1 (f - 1/2)^{\beta_2} \quad , \quad (3.28)$$

in which β_0, β_1 and β_2 are fitting parameters. An analogous functional form is used for $\gamma(f)$, $\delta(f)$, and $\epsilon(f)$. Because the simulation results for $f = 1/4$ were found to be consistent with the assumed scaling with $\overline{N}$ only for the longest two chain lengths, we knew that data for shorter chains at this composition could not fit any function of the form given in Eq. (3.25). We thus chose to focus on fitting data obtained for high values of $\overline{N}$, for which the assumed scaling with $\overline{N}$ appeared to be valid. We determined the parameters in this fit by performing a simultaneous least squares fit to results for $\overline{N}^{1/2}y$ vs. x_a using only data for the longest available value of $\overline{N}$ at $f = 0.5$, 0.375 and 0.25.

The results of an initial fit gave a value of $\epsilon(f)$ that was almost independent of f. To reduce the number of adjustable parameters, we thus chose to require ϵ to be independent of f, while allowing the other parameters to be smooth functions of f. Reoptimizing all parameters was then found to yield $\epsilon = 2.13$ and

$$\beta(f) = +126.1 - 1623(f - 1/2)^{0.2144} \tag{3.29}$$

$$\gamma(f) = +0.284 + 9.089(f - 1/2)^{2.585} \tag{3.30}$$

$$\delta(f) = -22.75 - 2143(f - 1/2)^{2.848} \quad . \tag{3.31}$$

Results of this global fit are compared to simulation results for $\overline{N}^{1/2}\delta y$ vs. x_a at $f = 0.5$, 0.375 and 0.25 in the three panels of Figure 3.12, where the results of this fit are shown as dashed lines.

Once an empirical approximation has been constructed for the function $\hat{K}(x_a, f)$, the resulting approximation can be used to predict the behavior of $cNS^{-1}(q^*)$ vs. $\chi_e N$ over a range of values of f and $\overline{N}$. Comparison of the resulting predictions to our simulation results is shown in Figure 3.13. The resulting approximation fits the raw data well for all values of $\overline{N}$ at $f = 0.5$ and 0.375. The model also fits the data well for $f = 0.25$ at the two largest values of $\overline{N}$, but does not fit results for $f = 0.25$ at the smallest value of $\overline{N} = 480$. The failure of the fit for $f = 0.25$ and the smallest value of $\overline{N}$ was expected in light of the failure of the representation shown in Figure 3.12 to collapse the data from these short chains onto the data obtained for two longer chain lengths. This failure thus reflects the fact that our empirical

model is based on an assumed dependence on $\overline{N}$ that breaks down for sufficiently short, asymmetric polymers.

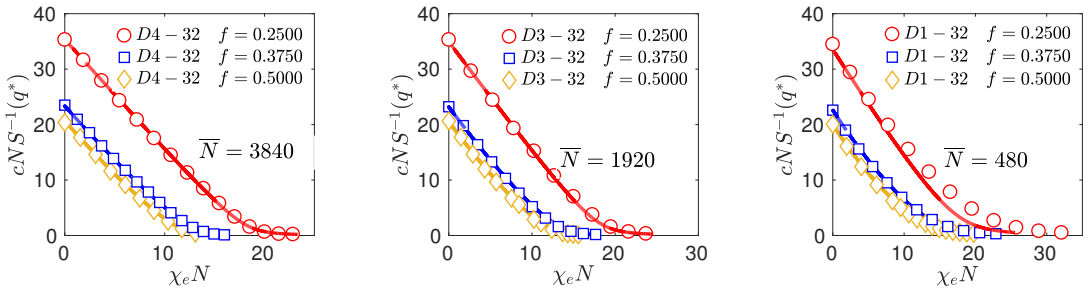

Figure 3.13: Comparison of simulation results (symbols) and empirical fit (lines) for $cN\delta S^{-1}(q^*)$ vs. $\chi_e N$ at several values of $\overline{N}$ = 3840 - 480 (left to right) and f.

Figure 3.14 shows the results of our fit to the function $K(x_a, f)$ plotted vs. x_a for $f = 0.5$, 0.375, and 0.25. The fact that this function diverges as $x_a = \chi_a^* N/(\chi N)_s$ approaches unity is necessary to produced the observed behavior of the normalized inverse peak intensity y for systems with large values of $\overline{N}$, in which y decreases approximately linearly with x for $x < 1$ and then saturates for $x > 1$. The shape of the dependence $K(x, f)$ on x, moreover, controls the width and shape of this crossover: The knee in a plot of y vs. x_a will be sharpest if $K(x_a, f)$ remains small until x_a approaches very close to $x = 1$ and then rapidly diverges, while the predicted knee in y will be more gradual if the increase in K with x_a starts earlier and is more gradual. With this in mind, it is notable that the results of our fit yields a plot of $K(x_a, f)$ vs. x that increases much more abruptly for the most asymmetric chains, with $f = 0.25$, then for more symmetric chains with $f = 0.375$ or $f = 0.5$. This representation of the data makes it particularly clear that, in the limit of long polymers to which our fit for K applies, the crossover to a regime of strong composition fluctuations occurs much more abruptly for highly asymmetric polymers than for symmetric polymers.

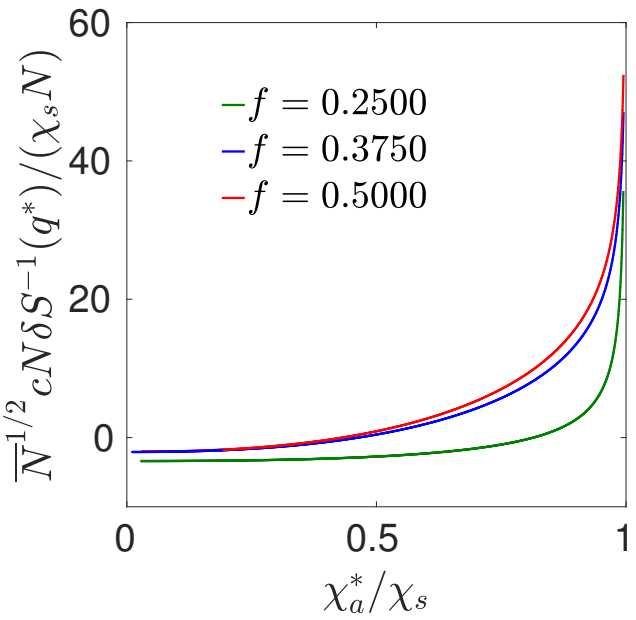

Figure 3.14: Results of a global fit to the function $K(x_a, f) = \overline{N}^{1/2} cN\delta S^{-1}(q^*)/(\chi_s N)$ vs. $x_a \equiv \chi_a^*/\chi_s$ at f =0.5000,0.3750,and 0.2500.

3.7 Conclusions

This contribution reports a study of how the position q^* and magnitude $S(q^*)$ of the peak in the structure factor $S(q)$ in disordered asymmetric diblock copolymer melts depends on parameters f, $\chi_e N$, and invariant degree of polymerization $\overline{N}$. The study focuses on systems with $f = 0.25 - 0.5$, and a range of values of $\overline{N} \simeq 500 - 4000$ that is relevant to many experiments. The work reported here expands on earlier simulation studies by our group that focused on the special case of symmetric diblock copolymers, with $f = 0.5$.

Previous simulation studies of symmetric block copolymers showed that simple coarse-grained simulation models exhibit behavior consistent with a proposed principle of corresponding states. The results presented in Sec. 4 of this chapter confirm that asymmetric diblock copolymers obey the same hypothesis. Specifically, we show here that equivalent results for q^* and $S(q^*)$ are obtained for pairs of systems with

equal values of f, $\chi_e N$ and $\overline{N}$ but different numbers of beads per chain and different values of other microscopic parameters. This conclusion is consistent with the results of an earlier comparison of a different pair of models by Sethuraman, Nguyen and Ganesan [53]. The identification of systems with nominally equal values of $\chi_e N$ was done here, as in the earlier work of [42] and [44], using a calibration of the relationship between χ_e and microscopic parameters that had been developed for each model in earlier studies of symmetric diblock copolymer melts. The fact that comparison of results for asymmetric copolymers with an estimate of χ_e that was obtained by analyzing results of symmetric copolymers indicates that the effective interaction parameter in these simple models is nearly independent of composition.

This conclusion that χ_e appears to be nearly independent of composition enormously simplified the analysis of the peak intensity presented here. The fact that this is true for the simple simulation models studied here does not imply that it must also hold for real polymers. The models studied here have structurally identical A and B blocks, which differ only in length. It has been shown previously [51] that the effective interaction parameter for this sort of structurally symmetric model is given to first order in an expansion in powers of the small parameter $\alpha = \epsilon_{AB} - \epsilon_{AA}$ by an expression $\chi_e(\alpha, f) = z_\infty \alpha / k_B T$ that is completely independent of composition. Composition dependence can, however, appear at second and higher order terms in a Taylor expansion in powers of α. Previous studies of symmetric copolymers [42, 45] suggest that the difference between $\chi_e(\alpha, f)$ and this linear approximation remains relatively small (i.e., typically of order 10% or less) over the range of values of α within which the disordered phase is stable for all of the chain lengths and models studied here. A value of $\chi_e(\alpha, f)$ with very little dependence on f would thus be expected for this type of structurally symmetric models as long as the relatively small nonlinear contribution does not exhibit a strong dependence on composition.

Earlier simulations of symmetric diblock copolymers showed that the behavior of $S(q)$ in the disordered phase is described surprisingly accurately in this special case by the renormalized one-loop (ROL) theory. These earlier studies also took advantage of this observation as the basis of a method estimating the relationship between Flory-Huggins interaction parameter and microscopic parameters in each

model of interest. ROL predictions for asymmetric copolymers are much less useful. ROL predictions for the relationship between q^* and the peak intensity $S(q^*)$ are reasonably accurate for modestly asymmetric copolymers and but tend to predict too large a decrease in q^* near the ODT for more asymmetric polymers. ROL predictions for the dependence of $S(q^*)$ on $\chi_e N$ are useful only over a narrow range of compositions near $f = 1/2$, because the theory exhibits unphysical behavior near the ODT when applied to asymmetric copolymers. Because of this breakdown of the ROL theory, there is thus currently no accurate theory for $S(q)$ in asymmetric copolymers.

In the absence of an accurate predictive theory, we have focused on characterizing our results for the behavior of the peak intensity at an empirical level, in a way that is inspired by the mathematical structure of the Fredrickson-Helfand and ROL theories. The dependence of the inverse peak intensity upon $\chi_e N$ in asymmetric polymers is found to be qualitatively very similar to that found for symmetric copolymers. Both symmetric and asymmetric copolymers, exhibit a crossover between a weakly fluctuating regime in which the behavior of the peak intensity is rather well described by the random phase approximation (RPA) and a strongly correlated regime in which the peak intensity is large but varies more weakly with changes in $\chi_e N$, with a crossover near the spinodal value $(\chi N)_s$ predicted by the RPA. It is shown that behavior obtained at different values of f can be nearly collapsed simply by scaling values of $cNS^{-1}(q^*)$ and $\chi_e N$ by the value of $\chi_e N$ at the RPA spinodal, i.e., by plotting $cNS^{-1}(q^*)/2(\chi N)_s$ vs. $\chi_e N/(\chi N)_s$. The dependence of the results on $\overline{N}$ can be reproduced for sufficiently long chains by an empirical relationship with a mathematical structure similar to that of the Fredrickson-Helfand theory, which assumes that deviations from the RPA scales as $\overline{N}^{-1/2}$. We report results of a global fit of our data for the peak intensity to a relationship of this form, which we hope others will find useful as a compact analytic representation of our results.

Close comparison of simulation results for systems with the same value of $\overline{N}$ but different values of f reveals that the width of the crossover between weak- and strong-fluctuation regimes depends on composition: The crossover in the behavior

of $S^{-1}(q^*)$ with increasing $\chi_e N$ is most gradual for symmetric polymers and becomes more abrupt for more asymmetric copolymers. We suspect that the change in the character of this crossover may be related to a corresponding change in the nature of the transition predicted by SCFT. SCFT predicts a second-order, continuous transition in the special case of symmetric diblock copolymers, with $f = 1/2$, but a first-order transition for $f \neq 1/2$, in which the degree of segregation of the ordered structure that appears at the ODT increases as $|1/2 - f|$ increases. Comparison of simulations of symmetric block copolymers to SCFT predictions indicate that in the strong-fluctuation regime, in which $\chi_e N$ lies between value at which SCFT predicts an ODT and the value at the actual ODT, the disordered phase consists of a bicontinuous structure of increasingly strongly segregated but disordered A and B domains. In the case of symmetric copolymers, these domains remain quite ill-defined and weakly segregated near the RPA spinodal value, reflecting the second-order nature of the underlying SCFT transition, but become steadily more strongly segregated with increasing χN. Scattering experiments on highly asymmetric sphere-forming block copolymers instead show evidence of a rather well defined "critical micelle temperature" (CMT) [58, 21, 59, 60, 61] at which, upon cooling, a high concentration of well segregated micelle-like structures appears over a narrow range of temperature. A SCFT study of the free energy of formation of an isolated spherical "micelle" within an otherwise disordered melt of highly asymmetric copolymers showed that the formation of micelles becomes favorable beyond a critical micelle value of χN somewhat below the RPA spinodal value and very close the value at which SCFT predicts an order-disorder transition [61]. The experimentally identified CMT, which presumably occurs very close to the value of χN at which the formation of well-segregated micelles becomes favorable, is accompanied by a rather rapid rise in the peak scattering intensity. The actual order-disorder transition in highly asymmetric copolymers, which occurs at a somewhat higher value of $\chi_e N$, is instead a crystallization transition in which micelles order on a lattice [59, 61, 60]. We assume that the crossover in the behavior of $S^{-1}(q^*)$ near the RPA spinodal is more abrupt for highly asymmetric copolymers because it corresponds to the rather sudden appearance of a dense but spatially disordered liquid of well-

defined "micelle"-like domains at the critical micelle temperature. Not much more can be done to test the validity of this picture in the composition range studied here by analyzing only the structure factor $S(q)$, as done in this simulation study and in scattering studies. More physical insight would at this point be gained from more real-space analysis of the size, structure, connectivity, and dynamics of domains in the strongly correlated regime of the disordered phase of simulated systems over a range of values of f and $\chi_e N$.

Chapter 4

Dynamics and Viscoelasticity of Disordered Symmetric Diblock Copolymers

Abstract: Simulations of simple bead-spring models are used to study the dynamics of chain motion, composition fluctuations, and stress relaxation in unentangled symmetric diblock copolymer melts. Extensive measurements are reported of the dynamic structure factor $S(q,t)$ as a function of wavenumber q, time t and χN, where χ is the Flory-Huggins interaction parameter and N is degree of polymerization. The relationship between $S(q,t)$ and the static structure factor $S(q) = S(q,t=0)$ is analyzed within the context of a simple linear Langevin equation, which is used to define an effective wavenumber-dependent diffusivity (or inverse mobility) $D(q)$. The ratio of the effective diffusivity $D(q)$ to the single-chain tracer diffusivity is shown to change very little with changes in χN, and to be a simple decreasing function of wavenumber q. The linear stress relaxation modulus $G(t)$ is also measured over a range of values of χN and compared to theoretical predictions. The modulus $G(t)$ agrees well with predictions of the Rouse model for low values of

χN, far from the order-disorder transition (ODT). Near the ODT, $G(t)$ develops an additional slowly decaying feature associated with composition fluctuations. The behavior of the $G(t)$ near the ODT is compared to a modified version of the model of Fredrickson and Larson, which relates the behavior of this slowly decaying component to the behavior of $S(q,t)$.

4.1 Introduction

In addition to their structure forming tendencies, diblock copolymers have interesting dynamical and viscoelastic properties[4]. We focus in this chapter on properties of disordered melts of unentangled symmetric diblock copolymers. Dynamical properties in this type of system vary with changes in χN, and are sensitive to proximity to the order-disorder transition (ODT). At low values of χN, sufficiently far from the ODT, dynamical and rheological properties of a melt of unentangled polymers is adequately described by the Rouse model, as is also true for unentangled homopolymers. As χN approaches the value $(\chi N)_{ODT}$ at the ODT, however, chain motion and stress relaxation are both affected by the appearance of strong, long-lived composition fluctuations. The relaxation of composition fluctuations can be characterized most directly by measuring the intermediate structure factor $S(q,t)$. In this chapter, we present extensive simulation results for the behavior of $S(q,t)$ and linear viscoelastic properties, as well as some characteristics of chain motion. We also discuss the relationship among these different measures of dynamical behavior.

4.2 Background

Dynamical behavior of block copolymer melts can be probed by measuring tracer diffusion, dynamics of composition fluctuations, and linear viscoelastic properties. In this section, we briefly review some relevant previous work.

Tracer Diffusion: They are several experimental techniques that can be used to measure self-diffusion of chains within a polymer melt, including forward recoil spectrometry [62, 63, 64], field gradient nuclear magnetic resonance spectrometry [65, 66], and forced Rayleigh scattering.

A theory of chain diffusion in a weakly ordered lamellar environment was developed by Fredrickson and Milner[67]. Numerical studies of Barrat and Fredrickson extended the Fredrickson-Milner study to the case of arbitrary strong composition fluctuations, deep in the ordered phase [68]. A theory of chain diffusion in the disordered phase of diblock copolymers near the ODT was first developed by Leibig and Fredrickson[69]. These authors extended the application of Rouse dynamics to conditions near the ODT by considering diffusion in a medium with strong composition fluctuations, which slow diffusion. The Leibig-Fredrickson theory was shown to be in qualitative agreements with experiments[69, 63].

One interesting experimental observation about diffusion block copolymer melts is that the average chain diffusion coefficient is almost unchanged upon crossing the order-disorder transition [62, 63, 64]. These experimental studies also showed that there is only a relatively small difference between the diffusion coefficient of homopolymers and that of a diblock copolymer made of those homopolymers with similar molecular weight. Comparison of diffusion coefficients for entangled and unentangled diblock copolymers by Dalvi tal revealed a strong depression of diffusivity in entangled diblock copolymers relative to unentangled copolymers[70]. However, the order-disorder transition did not seem to affect the diffusion coefficient, and it has also been shown that this conclusion is independent of the structure formed upon ordering[64, 71, 72, 73, 74].

Composition Fluctuations and Light Scattering: The dynamics of composition fluctuations in diblock copolymers was first studied theoretically in a series of publications by Akcasu et al. , using the so-called dynamic RPA [75, 76, 77]. The dynamic RPA is a dynamical mean-field approximation similar to that of the Leibler RPA[14], which can be used to derive the dynamic structure factor $S(q,t)$. In the dynamic RPA, a modified diffusion coefficient is defined to relate the dynamics of the interacting system to that of a non-interacting system[76].

Polarized dynamic light scattering (DLS) is a powerful technique used to study the dynamical properties of diblock copolymers. Dynamical light scattering is sensitive to spontaneous composition fluctuations and can provide insight into different relaxation modes of diblock copolymer melts and solutions. The dynamic RPA theory for monodisperse diblock copolymers predicts a single non-diffusive relaxation mode for a disorder melt of diblock copolymers, an internal relaxation process corresponding to the relative motion of the blocks usually referred to as the breathing mode[78]. This is in contrast with the experimental evidence obtained from dynamic light scattering (DLS) measurements, which show evidence for an additional diffusive mode of relaxation in melts and solutions of diblock copoymers [78, 79, 80, 81, 82, 83, 71, 84]. The theoretical interpretation of the dynamical structure factor results by Semenov et al. suggests the presence of an extra mode of relaxation in the copolymers melts, the heterogeneity mode[78], which arises from relative diffusion of fractions of different molecular weight within a slightly polydisperse melt. Semenov's theory explains the DLS observations with good qualitative agreement.[85]

Linear Viscoelasticity: Rheological measurements are the most common experiment probe of dynamical phenomena in block copolymer liquids. Measurements of linear viscoelasticity are useful in, part, as a way of identifying phase transitions. It was first demonstrated by Gouinlock and Porter and Chung that studies of the temperature dependence of the storage and loss moduli $G^{'}(\omega)$ and $G^{"}(\omega)$ can be used to identify order-disorder and order-order transitions in diblock copolymers[86, 87, 88].

Composition fluctuations in the disordered phase produce a unique signature in the linear viscoelastic moduli near the ODT. The first experimental evidence of this rheological signature of fluctuations within the disordered phase was reported by Bates et al. [6], who observed the appearance of a low-frequency shoulder in the storage modulus. Neutron scattering experiments on the same sample confirmed the presence of strong composition fluctuations[6, 7, 89].

Fredrickson and Larson [90] formulated a theory to explain the relations between the long-lived composition fluctuations in the melt near the ODT and the appearance of the secondary shoulder in the storage modulus. Their predictions for the stress

relaxation function produces a low-frequency feature in the complex shear stress modulus, in qualitative agreement with the observation by Bates et al. The work presented here provides a more quantitative test of the Fredrickson-Larson theory.

Simulation Studies:

Relatively few computational studies of disordered diblock copolymers have focused on characterizing dynamical or rheological behavior. Of those that have reported dynamical measurements, most have focused on diffusion, which is relatively easy to measure. Some of the earliest simulation studies of the dynamics of diblock copolymers were lattice Monte Carlo simulations by the Binder group, some of which characterized chain diffusion [8, 11]. Fried and Binder also reported some measurements of the dynamic structure factor, and used the appearance of a dramatic slow down of the relaxation time as a signature indicating approaching to the ODT [13, 91]. Pakula tal used cooperative motion algorithms in their Monte Carlo simulation to measure the center of mass diffusion, bond relaxation, and chain end-to-end auto-correlation time [92]. Murat tal used molecular dynamics simulations to study chain diffusion in the disordered and the order phase of diblock copolymers[93]. Yokoyama tal investigated chain diffusion in the asymmetric diblock copolymer melt in a periodic potential field for entangled and untangled polymeric systems. Their study revealed an exponential scaling of the diffusion constant as the strength of the potential field increases[94].

The simulation results presented in this thesis are intended to provide a clear picture of diblock copolymer dynamics in the disordered phase, and the relationships among chain motion, composition fluctuations, and rheology.

4.3 Simulation Methodology

The simulations presented here are molecular dynamics simulations of a simple coarse-grained model of a melt of symmetric diblock copolymers identical to the one used in several previous studies of equilibrium properties, which was referred to in Refs. [47, 42, 45] as model S1. The systems contained here are all melts of

symmetric AB copolymers with either $N = 16$ or $N = 32$ beads per chain, with equal numbers of A and B beads. All pairs of beads with monomer types i and j (which can each denote A or B) interact via nonbonded pair potential of the form

$$V_{ij}(r) = \frac{1}{2}\epsilon_{ij}\left(1 - \frac{r}{\sigma}\right)^2 \tag{4.1}$$

for $r < \sigma$ and $V_{ij}(r) = 0$ for $r > \sigma$, where σ is the range of interaction and ϵ_{ij} is a parameter with units of energy. All simulations use $\epsilon_{AA} = \epsilon_{BB} = 25k_{\mathrm{B}}T$ and variable values of a parameter $\alpha = \epsilon_{AB} - \epsilon_{AA}$. Here and herafter, k_{B} is Boltzmann's constant and T is absolute temperature. Consecutive beads in the same chain also interact via a harmonic bond potential

$$V_{\mathrm{bond}}(r) = \frac{1}{2}\kappa r^2 \tag{4.2}$$

with $\kappa = 3.406k_{\mathrm{B}}T/\sigma^2$.

The simulations presented here are all NVT molecular dynamics (MD) simulations in a cubic unit cell with periodic boundary conditions. All simulations were performed using a Nose-Hoover thermostat and a time step of $\Delta t = 0.005$ in natural simulation units in which bead mass, thermal energy $k_{\mathrm{B}}T$ and σ are set to 1. We choose to use an NVT ensemble in this study, as in our earlier work on properties of the disordered phase [42], rather than the NPT ensemble used in some work that focused on order-disorder transition [44, 45], in part to simplify the interpretation of measurements in which we measure stress-autocorrelations in order to infer the stress relaxation modulus.

The size of the simulation unit cell and the number of chains in the system were chosen so as give a concentration of $c = 3\sigma^{-3}$ beads per unit volume in all simulations. The length L of each edge of the cubic unit cell was selected such that $L \approx 10R_{g0}$, where $R_{g0} = \sqrt{Nb/6}$ is the random-walk radius of gyration of homopolymer chains, with $\alpha = 0.0$. Simulations of chains with 16 beads contained 2007 chains in a box of length $L = 22.04\sigma$, while simulations of chains with 32 beads contained 2839 chains in a box of length $L = 31.17\sigma$.

Simulations for each system are carried out over a range of values of α ranging from $\alpha = 0$ up to the value at the order-disorder transition (ODT). Values of the Flory-Huggins χ parameter are calculated for each value of α using the correlation that was developed for NVT simulations of model S1 in [42]. The ODT for each system was accurately identified by applying the well-tempered metadynamics algorithm described in previous work by our group [44, 45], which is applied here to NVT simulations rather than the NPT simulations used in our previous study of thermodynamic properties and phase transitions. SCFT predicts that symmetric diblock copolymers should undergo a second-order phase transition at a critical value of $\chi N = 10.495$. For the two systems studied here, we find that the ODT occurs at $\alpha = 4.69$ or $\chi N = 21.72$ for chains length $N = 16$ and at $\alpha = 2.11$ or $\chi N = 18.45$ for $N = 32$.

4.4 Single-Chain Dynamics

We characterize the dynamics of individual polymers within a disordered melt by measuring the mean-squared displacement of a bead near the middle of the chain and the auto-correlation function of the vector that connects the first and last bead in the chain.

Mean-Squared Displacement and Diffusivity: We measure the mean-squared displacement $g(t)$ of one of two beads that are nearest the center of a symmetric diblock copolymer, i. e.the first bead of the B block, which is bonded to the last bead of the A block. Let $g(t)$ denote the function

$$g(t) = \langle |\mathbf{R}(t) - \mathbf{R}(0)|^2 \rangle \quad , \tag{4.3}$$

in which $\mathbf{R}(t)$ denotes the position of this center bead. For large values of t, much greater than the longest internal relaxation time, the motion becomes diffusive, and is given by a linear function

$$g(t) = 6Dt \tag{4.4}$$

in which D is the tracer diffusion coefficient of the molecule.

Figure 4.1 and Figure 4.2 show the mean-square displacement $g(t)$ for chains of length $N = 16$ and $N = 32$, respectively, over a range of values of α or $\chi_e N$. Both axes are plotted using reduced units in which σ, $k_\mathrm{B}T$ and bead mass m are set to unity, giving a time unit $\tau_0 = \sigma/\sqrt{k_\mathrm{B}T/m} = 1$. Values of $\chi_e N$ range from $\chi_e N = 0$ up values very close to the ODT. The long time behavior of $g(t)$ becomes linear at sufficiently long times even near the ODT. The diffusion coefficient D each value of $\chi_e N$ has been extracted by fitting the late time behavior to a linear function of time.

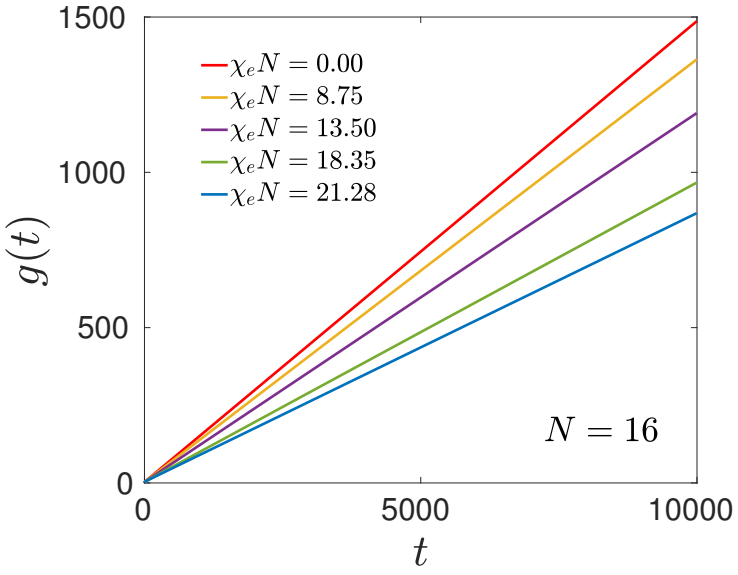

Figure 4.1: Mean-squared displacement $g(t)$ of a middle bead plotted versus time for chains of $N = 16$ beads, for several values of α or $\chi_e N$. Both time and mean-squared displacement are measured in reduced units in which σ, $k_\mathrm{B}T$ and bead mass m are equal to unity. The ODT for this system occurs at $(\chi_e N)_{ODT}$ =21.72

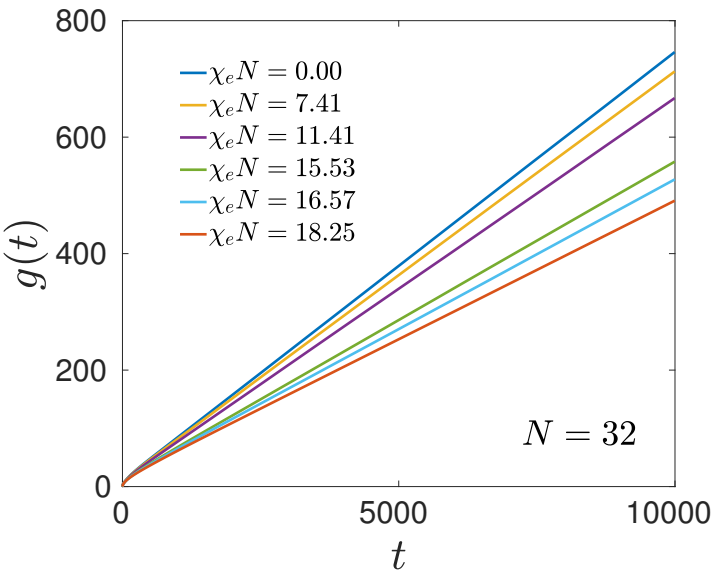

Figure 4.2: Mean-squared displacement $g(t)$ for a middle bead plotted versus time, in reduced units, for chains of $N = 32$ beads and several values of α or $\chi_e N$. The ODT for this system occurs at $(\chi_e N)_{ODT}$ =18.53

The Rouse model predicts that the chain diffusion coefficient in a homopolymer melt should vary with degree of polymerization N as

$$D = \frac{k_B T}{N\zeta} \tag{4.5}$$

where ζ is a bead friction coefficient. This prediction is consistent with our results for the homopolymer state obtained by setting $\alpha = \chi_e N = 0$. Analysis of the long time behavior of $g(t)$ at $\alpha = 0$ yields diffusion coefficients of $D = 0.0248$ for $N = 16$ and $D = 0.0125$ for $N = 32$ in Lennard-Jones units, corresponding to nearly equal values $\zeta = 2.5202$ for $N = 16$ and $\zeta = 2.5000$ for $N = 32$ for the bead friction coefficient.

Figure 4.3 shows how D varies with $\chi_e N$ for both chain lengths. In this plot, we show the ratio D/D_0 of D to its value in a homopolymer melt, which we denote by $D_0 = D(\chi_e N = 0)$. The ratio D/D_0 exhibits an almost identical dependence on $\chi_e N$ for both chain lengths, but reaches a lower value for the model with shorter

chains ($N = 16$), for which $\chi_e N$ reaches a larger value at the ODT. In both cases D/D_0 decreases to a value of $D/D_0 \sim 0.6$ near the ODT.

Figure 4.3 shows that D/D_0 remains near unity while $\chi_e N$ remains less than the critical value of $\chi_e N = 10.5$ predicted by SCFT, and that most of the decrease occurs at greater values of $\chi_e N$. It is known that the disordered phase develops increasing strongly segregated but disordered A and B domains over the range of values of $\chi_e N$ between the SCFT prediction and the true ODT. The observation that only a modest decrease in D (approximately 40%) occurs over this range does not necessarily imply that the chains can diffuse freely even near the ODT. In a state with sufficiently strongly segregated A and B domains, we expect the junction between A and B blocks in each block copolymer to become constrained to remain near interfaces between A and B domains. In the absence of entanglements, which do not occur in the soft-sphere model simulated here, we expect such chains to be able to move rather freely along these interfaces, but only infrequently hop between neighboring interfaces. Free motion along AB interfaces is enough to give diffusivity that is a large fraction of that obtained in the homopolymer state. In the simple case of polycrystalline lamellar phase with a diffusivity $D_\parallel$ for motion parallel to a layer and much lower diffusivity $D_\perp$ for diffusivity along the direction normal to the layers, with $D_\perp \ll D_\parallel$, we would expect an orientationally averaged diffusivity $D \simeq 2D_\parallel/3$. The value of the ratio $D/D_0 \sim 0.6$ that we obtain near the ODT is thus comparable to the value of $D/D_0 \simeq 0.67$ what we would expect in a polycrystalline lamellar phase with $D_\parallel \simeq D_0$. This is also similar to what we would expect for diffusion along the nearly minimal surface of a bicontinuous morphology. The roughly 40% drop in the value of D is thus consistent with the result one would expect from a crossover from fully three-dimensional diffusion to two-dimensional diffusion along interfaces between A and B rich domains in a co-continuous morphology.

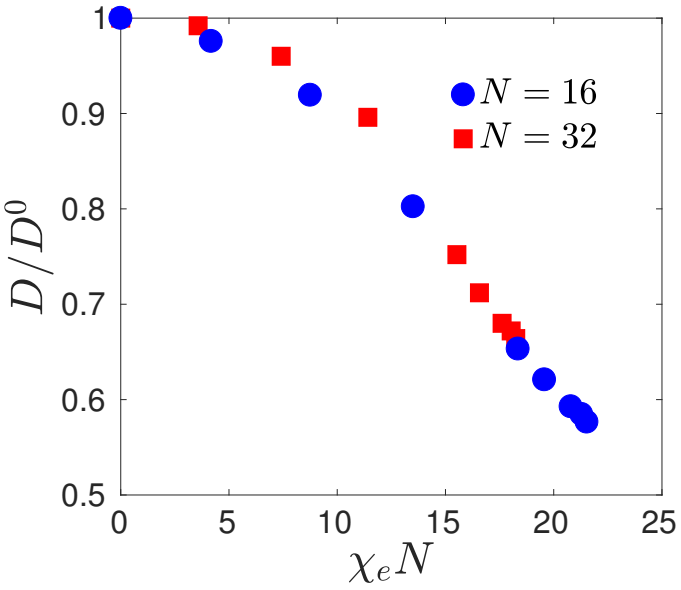

Figure 4.3: Tracer diffusivity D normalized by the value D_0 in a homopolymer melt, plotted versus $\chi_e N$ for disordered melts of symmetric diblock copolymers of lengths $N = 16$ (circles) and $N = 32$ (squares).

End-to-End Relaxation

We monitor the relaxation of chain conformations and chain orientation by measuring the end-to-end vector auto-correlation

$$E(t) = \langle \mathbf{R}_e(t) \cdot \mathbf{R}_e(0) \rangle \tag{4.6}$$

in which $\mathbf{R}_e(t)$ is the vector separation of the first and last bead of a randomly selected chain at time t.

The Rouse model for a continuous Gaussian chain in a homopolymer melt predicts

$$E(t) = \frac{8b^2N}{\pi^2} \sum_{p=1,3,\ldots}^{\infty} \frac{1}{p^2} \exp\left(-\frac{t}{\tau_p}\right) \tag{4.7}$$

where the sum is taken only odd values of $p = 1, 3, 5, \ldots, \infty$, $\tau_p = \tau_1/p^2$, and

$\tau_1 = \zeta N^2 b^2 / 3\pi^2 k_B T$. Note that the existence of a prefactor of $1/p^2$ in this sum yields an expression for $E(t)$ that is dominated by the contribution of the terminal $p = 1$ mode, since the prefactor for the $p = 3$ mode that is already 9 times smaller than that of the $p = 1$ mode. As a result, we expect $E(t)$ in a homopolymer melt to exhibit a nearly single exponential decay with a decay time τ_1.

Figure 4.4 shows simulation results for $E(t)$ for chains of length $N = 16$ in the $\alpha = 0.0$ homopolymer state in a semi-logarithmic plot. The results show that the behavior is indeed nearly single exponential after a small non-exponential transient at very early times. The dashed line shows a fit of late time behavior to a single exponential $E(t) \propto e^{-t/\tau_{e0}}$ from which we have extracted the value of the terminal end-to-end relaxation time, denoted here by τ_{e0}, which corresponds to the terminal time τ_1 in the Rouse model. This analysis yields $\tau_{e0} = 29.64$ in LJ time units. A similar analysis of chains of length $N = 32$ shows the same behavior, with a terminal relaxation time approximately four times longer, as predicted by the Rouse model.

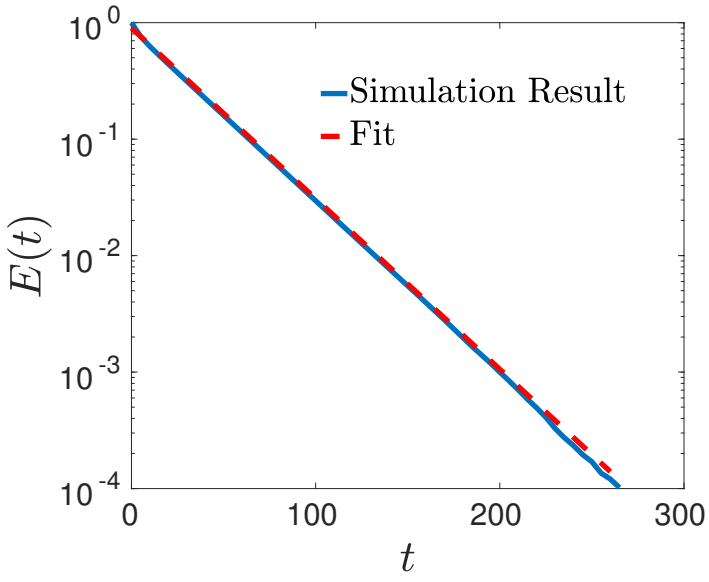

Figure 4.4: End-to-end auto-correlation $E(t)$ vs. time t chains of length $N = 16$ in the homopolymer limit, where $\chi_e N = 0.0$. Time t is shown in LJ time units, in which one LJ time unit is the time it takes a bead with a velocity equal to the root-mean-squared thermal velocity to move a distance equal to the cutoff length σ of the pair interaction. Dashed line is a fit to a single exponential $E(t) \propto e^{-t/\tau_{e0}}$, for which we obtain $\tau_{e0} = 29.46$ in LJ time units.

Figure 4.5 and Figure 4.6 show the evolution of the function $E(t)$ with increasing $\chi_e N$ for chains of length $N = 16$ and $N = 32$, respectively. Upon increasing $\chi_e N$, the behavior of $E(t)$ remains almost unchanged until $\chi_e N$ exceeds the SCFT critical point of $\chi_e N = 10.5$. In the range $10.5 < \chi_e N < (\chi_e N)_{ODT}$, $E(t)$ relaxes in two stages, with a fast initial decay at a rate similar to that obtained in the homopolymer and slower final exponential decay with a relaxation time that increases with increasing $\chi_e N$.

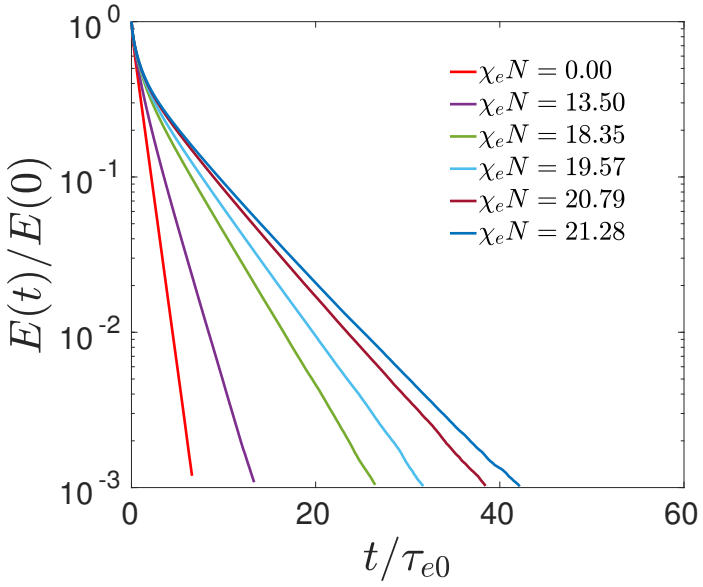

Figure 4.5: Normalized end-to-end auto-correlation function, $E(t)/E(t = 0)$ vs. time for chains of length $N = 16$, for varying values of $\chi_e N$. Values of $\chi_e N$ range from $\chi_e N = 0.00$ to very close to $(\chi_e N)_{ODT} = 21.72$.

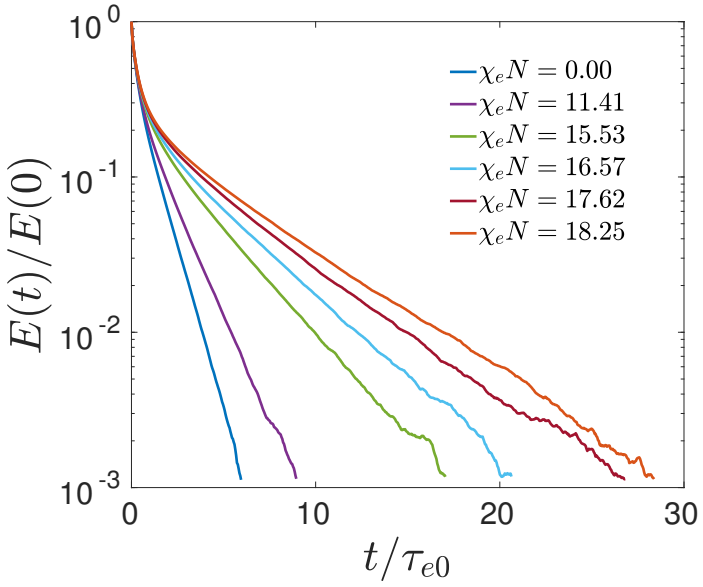

Figure 4.6: Normalized end-to-end auto-correlation function, $E(t)/E(t = 0)$ vs. time for chains of length $N = 32$, for varying values of $\chi_e N$. Values of $\chi_e N$ range from $\chi_e N = 0.00$ to very close to $(\chi_e N)_{ODT} = 18.53$.

We define a terminal end-to-end relaxation time τ_e at each value of α or $\chi_e N$ by fitting the long-time behavior of $E(t)$ to an exponential decay, $E(t) \propto e^{-t/\tau_e}$. To examine the relationship between measured values of τ_e and diffusivity D, we use the diffusivity D to define an effective friction coefficient ζ at each value of $\chi_e N$, by setting $D = k_B T/N\zeta$, and then define the "diffusion time" τ_d to be the value of τ_e predicted by the Rouse model with this friction coefficient (i. e., the predicted value of the longest Rouse relaxation time, τ_1). Values of τ_e and τ_d agree very well in the homopolymer state $\chi_e N = 0$, confirming the accuracy of the Rouse model in this limit. Figure 4.7 shows a comparison of τ_e and τ_d as functions of $\chi_e N$ for both chain lengths, N=16 and N=32. The ratio τ_d/τ_{e0} is very nearly equal to the inverse of the ratio D/D_0. Both τ_e/τ_{e0} and τ_d/τ_{e0} remain very close to unity in the weakly correlated regime $\chi_e N < 10.5$ and both increase at higher values of $\chi_e N$. The increase in τ_e/τ_{e0} is, however, much greater than the increases in τ_d/τ_{e0} or (equivalently) much greater than the decrease in diffusivity.

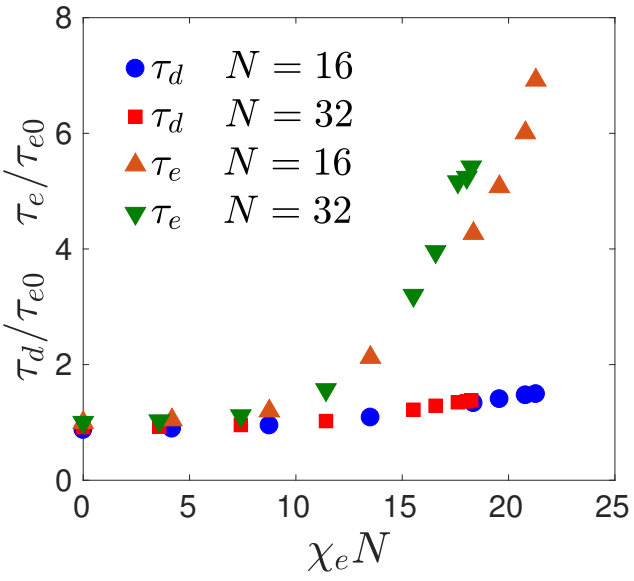

Figure 4.7: Evolution of the end-to-end auto-correlation terminal relaxation time τ_e and the diffusion time τ_d with $\chi_e N$. Both relaxation times are normalized by the value τ_{e0} of τ_e at $\chi_e N = 0.00$. The diffusion time τ_d is defined to be the time predicted by the Rouse model by using a friction coefficient ζ defined by fitting the diffusivity, by setting $D = k_B T/N\zeta$.

Figure 4.8 shows the same results for values of τ_d τ_e plotted vs. $\chi_a^* N$, rather than vs. $\chi_e N$. We define the "apparent" interaction parameter χ_a^* to be the value of χ that we would infer by fitting the measured peak scattering intensity $S(q^*)$ to the RPA prediction, which gives the definition

$$cNS^{-1}(q^*) = 2[10.495 - \chi_a^* N] \quad . \tag{4.8}$$

When plotted as functions of $\chi_a^* N$, values of τ_d/τ_{e0} and τ_e/τ_{e0} for two different chain lengths nearly collapse. Because $\chi_a^* N$ is a measure of the strength of composition fluctuations, this collapse suggests that the dependence of dynamical properties on $\chi_e N$ in the disordered phase is controlled primarily by the local degree of segregation.

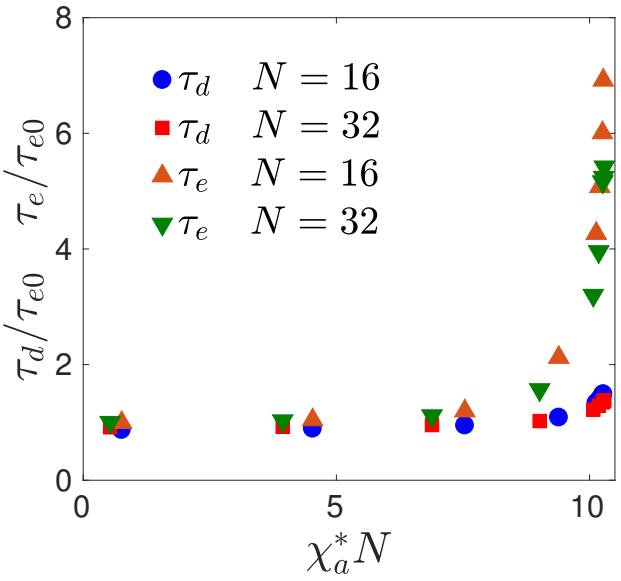

Figure 4.8: The normalized diffusion time τ_d/τ_{e0} and end-to-end autocorrelation time τ_e/τ_{e0} plotted versus the "apparent" segregation parameter $\chi_a^* N \equiv 10.495 - cNS^{-1}(q^*)/2$.

4.5 Dynamical Structure Factor

The dynamics of the relaxation of composition fluctuations in block copolymer melt can be quantified by studying the dynamic structure factor $S(\mathbf{q}, t)$. The function $S(\mathbf{q}, t)$ is an autocorrelation function for Fourier modes of the composition field. In a symmetric AB block copolymer melt, we define an instantaneous composition field

$$\psi(\mathbf{r}, t) = [c_A(\mathbf{r}, t) - c_B(\mathbf{r}, t)]/2 \tag{4.9}$$

at position $\mathbf{r}$ and time t, where $c_A(\mathbf{r}, t)$ and $c_B(\mathbf{r}, t)$ are the instantaneous concentrations of particles of types A or B, respectively, at position $\mathbf{r}$ and time t. The Fourier transform of this field, denoted here by

$$\hat{\psi}(\mathbf{q}, t) = \int d^3 \, e^{-i\mathbf{q}\cdot\mathbf{r}} \psi(\mathbf{r}, t) \quad , \tag{4.10}$$

can also be expressed as a sum over monomer positions,

$$\hat{\psi}(\mathbf{q},t) = \frac{1}{2}\sum_i e^{-i\mathbf{q}\cdot\mathbf{r}_i}\epsilon_i \quad , \tag{4.11}$$

in which i is a monomer particle index, $\mathbf{r}_i$ is the position of monomer i, the sum is taken over all monomers of both types (A and B) in a system containing many chains, and ϵ_i is a factor that is equal to $+1$ if particle i is of type A and -1 if particle i is of type B.

The dynamic structure factor $S(\mathbf{q},t)$ for wavevector $\mathbf{q}$ and time separation t is given by the correlation function

$$S(\mathbf{q},t) = \frac{1}{V}\langle\hat{\psi}^*(\mathbf{q},t)\hat{\psi}(\mathbf{q},0)\rangle \quad , \tag{4.12}$$

in which V is the total system volume. In a homogeneous, isotropic liquid, $S(\mathbf{q},t)$ depends only on the wavenumber $q \equiv |\mathbf{q}|$ and time t, and so can be expressed as a function $S(q,t)$. The static structure factor $S(q)$ that is commonly measured by quasi-elastic small angle X-ray and neutron scattering is given by the $t = 0$ value of the dynamics structure factor $S(q,t)$,

$$S(q) = S(q, t = 0) \quad . \tag{4.13}$$

The static structure factor in a diblock copolymer melt has a maximum at a value q^* of order the inverse radius of gyration. The random phase approximation (RPA) for symmetric diblock copolymers predicts a value $q^* R_{g0} = 1.95$, independent of $\chi_e N$, where $R_{g0} \equiv \sqrt{Nb^2/6}$. The peak wavenumber q^* measured in simulations and experiments instead generally decreases slightly with increasing $\chi_e N$, and is typically $10 - 25\%$ less than the RPA prediction near the ODT.

Results for $S(q,t)$

Figure 4.9 shows the decay of the ratio $S(q,t)/S(q,0)$ vs. normalized time t/τ_{e0} for chains of length $N = 16$ at $\chi_e N = 0$. Different lines correspond to different values

of q. The values of q shown here span a range $0.51 < qR_{g0} < 3.28$ that includes the peak in $S(q)$. In this and subsequent plots involving a time axis, we normalize time by the value τ_{e0} of the end-to-end autocorrelation time at $\chi_e N = 0$. The state $\chi_e N = 0$ examined in Figure 4.9 corresponds to a measurement in a homopolymer melt in which the two halves of each polymer have been artificially labelled A and B, analogous to a neutron scattering experiment in which half of each copolymer is deuterated in order to provide scattering contrast. The fact that the results for each value of q are nearly straight lines in this semi-logarithmic plot indicates that the dependence on time is nearly exponential over the range of values shown here. The dashed lines show fits to a simple exponential decay

$$S(q,t) \propto e^{-t/\tau(q)} \tag{4.14}$$

with a wavenumber dependent relaxation time $\tau(q)$ that is determined independently for each value of q.

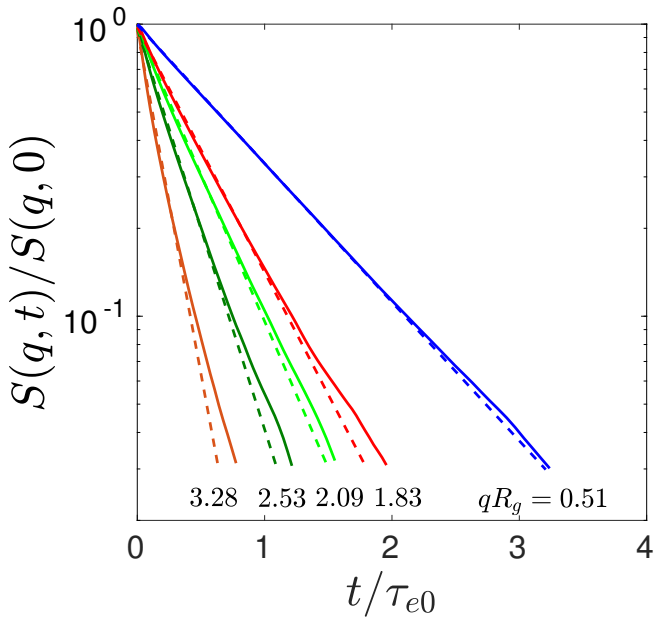

Figure 4.9: Normalized dynamic structure factor $S(q,t)/S(q,0)$ vs. normalized time t/τ_{e0} at $\chi_e N = 0.0$ ($\alpha = 0$) for several values of the normalized wavenumber qR_{g0}. Values of qR_{g0} are shown below each curve. Solid lines show simulation results, and dashed lines show results of a fit to an exponential time dependence $S(q,t) \propto e^{-t/\tau(q)}$.

Figures 4.9-4.12 show the evolution of $S(q,t)$ with increasing $\chi_e N$ for chains of length $N = 16$. Each figure shows results for $S(q,t)/S(q,0)$ vs. t/τ_{e0} at a single value of $\chi_e N$, for several values of q. The time dependence of $S(q,t)$ is nearly exponential over the range of values of q and t shown. The relationship between $\tau(q)$ and q changes, however, as $\chi_e N$ is increased. In Figure 4.12, which shows results closest to the ODT, the slowest decay occurs at a wavenumber $qR_{g0} = 1.52$ that is the chosen value of q that closest to q^*. Near the ODT, the most slowly evolving Fourier modes are thus those with wavenumber near q^*, for which we obtain values of $\tau(q)$ much greater than any obtained at $\chi_e N = 0$.

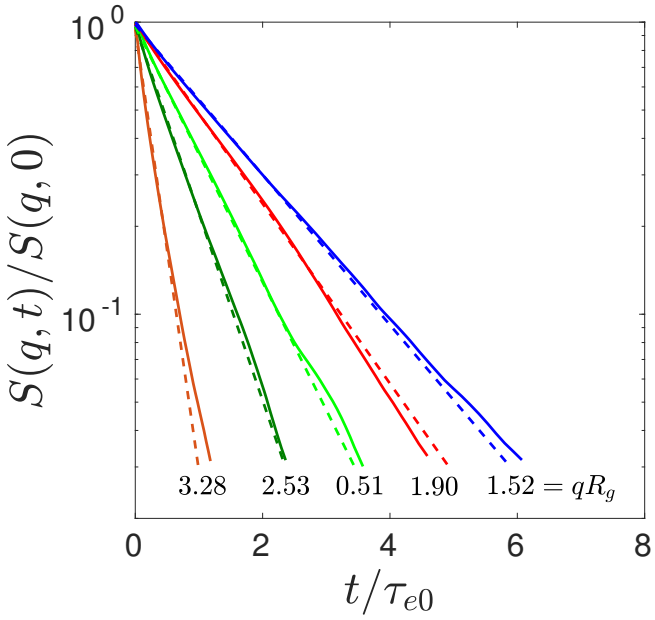

Figure 4.10: Normalized dynamic structure factor $S(q,t)/S(q,0)$ vs. normalized time t/τ_{e0} at $\chi_e N = 8.75$ ($\alpha = 2.0$) for $N = 16$. All symbols are the same as in Figure 4.9

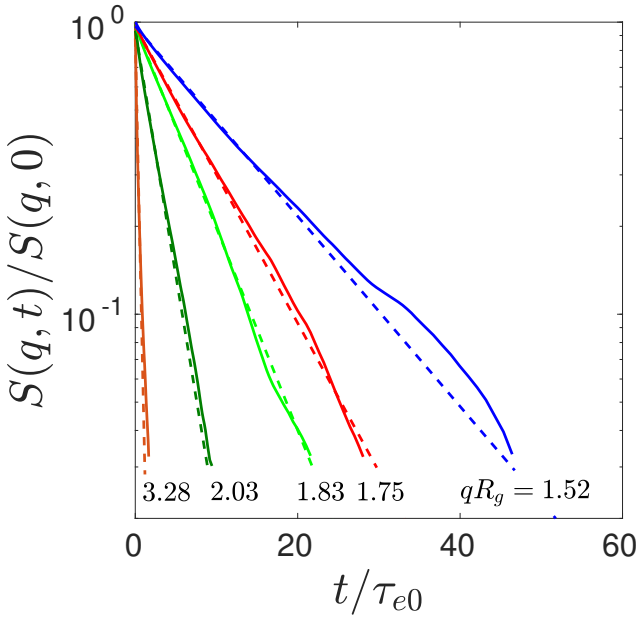

Figure 4.11: Normalized dynamic structure factor $S(q,t)/S(q,0)$ vs. normalized time t/τ_{e0} at $\chi_e N = 18.35$ ($\alpha = 4.0$) for $N = 16$. All symbols are the same as in Figure 4.9

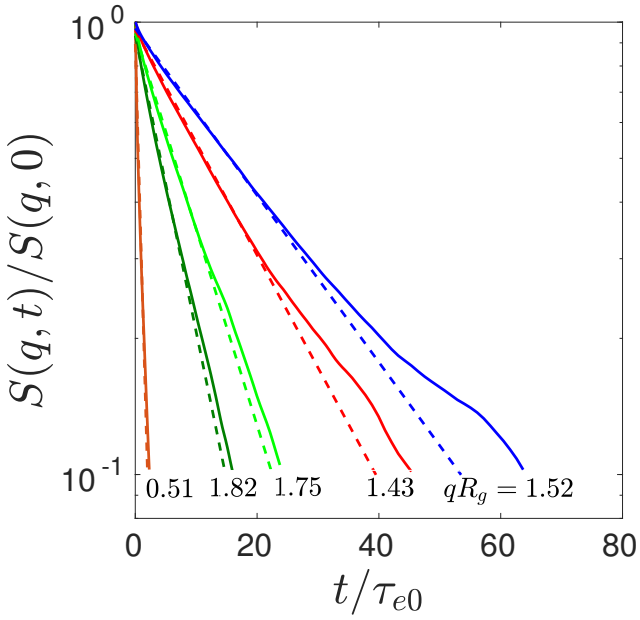

Figure 4.12: Normalized dynamic structure factor $S(q,t)/S(q,0)$ vs. normalized time t/τ_{e0} at $\chi_e N = 20.79$ ($\alpha = 4.5$) for $N = 16$. All symbols are the same as in Figure 4.9

Figures 4.9 - 4.12 show results for values of q that extend only to values slightly greater than q^*. The range of values for $S(q,t)/S(q,0)$ in each of these plots lwas chosen to include the range over which adequate statistics were obtained for the most slowly decaying modes, for which statistical accuracy is worst. Near the ODT, where the decay is slowest, the slowest decaying modes are those with $q \sim q^*$. Within the range of q and t shown in these figures, the time dependence of $S(q,t)$ is nearly single-exponential.

Measurements at higher q over a wider range of values of t show a more complicated time dependence. Figure 4.13 shows results for $S(q,t)/S(q,0)$ for $N = 16$ at a fixed, relatively large value of $qR_{g0} = 3.28$ at several values of $\chi_e N$. The relatively fast decay of correlations at this value of q allows us to obtain accurate measurements over a wider range of $S(q,t)/S(q,0)$ than that shown in Figures 4.9 - 4.12. The time dependence is not single-exponential, particularly near the ODT. Even at $\chi_e N = 0$, $S(q,t)$ shows a modest but clearly measurable deviation from single-

exponential decay. Results obtained near the ODT instead show a rapid, nearly exponential decay of $S(q,t)$ by approximately one decade followed by a small but more slowly decaying tail. Notably, the rate of the initial decay at this relatively high value of q is approximately independent of $\chi_e N$, as shown by the dashed line in the figure, while the rate of decay at longer times depends very strongly on $\chi_e N$ and is slowest near the ODT. We assume that the fast initial decay of $S(q,t)$ at high q is the result of an initial relaxation of composition fluctuations by relaxation of relatively high index Rouse modes of individual chains in an essentially static environment of disordered microdomains, and that the slowly relaxing tail is a result of relaxation of the micro-domain structure.

Our results for $S(q,t)$ for q similar to and less than q^* show almost single-exponential behavior. For the most slowly decaying modes, with $q \sim q^*$, our results are limited to approximately the range $S(q,t)/S(q,0) \geq 10^{-1}$ by limited statistical accuracy of measurements for slowly evolving modes. Deviations as large as those found near the ODT for $qR_g = 3.28$ would have, however, been detectable, and are not seen. Measurements of $S(q,t)$ at $q < q^*$ also show much smaller deviations than those found at $qR_{g0} > 3$. Even for the data shown for higher q near the ODT in Figure 4.13, the initial initial decay of $S(q,t)$ is reasonably well described as a single exponential for $S(q,t)/S(q,0) > 0.1$.

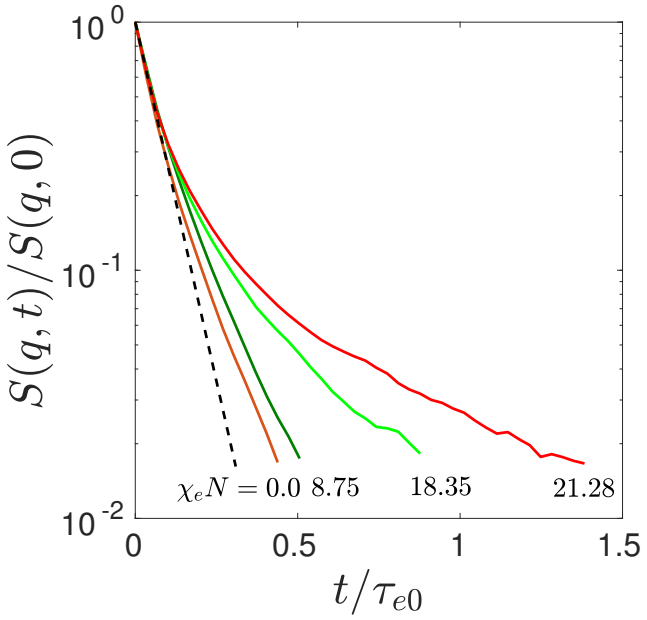

Figure 4.13: The dynamics structure factor $S(q,t)$ vs. time t plotted at a relatively high wave-number $qR_g = 3.28$ over a wide range of $\chi_e N = 0.00...21.28$. A single exponential fit to the early time behavior is shown as a dashed line.

Our data thus suggest that $S(q,t)$ is reasonably well described by a single exponential decay for $q \leq q^*$, and that the behavior at higher q is characterized by an exponential initial decay followed by a small, more slowly decaying tail. We have thus chosen to define a characteristic relaxation time $\tau(q)$ at all q by fitting the first decade of decrease of $S(q,t)$ at each q to an exponential, $S(q,t) \propto e^{-t/\tau(q)}$. For data taken at high q near the ODT, $\tau(q)$ should be understood to be the time associated with the initial decay, rather than with the more slowly decaying tail.

Figures 4.14 - 4.17 display the dependence of the relaxation time $\tau(q)$ on wavenumber q at four different values of $\chi_e N$, for chains of $N = 16$. Figures 4.18 - 4.21 show analogous data for $N = 32$. To illustrate the relationship between the relaxation time and static structure, each of these plots also includes simulation results for the static structure factor $S(q)$, for which the axis is shown on the right of each plot. At $\chi_e N = 0.0$, shown in Figure 4.14, the maximum of $\tau(q)$ appears to occur at $q = 0$. At higher values of $\chi_e N$, however, $\tau(q)$ exhibits a maximum at a value that rapidly

approaches the position q^* of the peak in $S(q)$ as $\chi_e N$. At the highest two values of $\chi_e N$ shown here, both $\tau(q)$ and $S(q)$ exhibit a sharp peak, and the peaks in both curves seem to have the same position and shape. Note that the maximum value of $\tau(q)$ increases dramatically as $\chi_e N$ increases, increasing by approximately a factor 15 over the range shown here. Also note, however, that $\tau(q)$ and $S(q)$ exhibit qualitatively different behavior near $q = 0$, because $S(q) \to 0$ as $q \to 0$, but $\tau(q)$ appears to approach a nonzero limit as $q \to 0$, with a limiting value $\tau(q = 0)/\tau_{e0} \simeq 1$ that changes very little with changes in $\chi_e N$.

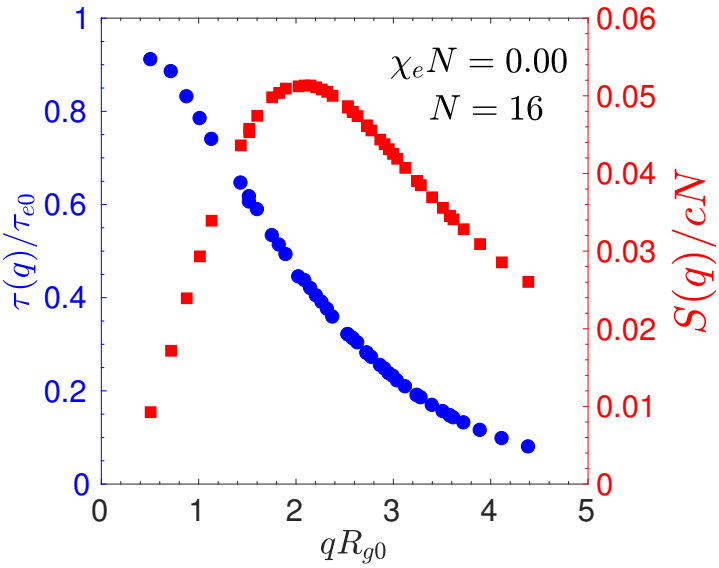

Figure 4.14: Structural relaxation time $\tau(q)$ (circles, left axis) and the static structure factor $S(q)$ (squares, right axis) plotted vs. qR_{g0} for chains of length $N = 16$ at $\chi_e N = 0$ ($\alpha = 0$).

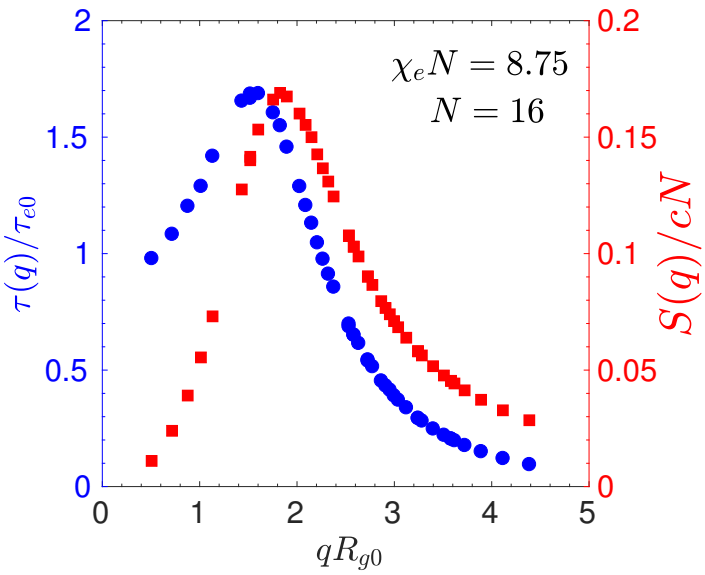

Figure 4.15: Structural relaxation time $\tau(q)$ (circles, left axis) and the static structure factor $S(q)$ (squares, right axis) plotted vs. qR_{g0} for chains of length $N = 16$ at $\chi_e N = 8.75$ ($\alpha = 2.0$).

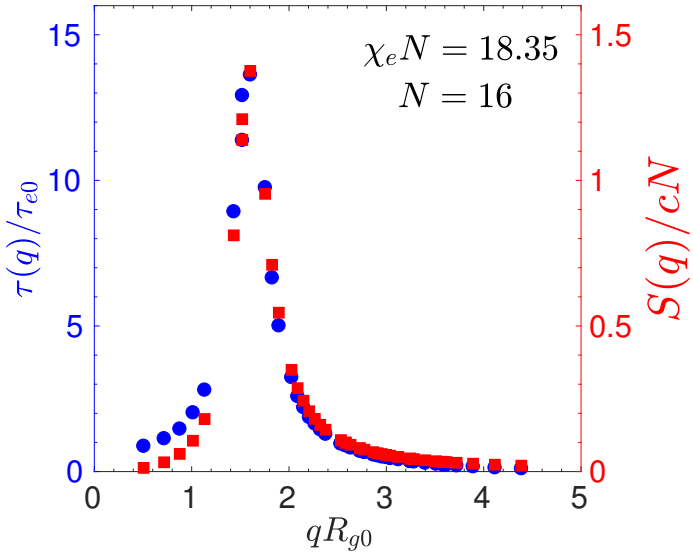

Figure 4.16: Structural relaxation time $\tau(q)$ (circles, left axis) and the static structure factor $S(q)$ (squares, right axis) plotted vs. qR_{g0} for chains of length $N = 16$ at $\chi_e N = 18.35$ ($\alpha = 4.0$).

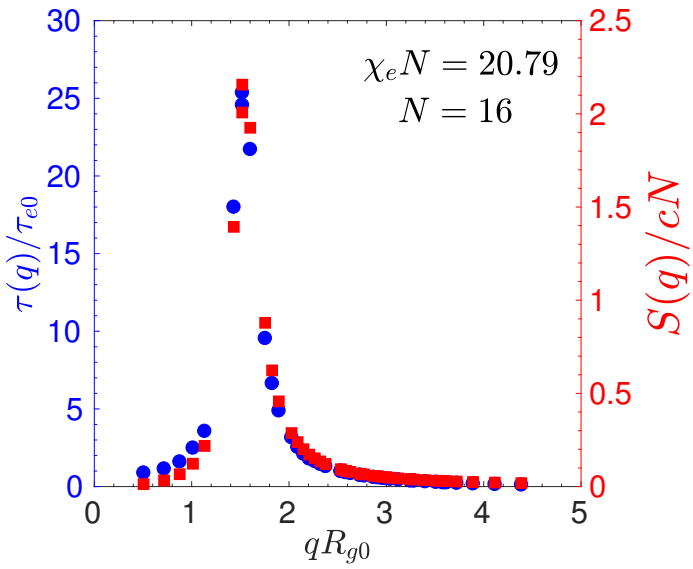

Figure 4.17: Structural relaxation time $\tau(q)$ (circles, left axis) and the static structure factor $S(q)$ (squares, right axis) plotted vs. qR_{g0} for chains of length $N = 16$ at $\chi_e N = 20.79$ ($\alpha = 4.5$).

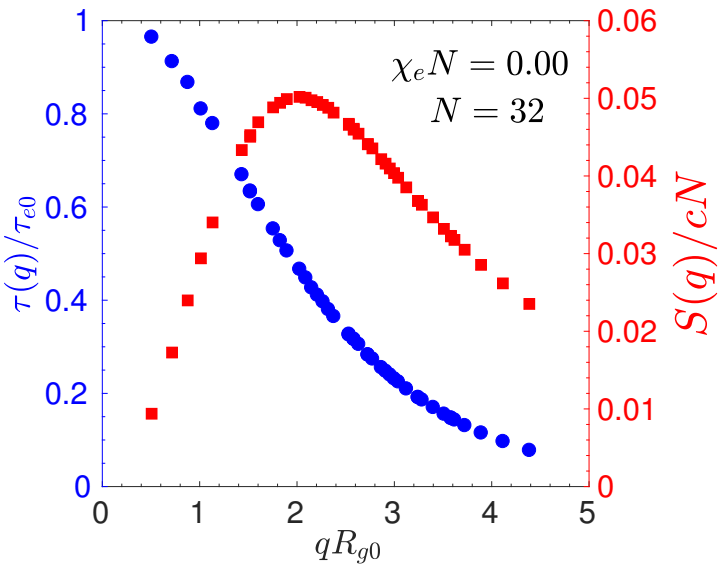

Figure 4.18: Structural relaxation time $\tau(q)$ (circles, left axis) and the static structure factor $S(q)$ (squares, right axis) plotted vs. qR_{g0} for homopolymers of length $N = 32$ at $\chi_e N = 0.0$ ($\alpha = 0.0$).

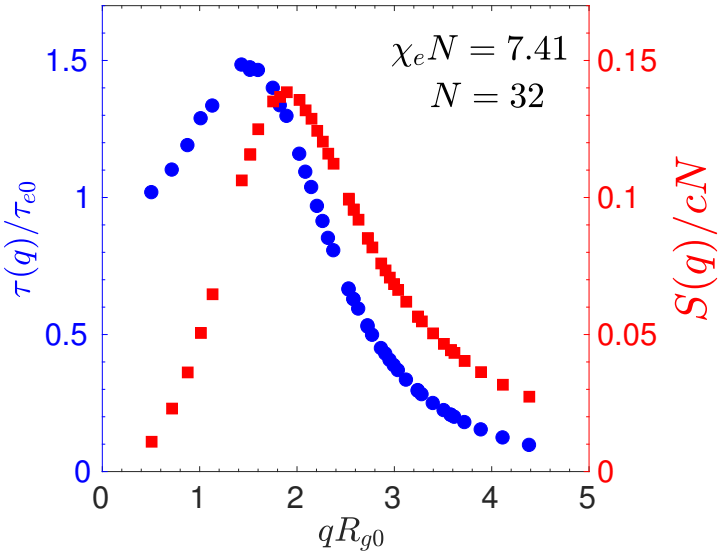

Figure 4.19: Structural relaxation time $\tau(q)$ (circles, left axis) and the static structure factor $S(q)$ (squares, right axis) plotted vs. qR_{g0} for $N = 32$ and $\chi_e N = 7.41$.

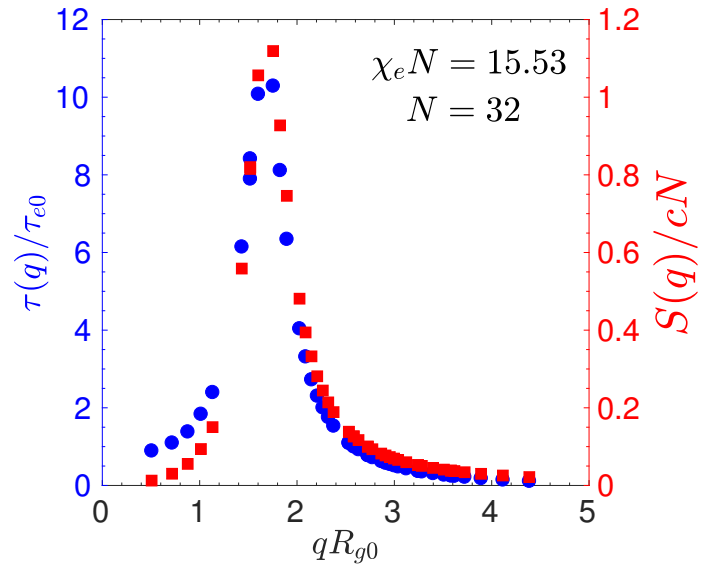

Figure 4.20: Structural relaxation time $\tau(q)$ (circles, left axis) and the static structure factor $S(q)$ (squares, right axis) plotted vs. qR_{g0} for $N = 32$ and $\chi_e N = 15.53$.

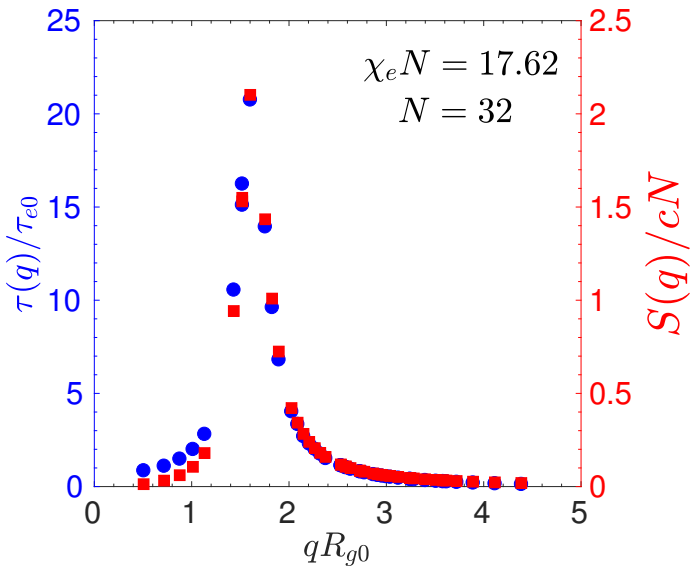

Figure 4.21: Structural relaxation time $\tau(q)$ (circles, left axis) and the static structure factor $S(q)$ (squares, right axis) plotted vs. qR_{g0} for $N = 32$ and $\chi_e N = 17.62$.

Linear Langevin Model Analysis of $\tau(q)$

We now discuss a simple phenomenological model for the behavior of $S(q,t)$, and analyze our data within the context of that model. The field $\psi(\mathbf{r},t)$ is a conserved order parameter, and so has dynamics controlled by a conservation equation

$$\frac{\partial \psi}{\partial t} = -\nabla \cdot \mathbf{J} \quad , \tag{4.15}$$

in which $\mathbf{J}(\mathbf{r},t)$ is a monomer flux. Because $\psi(\mathbf{r}) = [c_A(\mathbf{r}) - c_B(\mathbf{r})]/2$ is a field with units of monomer concentration, the flux is naturally written as a product

$$\mathbf{J} = c\mathbf{v} \tag{4.16}$$

in which c is the total monomer concentration and $\mathbf{v}$ is a relative velocity of A and B monomers. To construct a minimal model, let us assume for the moment that the velocity $\mathbf{v}$ is related to an exchange chemical potential $\mu(\mathbf{r}) = \delta F[\psi]/\delta\psi(\mathbf{r})$ by

a gradient

$$\mathbf{v} = -\frac{1}{\zeta}\nabla\mu \quad , \tag{4.17}$$

in which ζ is an effective bead friction coefficient. We know from equilibrium linear response theory that Fourier amplitudes of fluctuations in μ and ψ are related to linear order in ψ by the relation

$$\hat{\mu}(\mathbf{q}) = k_{\mathrm{B}}T\, S^{-1}(q)\hat{\psi}(\mathbf{q}) \quad . \tag{4.18}$$

Here, $\hat{\mu}(\mathbf{q})$ and $\hat{\psi}(\mathbf{q})$ denote Fourier components of the deviations of $\mu(\mathbf{r})$ and $\psi(\mathbf{r})$ from their values in a homogeneous reference state, and $S(q)$ is the static structure factor, which controls the free energy cost of small composition fluctuations. By substituting (4.18) and (4.17) into (4.15) and expressing the result in Fourier space (by replacing gradients by factors of $i\mathbf{q}$), we obtain

$$\frac{d\hat{\psi}(q,t)}{dt} = -q^2 DcNS^{-1}(q)\hat{\psi}(q,t) \quad , \tag{4.19}$$

where $D \equiv k_{\mathrm{B}}T/\zeta N$ is the molecular diffusion constant. We now generalize this expression so as to allow for the existence of a wavenumber dependent (i. e., nonlocal) effective friction, to account for the fact that polymers are extended objects, by replacing D by an unknown wavenumber dependent function $D(q)$. The resulting ordinary differential equation for the time depenence of $\psi(q,t)$ suggests that each mode relaxes with a relaxation rate

$$\frac{1}{\tau(q)} = D(q)q^2 cNS^{-1}(q) \quad . \tag{4.20}$$

Using this as the deterministic part of the relaxation of $\psi(q,t)$ in a linear Langevin equation for $\psi(q,t)$ would give a correlation function $S(q,t)$ with the same decay rate, $S(q,t) \propto e^{-t/\tau(q)}$. Note that this model predicts a decay time $\tau(q) \propto S(q)$, and will thus naturally predict the appearance of a sharp maximum in the relaxation time $\tau(q)$ when there is a sufficiently sharp peak in $S(q)$, as is true near the ODT.

We analyze our data by treating (4.20) as a definition of $D(q)$, and inferring

a value for $D(q)$ at each q from our measurements of $\tau(q)$ and $S(q)$. To put our expression for $D(q)$ into an appropriate universal scaling form, we consider the ratio where $D(q)/D_0$, in which D_0 is the chain diffusivity in the $\alpha = 0$ homopolymer state, normalize q by the length R_{g0}, and normalize $\tau(q)$ by the a time scale $\tau_0 \equiv R_{g0}^2/D_0$. This yields a non-dimensionalized equation for $D(q)/D_0$ as

$$\frac{D(q)}{D_0} = \frac{1}{q^2 R_{g0}^2} \frac{\tau_0}{\tau(q)} \frac{S(q)}{cN} \quad . \tag{4.21}$$

The ratio $S(q)/cN$ is known to be non-dimensional function of qR_{g0} and the state parameters $\chi_e N$ and $\overline{N}$. If we assume that $\tau(q)/\tau_0$ is also a universal function of these state parameters and qR_{g0}, it follows that $D(q)/D_0$ should also be a universal function of qR_g, $\chi_e N$ and $\overline{N}$, for which we expect a relatively weak dependence on $\overline{N}$.

Figures 4.22 and 4.23 show results for $D(q)/D_0$ vs. qR_{g0} for chains of 16 and 32 beads, respectively. Values of $D(q)$ were computed using measured values of $\tau(q)$ and $S(q)$ for all q in the range shown. Different symbols represent results obtained at different values of $\chi_e N$. The results for $D(q)/D_0$ for these two different values of N are very similar, consistent with our scaling hypothesis and the assumption of a weak dependence on $\overline{N}$. In fact, results for $D(q)/D_0$ also change relatively little with changes in $\chi_e N$, compared to the much more dramatic changes in $\tau(q)$ and $S(q)$ near the ODT. At any fixed value of $\chi_e N$, the function $D(q)$ is a smooth, monotonically decreasing function of q that appears to approach a nonzero value of $D(q)/D_0 \simeq 0.18 - 0.28$ as $qR_{g0} \to 0$, and appears to approach a lower asymptotic value at high q. Figure 4.24 shows a direct comparison of $D(q)/D_0$ for homopolymers ($\alpha = 0$) for chains of $N = 16$ and $N = 32$ beads, which shows that $D(q)/D_0$ appears to be independent of chain length in this limit. The ratio $D(q)/D_0$ does change somewhat with changes in $\chi_e N$. Values of $D(q)/D_0$ in the range $qR_{g0} \simeq 1.5 - 1.8$ in which the peak in $S(q)$ appears, however, change particularly little with changes in $\chi_e N$, and have values in the range

$$D(q^*)/D_0 \simeq 1.12 - 1.17 \tag{4.22}$$

for $\chi_e N$ ranging from 0 up to to $(\chi_e N)_{ODT}$, for both chain lengths. Notably, $D(q)$ is a much smoother function of both q and $\chi_e N$ than either the time scale $\tau(q)$ or the static structure factor $S(q)$. The appearance of a sharp peak in $\tau(q)$ near the ODT thus seems to almost entirely reflect the appearance of a corresponding peak $S(q)$.

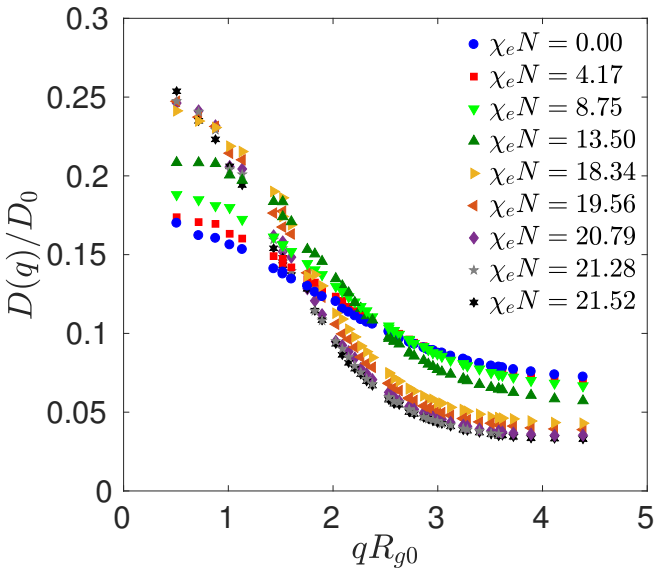

Figure 4.22: Values of the normalized effective diffusivity $D(q)/D_0$ vs. qR_{g0} for chains of $N = 16$ beads.

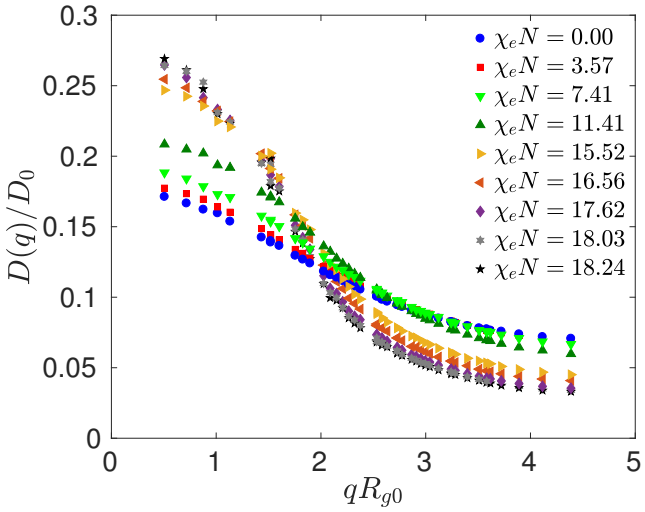

Figure 4.23: Values of the normalized effective diffusivity $D(q)/D_0$ vs. qR_{g0} for chains of $N = 32$ beads. Values of $D(q)$ are computed from measurements of $\tau(q)$ and $S(q)$, as described in the text.

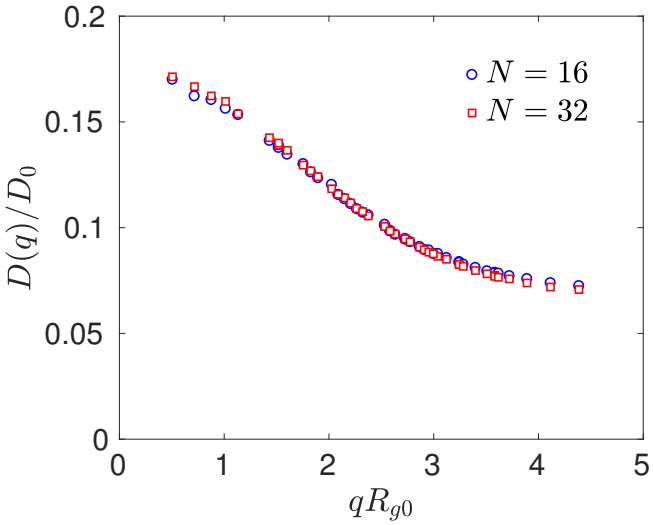

Figure 4.24: Values of the normalized effective diffusivity $D(q)/D_0$ vs. qR_{g0} for homopolymers of $N = 16$ and $N = 32$ beads ($\alpha = 0.00$).

Terminal Structural Relaxation Time:

The time constant $\tau(q)$ measures the time required for the value of a Fourier amplitude $\psi(\mathbf{q},t)$ to become de-correlated with its value at an earlier time. Near the ODT, the modes of largest mean-squared amplitude and longest relaxation time are those with $q \sim q^*$. The value of $\tau(q)$ for the most slowly decaying modes is thus a measure of how long it takes for a transient spatial arrangement of A- and B-rich regions to become re-randomized. We thus consider the behavior of the quantity

$$\tau_{\rm S} = \max_q \tau(q) \quad , \tag{4.23}$$

which we refer to as the termain structural relaxation time. This quantity is a function of $\chi_e N$ that increases rapidly with increasing $\chi_e N$ near the ODT.

Figure 4.25 shows simulation results for τ_S normalized by τ_{e0} as a function of $\chi_e N$ for chains of both 16 and 32 beads. At low values of $\chi_e N$, well below the SCFT critical value of 10.5, τ_S is nearly equal to the single chain terminal relaxation time τ_{e0}, and changes rather little with changes in $\chi_e N$. For $\chi_e N$ between 10.5 and $(\chi_e N)_{ODT}$, τ_S increases increasing rapidly with increasing $\chi_e N$, reaching a value of $25-30$ times greater than τ_{e0} at the ODT. The simulation results for these two systems indicate that the ratio of the value τ_S at the ODT to its value at $\chi_e N = 0$ is larger for shorter chains. More generally, this ratio is presumably larger for smaller values of $\overline{N}$, for which the degree of local segregation is larger at the ODT. Figure 4.26 shows the same comparison plotted vs. the "apparent" interaction $\chi_a^* N$. The near collapse of results with different chain lengths shows that the ratio τ_S/τ_{e0} is a nearly universal function of $\chi_a^* N$.

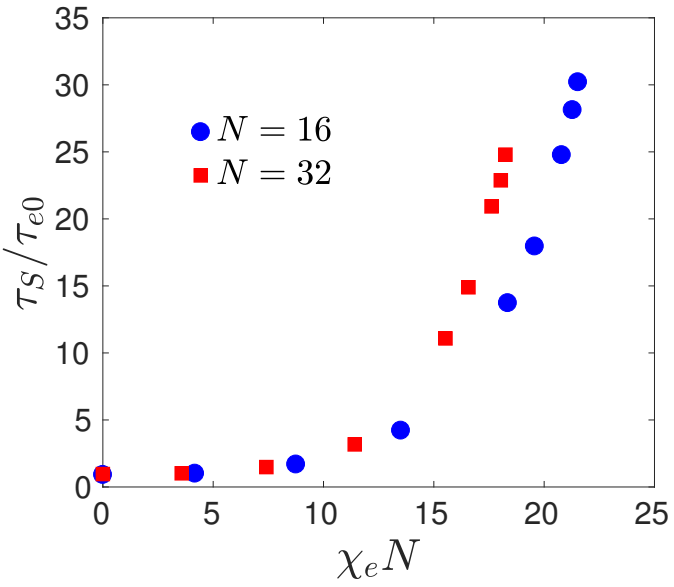

Figure 4.25: The structure factor relaxation time, τ_S, normalized to the end-to-end auto-correlation terminal time constants of the corresponding polymeric systems versus $\chi_e N$ over a wide ranged of $\chi_e N$ values, for chains of both 16 and 32 beads.

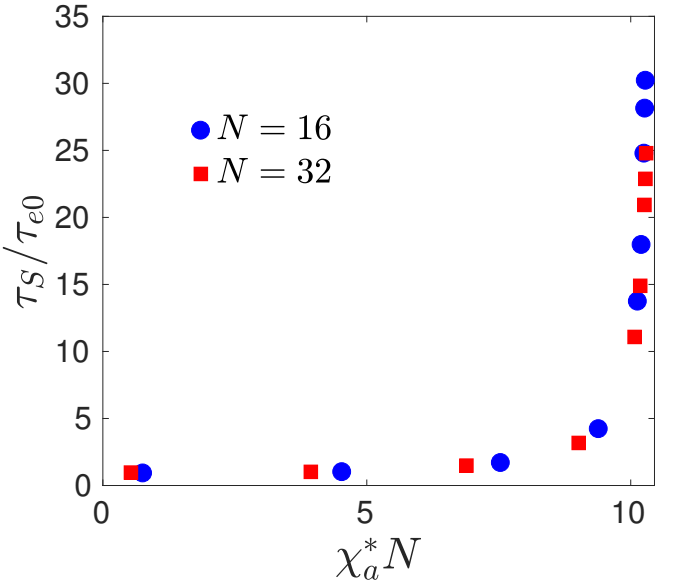

Figure 4.26: The normalized structure factor relaxation time, τ_S/τ_{e0} versus $\chi_a^* N$ for chains of both 16 an 32 beads.

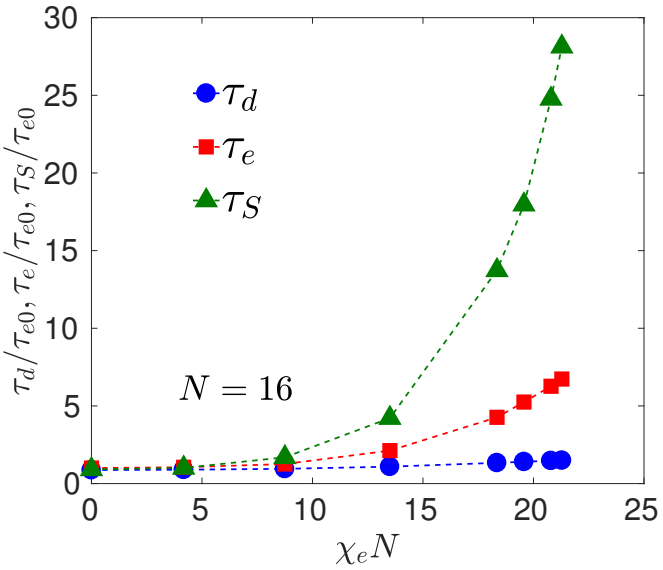

Figure 4.27: Different time constants for the system with $N = 16$ normalized to the end-to-end auto-correlation time constant(τ_{e0}) at $\chi_e N = 0.00$, plotted versus $\chi_e N$.

Figure 4.28 compares the behavior of the structure factor time τ_S, the end-to-end time τ_e and the diffusion time τ_d, plotted as functions of $\chi_e N$ for chains of length $N = 16$ and $N = 32$, respectively. All three times are very similar to each other, at low values of $\chi_e N$. Near the ODT, however, the τ_S becomes much larger than τ_e, and increases more rapidly than τ_e with increasing $\chi_e N$.

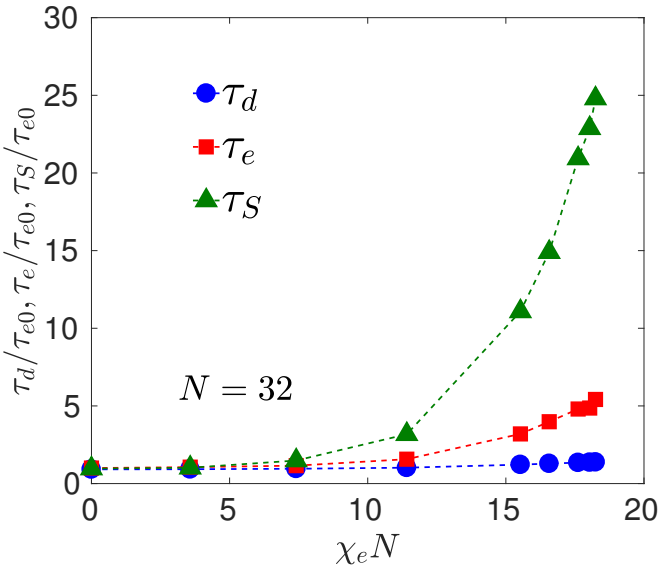

Figure 4.28: Different time constants for the system with $N = 32$ normalized to the end-to-end auto-correlation time constant(τ_{e0}) at $\chi_e N = 0.00$, plotted versus $\chi_e N$.

4.6 Linear Viscoelasticity

The most common experimental methods for characterizing dynamical properties of a polymer liquid are measurements of linear viscoelastic behavior. Measurements of linear viscoelastic properties also provide an excellent method of identifying order-disorder transitions in block copolymer melts. Here, we present measurements of the shear relaxation modulus $G(t)$ of the simulation model studied here in the disordered phase. The modulus $G(t)$ characterizes the decay of the macroscopic shear stress $\sigma(t)$ after step shear strain of magnitude γ, and is given by the limiting value of ratio $G(t) = \sigma(t)/\gamma$ in the limit of small strain γ.

Green-Kubo Relation

The results for $G(t)$ presented here were measured using the fluctuation-dissipation or Green-Kubo relationship that relates $G(t)$ to fluctuations in shear stress. In its

simplest form, this relationship states that $G(t)$ for an isotropic liquid is given by the autocorrelation function

$$G(t) = \frac{V}{k_{\mathrm{B}}T}\langle\sigma_{ij}(t)\sigma_{ij}(0)\rangle \quad , \tag{4.24}$$

where $\sigma_{ij}(t)$ is the instantaneous value at time t of any off-diagonal component of the stress tensor, with $i \neq j$, of a system of total volume V in thermal equilibrium at time t. To improve statistics of such a measurement, we use the equivalent relationship

$$G(t) = \frac{V}{10k_{\mathrm{B}}T}\sum_{i,j=1}^{3}\langle\tilde{\sigma}_{ij}(t)\tilde{\sigma}_{ij}(0)\rangle \quad , \tag{4.25}$$

in which $\tilde{\sigma}$ denotes the deviatoric (i. e., traceless) part of the symmetric stress tensor, with elements given by

$$\tilde{\sigma}_{ij}(t) = \sigma_{ij}(t) - \frac{1}{3}\delta_{ij}\sum_{i=1}^{3}\sigma_{ii}(t) \quad , \tag{4.26}$$

where $\sigma_{ij}(t)$ is an element of the full stress tensor.

The instantaneous stress tensor $\sigma(t)$ is given by a sum

$$\sigma_{ij} = \sigma_{ij}^{(\mathrm{kin})} + \sigma_{ij}^{(\mathrm{vir})} \tag{4.27}$$

of a kinetic component and virial component. The kinetic stress is given by a sum

$$\sigma_{ij}^{(\mathrm{kin})} = \frac{1}{V}\sum_{\alpha} m_\alpha v_{\alpha,i} v_{\alpha,j} \tag{4.28}$$

over all particles in the system, in which α is a particle index, m_α is the mass of particle α and $v_{\alpha,i}$ is the ith component of that particle's velocity. The virial compononent for a model with purely pairwise forces, such as the model used here,

is given by a sum over particle pairs,

$$\sigma_{ij}^{(\mathrm{vir})} = \frac{1}{V} \sum_{\alpha>\beta} r_{\alpha\beta,i} f_{\alpha\beta,j} \tag{4.29}$$

in which $r_{\alpha\beta,i}$ is a component of the separation of particles α and β and $f_{\alpha\beta,j}$ is a component of the force between these two particles.

The autocorrelation function for the traceless symmetric stress defined in (4.25) has been computed by measuring the stress every 10 molecular dynamics steps and averaging using the hierarchical averaging scheme introduced for this purpose by Likhtmann and Ramirez[95].

Because the model simulated here relies on a soft pair potential that allows chains to cut through one another, these simulations do not exhibit entanglement. The starting point for our analysis of results for $G(t)$ is thus a Rouse model of unentangled polymer melts. The Rouse model for a continuous Gaussian chain in a homopolymer melt predicts

$$G(t) = \frac{c k_{\mathrm{B}} T}{N} \sum_{p=1}^{\infty} \exp\left(-\frac{p^2 t}{\tau_R}\right) \tag{4.30}$$

in which c is the number concentration of monomers, N is the number of monomers in a chain, so that c/N is the number concentration of molecules, and τ_R is the terminal relaxation time for stress. The terminal stress relaxation time τ_R predicted by the Rouse model is half the relaxation time τ_1 for the mode amplitude of the most slowly decaying Rouse mode, $\tau_R = \tau_1/2$. The terminal relaxation time τ_e for the end-to-end autocorrelation function $E(t)$ introduced previously in (4.7) is instead equal to τ_1, $\tau_e = \tau_1$. The Rouse model predicts a power law decay $G(t) \propto t^{-1/2}$ times $t \ll \tau_R$ followed by exponential decay at times $t > \tau_R$.

Overview of Results

Figure 4.29 shows the evolution of the behavior of $G(t)$ with increasing degree of segregation within the ordered phase. In this and subsequent plots of $G(t)$ vs. time,

time t is normalized by the terminal time $\tau_{e0}/2$ predicted by the Rouse model for a homopolymer, while the modulus $G(t)$ is normalized by the prefactor $ck_{\mathrm{B}}T/N$ that appears in the Rouse model prediction of Eq. (4.30).

At $\chi_e N = 0$, the simulation model considered here reduces to a model of a homopolymer melt. We show in what follows that, in this limit, the behavior of $G(t)$ is predicted nearly perfectly by the Rouse model. At relatively low but nonzero values of $\chi_e N$, up to $\chi_e N \simeq 10$, the behavior remains similar to that found for a hompolymer. Throughout this regime of weak composition fluctuations, $G(t)$, is characterized by a single crossover from a power law decay at early times to exponential decay after a terminal relaxation time, with a crossover time that increases slightly with increasing $\chi_e N$.

At higher values of $\chi_e N$, closer to the ODT, the function $G(t)$ develops a second feature that is a result of strong composition fluctuations. At the two highest values of $\chi_e N$ shown in Figure 4.29, a second shoulder develops at long times, which becomes more prominent as $\chi_e N$ increases. We show in what follows that the decay time associated with this new feature is approximately the same as the terminal relaxation time τ_S for the relaxation of the composition fluctuations.

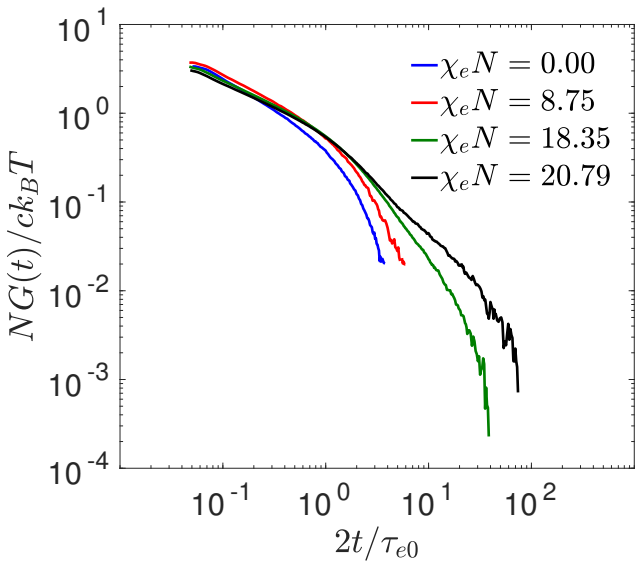

Figure 4.29: Normalized stress relaxation modulus, $NG(t)/ck_{\rm B}T$ for disordered melts of chains of length $N = 16$ over a wide range of values of χ_eN. The value at the ODT is $(\chi_eN)_{ODT} = 21.72$.

Figure 4.30 shows the rheological signature of the spontaneous formation of lamellar order. The highest two values of χ_eN shown in this plot ($\chi_eN = 22.02$) and $\chi_e = 22.26$) are slightly above the value $\chi_eN = 21.72$ at the equilibrium ODT. Both of these samples spontaneously crystallized into lamellar structures. The formation of lamellar order is visible in our measurement of $G(t)$ by the appearance of a plateau in $G(t)$ at long times. To explain why a plateau forms in the lamellar phase, recall that $G(t)$ is measured by measuring an auto-correlation of the deviatoric (i. e., traceless) part of the stress tensor, denoted by $\tilde{\sigma}$. In a lamellar phase with layers oriented perpendicular to a normal vector $\mathbf{n}$, the system stress can have a nonzero average uniaxial stress of the form $\tilde{\sigma} = \sigma_0(n_in_j - \delta_{ij}/3)$, in which σ_0 is a slight tensile or compressive stress arising from any mismatch between the actual layer spacing and the preferred layer spacing at which the tensile stress vanishes. Such a mismatch will generally arise because the periodic boundary conditions only allow lamellar alignment along specific directions, none of which may allow the formation of a structure with a spacing exactly equal to the preferred spacing. Formation of a

persistence stress of this form yields a plateau of magnitude $G(t) = V\sigma_0^2/15k_{\mathrm{B}}T$ as $t \to \infty$ in the stress inferred from (4.25).

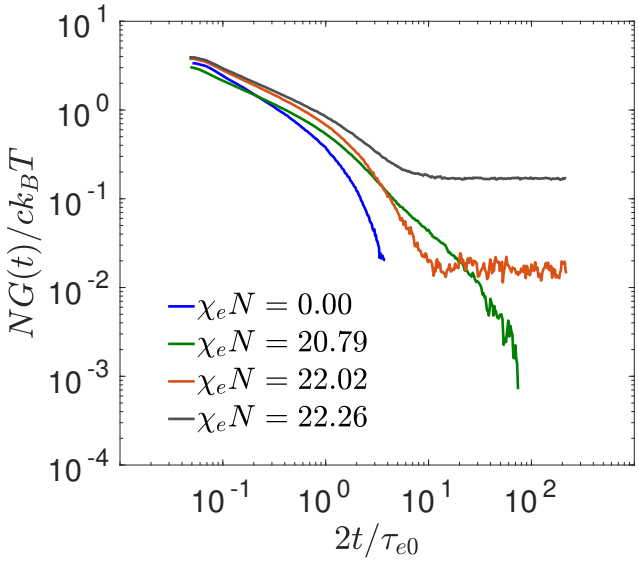

Figure 4.30: Normalized stress relaxation response, $NG(t)/ck_{\mathrm{B}}T$ for chains of length $N = 16$ over a range of values of $\chi_e N$ that includes the order-disorder transition at $(\chi_e N)_{ODT} = 21.72$. Measurements of $G(t)$ in samples that have spontaneously ordered show an elastic plateau at long times.

Weak Correlation Regime: Rouse Model

Figure 4.31 shows a comparison of Rouse model predictions to results for $G(t)$ in the limit $\chi_e N = 0.0$, corresponding to a hompolymer melt. In this comparison, the time constant τ_1 was taken to be equal to the terminal relaxation time τ_{e0} obtained from an independent measurement of the end-to-end autocorrelation function $E(t)$. For a homopolymer, excellent agreement with the Rouse model is obtained with no adjustable parameters.

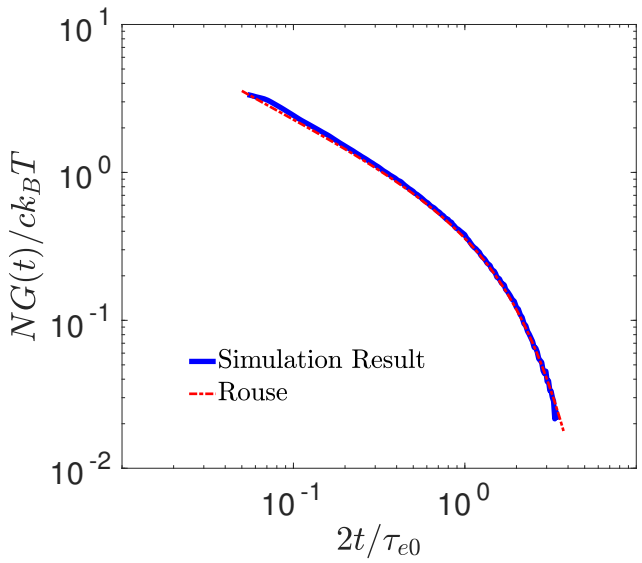

Figure 4.31: Normalized relaxation modulus $NG(t)/ck_BT$ vs. normalized time for chains of $N = 16$ beads at $\chi_e N = 0.00$, corresponding to homopolymers. Simulation results shown by red dotted line. Rouse model predictions computed using $\tau_1 = \tau_{e0}$ are shown by solid blue line.

Figures 4.32, 4.33, and 4.34 show fits of the Rouse model to results obtained at relatively low values of $\chi_e N$ =0.00, 4.21, 8.94, and 13.97(α =0.00, 1.00, 2.00, 3.00), in which the stress relaxation time $\tau_R = \tau_1/2$ has been adjusted to fit these data. The fits yield values of τ_1 that increase slightly with increasing $\chi_e N$, giving $\tau_1/\tau_{e0} =$ 1.051, 1.259, and 2.123 at $\chi_e N = 4.21$, 8.95, and 13.97, respectively. Allowing adjustment of τ_R is found to be sufficient to fit this data for the first three values of $\chi_e N = 0.0$, 4.21 and 8.94 for which $\chi_e N < 10$. For $\chi_e N = 13.97$, however, we can see an additional shoulder in $G(t)$ beginning to appear at long times, near the end of the range of times shown here.

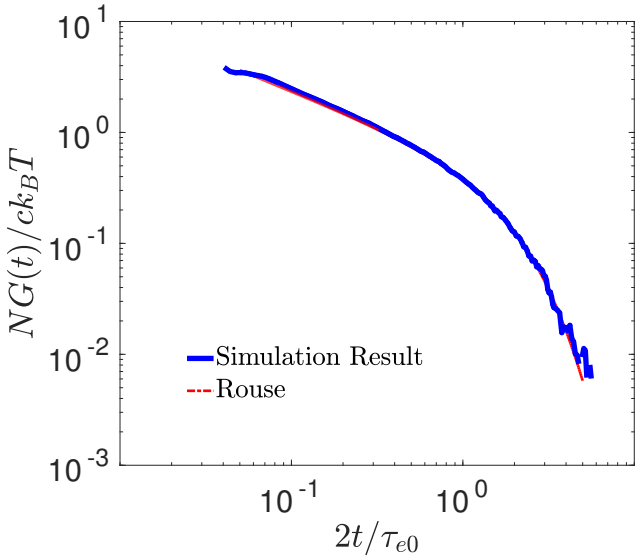

Figure 4.32: Normalized relaxation modulus $NG(t)/ck_{\mathrm{B}}T$ vs. normalized time for symmetric diblock copolymers chains of $N = 16$ beads at $\chi_e N = 4.17$ ($\alpha = 1.0$). Simulation results shown by red dotted line. A fit to the Rouse model computed using τ_R as the only fitting parameter is shown by solid blue line.

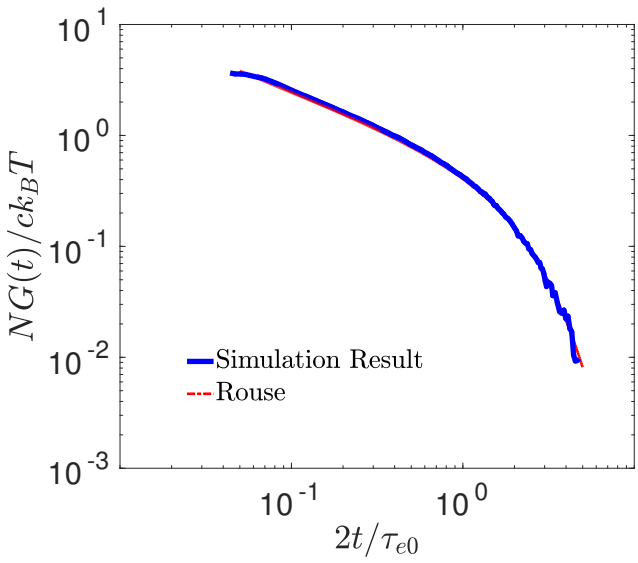

Figure 4.33: Normalized relaxation modulus $NG(t)/ck_{\mathrm{B}}T$ vs. normalized time for symmetric diblock copolymers chains of $N = 16$ beads at $\chi_e N = 8.75$ ($\alpha = 2.0$). Simulation results shown by red dotted line. A fit to the Rouse model computed using τ_R as the only fitting parameter is shown by solid blue line.

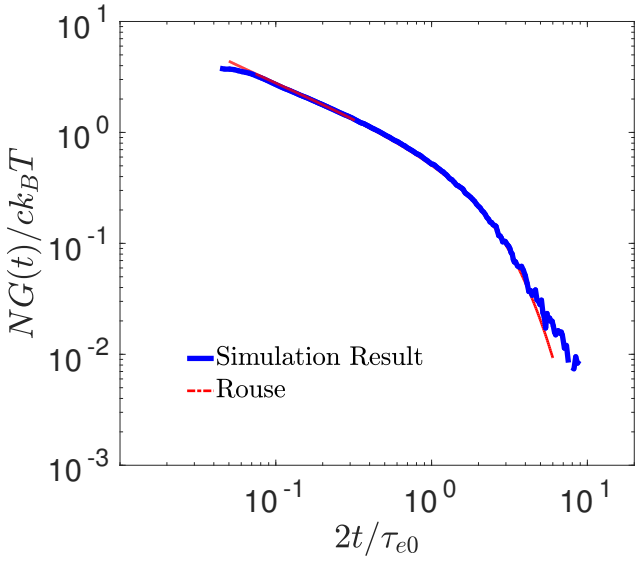

Figure 4.34: Normalized relaxation modulus $NG(t)/ck_{\mathrm{B}}T$ vs. normalized time for symmetric diblock copolymers chains of $N = 16$ beads at $\chi_e N = 13.50$ ($\alpha = 3.0$). Simulation results shown by red dotted line. A fit to the Rouse model computed using τ_R as the only fitting parameter is shown by solid blue line.

The shoulder in $G(t)$ at long times becomes more pronounced as $\chi_e N$ increases, causing the attempt to fit the data with a Rouse model to fail closer to the ODT. This can be seen in Figure 4.35, where we show a failed attempt to fit results for $G(t)$ at $\chi_e N = 18.35$ by the Rouse model.

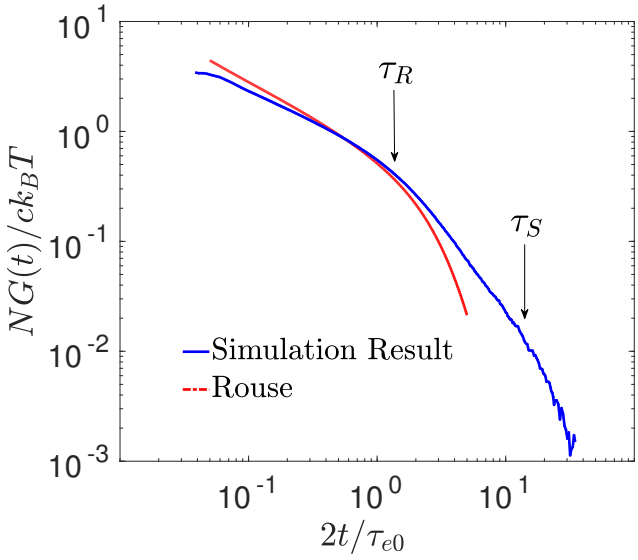

Figure 4.35: Normalized relaxation modulus $NG(t)/ck_{\rm B}T$ vs. normalized time for symmetric diblock copolymers chains of $N = 16$ beads at $\chi_e N = 18.35$ ($\alpha = 4.0$). Simulation results shown by red dotted line. The blue line shows an unsuccessful attempt to fit this data to the Rouse model using τ_R as an adjustable parameter.

The time constants associated with the two shoulders in $G(t)$ differ by an order of magnitude at $\chi N = 18.35$ ($\alpha = 4.0$), and seem to grow further apart as we increase χN. The presence of the second shoulder can be understood as a result of the appearance of transient well-segregated domains in the disordered melt. Upon exerting an external strain, a diblock copolymer melt with strong composition fluctuations reacts in two stages. First, individual molecule relax relative to an essentially fixed composition profile, which provides the chemical potential landscape for individual chains. Over a somewhat longer period of time, collective motion of many chains leads to relaxation of the composition profile. This relaxation of composition fluctuations is directly measured by $S(q,t)$, and is complete only at times longer that the longest structural relaxation time τ_S obtained in measurements of $S(q,t)$. This picture suggests that the terminal viscoelastic relaxation time should be given by τ_S, in agreement with our results. Therefore, we assume that the initial decay and the first shoulder in $G(t)$ is related to molecular relaxations in a system of

nearly constant composition field, and the second shoulder is caused by relaxation of residual stress associated with the slower relaxation of composition fluctuations.

Strongly Correlated Regime: Theory

Upon increasing $\chi_e N$, the main new feature of viscoelastic behavior near the ODT is the appearance of a slowly decaying shoulder in $G(t)$, in addition to the more rapidly decaying shoulder observed at lower values of χN. The appearance of this feature in $G(t)$ is consistent with the appearance of a corresponding low-frequency shoulder in the frequency dependent storage modulus $G'(\omega)$ in experiments on disorder diblock copolymers near the ODT. Near the ODT, the disordered phase is characterized by long lived composition fluctuations. Relaxation of these composition fluctuations is characterized most directly by $S(q,t)$, which yields a terminal structural relaxation time τ_S much longer than the time required for relaxation of individual chains in a fixed environment. When a strongly correlated diblock copolymer melt is subjected a macroscopic strain, relaxation of stress and $G(t)$ thus proceeds in two stages: First, over a time comparable to τ_{e0}, the distribution of conformations of individual chains relaxes to a state of local equilibrium in a nearly constant composition landscape. Over somewhat longer times, the composition field itself re-equiibrates, with a terminal time similar τ_S. The component of the stress that persists to long times is the stress of a system in which chains are in local equilibrium in an evironment defined by a more slowly evolving composition field.

In an attempt to model this slowly decaying component of the stress, we have compared our simulation results to a variant of the Fredrickson-Larson model (FL) of low-frequency stress relaxation [90]. The original derivation of this model was presented in the frequency domain, by considering an oscillatory strain and using the response to compute $G'(\omega)$ and $G''(\omega)$. Because we use the model here in the time domain, to predict $G(t)$, we begin by outlining a derivation of the FL theory in the time domain.

Fredrickson-Larson theory in the Time Domain: The Fredrickson-Larson theory attempts to describe linear viscoelastic behavior at long times or low frequencies in a

melt of very long diblock copolymer near the ODT. It assumes that the instantaneous stress in this regime can be approximated by the stress generated from a quasi-equilibrium free energy $F[\hat{\psi}]$ that is a functional of the slowly relaxing composition field. The functional $F[\hat{\psi}]$ is further approximated by a harmonic approximation

$$\frac{F[\hat{\psi}]}{Vk_{\rm B}T} \simeq \frac{1}{2}\int \frac{d^3q}{(2\pi)^3} S_{eq}^{-1}(q)|\hat{\psi}(q)|^2 \quad , \tag{4.31}$$

where $S_{eq}(q)$ is the equilibrium structure factor. The quasi-equilibrium stress arising from this free energy can be computed using the principle of virtual work, by computing the change in free energy induced by an affine deformation of the composition field. This yields a stress given to within an isotropic component by

$$\sigma_{ij}(t) = -k_{\rm B}T \int \frac{d^3q}{(2\pi)^3} q_i q_j \frac{dS_{eq}^{-1}(q)}{d(q^2)} \delta S_{ne}(\mathrm{q},t) \quad , \tag{4.32}$$

as given in Eq. (2.12) of Ref. [90], in which we use $S_{ne}(\mathbf{q})$ to denote the equilibrium value of the static structure factor, and

$$\delta S_{ne}(\mathbf{q},t) = S_{ne}(\mathbf{q},t) - S_{eq}(\mathbf{q}) \tag{4.33}$$

to denote the deviation of the instantaneous $S_{ne}(\mathbf{q},t)$ static structure factor from this equilibrium value. The subscript "ne" on the symbols $S_{ne}(\mathbf{q},t)$ and $\delta S_{ne}(\mathbf{q},t)$ denotes "non-equilibrium", which is used to indicate that $S_{ne}(\mathbf{q},t)$ is the instantaneous non-equilibrium value of the static structure factor

$$S_{ne}(\mathbf{q},t) = \langle|\hat{\psi}(\mathbf{q},t)|^2\rangle/V \tag{4.34}$$

evaluated at time t after a step strain. The subscript is needed to distinguish this quantity from the equilibrium dynamic structure factor $S(q,t)$ measured in Sec. 4.5, which is instead given by the equilibrium autocorrelation function $S(q,t) = \langle\hat{\psi}^*(\mathbf{q},t)\hat{\psi}(\mathbf{q},0)\rangle/V$.

To describe relaxation after a step strain, the function $\delta S_{ne}(\mathbf{q},t)$ is assumed to

decay exponentially with time t after a step strain, giving

$$\delta S_{ne}(\mathbf{q},t) = \delta S_{ne}(\mathbf{q},0^+)e^{-2t/\tau(q)} \quad . \tag{4.35}$$

Here, $\delta S_{ne}(\mathbf{q},0^+)$ is the deviation immediately after a step deformation, and $\tau(q)/2$ is a wavenumber dependent decay time. The time scale $\tau(q)$ that appears in (4.35) is taken to be equal to the relaxation time of the equilibrium dynamic structure factor $S(q,t)$ measured in Sec. 4.5. The prediction that the relaxation time $\tau(q)/2$ for the relaxation of the non-equilibrium structure factor is half the relaxation time $\tau(q)$ of the correlation function $S(q,t)$ follows from a linear stochastic model in which each Fourier amplitude $\hat{\psi}(\mathbf{q})$ behaves like an overdamped Brownian harmonic oscillator with a decay rate $1/\tau(q)$. Such a model generically gives a decay rate for quantities such as $S_{ne}(\mathbf{q},t)$ that are quadratic in the oscillator amplitude that is twice the decay time of the oscillator amplitude, or of the associated equilibrium auto-correlation function. This is also the reason that, in the Rouse model, the stress component associated with each Rouse mode decays with a decay time half of that seen in the corresponding contribution to the end-to-end autocorrelation time.

The initial deviation $\delta S_{ne}(\mathbf{q},t=0)$ caused by a small amplitude step deformation is computed by assuming an affine deformation of the equilibrium distribution. We consider a deformation characterized by a strain tensor γ, in which a material element at $\mathbf{r}$ is displaced to $\mathbf{r}+\gamma\mathbf{r}$. Assuming that $S_{ne}(\mathbf{q}) = S_{eq}(\mathbf{q})$ prior to the deformation yields

$$\delta S_{ne}(\mathbf{q},0^+) = 2\frac{dS_{eq}(q)}{d(q^2)}\sum_{ij} q_j q_i \gamma_{ij} \quad . \tag{4.36}$$

To compute the resulting stress σ_{ij}, we must combining Eqs. (4.32), (4.35) and (4.36). After defining a unit vector $\hat{\mathbf{q}} = \mathbf{q}/q$, where $q = |\mathbf{q}|$, and explicitly carrying out averages over orientation of the unit vector $\hat{\mathbf{q}}$, we obtain a stress $\sigma(t) = G(t)[\gamma + \gamma^T]$ characterized by a modulus

$$G(t) = \frac{2k_{\rm B}T}{15}\int \frac{d^3q}{(2\pi)^3}\left[q^2\frac{d\ln S_{eq}(q)}{dq^2}\right]^2 e^{-2t/\tau(q)} \tag{4.37}$$

or, equivalently,

$$G(t) = \frac{k_B T}{15\pi^2} \int_0^\infty dq\, q^2 \left[q^2 \frac{d \ln S_{eq}(q)}{dq^2} \right]^2 e^{-2t/\tau(q)} \tag{4.38}$$

Rouse/ Fredrickson-Larson Theory: The FL theory was intended to describe the behavior of $G(t)$ or $G^*(\omega)$ at very long times, or low frequencies in diblock copolymer melts with $\overline{N} \gg 10^4$ very close to the ODT. The theory assumes the existence of a large separation between the terminal structural relaxation time τ_S and time required for local equilibration of chain conformations. It was never intended to be used to describe the behavior of $G(t)$ at early times or low or intermediate values of $\chi_e N$. The simulation data shown here includes data over a wide range of values of time and $\chi_e N$, in which the separation between the terminal structural relaxation time and the shorter time for chain equilibration never exceed more than about one order of magnitude. We know that the behavior observed at low and intermediate values of $\chi_e N$ is well described by a Rouse model in which we treat the terminal Rouse time as an adjustable parameter. It appears likely that the first feature in the behavior observed near the ODT might also be reasonably well described by a Rouse like contribution. Because the Fredrickson-Larson model assumes local equilibration of the distribution of chain conformations in a slowly evolving composition lanscape, it cannot describe the Rouse-like relaxation of $G(t)$ at early times that occurs even in systems near the ODT, and would yield qualitatively incorrect behavior at all times if applied without modification to systems with lower values of $\chi_e N$.

In order to combine the realistic aspects of the Rouse and Fredrickson-Larson models, we propose an approximation for $G(t)$ as a sum

$$G(t) = G_R(t) + \delta G_{FL}(t) \tag{4.39}$$

in which $G_R(t)$ is a contribution that is computed using the Rouse model with an adjustable terminal time scale, and in which $\delta G_{FL}(t)$ is the difference between the prediction of the FH model at the value of $\chi_e N$ of interest and that at $\chi_e N = 0$.

More explicitly,

$$\delta G_{FL}(t) = G_{FH}(t, \chi_e N) - G_{FH}(t, \chi_e N = 0) \tag{4.40}$$

where $G_{FH}(t, \chi_e N)$ denotes the FL prediction for $G(t)$ at a specified value of $\chi_e N$, and $G_{FH}(t, \chi_e N = 0)$ represents the corresponding prediction for a homopolymer, with $\chi_e N = 0$. By construction, this model reduces to a Rouse model in the homopolymer limit $\chi_e N = 0$, and always contains a Rouse-like feature at early times. In addition, the model yields a contribution $\delta G_{FL}(t)$ for which both the magnitude and long decay time increase gradually with increasing $\chi_e N$, which becomes important only at relatively high values of $\chi_e N$.

Strongly Correlated Regime: Analysis of Simulations

Figure 4.36 shows a comparison of simulations results at $\chi_e N = 19.17$ to predictions of the Rouse / Fredrickson-Larson model for chains of $N = 16$ beads. The only adjustable parameter in this comparison is the terminal Rouse relaxation time $\tau_R = \tau_1/2$ used in the Rouse contribution to the model, for which we used $\tau_1/\tau_{e0} = 1.34$. Both the magnitude and time dependence of the contribution $\delta\delta G_{FL}(t)$ that produces the second shoulder has been predicted using information obtained from measurements of the intermediate structure factor $S(q, t)$. This theory yields a prediction for the behavior of $G(t)$ near the second shoulder in which the terminal time is and functional form of the time dependence is predicted correctly, but in which the magnitude of $G(t)$ is slightly large in this region, by a nearly constant multiplicative factor.

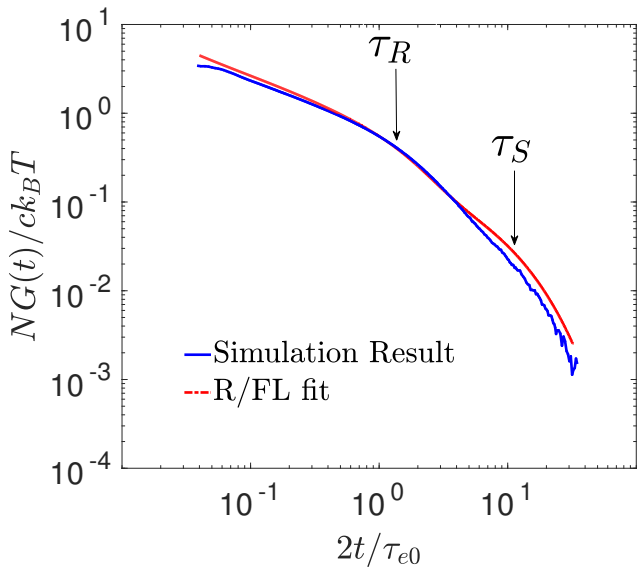

Figure 4.36: Comparison of the normalized stress relaxation modulus $NG(t)/ck_{\rm B}T$ to predictions of the Rouse/Fredrickson-Larson model, for chains of $N = 16$ beads at $\chi_e N = 18.35$ ($\alpha = 4.00$). The indicated value of τ_S was obtained from independent measurements of $S(q,t)$. The terminal Rouse stress relaxation time τ_R in the Rouse contribution $G_R(t)$ has been treated as an adjustable parameter, for which we used $\tau_R = \tau_1/2$ and $\tau_1/\tau_{e0} = 1.34$.

Figure 4.37 shows a similar comparison of results for $G(t)$ at $\chi_e N = 20.79$ to predictions of the Rouse/ Fredrickson-Larson model described above. The model again predicts somewhat too large a value for $G(t)$ in the vicinity of the second shoulder.

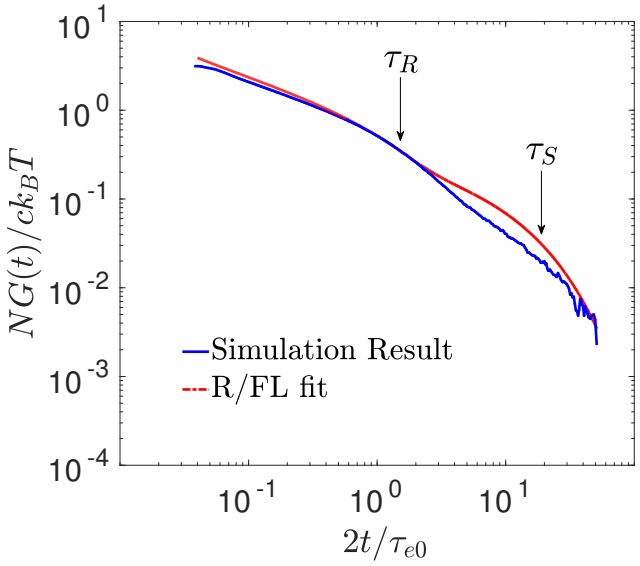

Figure 4.37: Comparison of the normalized stress relaxation modulus $NG(t)/ck_{\rm B}T$ to predictions of the modified Fredrickson-Larson model, for chains of $N = 16$ beads at $\chi_e N = 20.79$ ($\alpha = 4.5$). The terminal Rouse relaxation time in the Rouse contribution $G_R(t)$ has been treated as an adjustable parameter, for which we have used $\tau_R = \tau_1/2$ and $\tau_1/\tau_{e0} = 1.47$.

Figures Figure 4.38 and Figure 4.39 show the results of a somewhat *ad hoc* modification of the Rouse / Fredrickson-Larson model in which we have simply replaced the original theory by a sum of the form

$$G(t) = G_R(t) + \lambda \delta G_{FL}(t), \tag{4.41}$$

in which the contribution $\delta G_{FL}(t)$ arising from composition fluctuations is simply multiplied by an arbitrary factor λ whose value is chosen to fit the data. A value of $\lambda = 2/3$ was used to generate both Figure 4.38 and Figure 4.37, using the same value of λ for both values of $\chi_e N$. The fact that this modified theory fits the data reasonably well shows that the prediction of the time dependence of the fluctuation contribution is consistent with our simulation results for $G(t)$, even though the unmodified theory predicts slightly too large a magnitude for the slowly decay-

ing shoulder. More specifically, the comparison shows that the simulation data is consistent with the existence of a terminal rheological time equal to $\tau_S/2$.

Our results show that the Rouse / Fredrickson-Larson model slightly overpredict the magnitude of $G(t)$ in the long time regime in which stress is controlled by relaxation of composition fluctuations. Because the theory is based on several approximations, it is not entirely clear which approximation is the main source of this discrepancy. One possibility is that the error may be primarily a consequence of the limitations of the harmonic approximation for the free energy functional that is used here to compute stress. This expression for the stress is being applied here to states near the ODT in which composition fluctuations are known to be quite strong, and in which anharmonic contributions to the free energy are thus potentially important. The fact that the model is based on measured values of the relaxation times $\tau(q)$ inferred from the relaxation of $S(q,t)$ appears, however, to allow it make meaningful predictions about the spectrum of relaxation times in $G(t)$.

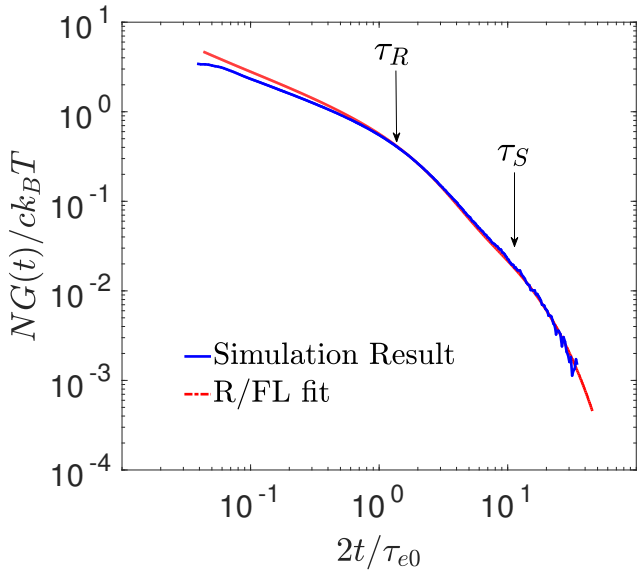

Figure 4.38: Comparison of the normalized stress relaxation modulus $NG(t)/ck_BT$ for a melt with $N = 16$ and $\chi_e N = 18.35(\alpha = 4.00)$ to predictions of the modified Fredrickson-Larson model of Eq. (4.41), using a prefactor $\lambda = 2/3$.

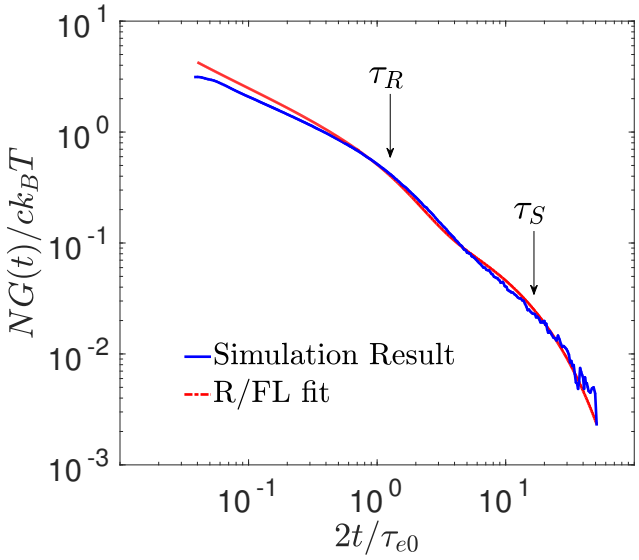

Figure 4.39: Comparison of the normalized stress relaxation modulus $NG(t)/ck_BT$ for a melt with $N = 16$ and $\chi_e N = 20.79$ to predictions of the modified Fredrickson-Larson model of Eq. (4.41), using $\lambda = 2/3$.

4.7 Conclusions

Simulations of simple bead-spring models have been used to single-chain properties (tracer diffusion, end-to-end autocorrelation), the dynamic structure factor $S(q,t)$, and the linear viscoelastic stress relaxation modulus $G(t)$ in the disordered phase of a symmetric diblock copolymer, and to characterize how these dynamical properties change with changes in the segregation parameter χN.

These dynamical properties (like equilibrium properties) behave somewhat differently in a regime in a weakly-correlated parameter regime in which $\chi N < (\chi N)_{ODT}^{SCFT}$ and in strongly correlated regime in which $(\chi N)_{ODT}^{SCFT} < \chi N < (\chi N)_{ODT}$, where $(\chi N)_{ODT}^{SCFT} = 10.5$ is the value at which SCFT predicts an ODT, and $(\chi N)_{ODT}$ denotes the value at the observed ODT for a system of finite $\overline{N}$. In the weakly correlated regime $(\chi N) < (\chi N)_{ODT}^{SCFT}$, where effects of composition fluctuations are small, all of the measured dynamical properties are reasonably well described by

a Rouse model, with an effective friction coefficient that is almost independent of χN. In the strongly correlated regime closer to the ODT, all dynamical properties show evidence of the formation of increasingly strongly segregated transient microdomains. The effects of composition fluctuations show up much more strongly in some measured quantities than in others.

The effect of composition fluctuations upon tracer diffusivity is relatively weak. In the two systems studied here, the value of the diffusion coefficient at the ODT was 0.55-0.65 of its value in the homopolymer state, at $\chi N = 0$. A reduction of approximately this magnitude would be expected in a system of unentangled chains, even if the formation of microdomains were to constrain chains to follow interfaces between A and B domains as the result of relatively free diffusion along AB interfaces within a bicontinuous structure.

Composition fluctuations have a somewhat larger effect on the relaxation of the end-to-end vector. In the strongly correlated regime, the end-to-end autocorrelation function $E(t)$ shows evidence of a two-stage relaxation. The rate of initial relaxation is similar to that seen in the homopolymer and is assumed to represent the relaxation of chains to a state of local equilibrium in a nearly fixed composition landscape. The relaxation time τ_e associated with the final relaxation reaches a value at the ODT that is 6-7 times the value obtained in the homopolymer for the two systems studied here. A somewhat larger fractional increase is observed for shorter chains, which reach a somewhat higher level of local segregation before crystallizing into a lamellar phase. Because the time scale τ_e is significantly slower than the terminal time for the relaxation of composition fluctuations at the ODT (discussed below), we speculate that final relaxation of $E(t)$ may occur in part via diffusion of chains along interfaces between domains in a more slowly evolving composition landscape.

The time dependence of the dynamic structure factor $S(q,t)$ can be described reasonably well as a single-exponential decay at wavenumbers similar to or less than the peak wavenumber q^*. Near the ODT, the relaxation time $\tau(q)$ at wavenumber q exhibits a peak at q^*. We have analyzed the relationship between $\tau(q)$ and the static structure factor $S(q)$ in terms of a phenomenological Langevin equation in which the relationship between the relaxation rate $\tau(q)^{-1}$ and the free energy gradient driving

that relaxation is controlled by a wavenumber dependent diffusivity $D(q)$. This effective diffusivity (or inverse mobility) for composition modes of wavenumber q is a monotonically decreasing function of q that scales like the single chain diffusion coefficient, and depends on weakly on χN. The simplicity of the behavior of $D(q)$ suggests that an empirical correlation for $D(q)$ might be useful as the basis of a simple method of estimating $\tau(q)$ from knowledge of the static structure factor.

The stress relaxation modulus $G(t)$ was inferred measurements of spontaneous stress fluctuations, via the appropriate Green-Kubo relation. The behavior of $G(t)$ in the weakly-correlated parameter regime is very well described by the Rouse model of stress relaxation. Near the ODT, $G(t)$ exhibits a slowly decaying shoulder arising from stress that arises from the effect of strain upon slowly decaying composition fluctuations. The connection between this slowly decaying contribution to the stress and composition fluctuations is demonstrated more directly here than in experiments or previous simulations by showing that the terminal rheological relaxation time is indeed the same as the longest relaxation time τ_S obtained from independent measurements of $S(q,t)$.

Simulation results for $G(t)$ near the ODT are rather well described by a slightly modified variant of the Fredrickson-Larson theory of stress relaxation. The Rouse / Fredrickson-Larson model to which we compare is obtained by modifying the original Fredrickson-Larson model so as to guarantee that Rouse-like behavior is recovered at early times and low values of χN. This theory was then evaluated using independently measured values of the static structure factor $S(q)$ and $\tau(q)$ as inputs. The main deficiency of the resulting theory is that it predicts slightly too large a value for the magnitude of the slowly decaying shoulder in $G(t)$. We suggest that this may reflect a limitation of the harmonic approximation for the free energy functional that underlies expression for the stress in the Fredrickson-Larson theory.

The work presented here provides both a relatively simple description of the behavior of $S(q,t)$ from knowledge $S(q)$, in terms of an effective diffusivity $D(q)$ that we have characterized empirically, but have not attempted to predict from first principles. This work also provides partial validation of a theory that predicts $G(t)$ from knowledge of $S(q,t)$. Taken together, these results provide a method

of estimating expected linear viscoelastic properties in unentangled symmetric diblock copolymers from knowledge of homopolymer viscosities (to calibrate friction coefficients) and the static structure factor $S(q)$.

Chapter 5

Order-Disorder Transitions and Free Energies in Asymmetric Diblock Copolymers

Abstract: Simulations of simple bead-spring models of asymmetric diblock copolymers are used to study the dependence of order-disorder transitions and free energies upon the invariant degree of polymerization $\overline{N}$. Well-tempered metadynamics is used to determine values of $(\chi N)_{ODT}$ along the lamellar-disorder, and hexagonal-disorder transitions, where χ is an effective Flory-Huggins interaction parameter, N is the degree of polymerization, and $(\chi N)_{ODT}$ is a value of χN at the order-disorder transition(ODT). Equivalent results for both phase boundaries and free energies are obtained for a pair of systems with different numbers of beads per chain but matched values of the invariant degree of polymerization $\overline{N}$, in agreement with the corresponding states hypothesis. A comparison of results for $(\chi N)_{ODT}$ with several different values of $\overline{N}$ over a range $0.25 \geq f \leq 0.5$ of values of the fraction f of beads in the minority block show the expected systematic decrease of $(\chi N)_{ODT}$ with increase $\overline{N}$, consistent with an approach to the self-consistent field pre-

diction as $\overline{N} \to \infty$. Results for the free energy per chain in the disordered and hexagonal phases of systems with $f = 1/4$ show that SCFT gives rather accurate predictions for the free energy in the ordered hexagonal phase, but that the random-mixing approximation underlying SCFT significantly overestimates the free energy of the disordered phase.

5.1 Introduction

Diblock copolymers melts can undergo an order-disorder transition (ODT) from a disordered state to any of several periodically ordered phases upon changing temperature. [18, 3] The resulting ordered structures can include lamellar, hexagonal, gyroid, and spherical structures, depending on the composition of the copolymer (i.e., the relative sizes of the two blocks). Recent simulations by our research group of the lamellar-disorder transition of symmetric AB diblock copolymers, with A and B blocks of equal length, have yielded significant improvements in quantitative understanding of the ODT for this particular case. The present chapter extends this work by using similar techniques to quantify the location of order-disorder transitions and the behavior of the free energy for asymmetric AB copolymers over a range of values of the invariant degree of polymerization.

Theoretical understanding of the ODT transition is based on a combination of self-consistent field theory (SCFT) [23] and theories that attempt to take into account effects of composition fluctuations that are ignored by SCFT [22, 40]. Throughout what follows, we consider AB diblock copolymers with a degree of polymerization N with an A block containing fN monomers, and equal statistical segment lengths for both monomer types. SCFT predicts that the ODT for such a system should occur when the product χN exceeds a critical value $(\chi N)_{ODT}$ that depends on the composition(f) of the diblock copolymer, where χ is an effective Flory-Huggins interaction parameter. SCFT has been shown to accurately predict the nature and sequence of the preferred ordered phases in copolymer melts [23], and appears to give reasonably accurate predictions for the locations of transitions

between ordered phases, but gives much less accurate predictions for the value of $(\chi N)_{ODT}$ for order-disorder transitions in systems containing polymers with typical experimental molecular weights [96, 18, 21]. The quantitative inaccuracy of SCFT predictions for ODTs is known to be primarily a result of the effects of strong composition fluctuations in the disordered phase in the vicinity of the order-disorder transitions[18]. The Fredrickson-Helfand theory [22] of the ODT of symmetric copolymers and the related renormalized-one loop (ROL) theory of correlations [40] suggest that the magnitude of resulting corrections to SCFT predictions $(\chi N)_{ODT}$ is controlled by the magnitude of the invariant degree of polymerization $\overline{N}$, with stronger fluctuation effects for smaller $\overline{N}$. These theories suggest that the value of $(\chi N)_{ODT}$ should depend on both f and $\overline{N}$, and should approach the SCFT predictions in the limit $\overline{N} \to \infty$.

Simulations of simple coarse-grained models of block copolymer melts have been performed by many authors over several decades. Most of the early simulations were lattice Monte Carlo simulations [97, 98, 13, 91, 99]. Some properties of these materials are much easier to measure in simulations than others. Properties of the disordered phase are particularly amenable to simulation, and were the focus of much of the earliest simulation work [97, 13, 91]. Simulations of properties of ordered phases must contend with the need to assure that the dimensions of the periodic unit cell used in the simulations are commensurate with the natural domain spacing of the ordered phase. This problem has been largely solved in continuum bead-spring simulations of the lamellar phase by the use of flexible unit cells with dimensions that can adjust in response to anisotropic stress components. The accuracy of simulations that attempt to identify the order-disorder transition by straightforward simulation of spontaneous crystallization and melting is limited by the existence of hysteresis, and are also complicated by effects of incommensurability between the simulation unit cell and the preferred domain size of the ordered phase. Precise identification of the location of transitions between different ordered phases poses a particularly severe problem for particle-based simulations that, in our opinion, has not yet been solved.

Most simulations that have attempted to identify order-disorder transitions have

relied on the study of spontaneous crystallization and melting, using a variety of methods to identify the appearance of periodic order. Fried and Binder gave an estimate of the location of the lamellar-disorder by identifying the transition with a drastic slow-down of the relaxation time for composition fluctuations[13]. Other studies have relied on identification of a discontinuity in the average value of a thermodynamic property (e.g., in the energy arising from contact between unlike A and B pairs), or the appearance of a spike in the heat capacity [100]. A transition can also be identified, somewhat more directly, by a discontinuous change in the structure factor and the appearance of a Bragg peak[101, 102]. Vassiliev and Matsen introduced a collective variable that is sensitive to the appearance of long-range spatial correlations.[103].

Several studies have used more sophisticated methods to identify order-disorder transitions that reduce or eliminate the problems caused by hysteresis. Mueller et al., used thermodynamic integration to identify the order-disorder transition[104]. de Pablo et al. identified the lamellar-disorder transition by calculating the excess chemical potential in the disordered and the lamellar phases of diblock copolymers[105]. Beardsley and Matsen relied on a parallel tempering technique. [106] Most recently Glaser, Medapuram, and coworkers [45] introduced the use of well-tempered metadynamics (WTMD) method to very precisely identify the lamellar-disorder transition of symmetric diblock copolymers. The WTMD method of Glaser et al. is used here to identify both lamellar-disordered and hexagonal-disordered transitions.

A few authors have previously mapped out the dependence order-disorder transitions on volume fraction f for asymmetric chains of fixed total length. Matsen and coworkers have mapped out the phase diagram of an FCC lattice model for chain of $N = 30$ monomers with $\overline{N} \simeq 230$ [107, 106]. Escobedo et al. used molecular dynamics polymeric models to sketch an approximate phase diagram by studying the spontaneous formation of different phases over a wide range of composition and χN [108]. We are not aware of any previous systematic study of the dependence of the value of $(\chi N)_{ODT}$ on $\overline{N}$ for asymmetric polymers.

Until recently, it has been difficult to quantitatively compare results of coarse-grained simulations to theoretical predictions, or to compare results of different sim-

ulation models to one another, because of the absence of an adequate operational definition of the Flory-Huggins χ parameter. A partial solution to this problem was provided in recent work by our research group that introduced an improved method of estimating the χ parameter in simple simulation models [42, 45]. This method of estimating χ relies on a combination of thermodynamic perturbation theory and fitting of simulation results for the structure factor in disordered melts of the symmetric copolymer to predictions of the ROL theory. The resulting estimates of χ have been shown to be accurate enough to allow consistent results to be obtained from a variety of different simulation models of symmetric diblock copolymers. Studies of correlations in the disordered phase in asymmetric diblock copolymers have also shown that this estimate of χ yields consistent results when applied to analogous models of asymmetric copolymers. [52]

Simulations by Glaser, Medapuram and coworkers [42, 45] have demonstrated that thermodynamic properties of symmetric copolymers exhibit a universal dependence on the state parameter χN and $\overline{N}$. Specifically, this work showed for symmetric copolymers that $(\chi N)_{ODT}$ at the ODT is a universal function of $\overline{N}$, and that the free energy per chain is a universal function of χN and $\overline{N}$, and quantitatively characterized these properties.

In this chapter, we use simulation and analysis techniques similar to those of Glaser et al. to study the order-disorder transitions and thermodynamic properties of asymmetric AB copolymers. We focus here on bead-spring models with structurally similar A and B monomers, which thus have equal A and B statistical segment lengths, in which the A and B blocks contain different numbers of monomers. In this case, the principle of corresponding states suggests that thermodynamic properties should exhibit a universal dependence on f, as well as χN and $\overline{N}$. The main results presented in this chapter are: (1) a study of the dependence of $(\chi N)_{ODT}$ upon f along the lamellar-disordered and hexagonal-disordered phase boundaries for two models (D1-32 and D3-32) with different values of $\overline{N} = 480$ and 1920, and (2) a detailed study of the dependence of the free energy upon χN and $\overline{N}$ at a single value of $f = 1/4$ for which the melt undergoes a hexagonal-disordered transition.

The work presented in this chapter does not include any estimates of the location of the gyroid-disorder transition, nor any estimate of the range of compositions over which such a transition exists. The results for the lamellar-disorder and hexagonal-disorder transitions presented here instead include results obtained in a range of values of f in which the gyroid phase is presumably stable, and in which the lamellar-disorder and hex-disorder transitions are transitions between metastable states that would not be observed in an experiment. Precise identification of the gyroid-disorder transition was found to pose unique technical difficulties, which I have chosen to discuss in a separate chapter of this thesis, Chapter 6.

5.2 Simulation Methodology

All simulation results presented here were obtained from constant temperature, constant pressure (NPT) molecular dynamics simulations of simple bead-spring models of diblock copolymer melts. Equilibrium domain spacings in the ordered lamellar and hexagonal phases were determined using constant pressure simulations in flexible unit cells in which the unit cell dimensions adjust to create a state of isotropic stress. Locations of lamellar-disordered and hexagonal-disordered transitions were determined using the well-temperated metadynamics method of Glaser et al.

Models

The bead-spring simulation models reported in this study all have harmonic bond potential

$$V_{bond}(r) = \frac{1}{2}kr^2 \tag{5.1}$$

That acts between neighboring monomers in each chain, where κ is a spring constant. All monomers interact via non-bonded pair potential similar to that used in dissipative particle dynamics (DPD), in which the interaction between a pair of

beads of types i and j of the form

$$V_{ij}(r) = \frac{1}{2}\epsilon_{ij}\left(1 - \frac{r}{\sigma}\right)^2 \quad , \tag{5.2}$$

where σ is a range of interaction and ϵ_{ij} is an interaction energy parameter. The parameters $\epsilon_{AA} = \epsilon_{BB}$ are set fixed to a fixed value $\epsilon_{AA} = 25k_{\mathrm{B}}T$, while the difference $\alpha = \epsilon_{AB} - \epsilon_{AA}$ is varied to control the level of incompatibility between the A and B beads.

Well-Tempered Metadynamics

Following Glaser et al. , we use well temperature metadynamics (WTMD) to identify order-disorder transitions. Well-tempered metadynamics is an adaptive biasing technique that allows sampling of rare states in molecular dynamics simulations. WTMD simulations used forces that are defined as derivatives of a modified Hamiltonian

$$H(\Psi) = H_0 + V(\Psi, t) \tag{5.3}$$

In which H_0 is the unmodified physical Hamiltonian of the system of interest, and $V(\Psi)$ is a biasing potential that is a function of an appropriate collective variable Ψ. The potential evolves over the course of the simulation in a manner that tends to raise the value of $V(\Psi, t)$ at values of Ψ that have been visited previously[109].

The choice of an appropriate collective variable is of crucial importance in the successful application of metadynamics. The variable introduced by Glaser et al. , which we denote here by Ψ_4, is given by a generalized n-norm of the form

$$\Psi_n \equiv \left[\sum_{\mathbf{q}} |A(\mathbf{q})|^n f(|\mathbf{q}|)\right]^{1/n} \tag{5.4}$$

with $n = 4$. The sum over $\mathbf{q}$ in this expression is a sum over all wavevectors that are commensurate with the periodic simulation unit cell, and $A(\mathbf{q})$ is a normalized Fourier amplitude of the composition field $\psi(\mathbf{r}) = [c_A(\mathbf{q}) - c_B(\mathbf{q})]/2$. The function

$f(|\mathbf{q}|)$ is a smooth cut-off function that is chosen to suppress high wave-number contributions with $|\mathbf{q}| > q^*$. In a system containing M chains of N monomers with monomer positions $\mathbf{r}_1, \mathbf{r}_2, \ldots,$, the Fourier amplitude $A(q)$ is given by the ratio

$$A(\mathbf{q}) = \hat{\psi}(\mathbf{q})/MN \tag{5.5}$$

where

$$\hat{\psi}(\mathbf{q}) = \frac{1}{2}\sum_{i=1}^{MN} \epsilon_i e^{i\mathbf{q}\cdot\mathbf{r}_i} \tag{5.6}$$

in which $\epsilon_i = \pm 1$ is an index for which $\epsilon_i = +1$ for beads of type A and $\epsilon_i = -1$ for beads of type B. The exponent $n = 4$ was chosen because the corresponding collective variable Ψ_2 (the Euclidean norm, or 2-norm) was found to have very similar values in the disordered and lamellar phase at the ODT. The use of a larger integer $n = 4$ yields a greater difference between values of Ψ_n obtained in these two phases.

The results of a WTMD simulation yield an estimate of the constrained free energy $G(\Psi_4)$ as a function of the value of collective variable Ψ_4. Figure 5.1 shows an example of the resulting free energy $G(\Psi_4)$ obtained for a simulation of a slightly asymmetric copolymer ($f = 14/32$) that undergoes a lamellar-disorder transition, at a value of α very near the value at the ODT.

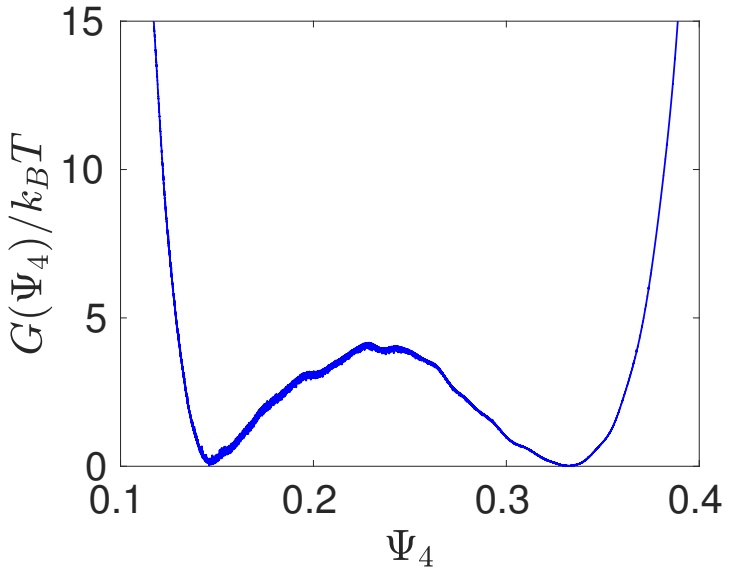

Figure 5.1: The constrained Gibbs free energy $G(\Psi)$ obtained from a well-tempered metadynamics simulation of model D1-32, with $\overline{N} = 960$, for $f = 14/32$ near the lamellar-disorder transition. This simulation has been performed at $\alpha = 2.365$. The simulation has been performed at constant temperature and pressure in a cubic simulation box with an average dimension of 30.52 with a total of 85280 particles inside the simulation box.

The probability density for the Ψ_4 is given by the exponential

$$P(\Psi_4, \alpha) \propto e^{-G(\Psi_4,\alpha)/kT} \quad . \tag{5.7}$$

We define the transition to be the value of α at which the regions associated with the two minima in $G(\Psi_4)$ yield equal contributions to the integral $\int P(\Psi_4, \alpha) d\Psi_4$. Results of simulations that are performed at a value of α near but not exactly at the ODT can be extrapolated slightly using a first order expansion

$$G(\Psi, \alpha + \delta\alpha) \simeq G(\Psi, \alpha) + \frac{\partial G}{\partial \alpha}\delta\alpha \tag{5.8}$$

in which the required first derivative is evaluated using the identity

$$\frac{\partial G(\Psi_4, \alpha)}{\partial \alpha} = \frac{\langle U_{AB} \rangle_{\Psi_4}}{\epsilon_{AB}} \tag{5.9}$$

where $\langle U_{AB} \rangle_{\Psi_4}$ denotes an average of the energy arising from interactions between A and B monomers, averaged over the subensemble of states with a constrained value of Ψ_4, and where $\epsilon_{AB} = \epsilon_{AA} + \alpha$.

Though the order parameter Ψ_4 was originally developed by Glaser et al. in order to study the lamellar-disorder transition, we show here that it works almost equally well as an identifier for the hexagonal-disordered transition. We show in the next chapter that this order parameter is not effective for the purpose of identifying the gyroid-disorder transition in a relatively small simulation unit cell.

Lamellar-Disordered Transition

Symmetric and slightly asymmetric diblock copolymers undergo a transition from a disordered phase to a lamellar phase upon increasing α, or upon (typically) decreasing temperature in an experiment. In what follows, we report results for the value of α along the lamellar-disorder transition, denoted by α_{ODT}, for models D1-32 and D3-32 for chains with $0.375 < f < 0.500$. The methods that we use to identify the lamellar-disorder transition are similar to those used previously by Glaser et al. , and are summarized here for completeness.

The first step in our procedure for identifying the ODT for a particular model is to perform a sequence of NPT simulations of the lamellar phase in a flexible simulation cell in order to determine the dependence of the equilibrium layer spacing on α. The initial state in each such simulation is an artificially induced lamellar state containing three layers aligned perpendicular to the unique axis of a flexible tetragonal unit cell. We create this state by creating generating a random, disordered state and then running a short simulation in which monomers are subjected to a periodic external field that acts differentiates A and B monomers, and is designed to segregate A and B monomers into different layers. Simulation with a flexible

unit cell and no external potential are then performed at several values of α. These simulations use a tetragonal unit cell with dimensions $a \times a \times c$ in which the two independent dimensions a and c can fluctuate independently, under the control of a barostat that imposes the same pressure in each direction. This geometry allows the unit cell dimensions to adjust to create a unit cell in which the average domain spacing is equal to its preferred value, which we denote by d^*. By performing such simulations over a range of values of α near and slightly above the expected value of α_{ODT}, we thus obtain an estimate of how the preferred domain spacing $d^*(\alpha)$ in the lamellar phase varies with α. Simulations in which α is chosen to below α_{ODT} melt into a disordered phase, thus giving an initial estimate of α_{ODT}.

Figure 5.2 shows a comparison of several different results or predictions for the value of a preferred wavevector q^* in simulations of model D1-32 with $f = 12/32 = 0.375$, over a wide range of values of α. The red squares show values of $q^* = 2\pi/d^*(\alpha)$ obtained from the simulations of the lamellar phase in a flexible tetragonal unit cell, as described above. The blue circles denote values wavenumber q^* at which the structure factor is maximum in the disordered phase, obtained using a fit. The asterisk shows the value of α at the ODT, which is 2.72 for this system. The dotted brown line and dashed green line represent predictions of SCFT for the value of q^* in the ordered lamellar and gyroid phases at this composition. These SCFT predictions have been calculated by computing the wavenumber corresponding to the primary peak in a relaxed unit cell over a range of values of χN, using the value of b for this model to convert to units with $\sigma = 1$, and using the empirical relation for $\chi(\alpha)$ obtained for this model to plot the results as functions of α. Note that the values of q^* obtained in the ordered and disordered phase extrapolate to almost the same value at the ODT, indicating the transition is almost perfectly epitaxial. Also note that the values of q^* for the lamellar and gyroid phase are quite close near the ODT, and are both about 2 % lower than the value of q^* at the ODT obtained from simulations.

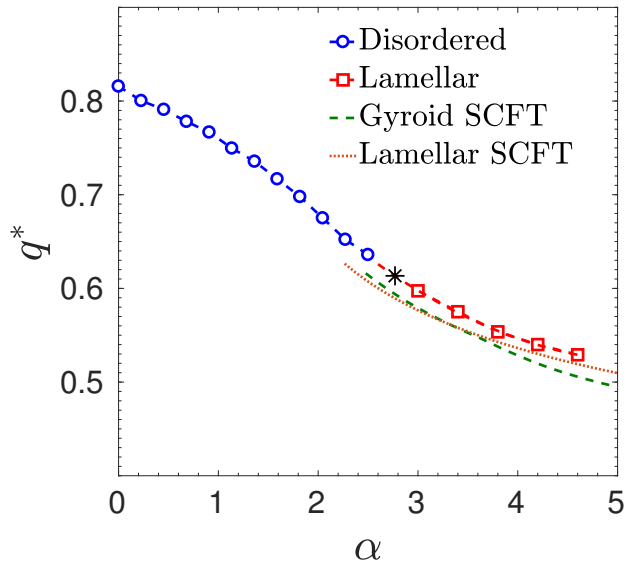

Figure 5.2: Values of q^* vs. α for model $D1-32$ at $f = 0.3750$. Blue circles show values of the wavenumber q^* at which the structure factor is maximum in simulations of the disordered phase. Red squares represent values of the primary Bragg peak $q^* = 2\pi/d$ obtained from the relaxation of three-layered lamellar structure in a tetragonal NPT-ensemble simulation box. The brown dotted and green dashed lines are the SCFT predictions for the magnitude of the primary Bragg peak in lamellar and gyroid systems at corresponding values of χN.

As the next part of our procedure, we perform simulations of spontaneous melting and crystallization in a cubic unit cell to obtain an improved estimate of α_{ODT}. For this purpose, we perform two sets of simulations at a set of values of α near our best estimate of α_{ODT}, in which one set of simulations is initialized with a disordered phase, and the other is initialized with an artificially induced lamellar phase. Both sets of these simulations are performed in a cubic cell in which the number of chains has been chosen to yield dimensions equal to three times our best estimate of the equilibrium layer spacing $d(\alpha_{ODT})$. We use a cubic $L \times L \times L$ box for a disordered phase because the dimensions of the simulation box fluctuate wildly in the disordered phase with a tetragonal unit cell with two independent dimensions. Therefore, leading to results in which the volume remains nearly constant but the shape can

vary from needle-like to pancake like states in which one or more dimension becomes very small. For simulations performed at low values of α, both initial states lead to a disordered final state, while at higher values of α, both initial states yield a final lamellar state. Near the equilibrium ODT, there is often also a narrow range of values of α in which the system exhibits hysteresis, such that initially disordered simulations remain disordered and initially ordered simulations remain ordered for tens of millions of MD steps. The value of α in the center of this hysteresis region is used as an updated estimate of α_{ODT}. This updated estimate of α_{ODT} is combined with extrapolation of our results for $d(\alpha)$ from simulations in a flexible unit cell to define a corresponding updated estimate of the equilibrium domain spacing at the ODT, $d(\alpha_{ODT})$.

Spontaneous crystallization or melting of lamellar order is easily identifiable either by visualizing the final state of the simulation or by inspecting the structure factor $S(q)$. Fig. 5.3 shows a comparison of results for the structure factor $S(q)$ obtained in simulations of the disordered phase and a lamellar phase of a system with $f = 0.4375$ at equal values of $\alpha = 2.39$, which is a value within the hysteresis region in which both disordered and lamellar are metastable. Both simulations were carried out in systems for which the unit cell was designed to accommodate three layers of the lamellar phase. The structure factor for the lamellar phase exhibits a Bragg peak that, for a system of this size, is approximately thirty times greater than the value of $S(q)$ at the maximum of the structure factor for a disordered structure.

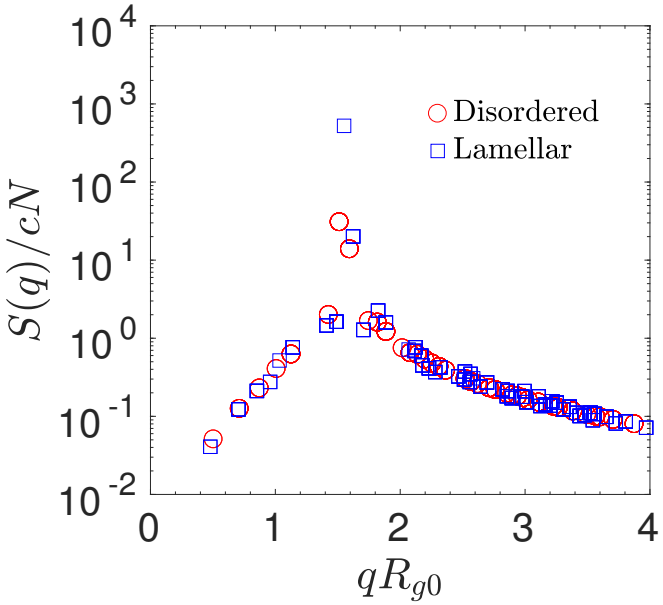

Figure 5.3: The structure factor results obtained for a lamellar phase and a disorder phase for model $D1-32$ with $f = 0.4375$ at the same value of $\alpha = 2.39$. Open red circles show results for $S(q)$ in the disordered phase, and blue squares represent results obtained in the lamellar phase. The disordered phase simulation has been performed in a cubic simulation cell of the size of 31.17σ. This simulation of the lamellar phase was performed in a flexible tetragonal box, with layers oriented perpendicular to the unique c axis. Results for $S(q)$ are averaged over wavevectors that are related by symmetry, assuming cubic point-group symmetry in the disordered phase and tetragonal symmetry in the ordered phase.

As the last stage of our determination of α_{ODT}, we perform a constant pressure WTMD simulation in a cubic $L \times L \times L$ simulation cell. The number of chains in this simulation is chosen to accommodate three layers of a lamellar structure at the ODT, such that the average of the cell dimension L is equal to three times our best estimate of $d(\alpha_{ODT})$. The results of WTMD simulations give a very accurate estimate of α_{ODT} for the selected system size. The resulting estimate of α_{ODT} is then combined the results for the function $d(\alpha)$ obtained from simulations with a flexible tetragonal unit cell to compute a refined estimate of $d(\alpha_{ODT})$. If the resulting value of $d(\alpha_{ODT})$ differs from the value obtained in WTMD simulations, this estimate is used to refine our estimate of the required number of chains, and

WTMD simulations are repeated until values of α_{ODT} from two iterations agree to within 1%. One iteration after the first is usually sufficient to achieve this.

Hexagonal-Disordered Transition

The procedure used here to identify the hexagonal-disorder transition for more asymmetric copolymers is closely analogous to that described above for the lamellar-disorder transition. Our procedure for identifying the hexagonal-disorder transition requires a combination of simulations in a flexible unit cell in order to determine the relationship between unit cell size and α, simulations of spontaneous melting and crystallization in approximately commensurate unit cell in which the ratio of unit cell dimensions are held fixed, and WTMD simulations in a simulation cell with fixed ratios of cell dimensions.

The simulation unit cell used to determine the equilibrium domain size for the hexagonal phase is an orthorhombic cell designed to contain four layers of cylinders in which each layer contains three cylinders. In a hexagonal phase in which the distance between nearest neighbor cylinders is denoted by D, with cylinders aligned parallel to the c axis, this gives a simulation cell of dimensions $a \times b \times c$ with $a = 3D$ and $b = 2\sqrt{3}D$. An example of the initial state used in simulations of artificially seeded hexagonal phase is shown in Fig. 5.4. Simulations used to determine the equilibrium domain spacing used an orthorhombic unit cell, in which the dimensions a, b and c can fluctuate independently, but converge to a structure in which the distance between nearest neighbors is equal in all directions.

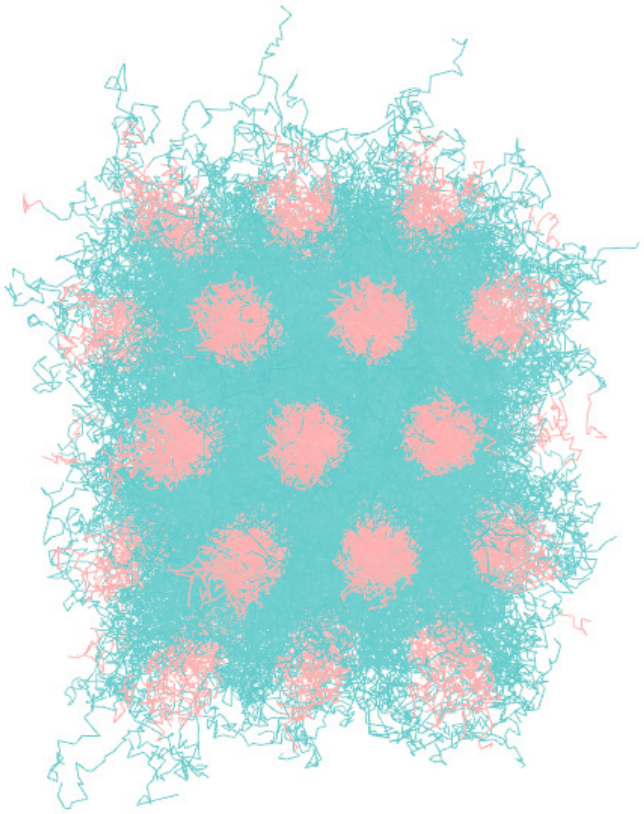

Figure 5.4: An example of the simulation unit cell used in simulations of the hexagonal phase.

Simulations of spontaneous melting of initially ordered states and spontaneous melting of initially disordered states were performed in a unit cell in which a fixed ratio $a/b = \sqrt{3}/2$ was imposed on the two directions perpendicular to the cylinder axes. The hexagonal and disordered states are easily distinguished by inspecting the structure factor. Fig. 5.2 shows a comparison of results for the structure factor $S(q)$ in the disordered and hexagonal phase of model D1-32 with $f = 0.3125$ at a value of $\alpha = 3.12$ in which both phases remain metastable. The appearance of a six Bragg peak is discernible a simulation cell of this size. This primary peak represents scattering from the six wavevectors that are related by symmetry. The magnitude of difference between the magnitudes of the Bragg peaks and the magnitude of $S(q^*)$

in the disordered phase is less for the hexagonal phase than for the lamellar phase, because of the spreading of the mean-square intensity over six primary peaks in the hexagonal phase, rather than over 2 primary peaks in the lamellar phase.

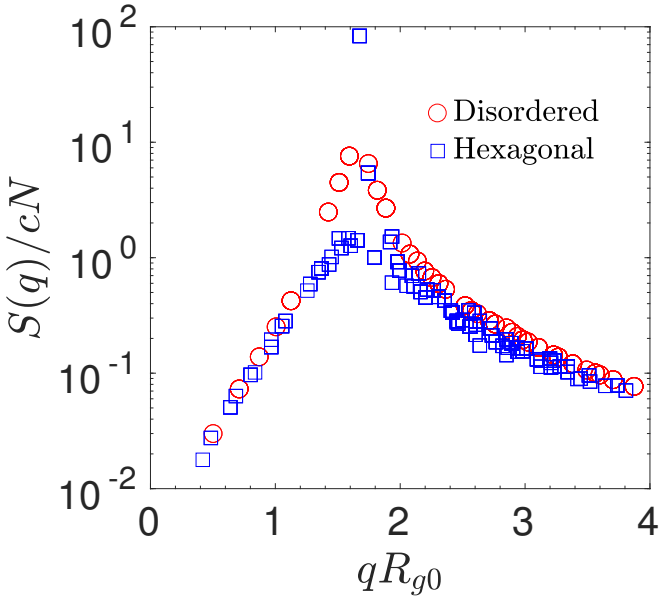

Figure 5.5: The structure factor results obtained for hexagonal and disordered phase of a system with $f = 10/32 = 0.3125$ at equal values of $\alpha = 3.12$ near the ODT. Red circles show results obtained in the disordered phase, while blue square show results in the ordered hexagonal phase.

Fig. 5.6 shows results for the free energy $G(\Psi_4)$ as a function of the order parameter Ψ_4 for a system with $f = 10/32$ that undergoes a hexagonal-disorder transition, which was obtained in a simulation with a nearly commensurate box at a value of α near α_{ODT}. Applying WTMD with the same collective variable, Ψ_4, to the study of hexagonal forming structures produces free energy landscape very similar that obtained for the lamellar-disorder transition of lamellar-forming structures. There are still two minima in the free energy landscape, one corresponding to the ordered hexagonal structure and the other corresponding to the disordered phase. The most probable value of the collective variable Ψ_4 corresponding to the hexagonal structure is equal to a value of $\Psi_4 = 0.22$ that is significantly smaller than the value of $\Psi_4 = 0.33$ obtained for a lamellar phase, but is sufficiently well separated from

the value in the disordered phase to allow two minima to be clearly distinguished. There also exists a clear barrier separating the hexagonal phase minimum and the disordered phase minimum. Despite this quantitative difference, the WTmetaD collective variable originally designed for lamellar structure also works well to identify the hexagonal-disorder transition.

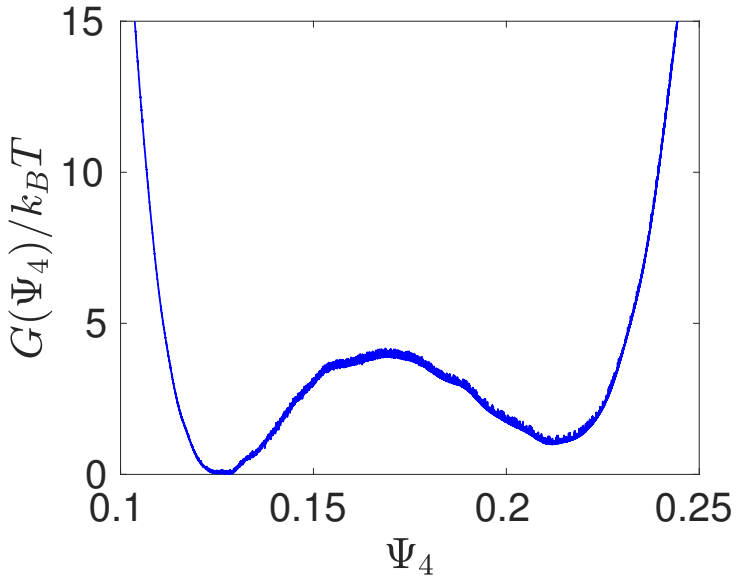

Figure 5.6: The constrained Gibbs free energy of $G(\Psi)$ of a simulation of model D1-32, with $\overline{N} = 960$, for $f = 10/32$ near hexagonal-disorder transition. The simulation box has the dimensions of $(29.18, 39.91, 34.61)$ with the total of 120896 particles inside the simulation box

5.3 Phase Boundaries

Fig. 5.7 summarizes our results for values of α_{ODT} for model D1-32 along the lamellar-disordered and hexagonal-disordered phase boundaries over the range $0.1875 \geq f \leq 0.5$ over which we have performed simulations for this model. Analogous results for model D3-32 are show in Figure 5.8 In each of these figures, we only show the region $f_A \leq 1/2$ in which A is the minority component because the other half of the phase map is related to this region by symmetry. Results for numerical values of

α and $\chi_e N$ at the ODT are tabulated for both models in Tables 5.1 and 5.2. The calibration developed for symmetric diblock copolymers to convert values of α to corresponding values of χ_e.

In model D1-32 found that a metastable lamellar phase could be created near the ODT only for chains with $N_A \geq 11$, or $11/32 \leq f_A \leq 1/2$, and that a hexagonal phase could be created only for $N_A \leq 11$. The only system for which we could identify both a metastable lamellar-disorder and a hexagonal-disorder transition was the system with $N_A = 11$, or $f_A = 0.34375$, for which the values of α_{ODT} along these two metastable boundaries are almost equal. A simulation that was performed with a lamellar initial state at composition $f = 10/32 = 0.3125$ were instead found to transform spontaneously into a distorted hexagonal structures. Simulations performed with a hexagonal initial state at composition $f = 12/32 = 0.3750$ were found to undergo a spontaneous transformation into a lamellar structure. Results for the value of α at the hex-disordered and lamellar-disordered were nearly equal at $f = 11/32$, indicating that the two (metastable) phase boundaries intersect near this composition.

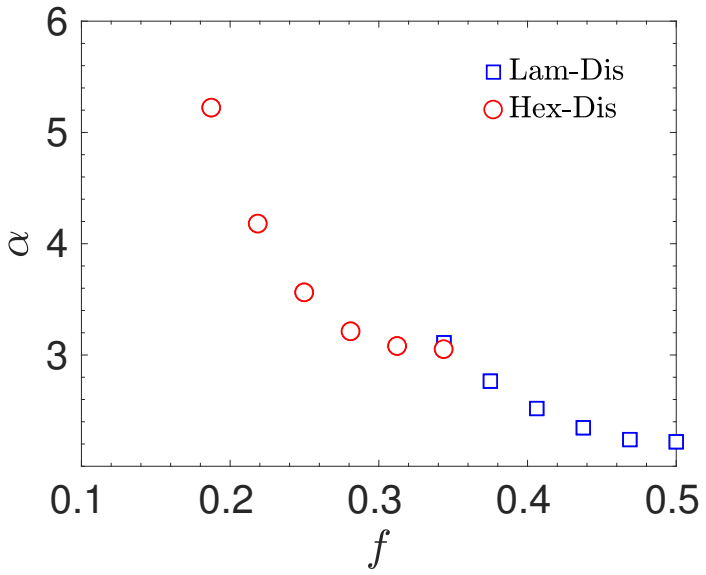

Figure 5.7: Values of α along the hexagonal-disordered transition (red circles) and lamellar-disordered transition (blue squares) plotted vs. f for model D1-32, for which $\overline{N} = 480$.

Similar results were obtained for model D3-32, with an intersection of the hexagonal-disorder and lamellar-disorder transition lines at a value of f slightly greater than $f = 11/32$, as shown in Figure 5.8.

The simulations that we used to determine these phase boundaries used unit cells that were carefully designed to be commensurate with a particular orientation of either the hexagonal or lamellar phase, and were thus designed to favor formation of a particular phase. Because the resulting unit cells were not commensurate with the preferred dimensions of a gyroid phase, we did not expect and did not observe spontaneous formation of a gyroid phase in these simulations. At compositions near $f = 11/32$ where the lamellar-disorder and hexagonal-disorder transitions meet, these are presumably metastable transitions in a region in which the true equilibrium phase of an infinite system is a gyroid phase that melts at some slightly lower value of α_{ODT}.

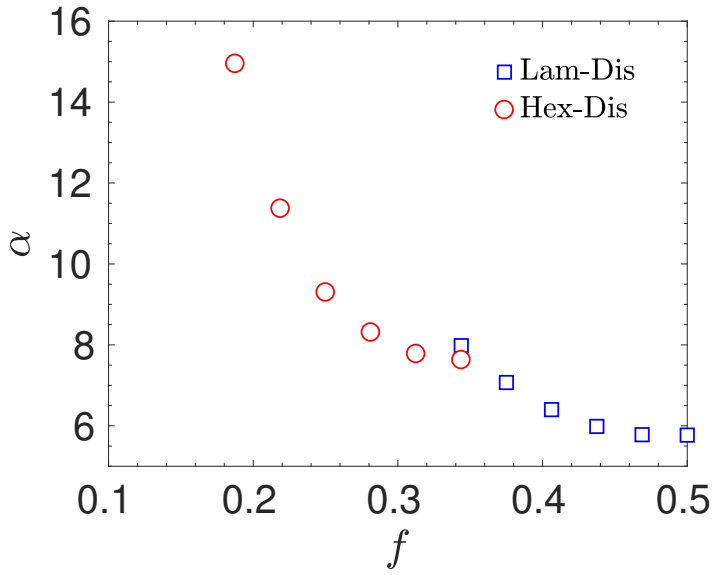

Figure 5.8: Values of α along the hexagonal-disordered transition (red circles) and lamellar-disordered transition (blue squares) plotted vs. f for model D3-32, for which $\overline{N} = 1920$.

f	Phase	α_{ODT}	$(\chi N)_{ODT}$
0.1875	HEX	5.22	48.66
0.2188	HEX	4.18	38.44
0.2500	HEX	3.56	32.42
0.2812	HEX	3.21	29.03
0.3125	HEX	3.08	27.76
0.3438	HEX	3.05	27.49
0.3438	LAM	3.11	28.07
0.3750	LAM	2.77	24.75
0.4062	LAM	2.52	22.41
0.4375	LAM	2.35	20.76
0.4688	LAM	2.24	19.76
0.5000	LAM	2.22	19.57

Table 5.1: The D1-32 Hexagonal-Disorder and Lamellar-Disorder transitions.

f	Phase	α_{ODT}	$(\chi N)_{ODT}$
0.1875	HEX	14.95	35.38
0.2188	HEX	11.37	28.37
0.2500	HEX	9.30	23.92
0.2812	HEX	8.31	21.68
0.3125	HEX	7.78	20.45
0.3438	HEX	7.63	20.10
0.3438	LAM	7.98	20.92
0.3750	LAM	7.07	18.77
0.4062	LAM	6.40	17.16
0.4375	LAM	5.98	16.14
0.4688	LAM	5.78	15.63
0.5000	LAM	5.77	15.61

Table 5.2: The D3-32 Hexagonal-Disorder and Lamellar-Disorder transitions.

Fig. 5.9 shows our results for both lamellar-disordered and hexagonal-disordered transitions for models D1-32 ($\overline{N} = 480$) and D3-32 ($\overline{N} = 1920$) plotted on map of χN vs. f. In this plot, our results are compared to earlier lattice Monte Carlo simulations of Beardsley and Matsen for $\overline{N} = 130$ and to SCFT predictions, which are expected to yield the limit $\overline{N} = \infty$. The most obvious and important feature of this graph is the fact that the order-disorder boundary shifts systematically to higher values of χN with decreasing $\overline{N}$ at all values of f. Strong correlations in the disordered phase reduce the free energy of the disordered phase relative to that predicted by SCFT, therefore postponing the order-disorder transition. The results appear to be consistent with the assumption that order-disorder line approaches the SCFT prediction for the ODT as $\overline{N} \to \infty$.

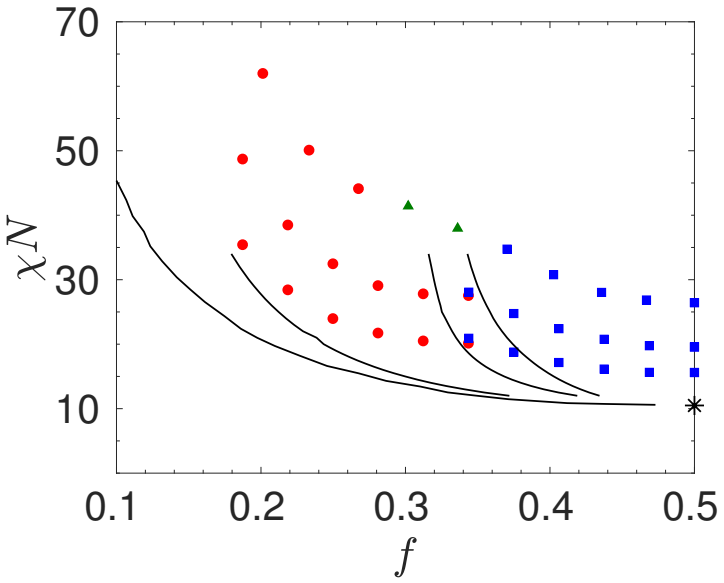

Figure 5.9: Comparison of simulation results for values of $(\chi N)_{ODT}$ (symbols) vs. f for three different simulation models with differing value of $\overline{N}$ to SCFT predictions (solid lines). Simulations results for $(\chi N)_{ODT}$ are shown for model D3-32 ($\overline{N} = 1920$), model $D1-32$ ($\overline{N} = 480$, and the lattice Monte-Carlo model of Beardsley and Matsen [106], for which $\overline{N} = 130$. Models with smaller values of $\overline{N}$ yield higher values of $\overline{N}$. Values for the two bead-spring models are shown for the lamellar-disorder (blue squares) and hexagonal-disorder transition (circle), even in the region near the intersection of the transitions where we expect a gyroid phase. Results of Beardsley and Matsen for the estimated location of the gyroid-disorder transition are shown as green triangles at the two compositions at which they observed such a transition. Solid lines represent SCFT predictions for the BCC-Dis, BCC-Hex, Hex-Gyr, and Gyr-Lam transitions, from left to right or bottom to top.

Note that the points at which the lamellar-disorder and hexagonal-disorder transitions for models D1-32 and D3-32 intersect appear to both lie within the region in which SCFT predicts a stable gyroid phase. If a gyroid phase exists and exhibits a direct gyroid-disorder transition, then the gyroid must be stable at the intersection of these two metastable phase boundaries. The fact that this point lies within the relatively narrow gyroid region predicted by SCFT is consistent with the evidence that SCFT yields more accurate predictions for free energies in ordered phases than in the disordered phase [45], and should thus yield much more accurate predictions

for order-order transitions than for order-disorder transitions. The results presented here suggest that the lamellar-gyroid and gyroid-hexagonal order transitions may lie rather close to the corresponding SCFT predictions, even when order-disorder transitions are shifted substantially by effects of composition fluctuations.

Fig. 5.10 shows the dependence of the value of χN at the ODT for a series of simulations of systems with a fixed value of $f = 1/4$ but widely varying values of $\overline{N}$. The SCFT prediction at $f = 1/4$ is $(\chi N)_{ODT} = 16.99$. The line through the data is an empirical fit through the data for which the functional form is constructed so as to approach the SCFT prediction as $\overline{N} \to \infty$. The results show that $(\chi N)_{ODT}$ is a smoothly decreasing function of $\overline{N}$, and are consistent with the assumption that $(\chi N)_{ODT}$ approaches the SCFT prediction as $\overline{N} \to \infty$.

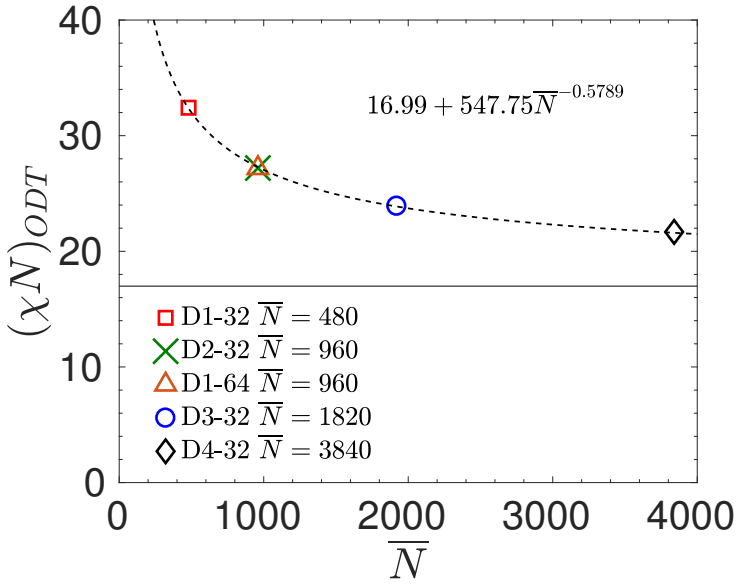

Figure 5.10: Variation of $(\chi N)_{ODT}$ with $\overline{N}$ for the hexagonal-disorder transition at $f = 1/4$. The black line shows an empirical fit through the simulation data points.

5.4 Free Energies at $f = 1/4$

In this section, we report a more detailed study of the dependence of the free energy per chain upon χN and $\overline{N}$ for systems with $f = 1/4$, which undergo a hexagonal-

disorder transition. We present results here for a sequence of models D1-32, D2-32, D3-32, and D4-32 that all have $N = 32$ beads per chain, but different values of $\overline{N} =$ 480, 960, 1920, and 3840, respectively. As a test of the principle of corresponding states, we also present results for a single pair of models, D2-32 and D1-64, that have different numbers of beads per chain (32 vs. 64) but matched values of $\overline{N} = 960$.

Let g denote the free energy per chain divided by $k_{\mathrm{B}}T$, or

$$g = G/MkT \quad , \tag{5.10}$$

where G is total Gibbs free energy, and M is the total number of chains in a system. The principle of corresponding states predicts that, for diblock copolymers chains with short-range interactions and enough beads to be modeled by a continuous random walk model, for systems with structurally similar A and B monomers, g should be given by a universal function

$$g = g(f, \chi_e N, \overline{N}) \tag{5.11}$$

of f, χN and $\overline{N}$ alone. Furthmore, g should approach the SCFT prediction for g in the limit $\overline{N} \to \infty$.

Let $g'(f, \chi_e N, \overline{N})$ denote the partial derivative

$$g'(f, \chi_e N, \overline{N}) \equiv \frac{\partial g(f, \chi_e N, \overline{N})}{\partial(\chi_e N)} \tag{5.12}$$

we can connect the quantity g' to properties that can be measured in a simulation by using identity

$$\frac{\partial g}{\partial \alpha} = \frac{1}{k_{\mathrm{B}}T} \frac{\langle U_{AB} \rangle}{M \epsilon_{AB}} \quad . \tag{5.13}$$

We use this identity to compute values of g in the disordered phase, relative to the free energy in a state with $\alpha = 0$ (a homopolymer) by performing a series of simulations at evenly spaced values of α, and performing a numerical integration, using Simpson's rule for integration. Values of g in the disordered phase can then be computed in the ordered phase by using the results of WTMD for the location of

the ODT and requiring that the free energies of the two phases match at the ODT. After computing g as a function of α, the results can then be plotted vs. $\chi_e N$ by using the empirical relation between χ_e and α that was obtained for each model by studying symmetric copolymers.

The value of the derivative g' at any value of α can be computed somewhat more directly by using Eq. 5.13 and the chain rule to show that

$$g'(f, \chi_e N, \overline{N}) = \frac{\partial g(f, \chi_e N, \overline{N})}{\partial(\chi_e N)} \tag{5.14}$$

$$= \frac{1}{k_{\mathrm{B}}T} \frac{\langle U_{AB} \rangle}{M \epsilon_{AB}} \left[N \frac{d\chi_e(\alpha)}{d\alpha} \right]^{-1} \quad . \tag{5.15}$$

This thermodynamic identity can be used to relate g' to the AB pair energy, and thus to the number of AB contacts per monomer, by using the nonlinear calibration of $\chi_e(\alpha)$. The derivative $\partial g / \partial \alpha$ is not expected to be a universal function, but the value of g' is expected to be a universal (i.e., model independent) function of f, $\chi_e N$, and $\overline{N}$, if evaluated using an accurate estimate of $\chi_e(\alpha)$.

Figs. 5.11 and 5.12 show SCFT predictions for the dependence of g and on χN for $f = 1/4$. At this composition, SCFT predicts a transition from the disordered phase to a BCC phase at $\chi N = 16.6$ and a transition from a BCC to hexagonal phase at $\chi N = 19.2$. At the relatively small values of $\overline{N} \simeq 500 - 4000$ used in our simulations, systems with $f = 1/4$ are instead expected to undergo a direct transition from the disordered to a hexagonal phase. SCFT predictions of free energies for the metastable disordered and hex phases become equal at $\chi N = 16.99$.

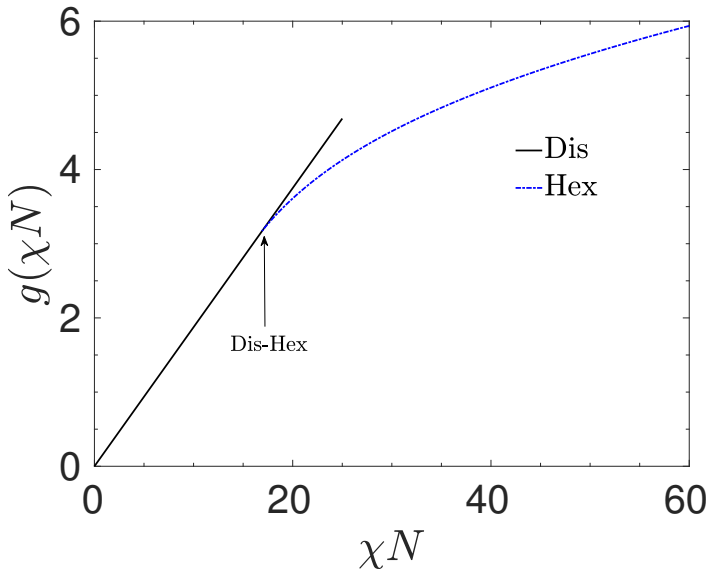

Figure 5.11: SCFT predictions for the free energy $g(\chi N)$ vs. χN for the disordered and hexagonal phases for systems with $f = 1/4$.

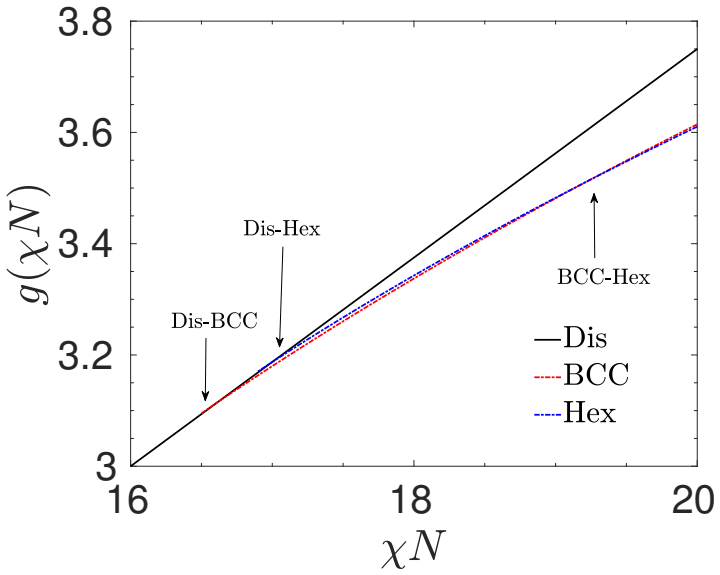

Figure 5.12: SCFT predictions for the free energy $g(\chi N)$ vs. χN for the disordered, BCC and hexagonal phases of systems with $f = 1/4$, shown over a relatively narrow range of values of χN that includes the disorder-BCC and BCC-Hex transitions.

Fig. 5.13 show SCFT predictions for the dependence of g' on χN for $f = 1/4$. The value of $g'(\chi N)$ predicted by SCFT is equal to the spatial average of the product $\phi_A(\mathbf{r})\phi_B(\mathbf{r})$. This yields a constant value of $g' = (3/4)(1/4) = 0.1875$ in the disordered phase, which is the horizontal line in Fig. 5.13. SCFT predicts a discontinuity in g' at the BCC-disorder transition, and then a smaller discontinuity (which is not visible in this graph) at the BCC-Hex transition.

Fig. 5.14 shows a comparison of simulation results for $g'(\chi N)$ for four different values of $\overline{N}$ for systems with $f = 0.25$ to SCFT predictions. The plot in the upper right, which shows results for systems with $\overline{N} = 960$, includes results for both models D2-32 and D1-64. The fact that essentially identical values of $g'(\chi N)$ are obtained for these models confirms that $g'(\chi N)$ is model-independent, in agreement the principle of corresponding states, and with results obtained earlier for symmetric copolymers [110, 45]. The first of two vertical lines in each plot is the SCFT prediction for the metastable hexagonal-disorder transition, while the second is the location of the actual hexagonal-disorder transition observed in the simulations.

The most striking feature of the comparison shown in Fig. 5.14 is the very close agreement between SCFT predictions for $g'(\chi N)$ in the hexagonal phase and the values measured in simulations of the hexagonal phase at corresponding values of χN. Simulation results for $g'(\chi N)$ in the disordered phase near the ODT are instead much lower than the value of $g' = 0.1875$ predicted by SCFT for the disordered phase, and are instead much closer to the value predicted by SCFT for the hexagonal phase. This behavior is consistent with that found previously for symmetric copolymers [110, 45].

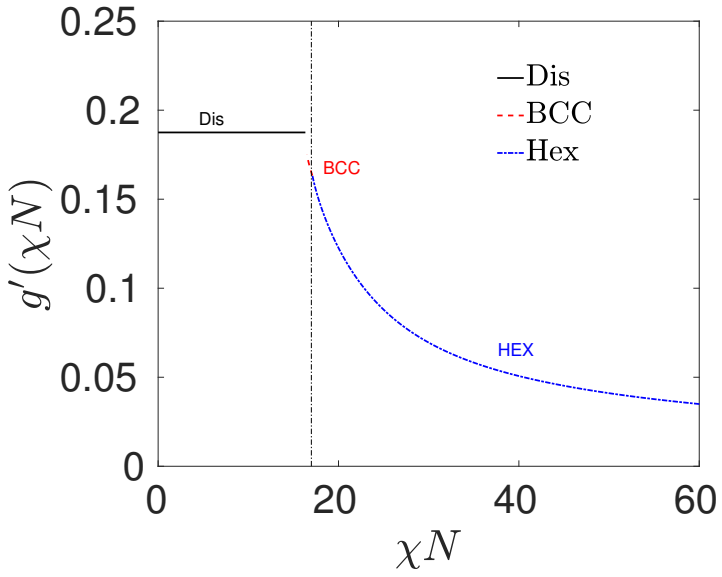

Figure 5.13: The SCFT theory prediction for g' is plotted versis χN for $f = 1/4$. The stable phase at each range of χN has been identified and plotted with a different color and line style.

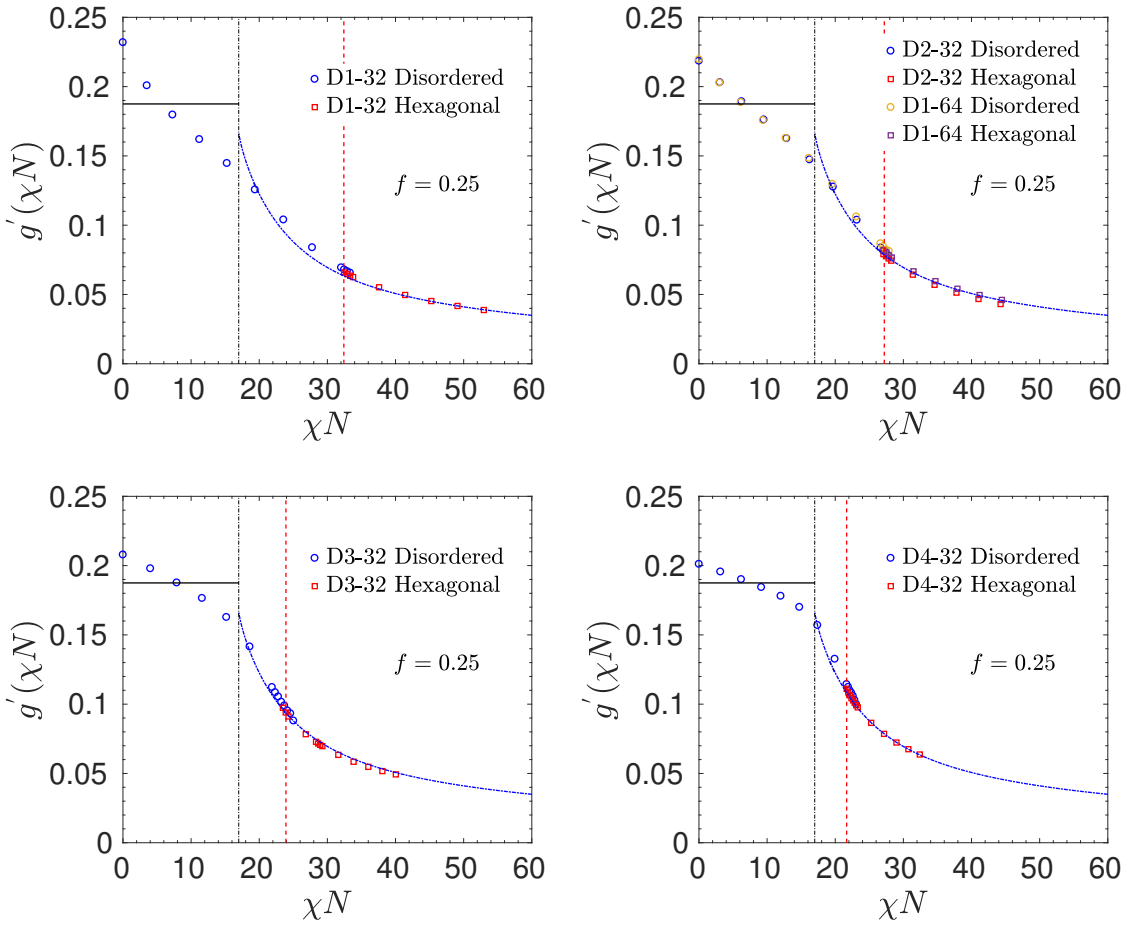

Figure 5.14: The Gibbs free energy derivative with respect to χN for different polymeric models with $\overline{N} = 480, 960, 1920, 3840$. Results are show for model D1-32 ($\overline{N} = 480$, upper left), models D2-32 and D1-64 ($\overline{N} = 960$, upper right), model D3-32 ($\overline{N} = 1920$, lower left) and D4-32 ($\overline{N} = 3840$, lower right). SCFT predictions for $g'(\chi N)$ are shown by solid lines. In the disordered phase, SCFT predicts a constant value of $g' = f(1-f) = 0.1875$. The vertical black dashed line shows the location of the SCFT prediction for the metastable hexagonal-disorder transition, at $\chi N = 16.99$. The vertical red dashed line shows the position of the actual ODT, as determined using well-tempered metadynamics.

Because the hexagonal-disorder transition is a first-order phase transition, values of the enthalpy per molecule and the related derivative g' are discontinuous across the transition. This slight discontinuity is too small to be easily visible in Fig. 5.14.

The magnitude of the difference $\Delta g' = g'_{Dis} - g'_{Hex}$ between the values of g' in the two phases at the ODT is shown as a function of $\overline{N}$ in Fig. 5.15. Fig. 5.16 instead shows the magnitude of the fractional change $\Delta g'/g'_{Hex}$ in the value of g' across the transition. The similarity of values of g' in the ordered and disordered phase suggests that the degree of local segregation is quite similar in the two phases. An analogous study of the lamellar-disordered transition of symmetric copolymers showed that both the disordered and ordered phases have well-segregated, nearly pure domains of A and B near the ODT over the experimentally relevant range of values of $\overline{N}$, creating structures in which contact between A and B monomers occurs primarily along interfaces between A and B domains. In this regime, the fractional change $\Delta g'/g'_{Hex}$ can be interpreted as a fractional decrease in the amount of interfacial area per unit volume when the system crystallizes into a hexagonal phase. Over the range of values studied here, this ratio appears to have a nearly constant value of 3-4 %, which is about half as large as the fractional change of 6-7% found for the lamellar-disordered transition of symmetric copolymers [110, 45].

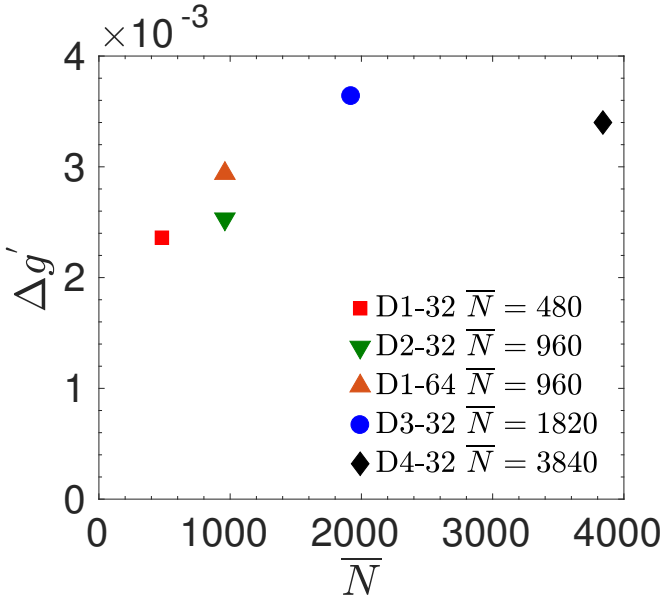

Figure 5.15: Magnitude $\Delta g' = g_{Dis} - g_{Hex}$ in the free energy derivative g' at the ODT for a variety of models with $f = 1/4$ plotted vs. $\overline{N}$.

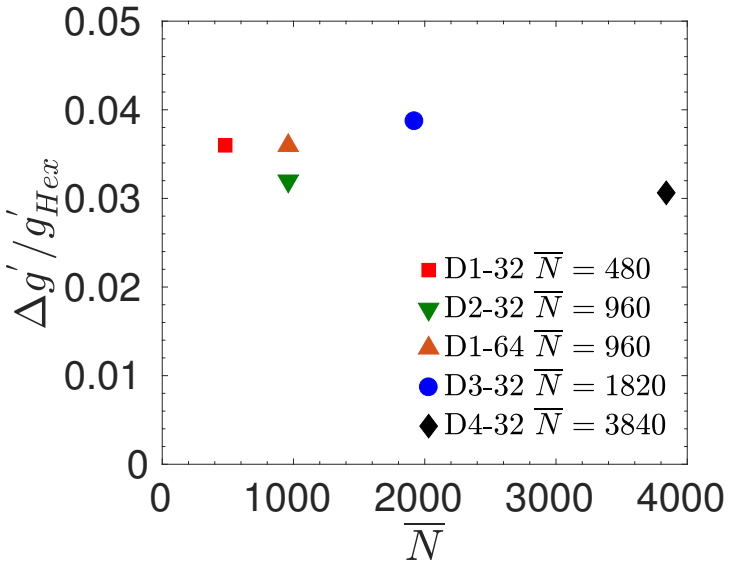

Figure 5.16: The ratio $\Delta g'/g'_{Hex}$ of the change in the Gibbs free energy derivative at the ODT to the value in the hexagonal phase for a variety of models with $f = 1/4$, plotted vs. $\overline{N}$.

Fig. 5.17 shows results for $g(\chi N)$ plotted vs. χN for systems with $f = 1/4$ at the same set of four values of $\overline{N}$. Simulation results and SCFT predictions for $g(\chi N)$ agree rather well within the range of values in which the ordered hexagonal phase is stable. The level of agreement is similar to that found previously for the lamellar phase of symmetric copolymers.

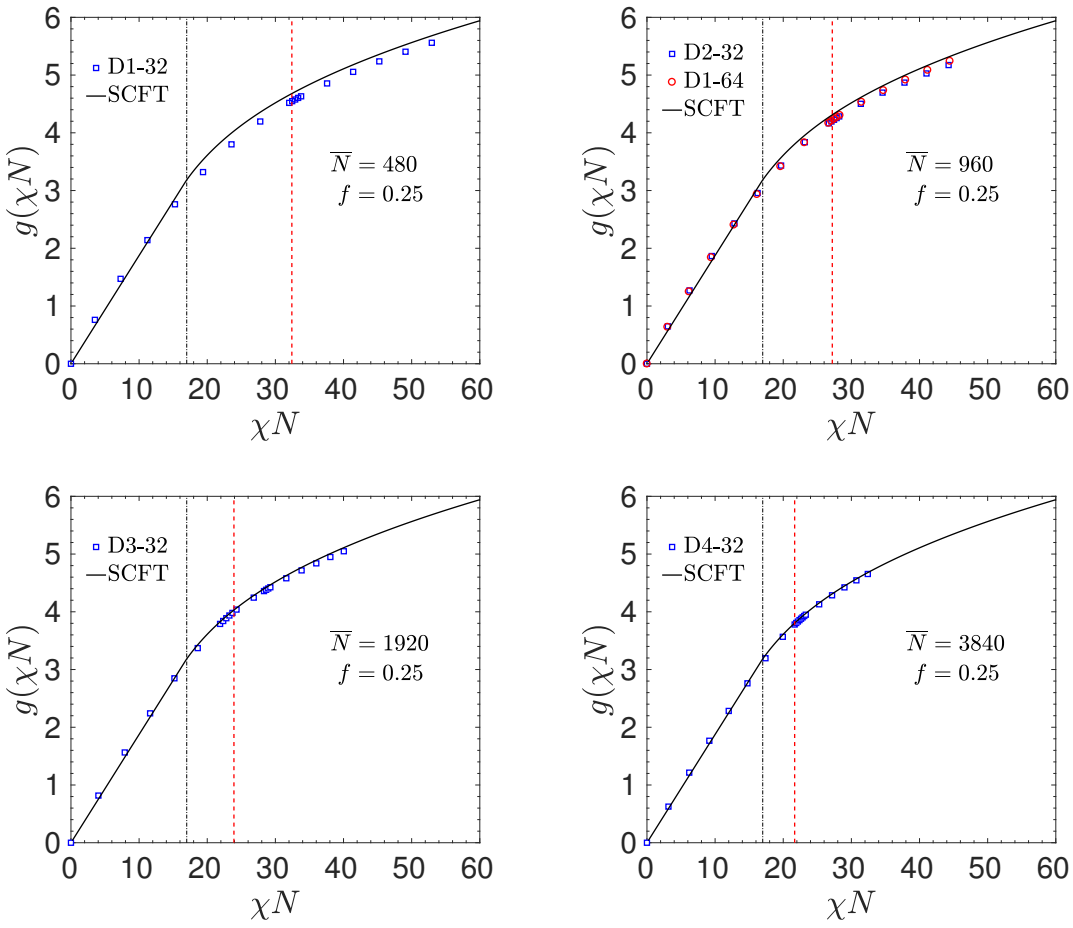

Figure 5.17: The Gibbs free energy per chain g plotted versus χN for different polymeric models with $\overline{N} = 480, 960, 1920, 3840$. Results are show for model D1-32 ($\overline{N} = 480$, upper left), models D2-32 and D1-64 ($\overline{N} = 960$, upper right), model D3-32 ($\overline{N} = 1920$, lower left) and D4-32 ($\overline{N} = 3840$, lower right). SCFT predictions are shown by solid lines. The vertical black dashed line shows the location of the SCFT prediction for the metastable hexagonal-disorder transition, at $\chi N = 16.99$. The vertical red dashed line shows the position of the actual ODT, as determined using well-tempered metadynamics

5.5 Conclusions

We have used simulations to investigate effects of composition fluctuation effects and finite chain length on the location of order-disorder transitions and the behavior of the free energy in melts of asymmetric diblock copolymers. This work builds directly upon a previous study of symmetric copolymers by Glaser, Medapuram, and coworkers,[45] and uses similar techniques to estimate values of the χ parameter, identify order-disorder transitions, and compute free energies.

Results for the composition dependence of the lamellar-disorder and hexagonal-disorder phase transitions for two different values of $\overline{N}$ shows that $(\chi N)_{ODT}$ increases systematically with decreasing $\overline{N}$ at any value of f. Equivalent results for $(\chi N)_{ODT}$ are obtained for a pair of systems with equal values of $f = 1/4$ and $\overline{N}$ but different numbers of beads per chain (models D1-64 vs. D2-32). This is consistent with the corresponding-states hypothesis, which requires that $(\chi N)_{ODT}$ be a universal function of f and $\overline{N}$ for diblock copolymers with $b_A = b_B$. Results for the dependence of $(\chi N)_{ODT}$ on $\overline{N}$ for systems with $f = 1/4$ are consistent with the assumption that the value of $(\chi N)_{ODT}$ for the direct hexagonal-disorder transition approaches the value predicted by SCFT for this this transition as $\overline{N} \to \infty$. A fit of the difference $\Delta(\chi N)_{ODT}$ between the observed value of $(\chi N)_{ODT}$ and the SCFT to a power law $\Delta(\chi N)_{ODT} \propto \overline{N}^{-\beta}$ yields an exponent $\beta \simeq 0.58$ similar to the effective exponent found at small values of $\overline{N}$ for the lamellar-disorder transition of symmetric copolymers.

A detailed study is presented of the dependence of the free energy per chain on χN and $\overline{N}$ for systems with a single value of $f = 1/4$. The results show that SCFT makes rather accurate predictions for the free energy within the ordered hexagonal phase, but poor predictions for the free energy of the disordered phase near the ODT, consistent with the results of prior simulations of symmetric diblock copolymers, with $f = 1/2$.

The main conclusions of this study of asymmetric diblock copolymers are, for the most part, very similar to the conclusions of a prior simulation study of symmetric copolymers[44, 45]. The case of symmetric diblock copolymers, with $f = 1/2$, is

somewhat special because it is the only composition for which SCFT predicts a continuous transition, and is the only case to which the Brazovskii/Fredrickson-Helfand theory of weakly first-order crystallization is rigorously applicable. The present work shows that conclusions about, e. g.the validity of the principle of corresponding states and accuracy of SCFT in the ordered phase, transcend the range of applicability of the Brazovskii weak-crystallization theory, and apply more generally to asymmetric as well as symmetric diblock copolymers.

Chapter 6

Identifying the Gyroid-Disorder Transition

6.1 Introduction

One of the most interesting structures formed by diblock copolymers is the gyroid network structure. The gyroid structure is stable only over a relatively narrow range of the volume fraction f, between the regions of stability of the lamellar and hexagonal phases. The gyroid structure is a tri-continuous morphology with space group $Ia\bar{3}d$ that contains two intertwined but unconnected networks of the minority component immersed in a matrix of the majority component. This structure is sometimes referred to as a double-gyroid structure, to reflect the fact that it contains two networks of the minority phase. The multi-continuous morphology leads to many potential applications, ranging from high-performance membranes and porous materials to possible applications as a template for photonic materials.[96, 16, 18, 111, 112]

The first observation of the gyroid phase in the diblock copolymers melt was made by Thomas et al. [113]. Subsequently, several studies confirmed the existence of a gyroid structure and showed the presence of a direct transition between the gyroid and disordered states [114, 115, 116]. However, the range of stability of

the gyroid phase was initially unclear. Early experimental observations found a gyroid phase at low values of χN but found a perforated lamellar structure between the lamellar and hexagonal phases at higher values of χN [96, 16, 18, 111]. The perforated lamellar structure was later shown both experimentally and theoretically to be a meta-stable structure that could spontaneously transform to a gyroid phase upon annealing. [23, 2, 117].

The self-consistent field theory (SCFT) of diblock copolymers predicts that the gyroid phase is stable over a narrow range of values of f between the hexagonal and lamellar phase [23, 2, 118]. Experiments have demonstrated that the gyroid phase remains stable to large values of χN values [119].

Relatively few simulation studies have focused on the gyroid phase or the gyroid-disorder transition in diblock copolymer melts. Most simulation studies in which a gyroid phase was observed have been performed for two-component copolymer/solvent mixtures or for triblock copolymer systems in which the gyroid phase has a wider window of stability[120, 121, 122, 123, 124, 125, 121, 122, 123]. Only a few simulation studies of diblock copolymer melts have reported spontaneous formation of a gyroid phase. Several computational studies of pure diblock copolymers have instead found evidence of only the hexagonal, perforated lamellar, and lamellar phases[126, 127, 128, 56, 129]. Spontaneous formation of a gyroid phase from a disordered melt was first observed in a simulation in molecular dynamics studies of Martinez-Veracoechea and Escobedo [130, 108], and later also found in lattice Monte Carlo simulations of Beardsley and Matsen. [106]. In both of these case, the authors performed simulations with cubic simulation cells of varying cell size near the expected cell size of the gyroid phase, and found that a gyroid would form only in a narrow range of values of the unit cell dimensions in which the simulation cell dimensions were commensurate with the preferred dimensions of the gyroid unit cell.

Simulation studies that attempt to identify a gyroid-disorder transition face several technical challenges that are more severe than those encountered when trying to identify a lamellar-disorder or hexagonal-disorder transition. Among these challenges are: (1) the narrow range of composition over which the gyroid phase is stable,

(2) the resulting close competition of the gyroid phase in free energy with competing hexagonal and lamellar phases, (3) the sensitivity of the gyroid free energy to the choice of unit cell dimensions, and (4) the large size of the gyroid unit cell, which makes it expensive to perform a simulation large enough to contain more than one unit cell in each of three directions.

When any periodic structure is simulated in a finite periodic unit cell, the free energy of the structure is sensitive to the dimensions of the simulation unit cell. This sensitivity to boundary conditions is a much more severe problem for the gyroid phase than for a lamellar phase and (to a lesser extent) than for the hexagonal phase. A lamellar phase that forms spontaneously from a disordered melt has some freedom to adjust the layer spacing by forming with an orientation relative to the boundaries of the unit cell that minimizes the difference between the actual layer spacing and its preferred value. [131] A hexagonal phase that forms spontaneously in a large unit cell may also have some freedom to choose from among several possible orientations, though most possible orientations introduce some degree of distortion of the 2D hexagonal lattice. Bead-spring simulations of the ordered lamellar and hexagonal phases can guarantee the use of a commensurate unit cell by using constant pressure simulations of a flexible unit cell, which allow the simulation unit cell dimensions to adjust to accommodate the preferred unit cell dimensions of the ordered structure. Information from such simulations about how the preferred unit cell dimensions depend on physical parameters can be used to help choose approximately commensurate unit cell dimensions for simulations of spontaneous melting and crystallization of lamellar and hexagonal phases or biased simulation techniques. This was done as part of the procedure used in Chapter 5 of this thesis to identify lamellar-disorder and hexagonal-disorder transitions. Unfortunately, a flexible unit cell cannot be used in this way to identify the preferred unit cell of a cubic structure, because the unit cell size in a simulation of a cubic structure of a nearly incompressible material can only change substantially by changing the number of molecules in the simulation. In work presented in this chapter, we attempt to address this problem by relying on the observation that the primary peak of $S(q)$ appears to be very nearly continuous at the order-disorder transition, and use measurements of

the parameter dependence of q^* in the disordered phase as guide to the construction of a unit cell that is approximately commensurate at the gyroid-disorder transition.

The large size of the cubic unit cell presents a potential computational challenge. Most of our work on the identification of the disordered lamellar phase was carried using a cubic or approximately cubic unit cell designed to contain three layers of the lamellar structure. The number of beads in a single unit cell of the gyroid structure is comparable to the number of beads in this three-layer lamellar structure. The primary peaks of the gyroid structure belong to the $\{211\}$ family with $q^* = \sqrt{6}(2\pi/a)$, this gives a cubic unit cell of size $a = \sqrt{6}d^* = 2.45d^*$ where $d^* = 2\pi/q^*$ is the layer spacing of a hypothetical lamellar phase with the same value of q^*. One might reasonably question whether the simulation of a single unit cell of the periodic structure is enough to determine where the structure is stable, particularly in a problem in which the effects of composition fluctuations are known to be crucial. The next reasonable choice for the size of simulation cell is a $2 \times 2 \times 2$ cell designed to accommodate 2 gyroid unit cells in each direction, which contains eight times as many particles and is approximately eight times more expensive as a result. The question of how expensive it will be to identify the gyroid-disorder transition thus depends critically upon whether a simulation of a single unit cell is sufficient, or whether one must simulate a simulation unit cell at least eight times larger. The results presented here suggest that, unfortunately, a simulation cell that contains a single unit cell of the gyroid structure is too small to yield reliable results.

6.2 Simulation Methodology

All of the simulation presented in this chapter are NPT molecular dynamics simulation of model D1-32 at a single composition of $f_A = 12/32 = 0.375$, corresponding to a melt of chains with 12 A beads and 20 B beads.

The first step in the design of simulations of the system with $f = 0.375$ is to choose an appropriate size for the simulation unit cell. Our choice of an approximately commensurate box size is based on the experimental observation that the

value of the peak wavenumber q^* is almost precisely continuous through the transition, and has a similar value in competing phases at the ODT. Given an initial estimate of α_{ODT}, this allows us to estimate the preferred box size rather closely by extrapolating results for the dependence of q^* on α in the disordered phase. Our choice of unit cell size for model D1-32 with $f_A = 0.375$ is based on the data shown for q^* vs. α for this system in Figure 5.2 of chapter 5. This figure shows results for q^* in the disordered phase at values of α below the lamellar-disorder transition, which occurs at $\alpha = 3.77$, and values of the wavenumber q^* of the primary Bragg peak in the lamellar phase. Several measurements, summarized below, suggested that the system has gyroid-disordered at a slightly lower value of $\alpha \simeq 2.70$. Using the value of q^* obtained at this value gave us a predicted cell size of $a \simeq 25.0\sigma$ for each side of the gyroid cubic unit cell. All of our simulations were carried out using simulation cells in which the number of molecules was chosen to yield a cell size equal or nearly equal to this value.

Because the simulations presented here were carried out in NPT, the dimensions of the unit cell are not specified as inputs to the simulation, and fluctuate slightly during the simulation. In what follows, we define the "nominal" length of each size of the cubic simulation unit cell to be the length obtained by computing the volume by dividing the number of beads in the system by an assumed bead concentration of $c = 3.0\sigma^{-3}$, which is the concentration that would be obtained for model D1 in the limit of infinitely long homopolymers. The actual average dimensions differ slightly from this nominal length because the average bead concentration differs very slightly from this limiting value.

6.3 Simulations of a Single Unit Cell

We started the study of disorder-gyroid transition in simulations in which the simulation unit cell was designed to contain only a single unit-cell of the gyroid structure.

Existing Methods

Figure 6.1 shows the results of an attempt to identify spontaneous melting and crystallization of the gyroid in several slightly different simulation unit cell sizes. The quantity plotted here is the average energy U_{AB} of interaction between unlike A and B monomers. In each plot circles show results obtained from simulations that were initialized with a disordered initial state, while squares show results obtained form a separate set of simulations that were initialized with an artificially generated gyroid phase. In each simulation, averages were take over a period that excluded an initial equilibration period of 10 million molecular dynamics steps. In systems that show a clear first order transition with hysteresis near the transition, this sort of plot yields two lines corresponding to values in the ordered and disordered state, in which lower values of α in each set of simulations fall on a line of larger values of U_{AB} found in a disordered phase and values at higher values of α fall on a line of lower values found in the ordered phase, with a hysteresis loop near the transition in which the observed state depends upon the nature of the initial state used to seed the simulation. Our point in showing this data is to show that this sort of clear transition with discontinuous changes and hysteresis does not occur for this system. Instead, the dependence of U_{AB} on α appears to be smooth and independent of the initial state for each of these box sizes. This type of observation raised the question in our mind of whether a true first order gyroid-disorder transition might not exist in this small a simulation unit cell.

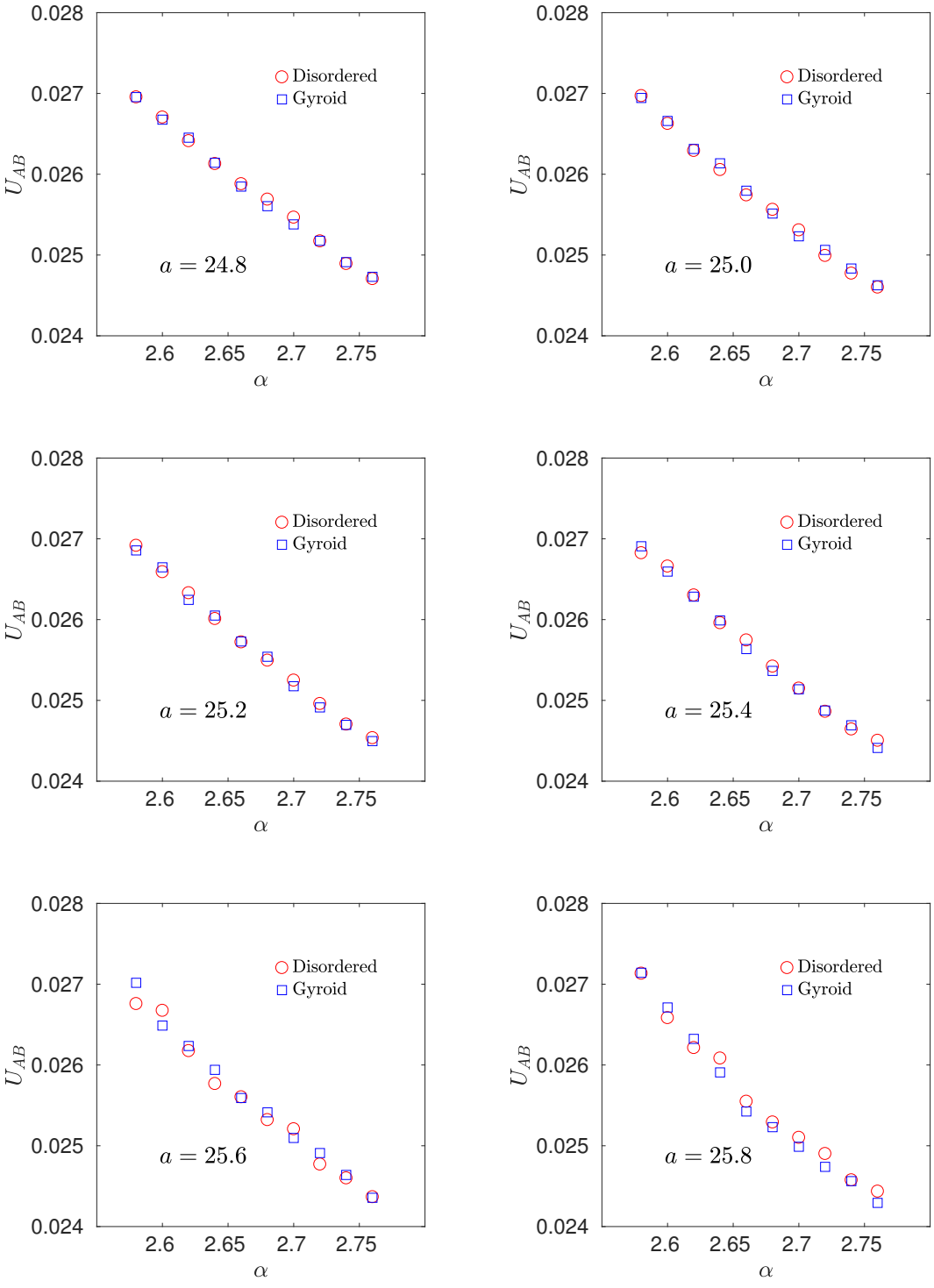

Figure 6.1: Values for the AB pair energy per monomer U_{AB} for simulations initialized with a gyroid structure (blue circles) and a disorder phase (red squares) in systems with nominal simulation unit cell sizes $L/\sigma = 24.8, 25.0, 25.2, 25.4, 25.6, 25.8$, for model D1-32, $f = 0.735$.

Figure 6.2 shows results for the structure factor obtained from simulations that were initialized either with disordered or gyroid structures, for simulations of systems with $a = 25.0$ at several values of α near the expected gyroid-disordered transition. The simulations from which these results were obtained were run for somewhat less simulation time than those shown in the previous figure to obtain some results that still reflect the nature of the initial state. We showed in chapter 5 that the distinction between a disordered state and an ordered lamellar state was obvious upon inspection of results for $S(q)$ for these phases. In the case of the hexagonal phase and (particularly) the lamellar phase, the formation of an ordered phase leads to a family of Bragg peaks with a magnitude much greater than the maximum magnitude of $S(q)$ in the disordered phase. In simulations of systems that contain a single unit cell of the gyroid phase, we instead find that that the magnitude of the primary $\{211\}$ family of peaks of the gyroid phase is almost indistinguishable from the magnitude of the same family of peaks in the disordered phase. The only signature of the formation of the gyroid phase in this unit cell that is visible in plots of $S(q)$ is the formation of an enhanced amplitude for a secondary peak corresponding to the $\{220\}$ family of reflections, which is visible in some plots of systems that were initialized with an artificially generated gyroid phase. The distinction between the gyroid phase and the disordered phase is much more subtle in this small unit cell than then difference between a disordered phase and a lamellar or hexagonal phase. We show later in this chapter that the distinction becomes more obvious in plots of $S(q)$ when we simulate a larger unit cell designed to contain eight gyroid unit cells.

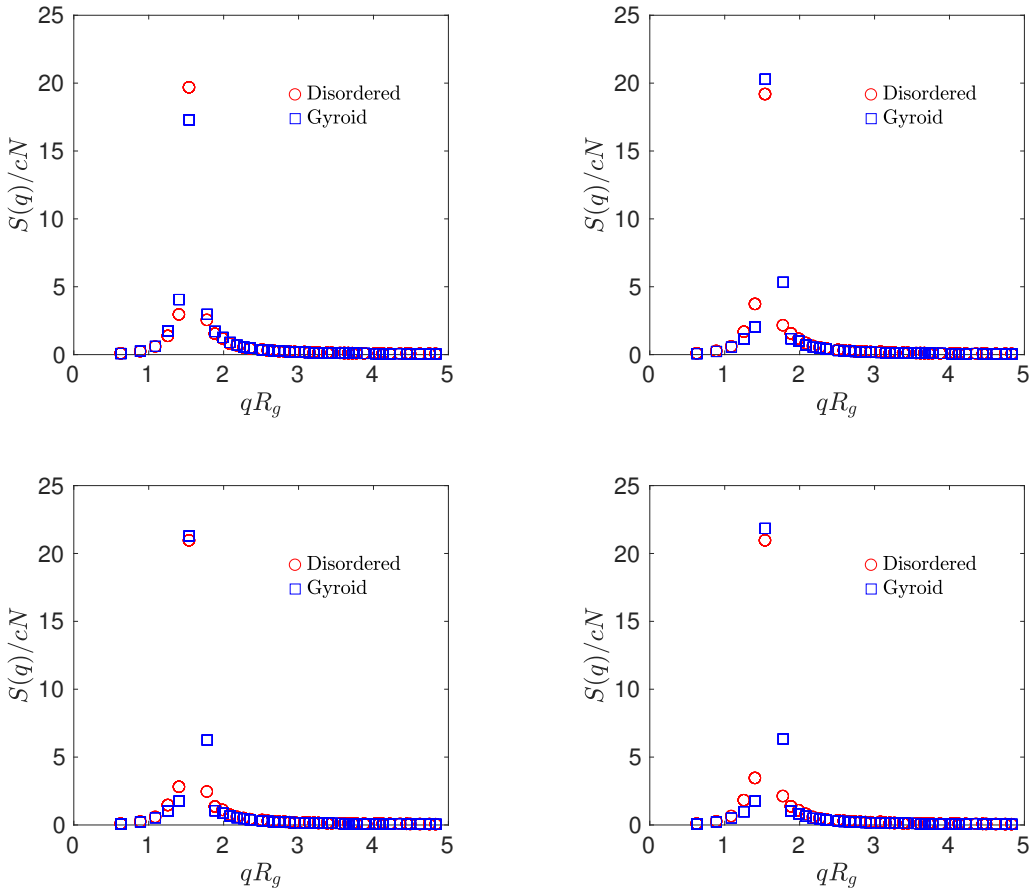

Figure 6.2: The structure factor results obtained for gyroid seeded phase and disorder seeded phase at various $\alpha = 2.64, 2.68, 2.72, 2.76$. The disordered and ordered phase simulations have been performed in a box size of 25.00 in cubic mode NPT simulation ensemble. The red square dots present the disordered seed structure factor results and the blue circle dots represent the gyroid seeded structure factor results at composition $f = 0.3750$ of D1-32 polymeric system, $\overline{N} = 480$.

As it can be seen in figure 6.2, the difference between the structure factor $S(q)$ in the gyroid and the disordered phase is quite small. Because the collective variable used in well-temperature metadynamics simulations is a function of the amplitudes of the composition modes, which are also reflected by $S(q)$, this suggests that values of Ψ_4 may also be less useful for distinguishing these two phases than it was for distinguishing disordered from lamellar or hexagonal phases.

Figure 6.3 shows results for the free energy $G(\Psi_4)$ obtained by performing metadynamics simulations analogous to those performed previously to identify the lamellar-disorder and hexagonal-disorder transitions, using the same collective variable Ψ_4 as that used in these studies.

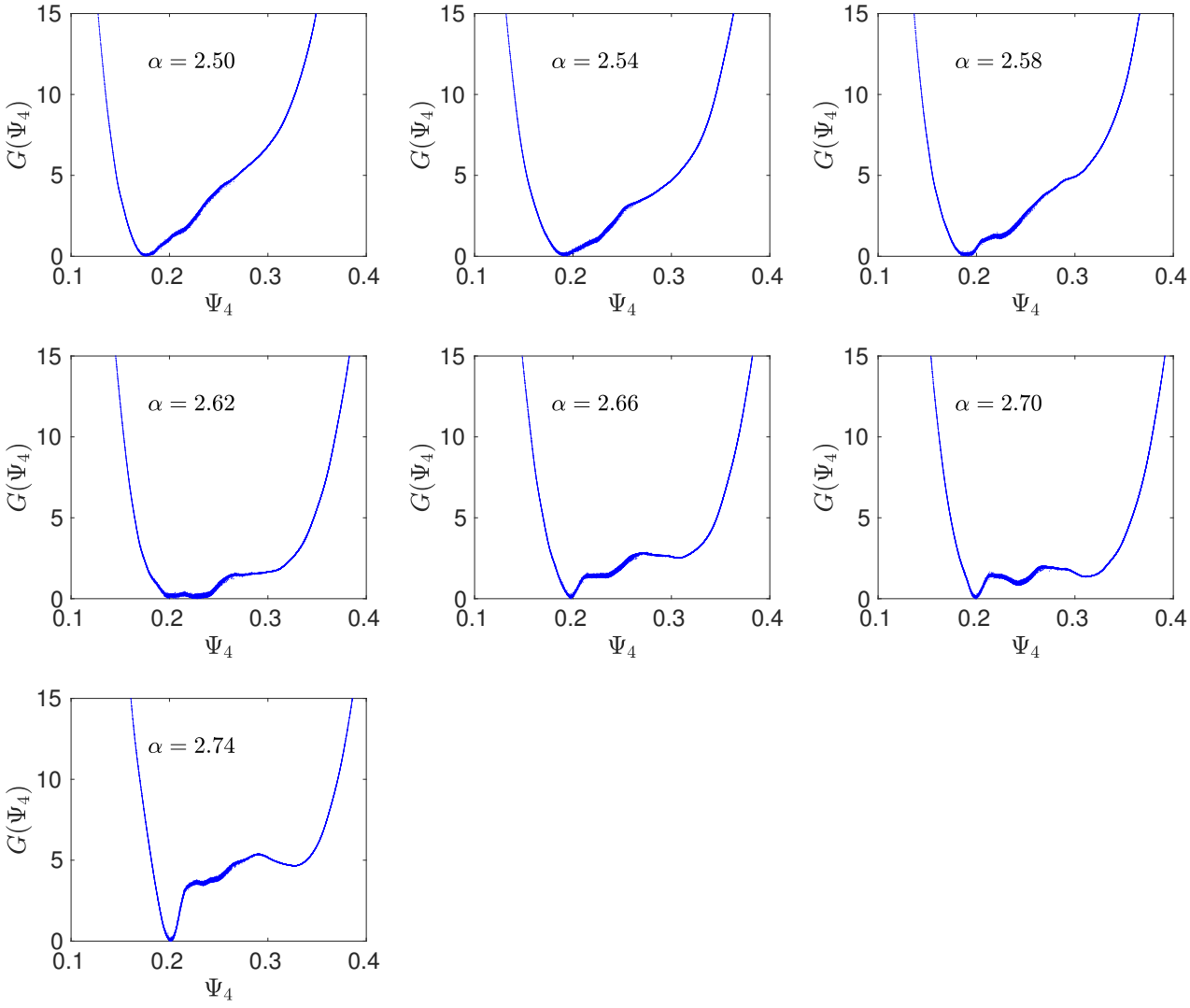

Figure 6.3: The constrained Gibbs free energy $G(\Psi_4)$ of D1-32 polymeric system, $\overline{N} = 960$, for $f = 12/32$ near order-disorder transition. Series of simulations have been performed over a range of $\alpha = 2.50, 2.54, 2.58, 2.62, 2.66, 2.70, 2.74$, for simulations of 1464 chains and 46848 beads with a nominal simulation unit cell dimension of $L = 25.0\sigma$.

We were initially puzzled to see that the results of these WTMD simulations contain three closely spaced minima in $G(\Psi_4)$ at some value of α, rather than only two. WTMD simulations performed at $\alpha = 2.50$ shows the presence of a single minimum at $\Psi_4 \simeq 0.18$, which we assume corresponds to a disordered phase. As values of α increase, a small indentation appears in the free energy landscape at slightly higher values of Ψ_4, which becomes deeper with increasing α. In addition, a third minimum appears at $\alpha > 2.62$ at a higher value of Ψ_4. The value of $\Psi_4 \sim 0.34$ is close to the value obtained previously for the lamellar phase near an ODT, suggesting that this third minimum might correspond to the formation of a closely competing lamellar phase. The appearance of three minima in this free energy landscape thus suggests the possible existence of three different structure with closely competing free energies. We tentatively identify these three structures as disordered, gyroid, and lamellar phase, and assume that minimum with the largest value Ψ_4 is probably a lamellar structure.

Figure 6.4 shows the time dependence of Ψ_4 during a conventional MD simulation performed at a value of $\alpha = 2.70$ near where we expect to find the ODT. The value of Ψ_4 appears to fluctuation for periods within one of three bands of values over short period of time, in which the range of value in each of these bands corresponds to one of the three minima found in the free energy landscape $G(\Psi_4)$, but also frequently "hop" between these bands of values. This suggests that the kinetic barriers between disordered, lamellar, and gyroid-like structures are so low that system can undergo relatively frequent spontaneous transitions between these states even in an unbiased MD simulation.

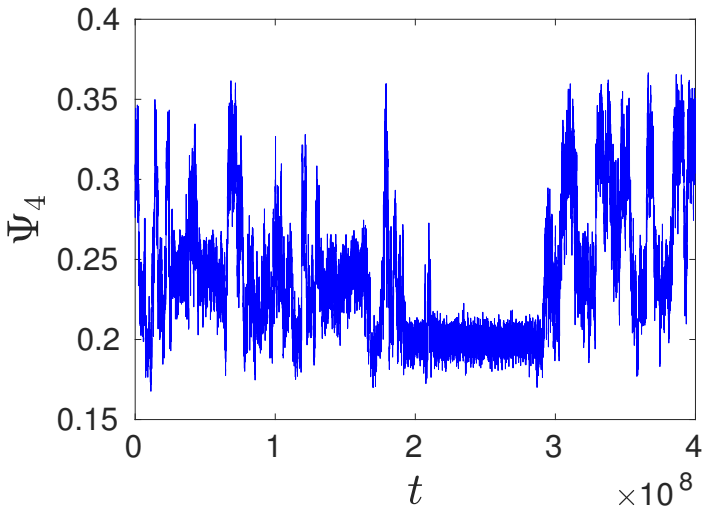

Figure 6.4: Time sequence of the evolution of Ψ_4 obtained from a molecular dynamics simulation at $\alpha = 2.70$ in a simulation box of nominal size 25.00σ that contains $MN = 46848$ particles.

The observation that the system appears to "hop" among three states associated with different values of Ψ_4 provides a possible observation of our failure to observe any hysteresis in measurements of the average AB pair energy in long simulations. In an MD simulation sufficiently long to contain many spontaneous transitions among different states, the time average of U_{AB} (or any other property) presumably corresponds to a weighted average of values arising from different states, with weights that may change smoothly with changes in α. In the absence of a barrier large enough to prevent spontaneous transitions between states over the course of a simulation, one thus does not expect to see either hysteresis or discontinuous change in the measured value of U_{AB} upon changing α.

Specialized Identifiers for Gyroid Structure

To more clearly identify the presence or absence of a gyroid structure in a simulation, we developed a collective variable that was designed specifically to identify the fingerprint of a gyroid structure, rather than simply to distinguish a disordered

structure from a generic ordered structure.

The primary wavevectors forming the gyroid structure are the twenty-four wavevectors in the {211} family. To identify the gyroid phase, we have developed an overlap collective variable:

$$\Psi_g = \max_{\mathbf{r}} \left(\sum_{i=0}^{i=23} e^{-i(\mathbf{k}_i \cdot \mathbf{r} + \phi_i)} A_i \right) \tag{6.1}$$

here the A_is are the measured complex amplitudes and ϕ_is and the values of ϕ_i are the expected relative phases of the 24 members of gyroid structure primary family of $(2,1,1)$ Bragg peaks. In the $Ia\overline{3}d$ space group of the gyroid phase, the expected phases all have values of $\phi_i = 0$ or $\phi_i = \pi$, corresponding to Fourier amplitudes that are either in phase or phase-reversed from amplitude associated with other wavevectors in this family. The phases in the idealized structure are defined relative to a unique inversion center that defines the origin of the conventional crystallographic unit cell. In an ideal gyroid structure with inversion center located at the origin of the simulation unit, all the twenty-four members of the $2,1,1$ family will have the same amplitudes with a unique pattern of relative phases. The sum in the above definition gives the inner product of the actual composition field with the symmetry-adapted basis function associated with the {211} family of Bragg peaks, when the inversion center associated with this basis function is located at a position $\mathbf{r}$. Because the definition of the phases of the Fourier amplitudes depend upon an arbitrary choice of an origin of space, or on the the relationship between the origin of the simulation cell and the inversion center of the gyroid (if one exists), we include a factor of $e^{i\mathbf{k}\cdot\mathbf{r}}$ in the definition of Ψ_g to allow the origin of the basis function to shift in response to any drift in the position the inversion center relative to the origin of the simulation cell. We then define Ψ_g to be the maximum of the sum over waves (i. e., the maximum value of the inner product), maximized with respect to all possible values of the assumed location $\mathbf{r}$ of the inversion center within the periodic unit cell.

To implement the required optimization with respect to $\mathbf{r}$, the code that evaluates this quantity first evaluates the value of the overlap for all values of $\mathbf{r}$ on a mesh inside the simulation unit cell. After identifies the value on the mesh for which the

inner product is maximum, it creates a refined mesh in the neighborhood of that point and repeats the process at least once to refine the choice of a value of the displacement $\mathbf{r}$. If the system is in a gyroid phase, this search will lead to a single well-defined value of $\mathbf{r}$ at which the overlap is maximum, and lead to a much larger value for Ψ_g than would be obtained in a disordered phase with essentially random phases.

To further simplify the identification of a gyroid phase, we also defined another collective variable, denoted by Ψ_{gn}, by normalizing the value of Ψ_g in a way that guarantees that $\Psi_{gn} = 1$ in a perfect gyroid phase. The normalized overlap collective variable is defined as a ratio

$$\Psi_{gn} = \frac{max\{\sum_{i=0}^{i=23} e^{-i(\mathbf{k_i}\cdot\mathbf{r}+\phi_i)} A_i\}}{\sum_{i=0}^{i=23} |A_i|} \quad . \tag{6.2}$$

This ratio is defined so as to give $\Psi_{gn} = 1$ in an idealized gyroid structure in which the Fourier amplitudes of all 24 wavevectors in the $\{211\}$ family have the same amplitude and the relative phases expected for a structure with space group $Ia\overline{3}d$.

Figure 6.5 shows a comparison of synchronized time sequences of Ψ_g, Ψ_{gn}, and Ψ_4 that were all obtained from the same simulation. It is clear that all three collective variables hop among three ranges of values related to three different physical states. We may identify the gyroid state with the state in which Ψ_{gn} is nearly equal to one, which corresponds to the state in which Ψ_g is largest and for which Ψ_4 is smallest. We tentatively identify the lamellar phase with the state in which Ψ^4 is largest, which corresponds to the state in which Ψ_{gn} and Ψ_g are smallest. If we assume that the three states are gyroid, lamellar and disordered, that suggests that the intermediate range of values in each order parameter corresponds to the disordered phase.

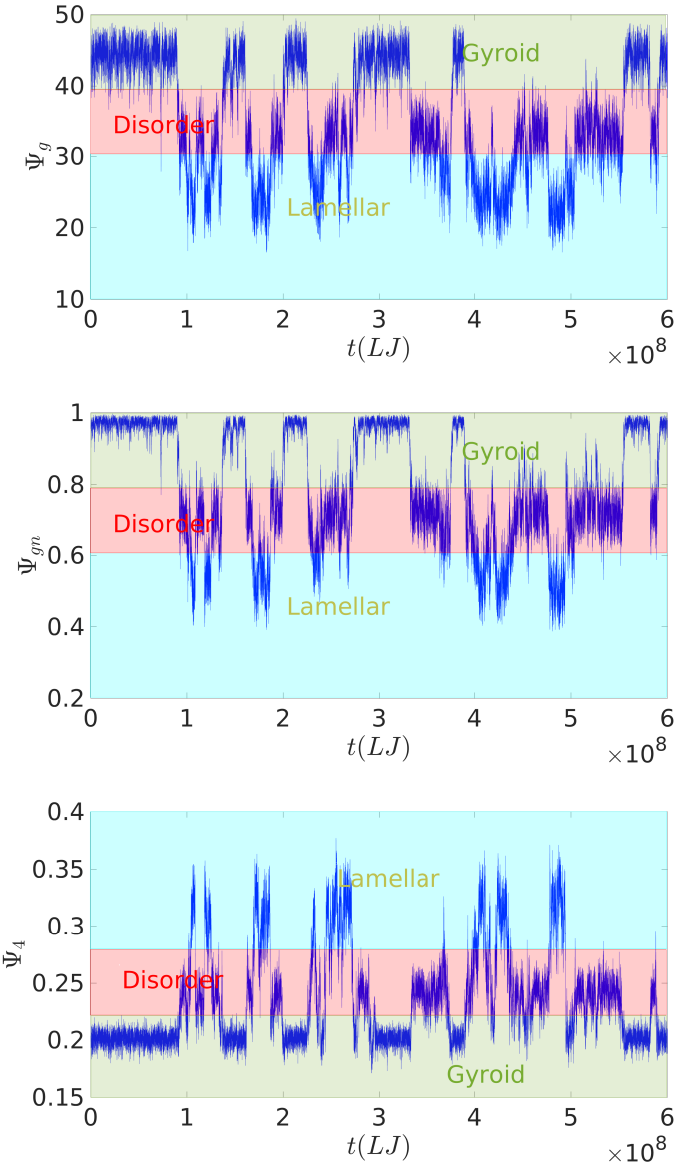

Figure 6.5: Time sequences of Ψ_g, Ψ_{gn} and Ψ_4 obtained from a molecular dynamics simulation in polymeric system D1-32 at composition $f = 0.3750$ at $\alpha = 2.74$ in a simulation box of size $a = 25.00$ that contains $MN = 46848$ particles.

Figure 6.6 shows examples of time sequences of Ψ_{gn} at several different values of α near the ODT. The results show that the system tends spend more time in the disordered state at the lowest value of α and more time in the gyroid state at

higher values of α, but that the crossover is gradual. The results also show that is also a substantial probability of finding the system in any of the disordered, gyroid or lamellar states at highest value of $\alpha = 2.78$ for which data is shown.

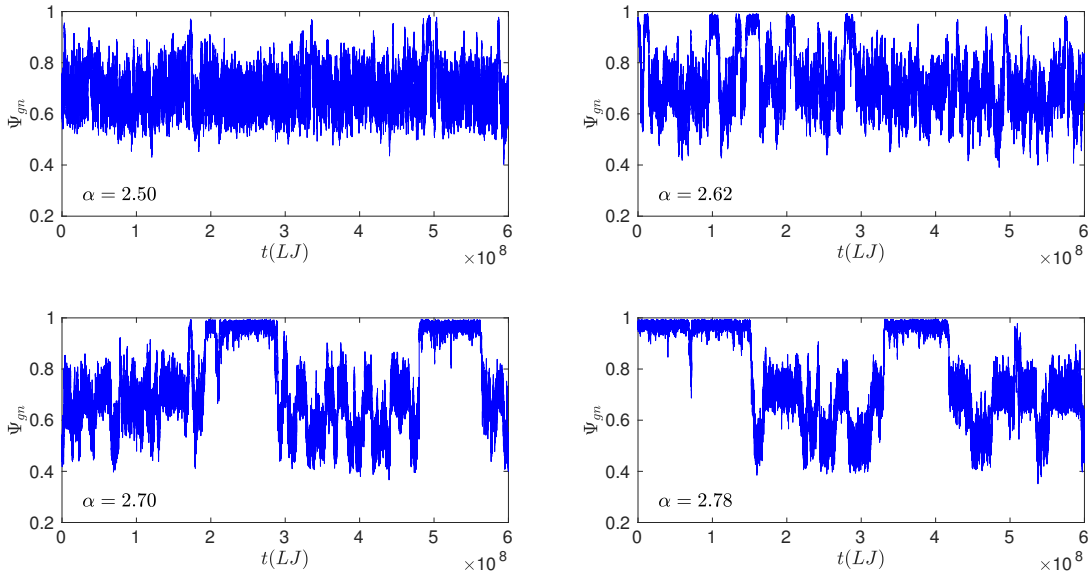

Figure 6.6: Time sequences for Ψ_{gn} time evolution from a molecular dynamics simulation of model D1-32, $f = 0.3750$ at several values of $\alpha = 2.50, 2.62, 2.70, 2.78$ in a simulation box of nominal size 25.00σ.

Figures 6.3, 6.3, and 6.3 show one-dimensional histograms of the three collective variables Ψ_4, Ψ_g and Ψ_{gn} that were all collected from unbiased MD simulations of a single unit cell of size $a = 25.0$ at $\alpha = 2.70$. A total of 5×10^9 molecular dynamics steps were performed to collect this data. The results show that there are three distinct maxima in the histograms for all three quantities, consistent our impression of the existence of three distinct preferred ranges of values in time sequences. The results also show, however, that three peaks are not separated from one another by clear empty valleys. None of these collective variables distinguishes these different states sufficiently to allow identification of three unique populations.

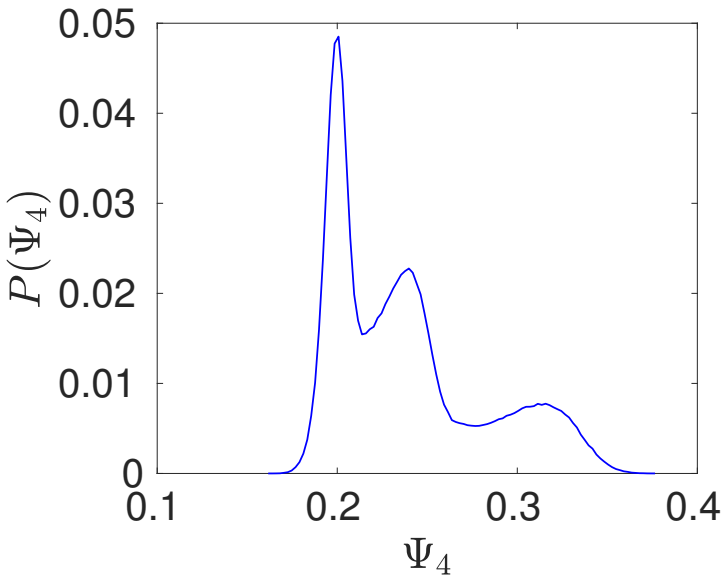

Figure 6.7: The Ψ_4 histogram obtained from a molecular dynamics simulation in polymeric system D1-32 at composition $f = 0.3750$ at $\alpha = 2.70$ in a simulation box of nominal size 25.00σ containing 46848 particles.

Figures 6.3 and 6.3 show histograms of collective variable Ψ_g and Ψ_{gn}, respectively. Both of those histograms also have three peaks. The peak with the highest value of Ψ_g or Ψ_{gn} corresponds to the gyroid structure, while the other two must be the disordered phase and lamellar phase peaks.

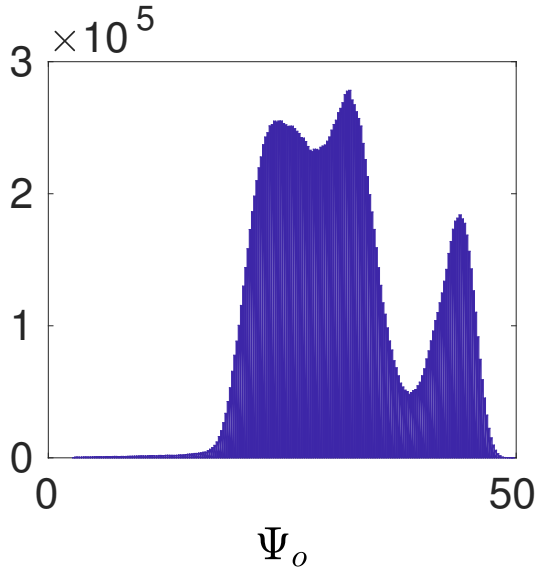

Figure 6.8: The Ψ_g histogram obtained from a molecular dynamics simulation in polymeric system D1-32 at composition $f = 0.3750$ at $\alpha = 2.70$ in a simulation box of nominal size 25.00σ. The simulation box includes $N = 46848$ particles.

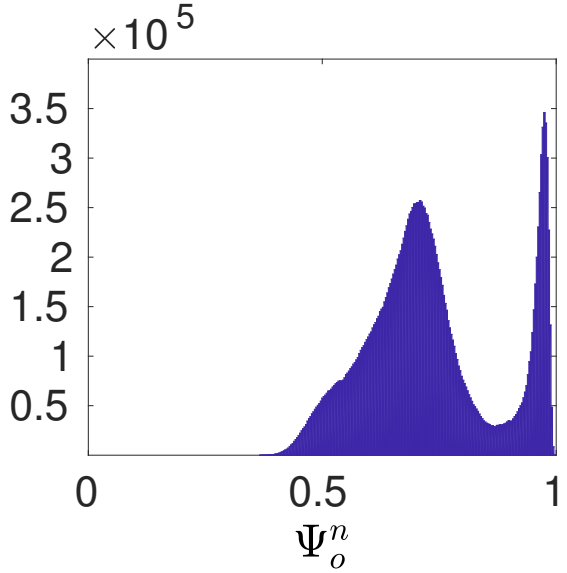

Figure 6.9: The Ψ_{gn} histogram obtained from a molecular dynamics simulation in polymeric system D1-32 at composition $f = 0.3750$ at $\alpha = 2.70$ in a simulation box of size 25.00. The simulation box includes $N = 46848$ particles.

As it turns out, none of the collective variables Ψ_4, Ψ_g, and Ψ_{gn} is by itself a good identifier for all three competing structure in simulations of a simulation cell that is designed to accommodate one unit cell of the gyroid phase. Therefore, we attempted to use a combination of collective variables to identify the three phases.

Figure 6.10 shows an example of a two-dimensional histogram of values of Ψ_4 and Ψ_g. It is clear that in this two-dimensional histogram there are three distinct peaks, which have been labeled as gyroid, disordered, and lamellar peaks, with clear valleys between. This 2D histogram appears to distinguish states well enough to allow us to define a reasonably clear division of the set of states generated by an MD simulation into subsets of gyroid, disordered, and lamellar states.

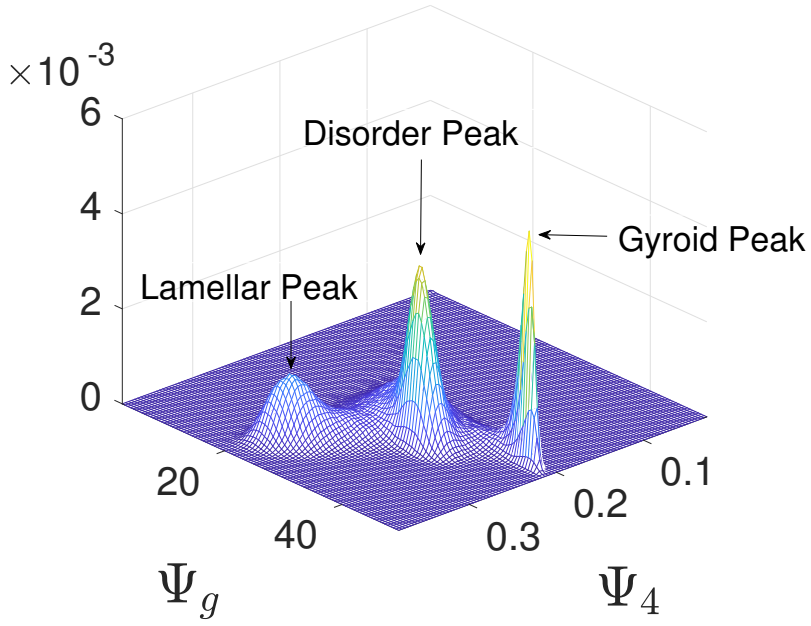

Figure 6.10: Two dimensional histogram of the Ψ_g and Ψ_4 obtained from a molecular dynamics simulation in polymeric system D1-32 at composition $f = 0.3750$ at $\alpha = 2.74$ in a simulation box of size 25.00. The simulation box includes $N = 46848$ particles.

To further clarify the state of the diblock copolymer melt under each of these three peaks, we have studied the distribution of the Fourier amplitudes within the 24 distinct members of the $2, 1, 1$ family for different subpopulations of microstates. For each subpopulation of interest, we have constructed a histogram by listing the 24 distinct Fourier amplitudes associated with each microstate in decreasing order, and then evaluating the average value of the largest Fourier amplitude, the average value of the second largest Fourier amplitude and so. This yields a list containing pairs of identical neighboring values, and pairs of identical average values, because pairs of vectors $\mathbf{k}$ and $-\mathbf{k}$ that are related by inversion have Fourier amplitudes that are complex conjugates of one another, and thus always have equal magnitude. We have applied this analysis to each of three subpopulations that we define by selecting states for which the value of Ψ_{gn} and Ψ_4 are within a small region around one of the maxima in the two-dimensional histogram. The first plot, which comes from states near the maximum that we previously identified as being a disordered population has the smoothly decreasing set of average values we would expect in a disordered phase. The second plot, which is a population that we identified as gyroid, has almost precisely equal Fourier amplitudes for all 12 distinct peaks, consistent with the interpretation of these states as being nearly perfect gyroid crystals. The third plot, which was obtained from states near the lamellar peak, shows that these are states in which 2 of the 24 peaks are much larger than the other 22, as expected for a lamellar phase that is aligned along one of the $\{211\}$ peaks. The combination of the amplitude plots and the histograms of the different collective variables make it completely clear which peak belongs to which structure.

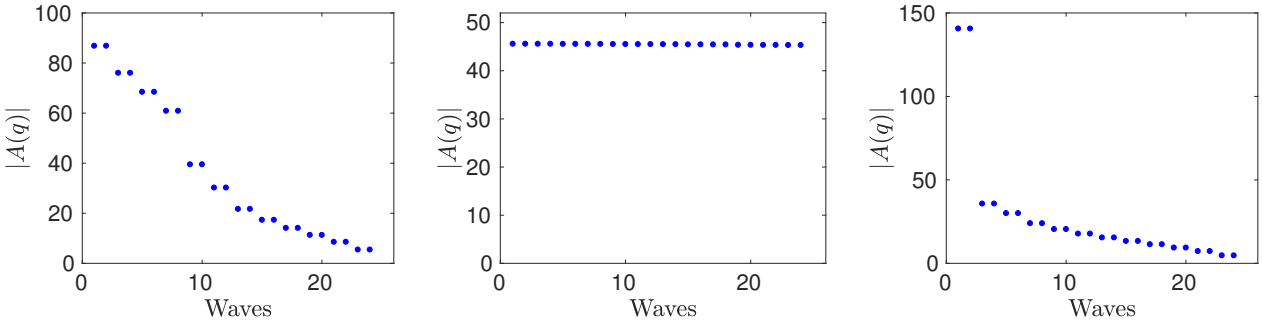

Figure 6.11: The distribution of the Fourier modulus among $2, 1, 1$ family members. The results has been obtained by selection a narrow regions around the three peaks in the two-dimensional histogram of Ψ_g and Ψ_4 corresponding to each peak.

Identifying Subpopulations

The disorder-gyroid transition in a single unit-cell simulation box hops between the disorder and the gyroid phase freely as a result of low activation barrier between the two phases. As a result, disorder-gyroid transition in a single unit-cell simulation box cannot be identified as a phase transition. However, the low activation barrier between the two phases gives us the opportunity to obtain the tendency of the system to form gyroid inside a single unit-cell simulation box. The two-dimensional histograms of Ψ_g and Ψ_4 obtained from relatively long simple molecular dynamics simulations would give us the opportunity to identify the probability that a state chosen at random from this MD sequences would be disordered, lamellar, or gyroid-like structure.

Figures 6.12 and 6.13 show the evolution of the 2D histograms of Ψ_g vs. Ψ_4 and Ψ_{gn} vs. Ψ_4 respectively, for a range of values of $\alpha = 2.50..2.74$. The simulation box size is set to 25.00, which we expect to be commensurate with gyroid dimensions near disorder-gyroid transition. Both plots show evidence of transfer of weight from the disordered phase to the gyroid phase, as well as some transfer of weight to the competing lamellar phase.

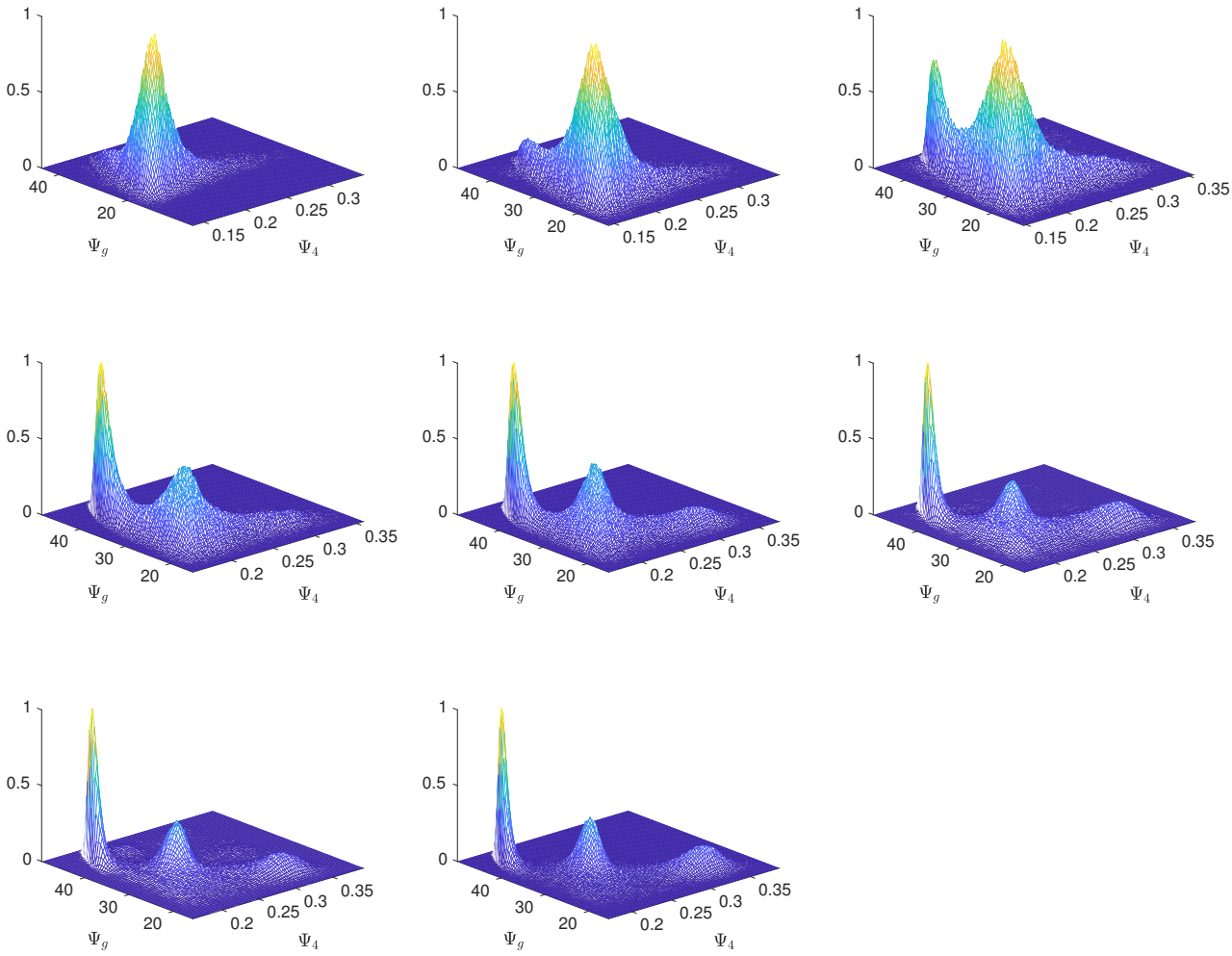

Figure 6.12: The evolution of the (Ψ_g,Ψ_4) two-dimensional histogram with increasing $\alpha = 2.50, 2.54, 2.58, 2.62, 2.66, 2.70, 2.74, 2.78$. The corresponding α value to each graph increases as we proceed from top to bottom and from left to right. The simulations are simple molecular dynamics simulations performed in a cubic box of dimensions 25.00.

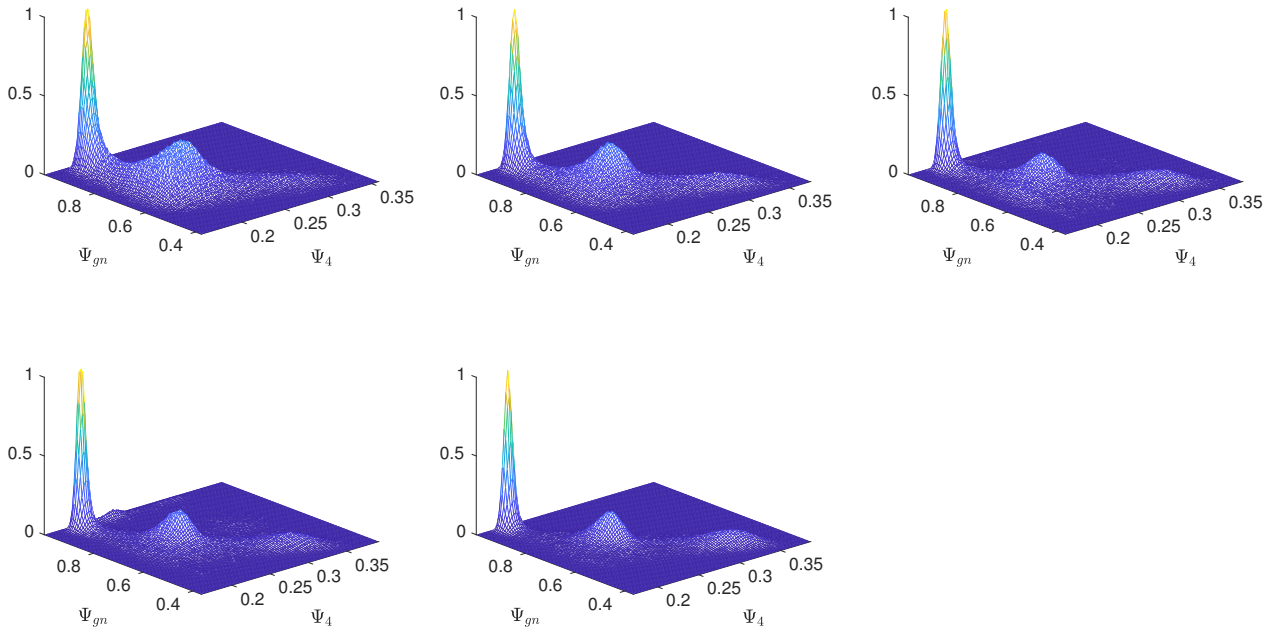

Figure 6.13: The evolution of the (Ψ_{gn},Ψ_4) two-dimensional histogram with increasing $\alpha = 2.62, 2.66, 2.70, 2.74, 2.78$. The corresponding α value to each graph increases as we proceed from top to bottom and from left to right. The simulations are simple molecular dynamics simulations performed in a cubic box of nominal size $L = 25.0\sigma$.

To define probabilities three populations, we have partitioned the histogram for Ψ_g and Ψ_4 along lines passing through the valleys between maxima, as illustrated for the case of $\alpha = 2.70$ in figure 6.3.

Figure 6.15 shows the resulting probabilities for the disordered, gyroid, and lamellar phases as functions of α over a range near the ODT. The results show that these simple MD simulations create a nearly pure disordered phase at the lowest value of $\alpha = 2.5$, but create a statistical mixture of gyroid, lamellar and disordered phases at the highest value of $\alpha = 2.8$ shown here. We have not extended this study of populations in a box of fixed size to higher values of α in part because the preferred domain sizes of both the gyroid and lamellar phases tend to increase with increasing α, and thus will get increasingly far from the preferred domain size at

$\alpha \simeq 2.70$ that this simulation unit cell size was chosen to accommodate.

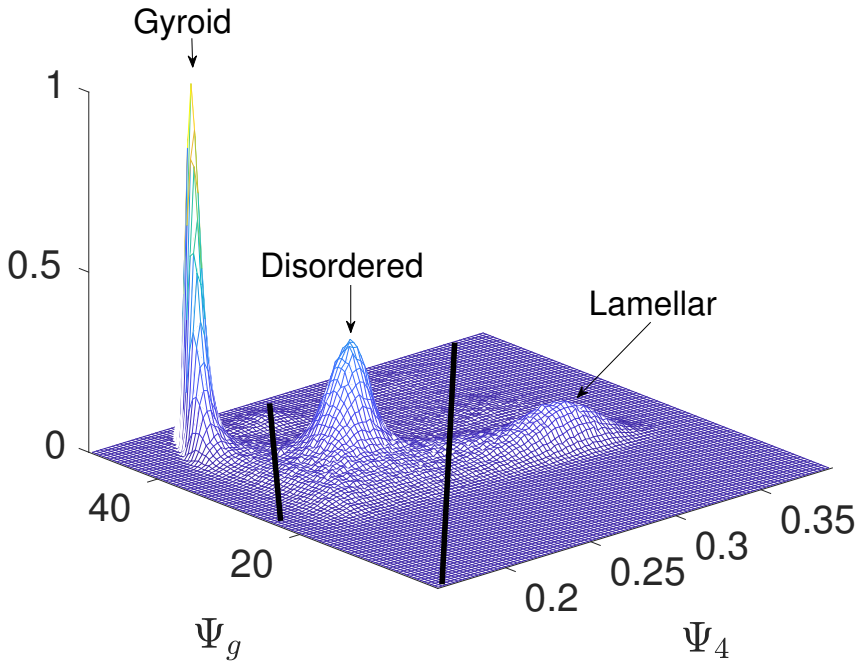

Figure 6.14: Partitioning of the (Ψ_g, Ψ_4) 2D histogram obtained from a molecular dynamics simulation in polymeric system D1-32 at composition $f = 0.3750$ at $\alpha = 2.70$ in a simulation box of nominal size 25.0.

Partitioning of the two-dimensional dimensional histgram of the Ψ_g and Ψ_4 obtained from a molecular dynamics simulation in polymeric system D1-32 at composition $f = 0.3750$ at $\alpha = 2.70$ in a simulation box of nominal size 25.0.

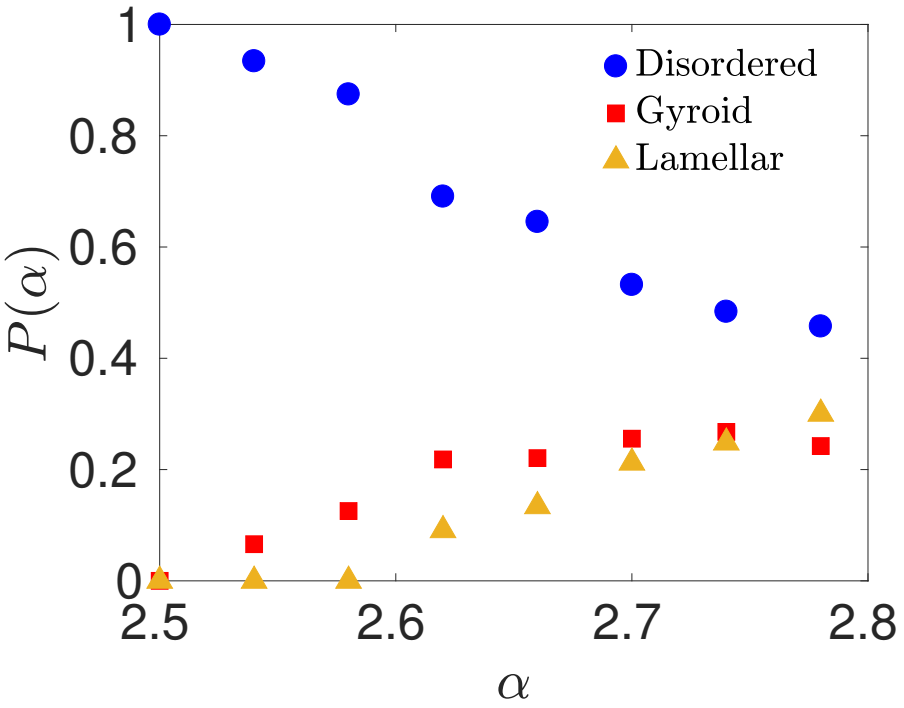

Figure 6.15: The probability of being in different phases obtained by partitioning different peaks of the 2D histograms of the (Ψ_g, Ψ_4) obtained from molecular dynamics simulations at different α values. The simulations have been performed for polymeric system D1-32 at composition $f = 0.3750$ in cubic simulation boxes of dimension 25.00.

6.4 Simulations in a Larger Simulation Cell

Our failure to identify a clear gyroid-disorder transition in simulations of the single gyroid unit cell suggests the use of a larger commensurate unit cell. The natural choice is to simulate the gyroid phase in a $2 \times 2 \times 2$ unit-cell.

Conventional NPT molecular dynamics studies have been performed using disordered and ordered gyroid initial states in a $2 \times 2 \times 2$ simulation unit cell designed to hold 8 unit cells of the gyroid structure. In contrast to the situation found in simulations of a single unit cell we find that simulations in this larger unit cell exhibit a range of values of α in which either a disordered phase or an artificially created

gyroid structure will remain stable over the length of MD runs of $10^7 - 10^8$ MD steps.

Within the range of values where different initial conditions lead to different long-lived states, results for the gyroid and disordered phase are easily distinguishable by inspection of the structure factor $S(q)$, as shown in Figure 6.16. In this larger unit cell, the structure factor of the gyroid phase contains a set of primary $\{211\}$ Bragg peaks with a magnitude approximately eight times the magnitude of the maximum value of $S(q)$ in the disordered phase. The difference between results obtained in simulation unit cells of different size is a straightforward result of the fact that the magnitude of contributions to $S(q)$ arising from Bragg peaks of a period structure is proportional to the number unit cells in the system, while the magnitude of $S(q)$ in the disordered phase is approximately independent of system size.

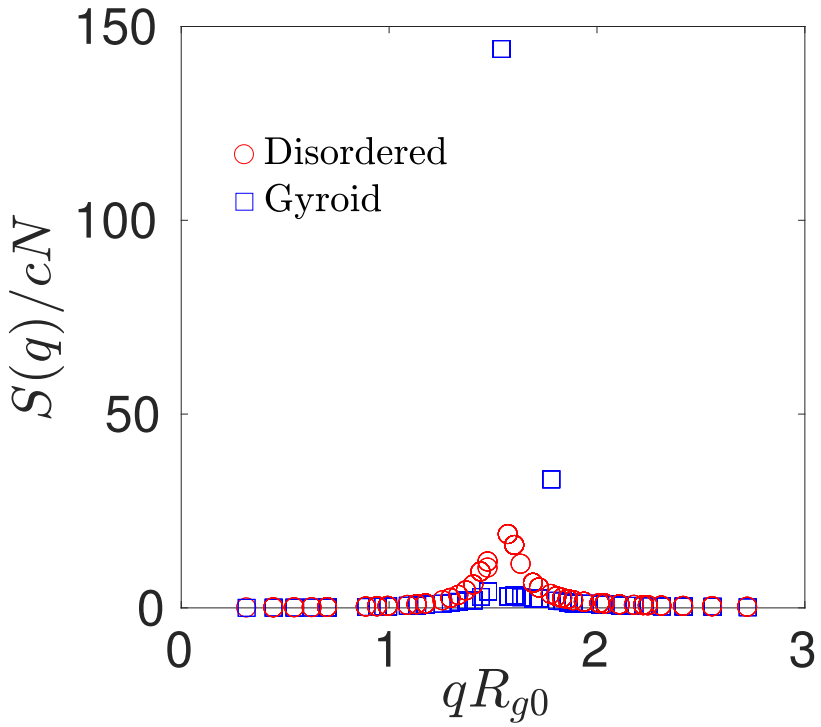

Figure 6.16: Simulation results for the structure factor $S(q)$ for simulations initialized with an ordered gyroif phase (blue squares) and initialize with a disordered phase (red circles) at a value $\alpha = 2.75$ for which both phases are metastable. The simulation has been performed in a box size of 50.00 containing 375000 particles that is designed to contain eight unit cells of the gyroid structure.

Figure 6.17 presents results for the average AB pair energy U_{AB} per particle for simulations in this larger unit cells that were initialized with either a disordered initial state (blue circles) or a gyroid initial state. Simulations were performed for several closely spaced values of the box size to examine commensurability effects. The

AB-pair energy hysteresis loop simulation studies of the gyroid-disorder transition in $2 \times 2 \times 2$ designed to understand the meta-stability of the gyroid phase in a $2 \times 2 \times 2$ simulation box has been performed in a series of boxes with closely spaced dimensions to understand the commensurability of the gyroid phase at $f = 0.3750$ of D1-32 model.

The hysteresis loops shown in Figure 6.17 are quite wide. Simulations that were initialized with an ordered gyroid phase all melt to disordered phase at low α values. Simulations that were initialized with a disordered structure do not, however, form a gyroid structure at high values of α, and instead form a lamellar phase. The fact that the structure formed spontaneously by crystallization at high values of α is not a gyroid phase is clear from these plots because the values of U_{AB} obtained from simulations of structures that crystallized spontaneously from a disordered phase at high values of α do not match the values obtained from simulations that were initialized with a gyroid structure. The formation of a lamellar phase may be favored by the fact that the preferred domain spacing changes with increasing α, and the simulation cell may not be sufficiently close to commensurate with the preferred gyroid cell size at the relatively high value of α where spontaneous crystallization occurs. Difference between the thermodynamically preferred unit cell size of the gyroid and the unit cell size imposed by the simulation boundary conditions tend to favor formation of a lamellar over a gyroid phase, because the lamellar phase has much more freedom to reorient in order maintain a domain spacing close to the equilibrium value. The SCFT phase diagram for this system also suggests that the phase sequence for this system may be DIS $\rightarrow$ GYR $\rightarrow$ LAM with increasing α at $f = 0.375$. This implies that the lamellar phase could also become the equilibrium structure at the value of α where crystallization occurs if crystallization d to sufficiently high values of α.

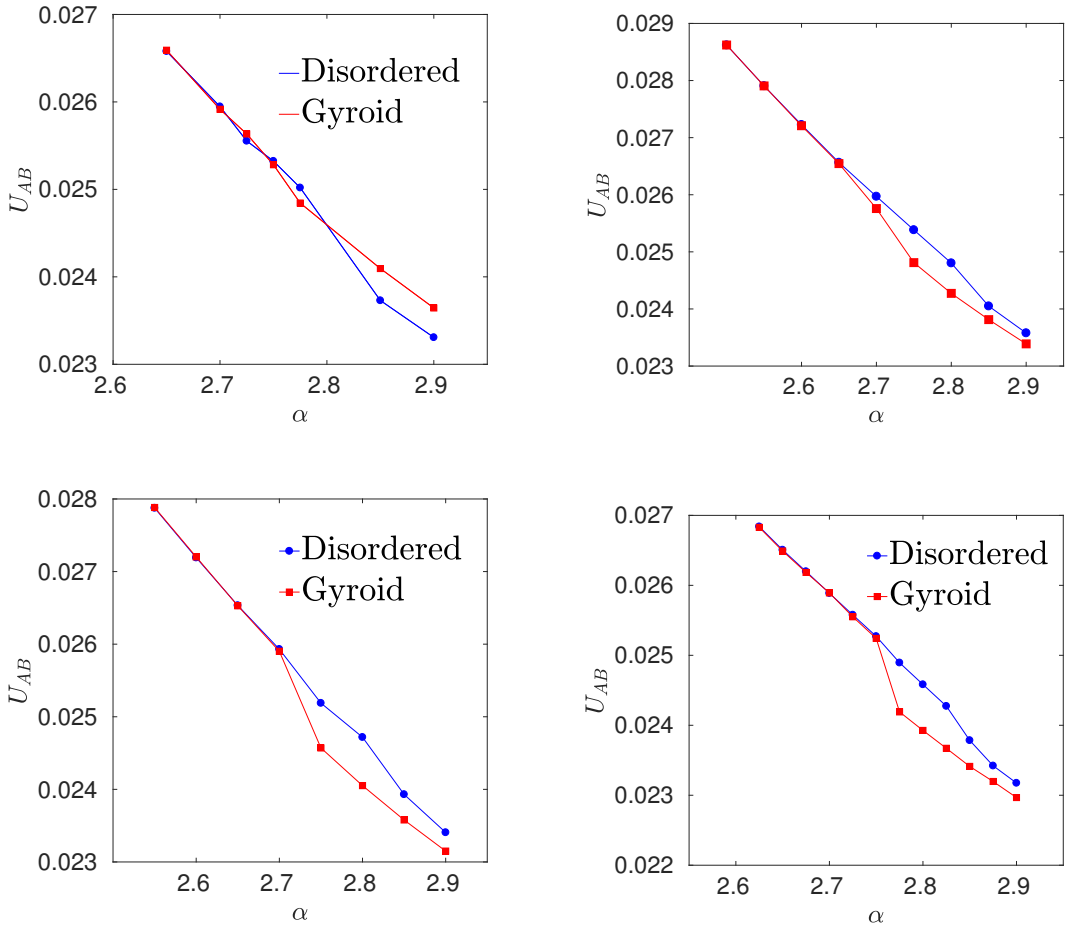

Figure 6.17: Values for the AB pair energy per monomer U_{AB} for simulations initialized with a gyroid structure (blue circles) and a disorder phase (red squares) in systems with nominal simulation unit cell sizes $L/\sigma = 49, 50, 51, 52$, for model D1-32, $f = 0.735$.

The melting α_{melt} values for different boxes can be used to infer the commensurate box dimension for the gyroid phase at the α_{ODT}. As it can be seen in figure 6.4, the α_{melt} values at which the gyroid phase melts strongly depend on the box dimensions. A quadratic fit to the α_{melt} versus the box dimensions are presented in figure 6.4. This box inferred from the $\alpha_{melting}$ result seems to suggest a unit cell dimension a between 25σ and 25.5σ, and melting transition at $\alpha_{ODT} \simeq 2.70$. In the

absence of data from spontaneous crystallization of the gyroid phase, this value of α_{ODT} at the spontaneous melting transition provides our best estimate of the value of α at the gyroid-disorder transition. The value of α at a spontaneous melting transition is expected to be somewhat below the true equilibrium value of α_{ODT}. The estimated value of $\alpha \simeq 2.7$ obtained from spontaneous melting is sufficiently close to the more precisely measured value of $\alpha_{ODT} = 2.77$ for the metastable disordered transition at this composition that we cannot rule out either the possibility of a direct disordered-lamellar transition or the existence of gyroid phase that remains stable only over a narrow range of values of α at this value of f.

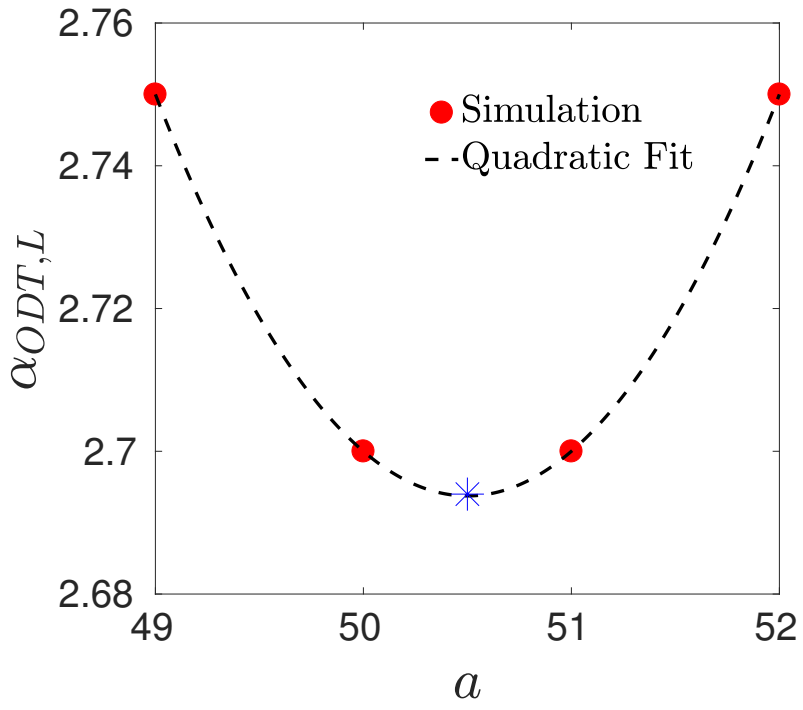

Figure 6.18: Estimates of α_{ODT} obtained from spontaneous melting of an artificially seeded gyroid structure in a $2 \times 2 \times 2$ unit cell, plotted vs. nominal box size.

6.5 Thermodynamic Integration

Thermodynamic integration is a powerful technique to identify first-order transitions. The technique relies on the fact that the difference in free energy between two thermodynamic states can be computed by integrating along a path through parameter space, and that the resulting difference in free energy between different states is independent of the choice of path. In order to use thermodynamic integration to identify a first order transition, one must identify a path through parameter space that continuously connects the two states of interest, thereby going "around" the discontinuious transition.

In this section, use thermodynamic integration to estimate the gyroid disorder transition. The technique used here is a variant of a method that was introduced by Müller and Daoulas [104], who used it to identify the lamellar-disorder transition in simulations of symmetric diblock copolymers. In this approach, we simulate a system with a modified Hamiltonian that is given by the sum of the physical Hamiltonian of the model of interest (here, model D1-32) and an additional external one-body potential U_{ext} that is chosen so as to artificially induce formation of the periodic structure of interest.

To artificially induce formation of a gyroid phase, we use an external potential energy of the form

$$U_{\text{ext}} = -\sum_{i=1}^{MN} \epsilon_i f(\mathbf{r}_i) \tag{6.3}$$

in which i is a particle index, summation is over all particles in the system, $\epsilon_i = \pm 1$ is a prefactor that is equal to $+1$ for particles of type A and -1 for particles of types B, $\mathbf{r}_i$ is the position of particle i, and $f(\mathbf{r})$ is a periodic function with the appropriate space group symmetry. Specifically, we use a function of the form

$$f(\mathbf{r}) = h \tanh[A\phi(\mathbf{r})] \tag{6.4}$$

in which h and A are parameters, and $\phi(\mathbf{r})$ is periodic eigenfunction of the Laplacian that is invariant under all elements of space group $Ia\overline{3}d$ of the gyroid phase. The

function $\phi(\mathbf{r})$ is given by a sum of the form

$$\phi(\mathbf{r}) = \sum_{\mathbf{G}} c_G e^{i\mathbf{G}\cdot\mathbf{r}} \tag{6.5}$$

in which $\mathbf{G}$ represents a wavevector in the primary $\{211\}$ family of wavevectors, where the sum is taken over all 24 such wavevectors, and c_G is a prefactor with a value $c_G = \pm 1$, with different signs for different vectors in this family in order to create a superposition with the correct space group symmetry. The value of the parameter h determines the strength of the external potential. The value of the parameter A determines the width of interfaces between regions with $f(\mathbf{r}) \simeq +h$ and $f(\mathbf{r}) \simeq -h$, with larger values of A yielding sharper interfaces.

The modified Hamiltonian, including this fictitious external potential, is treated as a function of two variable parameters, α and h. The physical parameter α controls the magnitude of repulsion between unlike monomers, and the parameter h controls the magnitude of the fictitious external potential. A fixed value is chosen for the parameter A, and for other parameters of the physical Hamiltonian. The original physical model is recovered in the one-dimensional subspace of the this two-dimensional parameter space within which $h = 0$. In order to identify the order-disorder transition, we integrate along the two paths shown in Fig. 6.19, which we will refer to as paths A and B. Both paths start from an initial point at which α is equal to some reference value α_0, and at which $h = 0$. Along path A (the green dashed line), α is increased along the line $h = 0$. Integration along this path gives the free energy in the disordered phase. Path B (the red dashed line) contains three segments that are each defined by a straight line in this parameter space. Along the first segment of path B, starting from the point $\alpha = \alpha_{ref}$, $h = 0$, h is increased from zero to a value $h_{\max}$ while α held constant at $\alpha = \alpha_0$. As h is increased along this path segment, the external potential induces the formation of a gyroid structure. Along the second segment, h is decreased to zero while α is increased to a value $\alpha_{\max}$, where $\alpha_{\max}$ is chosen to be signficantly greater than the expected value of α_{ODT}. The state at the end of this path segment is thus an ordered structure with $\alpha = \alpha_{\max}$ and no external field. In the last segment of path B, α is decreased to a

value slightly less than the α_{ODT} along the line $h = 0$. The free energy along this last segment of path B gives the free energy in the ordered phase as a function of α. The order-disorder transition is identified as the value of α at which the free energy computed by integrating along path A within the disordered phase intersects the free energy of the ordered phase computed by integrating along the last segment of path B.

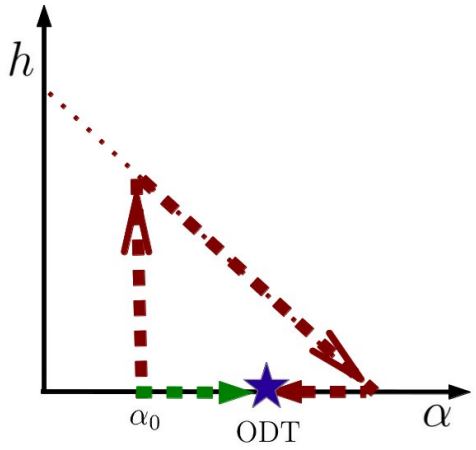

Figure 6.19: Paths through parameter space used in the thermodynamic integration scheme for estimating α_{ODT}.

Free energy differences along each of these paths are computed by numerical integration of derivatives of $G(\alpha, h)$. The required partial derivatives are given by the identities

$$\left.\frac{\partial G}{\partial \alpha}\right|_h = \frac{\langle U_{AB}\rangle}{\epsilon_{AB}} \tag{6.6}$$

$$\left.\frac{\partial G}{\partial h}\right|_\alpha = \frac{\langle U_{\text{ext}}\rangle}{h} \quad , \tag{6.7}$$

where $\epsilon_{AB}(\alpha) = \epsilon_{AA} + \alpha$. These partial derivatives can be used directly to integrate along "horizontal" path segments of constant $h = 0$, and along the "vertical" path segment of constant $\alpha = \alpha_0$, which is the first segment of path B. The required derivative of G with respect to α along the diagonal second segment of path B is

given by the sum

$$\frac{dG}{d\alpha} = \left.\frac{\partial G}{\partial \alpha}\right|_h + \frac{dh}{d\alpha}\left.\frac{\partial G}{\partial h}\right|_\alpha \quad , \tag{6.8}$$

where $dh/d\alpha$ is given by a constant value $dh/d\alpha = -h_{max}/(\alpha_{max} - \alpha_0)$ along this segment. Integration along each path segment is computed by carrying out a set of independent simulations at parameters corresponding to an odd number of equally spaced points along the path segment, including the segment endpoints, evaluating averages of the energy components $\langle U_{AB} \rangle$ and/or $\langle U_{\text{ext}} \rangle$ at each such state point, and using Simpson's rule to approximate the required numerical integral.

Figure 6.20 shows the results of an attempt to apply this method to simulations of a system designed to accomodate a single unit cell of the gyroid phase, using a system with a nominal simulation unit cell size of $L = 25\sigma$, using an initial condition with $\alpha_0 = 0$. The blue graph is the free energy difference obtained from path A, which is designed to give the free energy within the disordered phase. The red graph represents the free energy obtained from path B, which is designed to yield the free energy in the ordered phase.

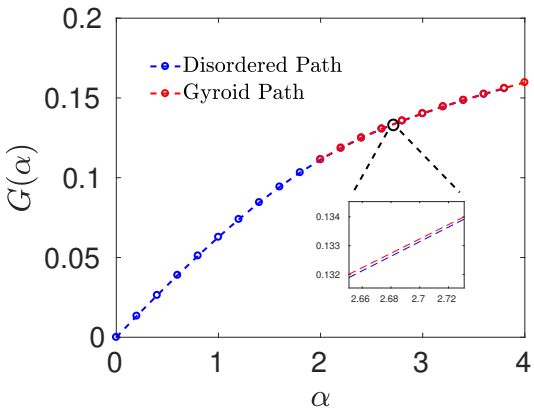

Figure 6.20: Gibbs free energies per monomer computed by thermodynamic integration for the disordered phase (blue line) and ordered (red line), for model D1-32, $f = 0.3750$ and a nominal box size of $L = 25.00\sigma$ that is designed to accomodate a single unit cell of the gyroid structure.

The two free energy curves illustrated in figure 6.20 come very close near the

expected ODT but never cross. In fact, the values of the free energies obtained around the two paths differ by less than statistical error in the region near the expected value of $\alpha_{ODT} \simeq 2.7$. This result is consistent with the observation that AB-pair energy shows no hysteresis for a simulation of a single unit cell, because the system actually has time too sample both ordered and disordered states within the time of a simulation. The fact that the same value for $\partial G/\partial\alpha = \langle U_{AB}\rangle/\epsilon_{AB}$ is obtained at each value of α for states that were seeded with a disordered or gyroid structure guarantees that the slopes of these two free energy curves must be equal, and thus that they cannot cross. The success of the thermodynamic integration method actually requires the existence of some hysteresis. The method only works if, near the transition, either of the two competing phases remain stable long enough to allow accurate average values of properties to be measured in either phase. For the gyroid-disorder transition, we can only satisfy this requirement by using a larger simulation unit cell that contains more than one unit cell of the gyroid structure.

Figure 6.21 shows the results of a thermodynamic integration computation that we performed on system of 375000 particles with a nominal simulation unit cell of $L = 50\sigma$, which was designed to accomodate $2 \times 2 \times 2$ unit cells of the gyroid structure. For this simulation we used an initial value of $\alpha_0 = 2.0$, rather than $\alpha_0 = 0.0$, to decrease the length of the paths along which we must integrate. Values of the free energy shown in Figure 6.21 are thus defined relative to the free energy of a disordered system with $\alpha = 2.0$ and $h = 0$. The results of the calculation with this larger unit cell yield equal values of the free energy of the ordered and disordered phase (i.e., a crossing of the red and blue lines) at $\alpha = 2.72$.

We can estimate the statistical error (i.e., the standard deviation) of this estimate of α_{ODT} as follows. We compute corresponding statistical errors on the average values of $\langle U_{AB}\rangle$ and $\langle U_{\rm ext}\rangle$ obtained at each state point. These errors are combined with the summation formula used in Simpson's rule for integration to compute a corresponding statistical error on the difference ΔG in free energy of the ordered and disordered phases near the ODT, assuming statistical independence of measurements obtained from different simulations performed using different parameters. This estimate of the error in ΔG is then converted into an error in our

estimate of α_{ODT} by dividing the error in ΔG by an estimate of $\partial \Delta G/\partial \alpha$, which is given by the difference in the values of $\partial G/\partial \alpha = \langle U_{AB} \rangle / \epsilon_{AB}$ in the two phases. This analysis yields an error estimate of $\alpha_{ODT} = 2.72 \pm 0.1$.

Thermodynamic integration using a $2 \times 2 \times 2$ unit cell thus yields an estimate of α_{ODT} that is consistent with estimates obtained by other methods, but suffers from a larger statistical error than we would like. Unfortunately, estimated the statistical error of $\Delta\alpha_{ODT} = \pm 0.1$ is large enough to include our previous estimate of the value of α at the lamellar-disorder transition, for which we obtained $\alpha_{ODT} = 2.77$ from a well-tempered metadynamics simulation. The statistical error in this case study of thermodynamic integration is thus too large to allow us to reliably distinguish the ODTs of the lamellar and gyroid phases, which appear to have very similar free energies in this model at $f = 0.375$.

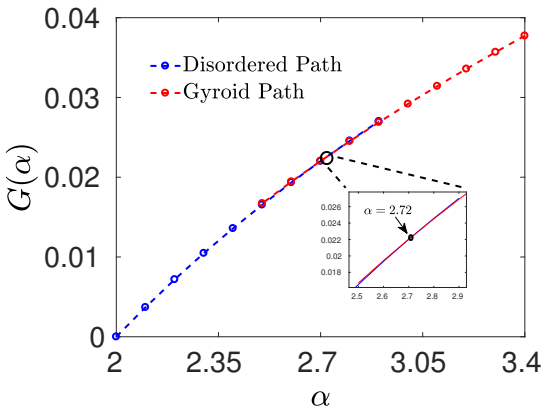

Figure 6.21: The Gibbs free energies per monomer calculated by thermodynamic integration for the disordered phase (blue line) and the ordered gyroid phase (red line) for model D1-32 with $f = 0.3750$ in a box of nominal size of $L = 50.00\sigma$. The simulation unit cell is designed to accomodate 2×2 unit cells of the gyroid structure. The calculated free energies of the two phases become equal at $\alpha_{ODT} \simeq 2.72$.

6.6 Conclusions

In this publication, we have attempted to identify the gyroid-disordered transition in a single model of diblock copolymers (model D1-32) at a single composition

$f = 12/32 = 0.375$. The choice of composition used for this study was chosen before we completed our study of the lamellar-disorder and hexagonal-disorder boundaries was completed, and may not have been the optimal choice. The fact that these metastable phase boundaries appear to intersect at $f = 11/32 = 0.34375$ suggests that the use of an A block of 11 rather than 12 A beads would have guaranteed the existence of stable gyroid phase and that a gyroid phase may or may not be stable at the composition we chose. We believe, however, that many of the lessons we learned about the nature (or existence) of the phase transition in different unit cell sizes would remain valid if the study were repeated at a slightly different composition, and have important implications for any further attempt to pin down the gyroid-disorder transition.

Our most important conclusion about the choice of unit cell is simply that a simulation designed to accommodate only unit cell of the gyroid structure appears to be too small to exhibit an identifiable first-order phase transition. Simulations performed in this relatively small unit cell showed clear evidence of spontaneous hopping among three states that resembled a disordered, gyroid-like and lamellar structure. As part of our effort to understand this behavior, we invented a new somewhat specialized collective variable that was designed specifically to identify a gyroid-like periodic structure, rather than merely to distinguish generic ordered and disordered states.

Conventional freezing and melting simulations in a larger $2 \times 2\times$ unit cell exhibited melting of an initially ordered gyroid phase at a reproducible value of α but showed crystallization of the disordered phase into a lamellar phase rather than into a gyroid phase. This could be a result of the sensitivity of the gyroid phase to lack of commensurability with the simulation unit cell, and the fact that the preferred domain size changes with alpha, making it difficult to maintaining commensurability over a range of values of α. It may also, however, indicate either that the disordered phase of an infinite system transforms directly to a lamellar phase at this composition, or that it exhibits a transition to a gyroid phase that is stable over only a very narrow range of values of α.

Our results indicate that further attempts to more precisely identify the gyroid-

disorder transition may need to use a rather expensive combination of a $2 \times 2 \times 2$ unit cell with methods of computing free energy differences that are precise enough to resolve the rather small differences between free energies of different phases in this parameter window.

Bibliography

[1] M. W. Matsen and F. S. Bates. Origins of complex self-assembly in block copolymers. *Macromolecules*, 29:7641, 1996.

[2] M. W. Matsen and F. S. Bates. Unifying weak- and strong-segregation block copolymer theories. *Macromolecules*, 29(4):1091–1098, January 1996.

[3] Frank S. Bates and Glenn H. Fredrickson. Block copolymers - designer soft materials. *Physics Today*, 52:32–38, 1999.

[4] Glenn H Fredrickson and Frank S Bates. Dynamics of block copolymers: theory and experiment. *Annual Review of Materials Science*, 26(1):501–550, 1996.

[5] Wayne W. Maurer, Frank S. Bates, Timothy P. Lodge, Kristoffer Almdal, Kell Mortensen, and Glenn H. Fredrickson. Can a single function for χ account for block copolymer and homopolymer blend phase behavior? *Journal of Chemical Physics*, 108(7):2989, 1998.

[6] Frank S Bates. Block copolymers near the microphase separation transition. 2. linear dynamic mechanical properties. *Macromolecules*, 17(12):2607–2613, 1984.

[7] Frank S Bates. Measurement of the correlation hole in homogeneous block copolymer melts. *Macromolecules*, 18(3):525–528, 1985.

[8] A Baumgärtner and K Binder. Dynamics of entangled polymer melts: A computer simulation. *Journal of Chemical Physics*, 75(6):2994–3005, 1981.

[9] Kristoffer Almdal, Jeffrey H. Rosedale, Frank S. Bates, George D. Wignall, and Glenn H. Fredrickson. Gaussian- to stretched-coil transition in block copolymer melts. *Physical Review Letters*, 65(9):1112–1116, 1990.

[10] Frank S. Bates and Glenn H. Fredrickson. Block copolymer thermodynamics: Theory and experiment. *Annual Review of Physical Chemistry*, 41(1):525–557, 1990. PMID: 20462355.

[11] Wolfgang Paul, Kurt Binder, Dieter W Heermann, and Kurt Kremer. Dynamics of polymer solutions and melts. reptation predictions and scaling of relaxation times. *Journal of Chemical Physics*, 95(10):7726–7740, 1991.

[12] Frank S. Bates, Jeffrey H. Rosedale, Glenn H. Fredrickson, and Charles J. Glinka. Fluctuation-induced first-order transition of an isotropic system to a periodic state. *Physical Review Letters*, 61(19):2229–2232, 1988.

[13] H. Fried and K. Binder. The microphase separation transition in symmetric diblock copolymer melts: A Monte Carlo study. *Journal of Chemical Physics*, 94(12):8349, 1991.

[14] Ludwik Leibler. Theory of microphase separation in block copolymers. *Macromolecules*, 13:1602–1617, 1980.

[15] Frank S. Bates, Jeffrey H. Rosedale, and Glenn H. Fredrickson. Fluctuation effects in a symmetric diblock copolymer near the order-disorder transition. *Journal of Chemical Physics*, 92(10):6255, 1990.

[16] Stephan Förster, Ashish K. Khandpur, Jin Zhao, Frank S. Bates, Ian W. Hamley, Anthony J. Ryan, and Wim Bras. Complex phase behavior of polyisoprene-polystyrene diblock copolymers near the order-disorder transition. *Macromolecules*, 27(4):6922, January 1994.

[17] Takeji Hashimoto, Toshihiro Ogawa, and Chang Dae Han. Determination of sharpness of order-disorder transition of block copolymers by scattering methods. *Journal of the Physical Society of Japan*, 63(6):2206–2214, 1994.

[18] Ashish K Khandpur, Stephan Förster, Frank S Bates, Ian W Hamley, Anthony J Ryan, Wim Bras, Kristoffer Almdal, and Kell Mortensen. Diblock copolymer phase diagram near the order-disorder transition. *Macromolecules*, 28:8796–8806, 1995.

[19] Naoki Sakamoto and Takeji Hashimoto. Order-disorder transition of low molecular weight polystyrene-block-polyisoprene. 1. SAXS analysis of two characteristic temperatures. *Macromolecules*, 28(20):6825–6834, 1995.

[20] Keiji Mori, Atsuo Okawara, and Takeji Hashimoto. Order-disorder transition of polystyrene-block-polyisoprene. i. thermal concentration fluctuations in single-phase melts and solutions and determination of χ as a function of molecular weight and composition. *Journal of Chemical Physics*, 104:7765, 1996.

[21] Naoki Sakamota, Takeji Hashimoto, Chang Dae Han, Do Kim, and Nitin Y Valdya. Order-order and order-disorder transitions in a polystyrene-block-polyisoprene-block-polystyrene copolymer. *Macromolecules*, 30:1621, 1997.

[22] Glenn H. Fredrickson and E. Helfand. Fluctuation effects in the theory of microphase separation in block copolymers. *J. Chem. Phys.*, 87(1):697–705, 1987.

[23] M. W. Matsen and M. Schick. Stable and unstable phases of a diblock copolymer melt. *Phys. Rev. Lett.*, 72:2660, 1994.

[24] M.W. Matsen and M. Schick. Microphases of a diblock copolymer with conformational asymmetry. *Macromolecules*, 27:4014, 1994.

[25] Eugene Helfand. Theory of inhomogeneous polymers: Fundamentals of the Gaussian random-walk model. *The Journal of Chemical Physics*, 62(3):999, 1975.

[26] Zhen-Gang Wang. Concentration fluctuation in binary polymer blends: χ parameter, spinodal and ginzburg criterion. *The Journal of Chemical Physics*, 117(1):481, 2002.

[27] Paul J. Flory. Thermodynamics of high polymer solutions. *J. Chem. Phys.*, 9(8):660–661, 1941.

[28] M. W. Matsen. The standard Gaussian model for block copolymer melts. *J. Phys.: Condens. Matter*, 14:R21–R47, 2002.

[29] M.W Matsen and M. Schick. Stable and unstable phases of a linear multiblock copolymer melt. *Macromolecules*, 27:7157, 1994.

[30] G.H. Fredrickson, V. Ganesan, and F. Drolet. Field-theoretic computer simulation methods for polymers and complex fluids. *Macromolecules*, 35:16–39, 2002.

[31] Frank S. Bates. Measurement of the correlation hole in homogeneous block copolymer melts. *Macromolecules*, 18:525–528, 1985.

[32] John N. Owens, Irena S. Gancarz, Jeffrey T. Koberstein, and Thomas P. Russell. Investigation of the microphase separation transition in low-molecular-weight diblock copolymers. *Macromolecules*, 22(8):3380–3387, 1989.

[33] Frank S. Bates and Mark a. Hartney. Block copolymers near the microphase separation transition. 3. small-angle neutron scattering study of the homogeneous melt state. *Macromolecules*, 18(12):2478–2486, 1985.

[34] V. T Bartels, V Abetz, K Mortensen, and M Stamm. Microphase separation of a symmetric poly(styrene-b-paramethylstyrene) diblock copolymer. *Europhysics Letters (EPL)*, 27(5):371–376, 1994.

[35] S. Brazovskiĭ. Phase transition of an isotropic system to a nonuniform state. *Sov. Phys JETP*, 41:85, 1975.

[36] Jean-louis Barrat and Glenn H Fredrickson. Collective and single-chain correlations near the block copolymer order–disorder transition. *J. Chem. Phys.*, 95(2):1281–1289, 1991.

[37] Piotr Grzywacz, Jian Qin, and David C. Morse. Renormalization of the one-loop theory of fluctuations in polymer blends and diblock copolymer melts. *Phys. Rev. E*, 76:061802, 2007.

[38] Renormalized one-loop theory of correlations in polymer blends. *The Journal of Chemical Physics*, 130(22):224902, June 2009.

[39] David C. Morse and Jian Qin. Relationships among coarse-grained field theories of fluctuations in polymer liquids. *The Journal of Chemical Physics*, 55455(2):084902, 2010.

[40] Jian Qin, Piotr Grzywacz, and David C. Morse. Renormalized one-loop theory of correlations in disordered diblock copolymers. *J. Chem. Phys.*, 135:84902, 2011.

[41] Jian Qin and David C. Morse. Fluctuations in symmetric diblock copolymers: Testing theories old and new. *Physical Review Letters*, 108:238301, 2012.

[42] Jens Glaser, Jian Qin, Pavani Medapuram, and David C Morse. Collective and single-chain correlations in disordered melts of symmetric diblock copolymers: Quantitative comparison of simulations and theory. *Macromolecules*, 47(2):851–869, 2014.

[43] J. Glaser, J. Qin, P. Medapuram, M. Müller, and D.C. Morse. Test of a scaling hypothesis for the structure factor of disordered diblock copolymer melts. *Soft Matter*, 8:11310–11317, 2012.

[44] J. Glaser, P. Medapuram, T. M. Beardsley, M. W. Matsen, and D.C. Morse. Universality of block copolymer melts. *Physical Review Letters*, 113:068302, 2014.

[45] Pavani Medapuram, Jens Glaser, and David C. Morse. Universal phenomenology of symmetric diblock copolymers near the orderdisorder transition. *Macromolecules*, 48(3):819–839, 2015.

[46] M Doi and S F Edwards. *The Theory of Polymer Dynamics*. Oxford University Press, Oxford, 1988.

[47] Jens Glaser, Jian Qin, Pavani Medapuram, Marcus Müller, and David Morse. Test of a scaling hypothesis for the structure factor of disordered diblock copolymer melts. *Soft Matter*, 8(44):11310–11317, 2012.

[48] Timothy M. Gillard, Pavani Medapuram, David C. Morse, and Frank S. Bates. Fluctuations, phase transitions, and latent heat in short diblock copolymers: Comparison of experiment, simulation and theory. *Macromolecules*, 48(8):2801–2811, 2015.

[49] Jian Qin. *Studies of block copolymer melts by field theory and molecular simulations*. PhD thesis, University of Minnesota, Sept. 2009.

[50] Pavani Medapuram. *Simulation of Symmetric Diblock Copolymers*. PhD thesis, University of Minnesota, Sept. 2016.

[51] David C. Morse and Jun Kyung Chung. On the chain length dependence of local correlations in polymer melts and a perturbation theory of symmetric polymer blends. *The Journal of Chemical Physics*, 130(22):224901, 2009.

[52] Taher Ghasimakbari and David C Morse. Correlations in disordered melts of asymmetric diblock ccopolymers. *Macromolecules*, 51:2335–2348, 2018.

[53] Vaidyanathan Sethuraman, Bryan H. Nguyen, and Venkat Ganesan. Coarse-graining in simulations of multicomponent polymer systems. *Journal of Chemical Physics*, 141(24):244904, 2014.

[54] Thomas M. Beardsley and Mark W. Matsen. Universality between experiment and simulation of a diblock copolymer melt. *Physical Review Letters*, 117:217801, 2016.

[55] David C. Morse and Jian Qin. Relationships among coarse-grained field theories of fluctuations in polymer liquids. *J. Chem. Phys.*, 134:084902, 2011.

[56] Robert D. Groot and Timothy J. Madden. Dynamic simulation of diblock copolymer microphase separation. *Journal of Chemical Physics*, 108(20):8713, 1998.

[57] Robert D. Groot and Patrick B. Warren. Dissipative particle dynamics: Bridging the gap between atomistic and mesoscopic simulation. *Journal of Chemical Physics*, 107(11):4423, 1997.

[58] Mario Schwab and Bernd Stühn. Thermotropic transition from a state of liquid order to a macrolattice in asymmetric diblock copolymers. *Physical Review Letters*, 76:924–927, Feb 1996.

[59] E. E Dormidontova and T. P Lodge. The order-disorder transition and the disordered micelle regime in sphere-forming block copolymer melts. *Macromolecules*, 34:9143–9155, 2001.

[60] Moon Jeong Park, Kookheon Char, Joona Bang, and Timothy P. Lodge. Order-disorder transition and critical micelle temperature in concentrated block copolymer solutions. *Macromolecules*, 38:2449–2459, 2005.

[61] Jiafang Wang., Zhen-Gang Wang, and Yuliang Yang. Nature of disordered micelles in sphere-forming block copolymer melts. *Macromolecules*, 38(13):5766–5773, June 2005.

[62] Dietmar Ehlich, Mikihito Takenaka, and Takeji Hashimoto. Forced Rayleigh scattering study of diffusion of block copolymers. 2. self-diffusion of block copolymer chains in lamellar microdomains and disordered melts. *Macromolecules*, 26(3):492–498, 1993.

[63] MC Dalvi and TP Lodge. Diffusion in block copolymer melts: the disordered region and the vicinity of the order-disorder transition. *Macromolecules*, 27(13):3487–3492, 1994.

[64] Mark W Hamersky, Matthew Tirrell, and Timothy P Lodge. Self-diffusion of a polystyrene-polyisoprene block copolymer. *Journal of Polymer Science Part B: Polymer Physics*, 34(17):2899–2909, 1996.

[65] SH Anastasiadis, K Chrissopoulou, G Fytas, M Appel, G Fleischer, K Adachi, and Y Gallot. Self-diffusivity of diblock copolymers in solutions in neutral good solvents. *Acta polymerica*, 47(6-7):250–264, 1996.

[66] Timothy P Lodge, Matthew A Blazey, Z Liu, and Ian W Hamley. Asymmetric block copolymers in neutral good solvents: self-diffusion through the ordering transition. *Macromolecular Chemistry and Physics*, 198(4):983–995, 1997.

[67] Glenn H Fredrickson and Scott T Milner. Tracer-diffusion in weakly-ordered block copolymers. *MRS Online Proceedings Library Archive*, 177, 1989.

[68] Jean Louis Barrat and Glenn H Fredrickson. Diffusion of a symmetric block copolymer in a periodic potential. *Macromolecules*, 24(24):6378–6383, 1991.

[69] Cora M Leibig and Glenn H Fredrickson. Tracer diffusion in fluctuating block copolymer melts. *Journal of Polymer Science Part B: Polymer Physics*, 34(1):163–171, 1996.

[70] MC Dalvi, CE Eastman, and TP Lodge. Diffusion in microstructured block copolymers: Chain localization and entanglements. *Physical Review Letters*, 71(16):2591, 1993.

[71] G Fleischer, F Rittig, P Štěpánek, K Almdal, and CM Papadakis. Self-diffusion of a symmetric PEP-PDMS diblock copolymer above and below the disorder-to-order transition. *Macromolecules*, 32(6):1956–1961, 1999.

[72] Frank Rittig, Jörg Kärger, Christine M Papadakis, Gerald Fleischer, Petr Štěpánek, and Kristoffer Almdal. Self-diffusion investigations on a series of PEP-PDMS diblock copolymers with different morphologies by pulsed field gradient NMR. *Physical Chemistry Chemical Physics*, 1(17):3923–3931, 1999.

[73] Frank Rittig, Gerald Fleischer, Jörg Kärger, Christine M Papadakis, Kristoffer Almdal, and Petr Štěpánek. Anisotropic self-diffusion in a hexagonally ordered asymmetric PEP-PDMS diblock copolymer studied by pulsed field gradient NMR. *Macromolecules*, 32(18):5872–5877, 1999.

[74] G Fleischer, Franz Fujara, and Bernd Stuehn. Restricted diffusion in the regime of the order-to-disorder transition in diblock copolymers: a field gradient NMR study. *Macromolecules*, 26(9):2340–2345, 1993.

[75] R Borsali and TA Vilgis. Dynamics of copolymer and homopolymer blends in strong solutions and bulk: The Edwards hamiltonian approach. *The Journal of Chemical Physics*, 93(5):3610–3613, 1990.

[76] A.Ziya Akcasu, M. Benmouna, and H. Benoit. Application of random phase approximation to the dynamics of polymer blends and copolymers. *Polymer*, 27(12):1935 – 1942, 1986.

[77] A. Ziya Akcasu and M. Tombakoglu. Dynamics of copolymer and homopolymer mixtures in bulk and in solution via the random phase approximation. *Macromolecules*, 23(2):607–612, 1990.

[78] T. Jian, S. H. Anastasiadis, A. N. Semenov, G. Fytas, K. Adachi, and T. Kotaka. Dynamics of composition fluctuations in diblock copolymer solutions far from and near to the ordering transition. *Macromolecules*, 27(17):4762–4773, 1994.

[79] S Vogt, T Jian, SH Anastasiadis, G Fytas, and Erhard W Fischer. Diffusive relaxation mode in poly (styrene-b-methylphenylsiloxane) copolymer melts above and below the order-disorder transition. *Macromolecules*, 26(13):3357–3362, 1993.

[80] SH Anastasiadis, G Fytas, S Vogt, and Erhard W Fischer. Breathing and composition pattern relaxation in "homogeneous diblock copolymers. *Physical Review Letters*, 70(16):2415, 1993.

[81] SH Anastasiadis, G Fytas, S Vogt, B Gerharz, and Erhard W Fischer. Diffusive composition pattern relaxation in disordered diblock copolymer melts. *EPL (Europhysics Letters)*, 22(8):619, 1993.

[82] CM Papadakis, K Almdal, K Mortensen, F Rittig, G Fleischer, and P Štěpánek. The bulk dynamics of a compositionally asymmetric diblock copolymer studied using dynamic light scattering. *The European Physical Journal E*, 1(4):275–283, 2000.

[83] CM Papadakis, F Rittig, K Almdal, Kell Mortensen, and P Štěpánek. Collective dynamics and self-diffusion in a diblock copolymer melt in the body-centered cubic phase. *The European Physical Journal E*, 15(4):359, 2004.

[84] Petr Stepanek, Kristoffer Almdal, and Timothy P Lodge. Polarized and depolarized dynamic light scattering from a block copolymer melt. *Journal of Polymer Science Part B: Polymer Physics*, 35(10):1643–1648, 1997.

[85] P Stepanek and TP Lodge. Dynamic light scattering from block copolymer melts near the order- disorder transition. *Macromolecules*, 29(4):1244–1251, 1996.

[86] Chan I Chung and John C Gale. Newtonian behavior of a styrene–butadiene–styrene block copolymer. *Journal of Polymer Science Part B: Polymer Physics*, 14(6):1149–1156, 1976.

[87] Edward V Gouinlock and Roger S Porter. Linear dynamic mechanical properties of an sbs block copolymer. *Polymer engineering & Science*, 17(8):535–543, 1977.

[88] Chan I Chung and Ming I Lin. Nature of melt rheological transition in a styrene–butadiene–styrene block copolymer. *Journal of Polymer Science Part B: Polymer Physics*, 16(3):545–553, 1978.

[89] Frank S Bates and Mark A Hartney. Block copolymers near the microphase separation transition. 3. small-angle neutron scattering study of the homogeneous melt state. *Macromolecules*, 18(12):2478–2486, 1985.

[90] Glenn H Fredrickson and Ronald G Larson. Viscoelasticity of homogeneous polymer melts near a critical point. *The Journal of Chemical Physics*, 86(3):1553–1560, 1987.

[91] K. Binder and H. Fried. Asymmetric block copolymer melts near the microphase separation transition: a Monte Carlo simulation. *Macromolecules*, 26(25):6878–6883, 1993.

[92] T. Pakula, K. Karatasos, S. H. Anastasiadis, and G. Fytas. Computer simulation of static and dynamic behavior of diblock copolymer melts. *Macromolecules*, 30(26):8463–8472, 1997.

[93] Michael Murat, Gary S. Grest, and Kurt Kremer. Statics and dynamics of symmetric diblock copolymers: A molecular dynamics study. *Macromolecules*, 32(3):595–609, 1999.

[94] Hideaki Yokoyama, Edward J Kramer, and Glenn H Fredrickson. Simulation of diffusion of asymmetric diblock and triblock copolymers in a spherical domain structure. *Macromolecules*, 33(6):2249–2257, 2000.

[95] Jorge Ramírez, Sathish K Sukumaran, Bart Vorselaars, and Alexei E Likhtman. Efficient on the fly calculation of time correlation functions in computer simulations. *Journal of Chemical Physics*, 133(15):154103, October 2010.

[96] Frank S. Bates, Mark F. Schulz, Ashish K. Khandpur, Stephan Forster, Jeffrey H. Rosedale, Kristoffer Almdal, and Kell Mortensen. Fluctuations, conformational asymmetry and block copolymer phase behaviour. *Faraday Discussions*, 98:7, 1994.

[97] B Minchau, B Dünweg, and K Binder. Microphase separation transition in block copolymers: a test of leibler's theory by monte carlo simulation. *Polymer Communications*, 31(9):348–350, 1990.

[98] Kurt Kremer and Kurt Binder. Monte Carlo simulation of lattice models for macromolecules. *Computer Physics Reports*, 7(6):259–310, 1988.

[99] RG Larson. Simulation of lamellar phase transitions in block copolymers. *Macromolecules*, 27(15):4198–4203, 1994.

[100] Andrea Weyersberg and Thomas A. Vilgis. Phase transitions in diblock copolymers: Theory and Monte Carlo simulations. *Physical Review E*, 48(1):377–391, 1993.

[101] Alexander Hoffmann, Jens-Uwe Sommer, and Alexander Blumen. Computer simulations of asymmetric block copolymers. *Journal of Chemical Physics*, 107(18):7559, 1997.

[102] Alexander Hoffmann, Jens-Uwe Sommer, and Alexander Blumen. Statics and dynamics of dense copolymer melts: A Monte Carlo simulation study. *Journal of Chemical Physics*, 106(16):6709, 1997.

[103] O. N. Vassiliev and M. W. Matsen. Fluctuation effects in block copolymer melts. *Journal of Chemical Physics*, 118(16):7700, 2003.

[104] Marcus Müller and Kostas Ch Daoulas. Calculating the free energy of self-assembled structures by thermodynamic integration. *Journal of Chemical Physics*, 128(2):024903, January 2008.

[105] F.A. Detcheverry, D.Q. Pike, P.F. Nealey, , M. Mueller, and J.J. de Pablo. Monte Carlo simulation of coarse grain polymeric systems. *Physical Review Letters*, 197801:2009, 102.

[106] T M Beardsley and M W Matsen. Monte Carlo phase diagram for diblock copolymer melts. *European Physical Journal. E, Soft Matter*, 32(3):255–64, July 2010.

[107] M W Matsen, G H Griffiths, R a Wickham, and O N Vassiliev. Monte Carlo phase diagram for diblock copolymer melts. *Journal of Chemical Physics*, 124(2):024904, January 2006.

[108] Francisco J Martínez-Veracoechea and Fernando A. Escobedo. Simulation of the gyroid phase in off-lattice models of pure diblock copolymer melts. *Journal of Chemical Physics*, 125(10):104907, September 2006.

[109] Alessandro Barducci, Giovanni Bussi, and Michele Parrinello. Well-tempered metadynamics: A smoothly converging and tunable free-energy method. *Physical Review Letters*, 100(2):020603, January 2008.

[110] Jens Glaser, Jian Qin, Pavani Medapuram, and David C. Morse. Collective and single-chain correlations in disordered melts of symmetric diblock copolymers: Quantitative comparison of simulations and theory. *Macromolecules*, 47(2):851–869, 2014.

[111] Damian A. Hajduk, Sol M. Gruner, Pratima Rangarajan, Richard A. Register, Lewis J. Fetters, Christian Honeker, Ramon J. Albalak, and Edwin L. Thomas. Observation of a reversible thermotropic order-order transition in a diblock copolymer. *Macromolecules*, 27(2):490–501, 1994.

[112] Vanessa Z-H Chan, James Hoffman, Victor Y Lee, Hermis Iatrou, Apostolos Avgeropoulos, Nikos Hadjichristidis, Robert D Miller, and Edwin L Thomas. Ordered bicontinuous nanoporous and nanorelief ceramic films from self assembling polymer precursors. *Science*, 286(5445):1716–1719, 1999.

[113] Edwin L Thomas, David B Alward, David J Kinning, David C Martin, Dale L Handlin Jr, and Lewis J Fetters. Ordered bicontinuous double-diamond structure of star block copolymers: a new equilibrium microdomain morphology. *Macromolecules*, 19(8):2197–2202, 1986.

[114] Hirokazu Hasegawa, Hideaki Tanaka, Komei Yamasaki, and Takeji Hashimoto. Bicontinuous microdomain morphology of block copolymers. 1. tetrapod-

network structure of polystyrene-polyisoprene diblock polymers. *Macromolecules*, 20(7):1651–1662, 1987.

[115] Karen I Winey, Edwin L Thomas, and Lewis J Fetters. The ordered bicontinuous double-diamond morphology in diblock copolymer/homopolymer blends. *Macromolecules*, 25(1):422–428, 1992.

[116] Richard J Spontak, Steven D Smith, and Arman Ashraf. Dependence of the OBDD morphology on diblock copolymer molecular weight in copolymer/homopolymer blends. *Macromolecules*, 26(5):956–962, 1993.

[117] Martin Etchells Vigild, Kristoffer Almdal, Kell Mortensen, IW Hamley, JPA Fairclough, and AJ Ryan. Transformations to and from the gyroid phase in a diblock copolymer. *Macromolecules*, 31(17):5702–5716, 1998.

[118] Eric W Cochran, Carlos J Garcia-Cervera, and Glenn H Fredrickson. Stability of the gyroid phase in diblock copolymers at strong segregation. *Macromolecules*, 39(7):2449–2451, 2006.

[119] Drew A Davidock, Marc A Hillmyer, and Timothy P Lodge. Persistence of the gyroid morphology at strong segregation in diblock copolymers. *Macromolecules*, 36(13):4682–4685, 2003.

[120] R. G. Larson. Monte Carlo simulations of the phase behavior of surfactant solutions. *Journal de Physique II France*, 6:1441–1463, 1996.

[121] Nélido González-Segredo and Peter V Coveney. Self-assembly of the gyroid cubic mesophase: lattice-boltzmann simulations. *EPL (Europhysics Letters)*, 65(6):795, 2004.

[122] I Rychkov. I. rychkov, macromol. theory simul. 14, 207 (2005). *Macromolar Theory and Simulations*, 14:207, 2005.

[123] Igor Rychkov and Kenichi Yoshikawa. Structural changes in block copolymer solutions under shear flow as determined by non-equilibrium molecular dynamics. *Macromolecular Theory and Simulations*, 13(3):257–264, 2004.

[124] MW Matsen. Phase behavior of block copolymer/homopolymer blends. *Macromolecules*, 28(17):5765–5773, 1995.

[125] Tomonari Dotera. Tricontinuous cubic structures in ABC/A/C copolymer and homopolymer blends. *Physical Review Letters*, 89(20):205502, 2002.

[126] Mark A. Horsch, Zhenli Zhang, Christopher R. Iacovella, and Sharon G. Glotzer. Hydrodynamics and microphae ordering in block copolymers: Are hydrodynamics required for ordered phases with periodicity in more than one dimension? *Journal of Chemical Physics*, 121(22):11455–11462, 2004.

[127] Andrew J. Schultz, Carol K. Hall, and Jan Genzer. Computer simulation of copolymer phase behavior. *Journal of Chemical Physics*, 117(22):10329, 2002.

[128] Andrew J Schultz, Carol K Hall, and Jan Genzer. Computer simulation of block copolymer/nanoparticle composites. *Macromolecules*, 38(7):3007–3016, 2005.

[129] Robert D Groot, Timothy J Madden, and Dominic J Tildesley. On the role of hydrodynamic interactions in block copolymer microphase separation. *Journal of Chemical Physics*, 110(19):9739–9749, 1999.

[130] Francisco J Martínez-Veracoechea and Fernando A Escobedo. Lattice monte carlo simulations of the gyroid phase in monodisperse and bidisperse block copolymer systems. *Macromolecules*, 38(20):8522–8531, 2005.

[131] Akash Arora, David C Morse, Frank S Bates, and Kevin D Dorfman. Commensurability and finite size effects in lattice simulations of diblock copolymers. *Soft Matter*, 11(24):4862–4867, 2015.